Imperial College London

Targeting mechanotransduction in myofibroblast like cells

Dariusz Lachowski

February 2019

Imperial College London

Department of Bioengineering

Submitted in partial fulfilment of the requirements for the degree of Doctor of Philosophy in Bioengineering of Imperial College London and the Diploma of Imperial College London

Copyright Declaration

The copyright of this thesis rests with the author. Unless otherwise indicated, its contents are licensed under a Creative Commons Attribution-Non Commercial 4.0 International Licence (CC BY-NC).

Under this licence, you may copy and redistribute the material in any medium or format. You may also create and distribute modified versions of the work. This is on the condition that you credit the author and do not use it, or any derivative works, for a commercial purpose.

When reusing or sharing this work, ensure you make the licence terms clear to others by naming the licence and linking to the licence text. Where a work has been adapted, you should indicate that the work has been changed and describe those changes.

Please seek permission from the copyright holder for uses of this work that are not included in this licence or permitted under UK Copyright Law.

Declaration of Originality

I hereby declare that the work presented in this thesis is entirely my own. Where others have contributed, every effort has been made to accurately reference and acknowledge their work.

Abstract

Mechanical stimuli applied by the extracellular matrix (ECM) and the cells play an important role in the maintenance of tissue homeostasis. Mechanosensing and mechanotransduction are two processes by which cells transform mechanical forces into biochemical signals and adapt to changes in the microenvironment. Imbalanced cell response can create a positive feedback loop and lead to the pathological conditions, such as pancreatic ductal adenocarcinoma, which is characterised by the presence of extensive fibrotic stroma produced and maintained by pancreatic stellate cells (PSC). Here, it is shown that PSC are reversibly activated through mechanosensing of fibrosis-mimicking stiff substrates. Under the application of this mechanical cue, PSC exhibit rigidity-guided movement (durotaxis). This pattern of migration, which is regulated by a stiffness-dependent asymmetric distribution of active and inactive focal adhesion protein, is also observed in hepatic stellate cells (HSC).

HSC, durotactically migrating to the fibrotic sites, can perpetuate the disease through their stiffness-initiated activation and resulting aberrant matrix remodelling capabilities. Experiments revealed a mechanical network allowing HSC to maintain fibrotic ECM by decreasing the matrix-digesting enzyme MMP-9 expression and activity, and increasing the activity of its secreted inhibitor, TIMP-1. Furthermore, these results shed light on a new mechanism, through which stiff matrix can initiate exocytosis. This is identified as an effect of membrane homeostasis maintenance, where an increase in plasma membrane tension via β1 integrin mechanosensing and RhoA activation is followed by tension-relieving secretion.

With RhoA and cell activation as a common factor in the cell mechanical response, final experiments focused on G protein-coupled receptor (GPER), here identified as a novel mechanoregulator in fibroblasts. GPER activation decreases RhoA activity and impacts overall mechanical response in cells, opening new possibilities for potential therapies in cancer and fibrosis.

Acknowledgements

First and foremost, I want to thank my supervisor Dr. Armando del Río Hernández for the continuous support of my studies. He taught me and provided me with all the resources to grow as a scientist. I am grateful for the time he spent on planning and analysing the projects with me, giving the feedback on my research and always listening to what I had to say. I would also like to thank Dr. Krista Rombouts for her support, encouragement and help with establishing the foundations of my work with hepatic stellate cells.

I thank those present and past members of Cellular and Molecular Biomechanics Laboratory and the Department of Bioengineering who I have worked with over the time of my PhD studies. I am grateful to Dr. Ernesto Cortes for his support and assistance with cell culture, Dr. Alistair Rice for teaching the magnetic tweezers and working on many great projects and publications with me, Dr. Benjamin Robinson for teaching and sparking passion for the microscopy. I am indebted for the time he spent on discussing the experiments with me even after he had finished his work in our group. I would also like to thank Carlos Matellan, Dr. William Haining, Dr. Tyler Lieberthal, Ashna Patel, Dr. Muge Sarper, Dr. Sahana Gopal, Dr. Stephen Thorpe, Daniel Pink and Julian Ashby for thoughtful discussions and help with the projects. I thank Alain Vella for all those coffee breaks I needed during my work and for many insightful conversations about our research and life outside the lab. I finally thank Gulcen Yeldag for helping me with transfections, microscopy and PCR, but most importantly for being an amazing, always supportive and patient, friend.

Lastly, I am deeply grateful to my family – my Mum, Ewa, Jacek, Ewelina and Remek for always believing in me, being encouraging and providing me with all the support I needed during my PhD.

Publication list

1. Lachowski D, Cortes E, Rice A, and del Río Hernández A. **Mechanoregulation in fibroblasts via G protein coupled receptor.** Under revision in Science Advances
2. Chronopoulos A, Thorpe S, Cortes E, Lachowski D, Rice A, Mykuliak V, Rog T, Lee DA, Hytonen VP, del Rio Hernandez A **Syndecan-4 tunes cell mechanics by activating the kindlin-integrin-RhoA pathway.** Accepted in Nature Materials
3. Cortes E, Sarper M, Robinson B, Lachowski D, Chronopoulos A, Thorpe S, Lee DA, and del Río Hernández A. **GPER is a mechanoregulator of pancreatic stellate cells and the tumor microenvironment**. EMBO reports 2018
4. Cortes E, Lachowski D, Robinson R, Sarper M, Teppo J, Thorpe S, Lieberthal T, Iwamoto K, Lee DA, Okada-Hatakeyama M, Varjosalo M, and del Río Hernández A. **Tamoxifen mechanically reprograms the tumor microenvironment and the survival of cancer cells via HIF-1A.** EMBO reports 2018
5. Lachowski D, Cortes E, Rice A, Robinson B, Thorpe S, Lee DA, Possamai LA, Wang H, Pinato D, and del Río Hernández A. **RAR-β is downregulated in HCC & cirrhosis and its expression inhibits myosin-driven activation and durotaxis in hepatic stellate cells.** Hepatology 2018
6. Cortes E, Lachowski D, Chronopoulos A, & del Río Hernández A. **Tamoxifen Reprograms Hepatic Stellate Cells to Mechanical Quiescence.** Oncogene 2018
7. Haining AWM, Rahikainen R, Cortes E, Lachowski D, Rice AJ, von Essen M, Hytönen VP, del Río Hernández A. **Mechanotransduction in talin through the interaction of the R8 domain with DLC1.** PLoS Biology 2018
8. Lachowski D, Cortes E, Rice A, Pinato D, Rombouts K, del Río Hernández A. **Matrix stiffness modulates the activity of MMP-9 and TIMP-1 in hepatic stellate cells to perpetuate fibrosis**. Scientific Reports 2018
9. Lachowski D, Cortes E, Robinson B, Rice A, Rombouts K, del Río Hernández A. **FAK controls the mechanical activation of YAP, a transcriptional regulator required for durotaxis.** FASEB Journal 2017
10. Rice A, Cortes E, Lachowski D, Cheung, CH, Karim SA, Morton J, del Río Hernández A **Matrix stiffness induces Epithelial-Mesenchymal transition and promotes chemoresistance in pancreatic cancer cells.** Oncogenesis 2017

11. Lachowski D, Cortes E, Pink D, Chronopoulos A, Karim SA, Morton JP, del Río Hernández A. **Substrate rigidity controls activation and durotaxis in pancreatic stellate cells.** Scientific Reports 2017
12. Chronopoulos A, Robinson B, Sarper S, Cortes E, Auernheimer V, Lachowski D, Attwood S, Garcia R, Ghassemi S, Fabry B, del Río Hernández A**. ATRA mechanically reprograms pancreatic stellate cells to suppress matrix remodelling and inhibit cancer cell invasion.** Nature Communications 2016.
13. Lachowski D, Cortes E, Robinson B, Rombouts K, del Rio Hernandez A. **Elucidating the Biomechanical Response of Human Hepatic Stellate Cells on Substrates Mimicking Healthy and Fibrotic Matrix Rigidity.** Journal of Hepatology 2016
14. Lachowski D, Cortes E, Robinson B, Rombouts K, del Rio Hernandez A. **Assaying the rigidity guided migration of human tumour stromal myofibroblasts (TSMs) on polyacrylamide substrates mimicking the healthy and fibrotic tissue transition boundary.** Convergent Science Physical Oncology 2016

Contents

Copyright Declaration 2
Declaration of Originality 2
Abstract 3
Acknowledgements 4
Publication list 5
Contents 7
List of figures 12
Abbreviations 15
Aims and objectives 18
General objectives 19
Working hypotheses 19
1 Introduction 20
1.1 Substrate mechanosensing and durotaxis 20
1.2 Plasma membrane 24
1.3 Cytoskeletal regulation of plasma membrane dynamics 27
1.4 Matrix metalloproteinases and their inhibitors 30
1.5 GPER signalling 33
1.6 Pancreatic cancer 35
1.7 Liver fibrosis 37
2 Substrate rigidity controls activation and durotaxis in pancreatic stellate cells 40
2.1 Introduction 40
2.2 Results 42
2.2.1 Matrigel induces PSC quiescence 42
2.2.2 Production of a physiomimetic model recapitulating soft and stiff substrates 44
2.2.3 Stiff matrices induce PSC activation 47

2.2.4 Soft matrices induce and maintain PSC quiescence 49
2.2.5 PSCs exhibit directed migration across a stiffness gradient 53
2.3 Discussion 58
2.4 Materials and methods 62
2.4.1 Cell culture and reagents 62
2.4.2 Quiescence induction using Matrigel assay 62
2.4.3 Preparation of polyacrylamide hydrogels of tuneable stiffness 62
2.4.4 Oil Red O staining 63
2.4.5 Immunofluorescence 63
2.4.6 Image acquisition and quantitative analysis 64
2.4.7 Quantification and analysis of durotaxis on polyacrylamide hydrogels 64
2.4.8 Real-time quantitative polymerase chain reaction 65
2.4.9 Mouse Tissues 65
2.4.10 Multiphoton Microscopy 65
2.4.11 Statistical analysis 66
3 FAK controls the mechanical activation of YAP, a transcriptional regulator required for durotaxis 67
3.1 Introduction 67
3.2 Results 68
3.2.1 Stiffness-induced YAP nuclear localization and activation requires FAK activity 68
3.2.2 Fabrication of a rigidity gradient for durotaxis assays 73
3.2.3 Directed migration in hepatic stellate cells 74
3.2.4 HSC durotaxis is dependent on a working FAK/YAP axis 76
3.3 Discussion 79
3.4 Materials and methods 83
3.4.1 Cell culture 83
3.4.2 Transfection 83

3.4.3 Polyacrylamide substrate fabrication 83
3.4.4 Immunofluorescence 84
3.4.5 Quantitative PCR 84
3.4.6 Atomic force microscopy 85
3.4.7 Quantification and analysis of durotaxis on polyacrylamide hydrogels 85
3.4.8 Statistical analysis 86
4 Matrix stiffness modulates the activity of MMP-9 and TIMP-1 in hepatic stellate cells to perpetuate fibrosis 87
4.1 Introduction 87
4.2 Results 90
4.2.1 Substrate rigidity inhibits MMP-9 gene expression 90
4.2.2 Substrate rigidity inhibits intracellular protein levels of MMP-9 and TIMP-1 92
4.2.3 Substrate rigidity modulates the activity of secreted MMP-9 and TIMP-1 94
4.2.4 TIMP-1 knockdown promotes extracellular MMP-9 activity 96
4.2.5 MMP-9 is downregulated in HCC 98
4.3 Discussion 99
4.4 Materials and methods 102
4.4.1 Tissues microarrays 102
4.4.2 Cell culture 102
4.4.3 Polyacrylamide substrate fabrication 103
4.4.4 Western blot 103
4.4.5 Quantitative PCR 104
4.4.6 Gelatin zymography and reverse zymography 104
4.4.7 Immunostaining 105
4.4.8 Statistics 106
5 Matrix stiffness promotes membrane tension and caveolae-dependent exocytosis 107
5.1 Introduction 107

5.2 Results 108
5.2.1 Substrate rigidity promotes membrane and cytoskeletal stiffening 108
5.2.2 Membrane mechanosensing requires β1 integrin 109
5.2.3 Substrate rigidity and membrane tension promote caveolae formation 113
5.2.4 Substrate rigidity promotes exocytosis 116
5.2.5 Dynamin-1 is required for caveolae formation in response to membrane stiffening 118
5.3 Discussion 121
5.4 Materials and methods 123
5.4.1 Cell culture 123
5.4.2 Polyacrylamide substrate fabrication 123
5.4.3 Quantitative PCR 124
5.4.4 Atomic force microscopy 125
5.4.5 Fluorescence Lifetime Imaging Microscopy 125
5.4.6 Focused Ion Beam scanning electron microscopy 126
5.4.7 Total Internal Reflection Microscopy 126
5.4.8 Statistical analysis 127
6 Mechanoregulation in fibroblasts by the G protein-coupled estrogen receptor 128
6.1 Introduction 128
6.2 Results 129
6.2.1 GPER activation modifies cell morphology and supresses RhoA activation 129
6.2.2 GPER activation reduces phosphorylation of myosin light chain 2 through RhoA 134
6.2.3 GPER modulates force generation and mechanosensing 137
6.2.4 GPER activation suppresses the myofibroblast-like phenotype 142
6.2.5 GPER regulates cell polarization and assembly of actin stress fibres 144
6.2.6 GPER activation inhibits actin polymerisation and synthesis of β-actin 147
6.2.7 GPER modulates focal adhesion formation and dynamics through RhoA 149

6.2.8 GPER inhibits YAP nuclear localisation and activation 151
6.3 Discussion 155
6.4 Materials and methods 156
6.4.1 Cell culture, transfection, and antibodies 156
6.4.2 Scanning Electron Microscopy 157
6.4.3 Immunofluorescence staining 157
6.4.4 YAP IF measurements 158
6.4.5 Traction forces using elastic pillars 158
6.4.6 Cell mechanosensing 159
6.4.7 Atomic force microscopy 159
6.4.8 Fluorescence Recovery After Photobleaching 160
6.4.9 RT–PCR 160
6.4.10 Western blotting 160
6.4.11 G-LISA assay for RhoA 161
6.4.12 Statistical analysis 162
7 Conclusions 163
8 References 168

List of figures

Figure 1.1 Integrin complex as a mediator between extracellular matrix and intracellular biomechanical signalling. 21
Figure 1.2 Force-mediated regulation of integrin adhesions. 23
Figure 1.3 Comparison of the functions of flippases, floppases and scramblases in the plasma membrane. 25
Figure 1.4 Structure of caveolae membrane vesicle. 26
Figure 1.5 Membrane lipids regulate the actin assembly....28
Figure 1.6. TIMPs regulate MMP function and activation....33
Figure 1.8 Hepatic stellate cells activation.. 39
Figure 2.1 Stiff matrices induce PSC activation.. 43
Figure 2.2 Bright field images of Oil Red O stained PSCs cultured on Matrigel.....44
Figure 2.3 Schematic representation of surface preparation for cell attachment on soft and stiff PAA gels. 46
Figure 2.4 Immunofluorescent images of aSMA and vimentin of PSCs seeded on matrices represented in Fig. 1a.. 48
Figure 2.5 Mechanical activation of PSCs by stiff substrates increases cell proliferation and fibronectin production....48
Figure 2.6 Soft matrices induce PSC deactivation. 50
Figure 2.7 Immunofluorescent images of αSMA and vimentin of PSCs seeded on matrices represented in Fig. 2a.. 52
Figure 2.8 Mechanical deactivation of PSCs by soft substrates decreases cell proliferation and fibronectin production.. 52
Figure 2.9 αSMA is highly expressed and co-localises with collagen-I in PDAC tissues but αSMA expression is markedly decreased in normal pancreatic tissues from mice.. 53
Figure 2.10 Durotactic response of PSCs. 55
Figure 2.11 FAK and myosin-II activities are required for durotaxis in PSCs.....57
Figure 2.12 Illustration of PSC mechano-sensory driven regulation within a PDAC microenvironment.. 60
Figure 3.1 Active FAK is required for YAP translocation to the nucleus and further activation 69
Figure 3.2 YAP nuclear localisation in HSCs cultured on different stiffness polyacrylamide gels 70

Figure 3.3 YAP nuclear localisation in y397FAK and myrFAK HFFs cultured on different stiffness polyacrylamide gels.. 71
Figure 3.4 Focal adhesion kinase (FAK) expression and FAK inhibition in Hepatic Stellate Cell durotaxis. 72
Figure 3.5 Stiffness transition boundary. 73
Figure 3.6 HSC-directed migration toward stiffer substrate in the rigidity gradient. 75
Figure 3.7 Durotaxis in HSCs depends on the FAK/YAP axis. 77
Figure 3.8 Durotaxis in HSCs depends on the FAK/YAP axis.. 79
Figure 3.9 Model illustrating the roles of FAK/YAP in HSCs durotaxis. 80
Figure 4.1 Changes in cell morphology are dependent on substrate stiffness. 90
Figure 4.2 MMP-2, MMP-9 and TIMP-1 mRNA expression on different gel rigidities. 91
Figure 4.3 GAPDH mRNA expression in hepatic stellate cells does not change when cultured on different rigidity substrates. 92
Figure 4.4 MMP-2, MMP-9 and TIMP-1 protein expression on different gel rigidities. 93
Figure 4.5 Western Blot analysis of protein expression in response to external rigidity. 93
Figure 4.6 MMP-2, MMP-9 and TIMP-1 assayed activity on different gel rigidities.. 95
Figure 4.7 Enzymatic activity of MMP 9 MMP 2 and TIMP 1 in response to external rigidity assessed by zymography and reverse zymography 96
Figure 4.8 TIMP-1 mRNA expression in cells treated with TIMP-1 siRNA. 97
Figure 4.9 MMP-9 activity with TIMP-1 knockdown. 98
Figure 4.10 MMP-9 is downregulated in stromal tissues of HCC patients.. 99
Figure 4.11 MMP-2, MMP-9 and TIMP-1 activity regulation on different gel rigidities. 100
Figure 5.1 Substrate rigidity affects the membrane and cytoskeleton stiffness. 109
Figure 5.2 β1 integrin and RhoA activity are required for substrate-stiffness membrane mechanosensing. 112
Figure 5.3 Substrate stiffness effect on caveolae formation. 114
Figure 5.4 Media osmotic concentration effect on caveolae formation. 115
Figure 5.5 Hypotonic medium-induced plasma membrane stiffening affects the TIMP-1 exocytosis in HSC. 117
Figure 5.6 Dynamin-1 presence in the plasma membrane is membrane tension dependant. 119
Figure 5.7 Dynamin-1 is required for increased caveolae presence in plasma membrane in response to high membrane tension. 120
Figure 6.1 GPER activation changes the morphology of human foreskin fibroblasts (HFFs) and inhibits RhoA activation. 131

Figure 6.2 GPER expression in human foreskin fibroblasts 132
Figure 6.3 GPER activation changes morphology in mouse embryonic fibroblasts (MEFs)…. 132
Figure 6.4 Images of the full membranes used in Western blots for RhoA and pRhoA 133
Figure 6.5 GPER activation supresses phosphorylation of myosin light chain 2 (MLC-2) but does not affect the expression of total MLC-2..... 135
Figure 6.6 Characterization of cell morphology in human foreskin fibroblasts (HFFs). 136
Figure 6.7 GPER activation supresses activation (phosphorylation) of MLC-2 but does not affect the expression of total MLC-2 in mouse embryonic fibroblasts (MEFs) cells..... 137
Figure 6.8 GPER activation reduces HFF force generation, cell stiffness, and mechanosensing.. 140
Figure 6.9 GPER activation induces HFF deactivation.. 143
Figure 6.10 GPER activation induces MEF deactivation. 144
Figure 6.11 Actin polymerisation rate and fibre thickness are dependent on the GPER/RhoA axis. 146
Figure 6.12 Full membranes for Western blot of β-actin and total protein in HFFs.. 148
Figure 6.13 GPER activation regulates the size and dynamics of focal adhesions in human foreskin fibroblasts (HFFs). 150
Figure 6.14 GPER activation decreases nuclear localisation of YAP in the nucleus and YAP activation. 152
Figure 6.15 GPER activation decreases nuclear YAP location via mechanical pathway in mouse embryonic fibroblasts (MEFs) cells. 154

Abbreviations

AFM – atomic force microscopy

aHSC – activated hepatic stellate cells

ANKRD – Ankyrin Repeat Domain

APS – ammonium persulfate

APTES – 3-aminopropyl)triethoxysilane

ASMA/αSMA – alpha smooth muscle actin

ATP – adenosine triphosphate

BSA – bovine serum albumin

CAF – cancer associated fibroblasts

cAMP – Cyclic adenosine monophosphate

CAV – caveolin

COPII – coat protein II

CTGF – connective tissue growth factor

Dyn-1 – dynamin 1

ECM – extracellular matrix

EGFR – epidermal growth factor receptor

ER – estrogen receptor

F-actin – fibrillar actin

FAK – focal adhesion kinase

FBS – foetal bovine serum

FIB SEM – focused ion beam scanning electron microscopy

G-actin – globular actin

GAP – GTPase-activating proteins

GEF – guanine nucleotide exchange factor

GFP – green fluorescent protein

GPER – G protein coupled receptor

HCC – hepatocellular carcinoma

HFF – human foreskin fibroblast

HSC – hepatic stellate cells

IL – interleukin

LATS1/2 – large tumour suppressor kinase 1/2

MEF – mouse embryonic fibroblasts

MLC-2 – myosin light chain 2

MMP – matrix metalloproteinase

myrFAK – myristoylated focal adhesion kinase

PAA - polyacrylamide

PanIN – pancreatic intraepithelial neoplasia

PDAC – pancreatic ductal adenocarcinoma

PFA - paraformaldehyde

PGDF – platelet derived growth factor

PI(4,5)P_2 – Phosphatidylinositol 4,5-bisphosphate

PI3K – phosphoinositide 3-kinase

PLC – phospholipase c

PSC – pancreatic stellate cells

qHSC – quiescent hepatic stellate cells

RFP – red fluorescent protein

SEM – scanning electron microscope

siRNA – small interfering RNA

TEMED – tetramethylethylenediamine

TGF-β – transforming growth factor beta

TIMP – tissue inhibitor of metalloproteinases

TNF-α – tumour necrosis factor alpha

YAP – yes-associated protein

Aims and objectives

Living cells receive biochemical and physical signals from their microenvironment, composed of neighbouring cells and extracellular matrix (ECM)[1]. ECM is secreted and controlled in a strict, tissue specific manner by the cells during tissue development and is maintained in response to physiological processes, such as matrix remodelling and post-injury repair[2,3]. Matrix properties can affect many cellular functions, such as growth, survival, differentiation, or migration[4,5], by exerting constant chemical and mechanical stimuli on the cells. To promote tissue homeostasis – proper function and integrity in response to the signals from the ECM, cell must be able to sense not only biochemical cues, but also the mechanical properties of the microenvironment[6].

The intracellular signalling process, through which tensional, compressive, and shear forces can be translated into biochemical signals allowing cells to adapt to the changes in the microenvironment, is known as mechanotransduction. It involves ECM components, such as fibronectin and collagens[7], to support and transmit the load through transmembrane receptors, primarily integrins that connect extracellular and intracellular structures via focal adhesions comprised of linker proteins (such as, focal adhesion kinase, paxillin, talin and vinculin) connecting receptors to the cytoskeleton, consisting of actin filaments and associated proteins, and transmit the mechanical signals within the cell[8,9]. The effect of mechanotransduction can be observed both as triggering biochemical signalling and exerting mechanical forces on the ECM[10].

The biomechanical homeostasis maintained between the microenvironment and cell is disrupted in a disease, such as fibrosis and cancer[11,12]. In the latter, tumour stroma and mechanical abnormalities developed during tumour growth are considered as leading regulatory factors[13,14]. Tumour microenvironment is composed of cancer cells, immune cells and fibroblasts, as well as hyaluronan, glycosaminoglycans and proteins (mostly fibronectin and collagen I)[15]. Biochemical signals (growth factors secreted by cancer cells) together with biomechanical signals from the stroma activate fibroblasts to start a chronic wound healing-like response resulting in abnormal cell contraction and fibrillar ECM protein deposition leading to desmoplasia – accumulation of rich, fibrotic stroma within and around the tumour[16]. ECM stiffening and desmoplasia characterise many tumour types and promotes their progression, including pancreatic[17,18] (pancreatic adenocarcinoma - PDAC) and liver[19,20] (hepatocellular carcinoma – HCC) cancer. Desmoplastic tissue is known to contribute to the

microenvironment stiffening and the increase of solid stress, due to the bidirectional force generation between the tumour and the host. Increased stiffness highly affects the fibroblasts, activating them and maintaining this state via cellular mechanoregulation through, for example, YAP[21] and RhoA[22] related pathways.

The recognition of cell sensing and regulation of mechanical properties of the extracellular matrix in healthy and fibrotic stroma is crucial for the understanding of the disease progression and the identification of new therapeutic targets. Integration and translation of these findings into the general mechanisms of mechanotransduction in the model cells provides a valuable insight that helps to more completely explain the role of mechanosignalling in tissue development and maintaining the homeostasis.

General objectives

- Characterisation of stellate cell and fibroblast biomechanical activation and durotaxis on substrates mimicking healthy and diseased pancreas & liver.
- Determination of the mechanism of substrate stiffness-triggered focal adhesion formation.
- Elucidation of the mechanism of cytoskeleton mediated plasma membrane mechanosensing.
- Assessment of GPER role as a mechanoregulator of fibroblast activation.

Working hypotheses

- Fibrosis or tumour mimicking substrates activate myofibroblasts transition, triggering TIMP secretion and FAK dependent durotaxis.
- Cells exhibit caveolin related exocytosis to maintain membrane homeostasis, in response to increased tension of plasma membrane caused by high substrate stiffness.
- GPER is a mechanoregulator and its activation can inhibit cell mechanical response to the external mechanical stimuli.

1 Introduction

1.1 Substrate mechanosensing and durotaxis

Cells adhering to the extracellular matrix probe the rigidity of the substrate. Pulling on their surroundings through integrins provides a structural connection between outer cellular contacts and cytoskeleton[23]. Focal adhesions (FAs) are adhesion plaques formed by binding complexes of integrins and proteins, for example focal adhesion kinase, paxillin, vinculin or talin. Focal adhesions are key as they play a role as a dynamic interface between cytoskeleton and extracellular matrix (ECM) transmitting mechanical forces through the cell membrane. FAs are dynamic structures physically interacting with the components of ECM, such as, vitronectin, fibronectin, laminins or collagens. Integrins, being one of the most studied focal adhesion proteins are heterodimers composed of α- and β- subunits[24]. Their assembly can be guided by the extracellular matrix composition and their specificity is defined by the combination of 24 α- and β- subunits and by alternative protein splicing[25]. Combination of those subunits provides the specificity and affinity to different ECM components. Extracellular mechanical stimuli can affect integrin activation via high affinity conformation change in a process called “inside out signalling”[26]. As a result of those events they cluster, reinforcing the molecular links at the cell-matrix interface (Figure 1.1). Integrin extracellular domain contacts the ECM, while the cytoplasmic domain interacts with cytoskeletal proteins through the core focal adhesion components[27].

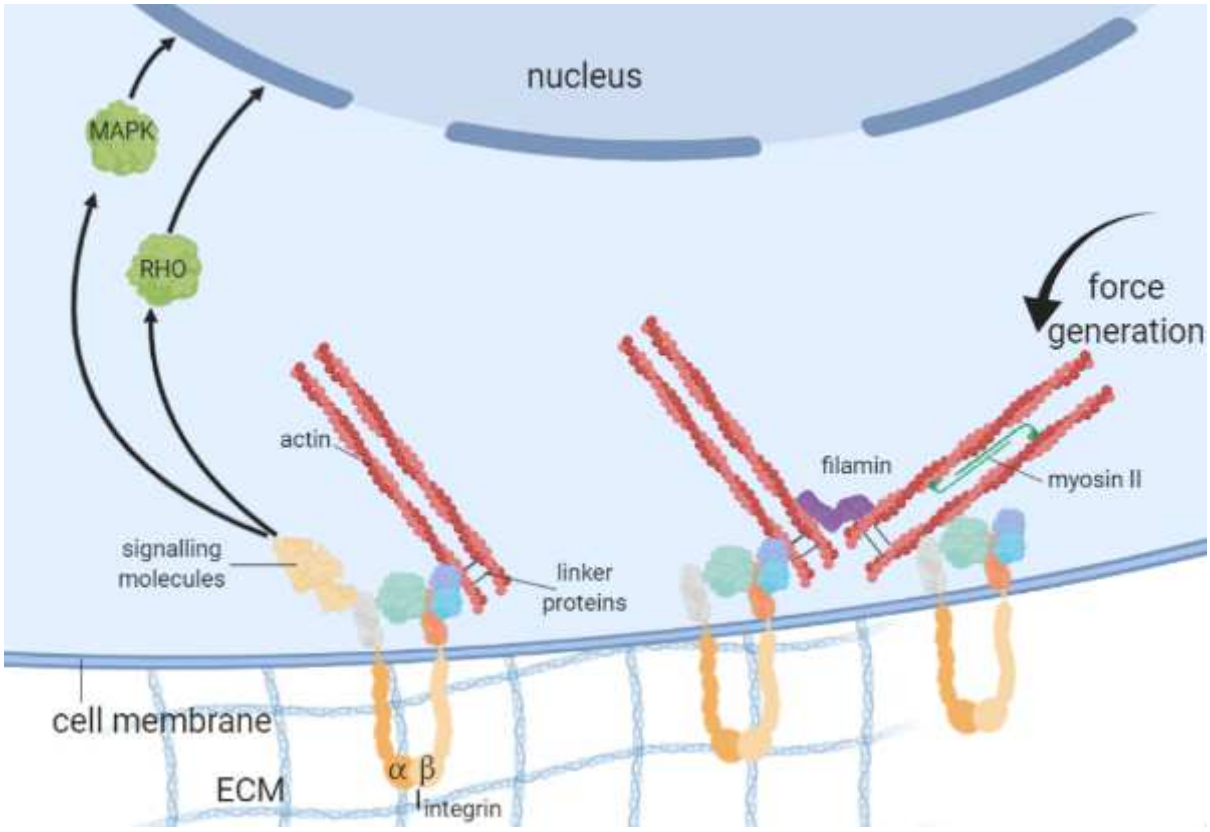

Figure 1.1 Integrin complex as a mediator between extracellular matrix and intracellular biomechanical signalling. Adapted from Humphrey 2014[28]

Cells can accommodate their own mechanical state not only by biochemical composition, but also by adjusting force generation, cytoskeletal tension and bulk cell elasticity in response to applied force. A good example of this mechanism is regulation of actin stress fibres by zyxin, re-orientation and alignment of integrins by actin flow affecting their clustering and function[29] and re-ordering of actin cytoskeleton in response to substrate stiffness[30]. The 'molecular clutch theory'[31,32] predicts and can be an explanation for the nanoscale contractions in the maturing focal adhesions. These events depend on the substrate rigidity[33] and the tyrosine kinases receptors activity[34].

Integrins are not the only components of focal adhesions taking part in sensing substrate rigidity[35,36]. One of the first studies conducted by Pelhalm and Wang demonstrated that the different response of fibroblastic NIH/3T3 cells to the elasticity of the surrounding matrix initiates at focal adhesion sites[37]. Fibroblasts are highly sensitive to mechanical stimuli and the mechanical properties of their matrix, similar to the other types of cells, for example

myofibroblasts. The level of stiffness at which the ECM can influence the cell differs depending on the cell type. Fibroblasts and endothelial cells increase the assembly of their cytoskeleton into actin stress fibres and focal adhesions at ~3 kPa, whereas neutrophil spreading is not sensitive to substrate stiffness that is reduced to 2 Pa[38]. Moreover, it is known that cells spread more on stiffer matrices versus soft ones[39]. They also exert higher tractions on stiff surfaces, whereas cells downregulate myosin-dependent contractility on softer substrates[40]. Cell migration speed shows a biphasic dependence on stiffness, being maximal at intermediate levels[41].

ECM remodelling, cell migration and other important cell functions can be driven by forces generated by acto-myosin stress fibres and transmitted to the ECM through focal adhesion. Cells can also sense substrate rigidity. Their response is observable in focal adhesions and stress fibres reassembling. Mechanosensing and mechanotransduction feedbacks are regulated by mutual relation of extracellular matrix rigidity and following cytoskeleton and focal adhesions assembly. This mechanism is responsible for regulating many cellular functions – differentiation, spreading area and migration.

Interestingly, extracellular matrix stiffness can affect cell fate. Soft matrices induce apoptosis of adherent cells, possibly the result of suppression of focal adhesion kinase and other integrin related signalling pathways on compliant extracellular matrix, and the requirement of ECM binding for cell survival [42]. Analogous effects may be important in wound healing, with low environment stiffness promoting myofibroblast apoptosis once tissue repair is complete and cell-induced tension has decreased. In this context, failed apoptosis is linked to tissue fibrosis.

Cell migration plays a crucial role in developmental morphogenesis[43] and tissue homeostasis, as well as disease progression in cancer[44]. Environmental cues can be sensed by cells and guide their movement. These cues may be diffusible chemical factors, as in chemotaxis or physical, including electric fields, topography, or extracellular matrix rigidity – in durotaxis[45]. This mechanism is thought to be crucial in epithelial-mesenchymal transition[46], development of the nervous system[38] and cancer metastasis[47]. Extracellular matrix stiffness in tissues can differ locally or change over time during development. It can differ in diseases such as cancer or liver fibrosis[48]. Durotaxis requires cells to probe and measure the spatial and temporal variability in the stiffness of extracellular matrix using mechanosensing via integrins and focal adhesions pathways – the cell must actively exert a force on the substrate, sense the resulting substrate

deformation and calculate the force and deformation ratio to measure rigidity. New studies are required to explain these phenomena in detail.

Cells mostly show a centripetal flow of the actin cytoskeleton toward the cell centre. Clutch models have proposed that forces and deformations experienced by the molecules linking this actin flow to the substrate depend on substrate rigidity (Figure 1.2)[28]. In this model, actin filaments flow backwards, towards the posterior side of the cell, over the immobile, ECM-bound integrins, being pulled by the central myosin II filaments and pushed by polymerization at the leading edge of the cell. Linker proteins are driven backwards at intermediate speeds, slowing down the actin flow and transmitting force through a sort of 'friction'[49]. Loading rate of the linkage between extracellular matrix, integrins and skeleton can be changed by ECM stiffness. On soft substrates, deformation of extracellular matrix buffers the rearward movement of actin, which slows down the loading rate on adhesions; on stiff substrates, the force on a focal adhesion increases faster.

Other mechanisms have been proposed based on the observation that cells augment force generation as substrate stiffness increases so as to maintain a constant substrate deformation. This finding has led to the hypothesis that cells probe substrate rigidity by measuring the force required to obtain a given substrate deformation sensed by either local contractile filaments, or by actin stress fibres operating at the whole cell scale. However, how exactly cells dynamically sample local differences in the extracellular matrix stiffness landscape in order to guide durotaxis has not yet been identified.

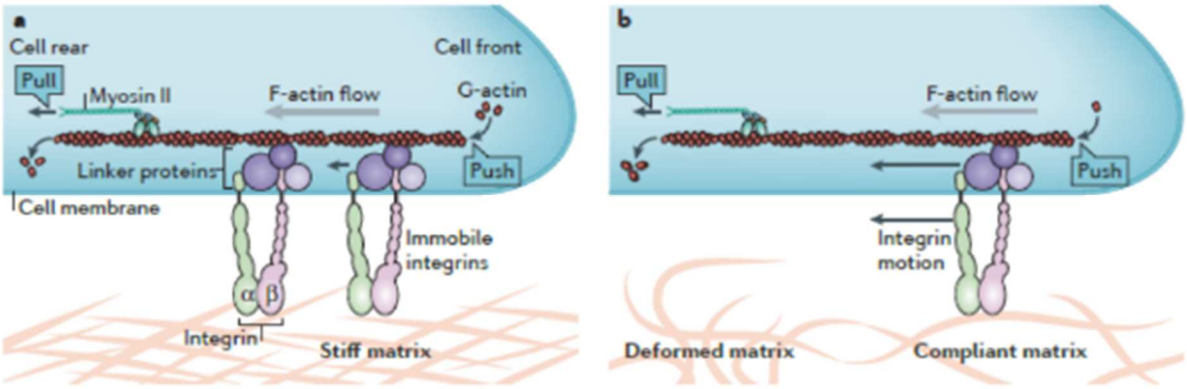

Figure 1.2 Force-mediated regulation of integrin adhesions. Schematic of the 'focal adhesion clutch' on stiff (a) versus soft (b) extracellular matrix (ECM)[28]

1.2 Plasma membrane

Biomembranes establish the cell and cellular organelle boundaries. They consist of a hydrophobic bilayer of phospholipids with differently bound proteins. The first accurate view on the structure of biomembranes was represented by Singer and Nicholson's "fluid mosaic"[50]. The model describes the membrane as a lipid bilayer that can be formed of phospholipids, glycolipids and sterols. It has an amphipathic character enabling the membrane to auto organise in water environment. The bilayer's hydrophobic tails face each other inward, whereas hydrophilic heads are oriented to the outer, aqueous side[51]. Proteins in the membrane can be bound to either headgroups or tails, residing either on the surface or being anchored inside the membrane[52]. Both proteins and lipids are in constant rotational, translational or transbilayer motion. Rotational motion occurs around the axis perpendicular to the membrane at frequencies in the order of 10^8–10^9 s^{-1} for the lipids and 10^3–10^5 s^{-1} for the proteins, under physiological conditions[53]. This movement is crucial for all membrane proteins and preventing the movement results in the loss of function. Translational motion of lipids and proteins occurs along the plane of the membrane. The diffusion coefficients are in the 10^{-8} - 10^{-9} cm^2 s^{-1} range (lipids) and 10^{-9}–10^{-11} cm^2 s^{-1} (proteins)[54]. Transbilayer (flip-flop) movement occurs either by very slow, due to the high energy barrier imposed by the lateral tension and the resistance to the passage of polar head groups through the core, spontaneous translocation of phospholipids across the bilayer[55] (10^{-15} s^{-1})[56] or by the aid of ATP-dependant lipid translocators – lipid selective flippases and floppases, and non-selective, energy - independant scramblases[55,57] . The former catalyses lipid transfer in the direction of the inward layer and the latter towards the outward layer.

Both types of ATP-dependant translocators are required to equalise the number of lipids at both sides of the biomembranes when new organelles are being generated, making the membrane more symmetric. They can also play an opposite role, providing the membrane asymmetry necessary in lipid vesiculation[58]. Flippases activity can result in the formation of the vesicles that can be involved in endofacial lipid and protein traffic[55], whereas floppases, members of the ATP-binding cassette superfamily, catalyse exofacial transport of lipids in membranes (Figure 1.3). The last major type of the lipid translocators are phospholipid scramblases. They are ATP-independent translocators involved in calcium-regulated bidirectional phospholipid transport, eliminating the membrane asymmetry[59].

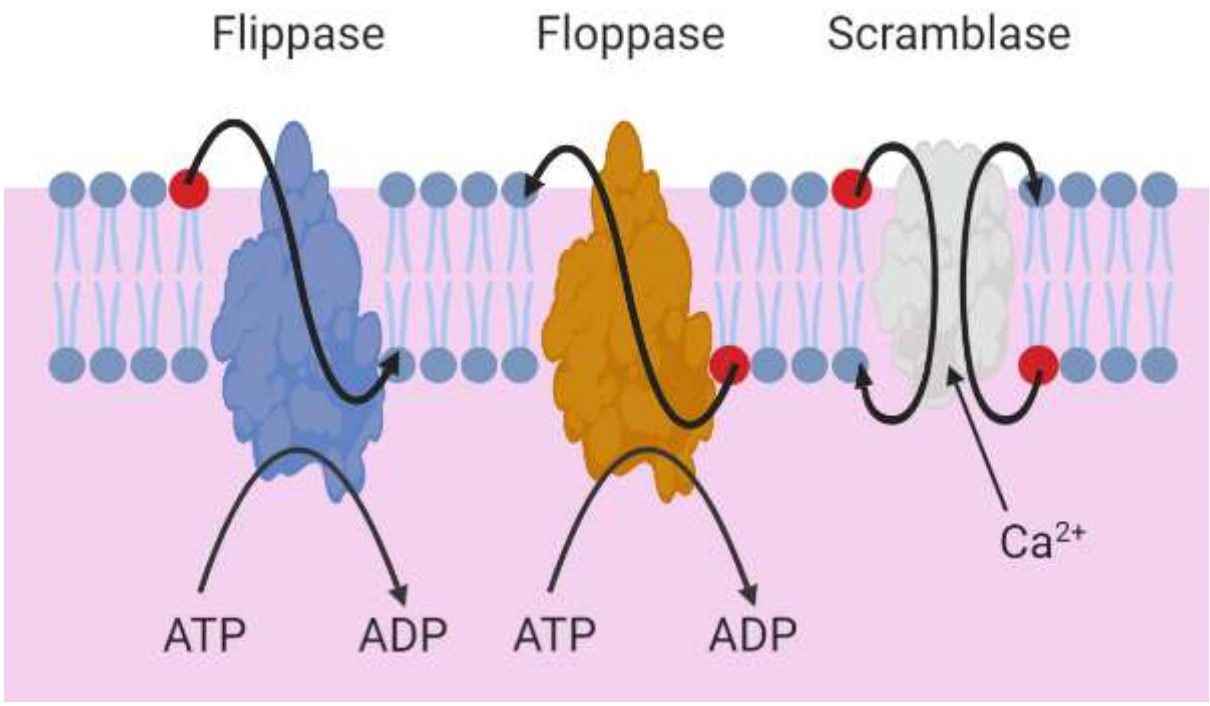

Figure 1.3 Comparison of the functions of flippases, floppases and scramblases in the plasma membrane. Adapted from Clark[60]

Membrane asymmetry, with the involvement of the translocators, is a part of the caveolae formation. Caveolae are bulb-shaped or cuplike uncoated membrane invaginations (Figure 1.4), while observed by transmission electron microscopy. Their presence, in contrast to clathrin coated vesicles, varies highly across different cell types[61]. This variation and mutations in caveolae proteins can have an implication in numerous disease conditions, such as cardiomyopathy, muscular dystrophy and pulmonary arterial hypertension[62].

Caveolae protein composition can be classified into lipids, core structural components and key accessory proteins. The second group, including caveolin-1 (CAV1), caveolin-3 (CAV3), cavin1 and fascin, are required for the caveolae formation. Key accessory proteins: caveolin-2 (CAV2), cavin2, cavin3 and cavin4 are responsible for caveolae shaping[63].

Caveolae formation requires coordinated action of the structural proteins, starting in the synthesis in the endoplasmic reticulum. Subsequently they are exported to the Golgi via a COPII pathway. The release of the caveolae pool from the Golgi can is facilitated by cholesterol addition[64] and it is inhibited after glycosphingolipid depletion[65]. The nascent caveolin-containing vesicles released from Golgi targeting the plasma membrane contain a defined

number of caveolin molecules similar to the mature ones and they do not disperse during the fusion with the membrane[66]. After reaching the membrane caveolae are fused in under the control of SNARE protein syntaxin-6[67] and ganglioside GM1[68]; forming a specialised lipid domain enriched in sphingomyelin[69], cholesterol[70], phosphatidylinositol (4,5)-bisphosphate [$PI(4,5)P_2$][71] and the glycosphingolipids ganglioside GD3, GM1 and GM3[69,72].

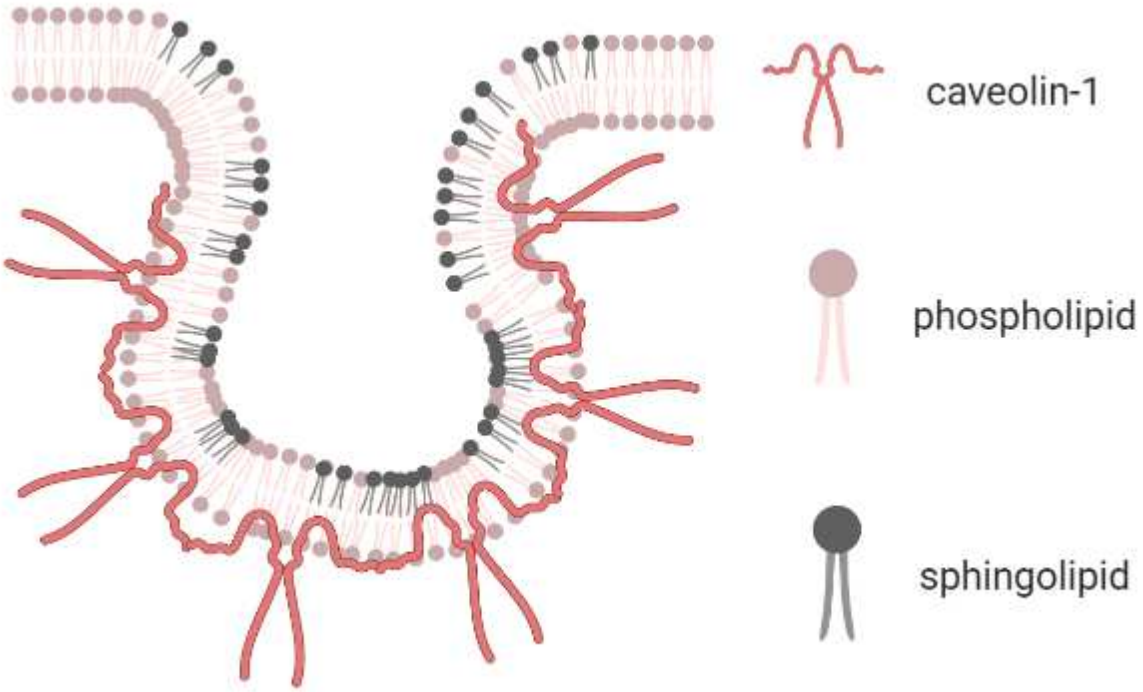

Figure 1.4 Structure of caveolae membrane vesicle.

1.3 Cytoskeletal regulation of plasma membrane dynamics

The cytoskeleton is responsible for the regulation of many cellular processes, such as mitosis, cell physiology, cell polarity and stiffness, cell division and ECM patterning. It forms a cortical shell around the cell periphery that is primarily composed of microtubules, septins and actin filaments associated with the inner face of plasma membrane. This connection relies on many weak bonds between actin-associated proteins (i.e. talin[73], myosins, filamin) and membrane proteins (i.e. integrins, focal adhesion protein) and it possesses properties specific to the plasma membrane, in contrast to intracellular membranes. The cytoskeleton receives, transmits and sends bidirectional extra- and intracellular signals, in many cases relying on membrane regulators[74]. Cells simultaneously assemble, maintain and disassemble filamentous actin (F-actin). They also create networks with a specific function, dynamics and organisation, created by coordinated actions of globular actin (G-actin) monomer binding, assembly, end capping, bundling and disassembling[75]. Actin associated plasma membrane regulation can have two major forms: actin monomer pool regulation by phosphoinositides and modulation of actin assembly by small GTP-ases[76].

Phosphoinositide lipids associate with both actin binding stimulators and inhibitors[77]. The first of them, WASP and WAVE, promote actin polymerisation through ARP2/3 complex upon binding phosphatidylinositol 4,5-bisphosphate ($PI(4,5)P_2$). In contrast, G-actin binding protein profilin and F-actin severing protein cofilin are inhibited by binding phosphatidylinositol 4,5-bisphosphate. One of the proposed mechanisms states phosphatidylinositol 4,5-bisphosphate hydrolyse by the external signal-mediated phosphorylation of phospholipase C (PLC), followed by a release of membrane bound profilin, to facilitate actin assembly by formin and Ena/VASP[78]. Another proposed mechanism suggests that sequestration of profilin to membrane regions with high concentrations of phosphatidylinositol 4,5-bisphosphate could lead of free G-actin, unbound to profilin. Free G-actin can preferentially bind to the branched actin filament networks generated by the Arp2/3 complex (**Figure 1.**). Regulation of actin binding stimulators and inhibitors by phosphoinositides is an emerging topic that could help explain the actin network maintenance and self-organisation.

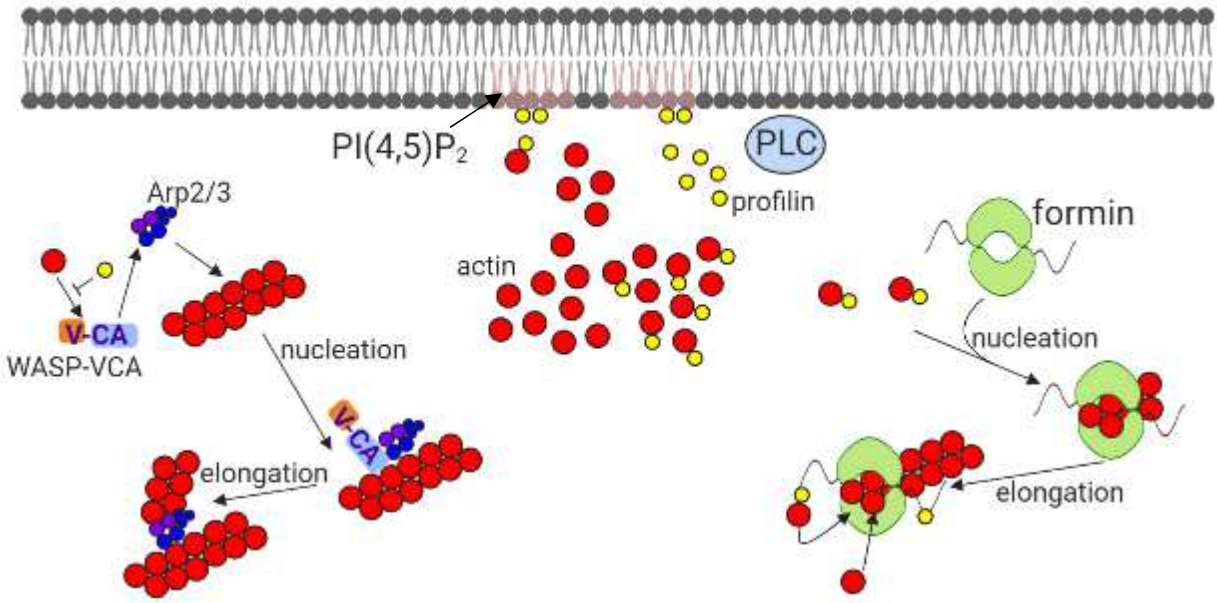

Figure 1.5 Membrane lipids regulate the actin assembly. Adapted from Bezanilla 2015[79]

Actin assembly and cortical actin remodelling is a process directly regulated by the Ras homolog family member Rho family. These activated small GTPases dock on the membrane through the exposed covalent lipid modification intercalating into the membrane. In the case of Arp2/3 complex, amongst many actin assembly factors, it has a GTPase binding domain, capable of binding to the active GTPase inducing a relief from the auto-inhibited state. Through this mechanism CDC42 and Rac1 GTPases activate Arp2/3 complex, promoting enucleation and elongation of the branched actin networks[74]. Another group of actin nucleation promoting factors, formins, can be activated by both CDC42 and RhoA[80]. The small GTPases also acts in a coordinated way as an antagonist of CDC42 and Rac1, or as an activator of protein kinases Rho-associated coiled-coil forming kinase (ROCK), RhoA activated, and p21-activated kinase (PAK), activated by CDC42 and Rac[81–83].

The family of small GTPases are crucial for the actin cytoskeleton remodelling and maintenance. Small changes to the cell surface have relatively small effect on the features of the cell membrane, including cell volume, providing matching levels of exo- and endocytosis keeping the homeostasis. However, more significant changes to the cell shape lead to increasing or decreasing cell membrane area through exocytosis and endocytosis[84].

Exocytosis is a process leading to the fusion of an intracellular vesicle with the plasma membrane. Cortical cytoskeleton interconnects with this process throughout most of the steps. RhoA GAP Gem interacting protein induces actin depolymerisation in the vesicles approaching the discharge into the membrane[85], followed by the vesicle fusion. Actin cytoskeleton remodelling aids the assembly of endocytic invaginations. The complex of CDC42 activated N-WASP together with Arp2/3 binds amphipathic protein. Caveolae formation in endocytosis requires the actin remodelling controlled by Rac1 and CDC42[86].

1.4 Matrix metalloproteinases and their inhibitors

The tissue biochemical and mechanical environment can affect cell fate and behaviour, as previously mentioned. Cells and their environment exist in a mutual relationship. In many tissues, for example in the liver, dysregulation of extracellular matrix production and degradation is present in the process of developing a pathological state. ECM components of normal liver: proteoglycans, laminin, fibronectin, matricellular proteins and collagens comprise approximately 0,5% of the wet weight[87]. These components can be remodelled and proteolysed in temporary, acute liver inflammation and a proper architecture is mostly restored. Contrary to transient injury, in sustained injury ECM accumulates and its degradation is disturbed. It leads to the formation of scar tissue and results in fibrosis[88]. In clinical trials dysregulation of the group of enzymes called matrix metalloproteinases is linked to liver pathological states[89–91], tissue damage and functional alterations.

The matrix metalloproteinases (MMPs) are a family of calcium- and zinc-dependent proteinases capable of extracellular matrix components degradation[92,93]. They have been divided in five categories according to their substrate specificity: gelatinases, collagenases, stromelysins, matrilysins and membrane-type. MMPs can be secreted into the cell surrounding or, as an inactive proenzymes, bound to the cell membranes. Gelatinases family members – MMP-2 – gelatinase A and MMP-9 – gelatinase B are important in regulation of fibrogenesis and scarring. Their activity is associated with ECM remodelling in wound healing, development, inflammation, fibrosis, angiogenesis, and tumour invasion. Their role is to degrade basement membrane collagen IV, collagen I and III. MMPs activity is regulated on different levels – transcription, proenzyme activation or inhibition by TIMPs – tissue inhibitors of metalloproteinases (Figure 1.6). However, there is the possibility of another mechanism of regulation i.e. by substrate mechanical properties. Hepatic stellate cells are known to be highly susceptible to mechanical stimulation and may play a key role during liver fibrosis by controlling the MMPs secretion in response to microenvironment stiffness.

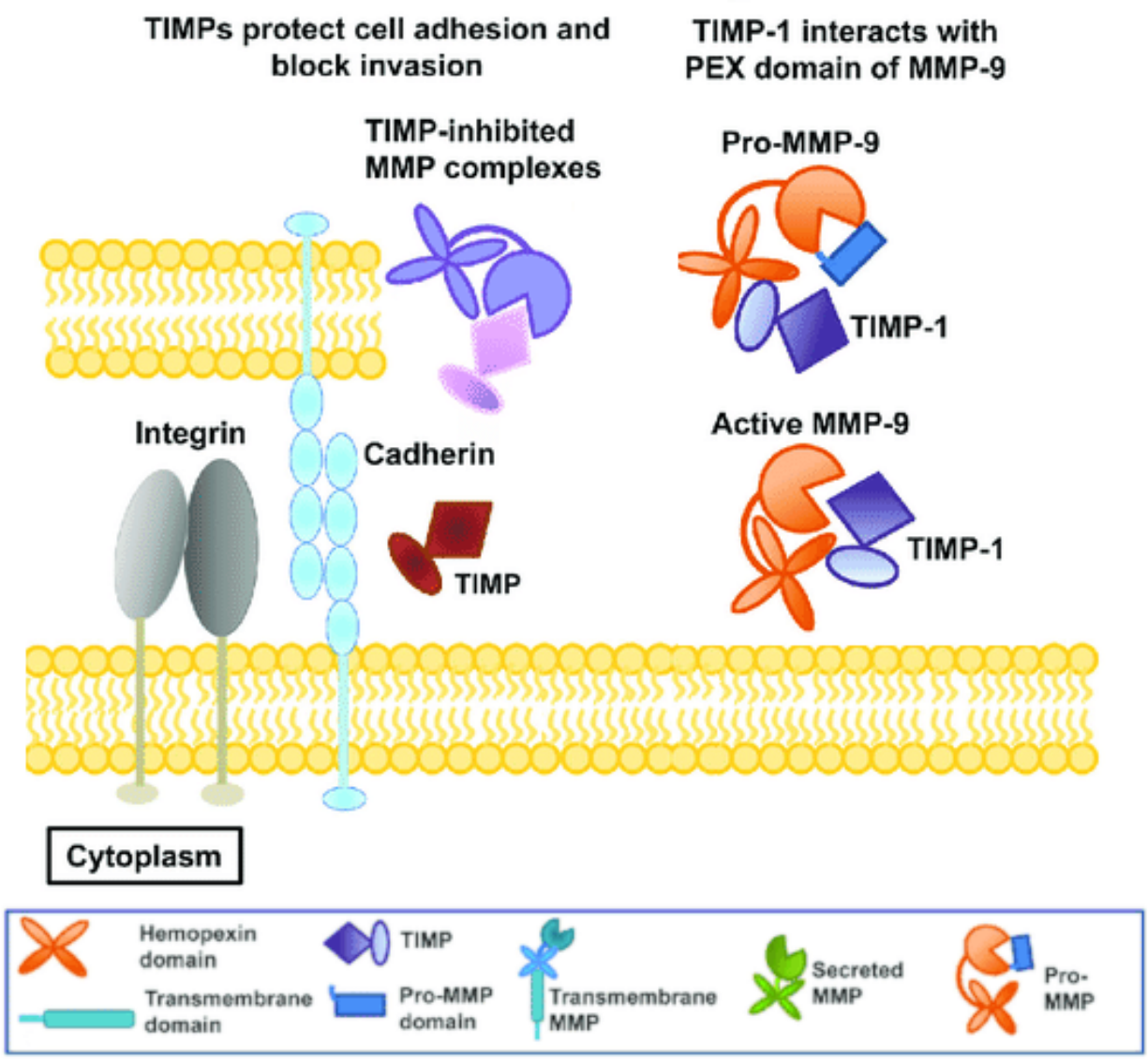

Figure 1.6 TIMPs regulate MMP function and activation. Adapted from Radisky 2017[94]

Homeostatic remodelling of the ECM matrix is achieved through a balance of deposition and degradation, with degradation largely governed by matrix metalloproteinases and their inhibitors, tissue inhibitors of metalloproteinases. Deviation from this balance can lead to multiple disorders such as atherosclerosis, arthritis and tumour growth[95]. Each MMP within the family exhibits a different substrate specificity and is inhibited by different TIMPs to different degrees. For example, MMP-9 has been shown to degrade both collagen I[96] and collagen IV[97], and is inhibited by TIMP-1 at nanomolar concentrations[98]. In the liver, HSCs secrete both MMP-9 and TIMP-1[99], and these contribute to ECM remodelling[100].

The stiffness of the extracellular matrix, across multiple cell types including HSCs, is known to induce intracellular signalling pathways through mechanotransduction. In HSCs, matrix stiffness has been shown to significantly decrease levels of MMP-9 mRNA and intracellular protein, acting as a positive feedback loop which prevents degradation. Stiffness also decreases levels of TIMP-1 mRNA and intracellular protein, representing a negative feedback loop[101]. Additionally, matrix stiffness is observed to promote exocytosis of TIMP1, and is expected to promote exocytosis of other molecules such as MMP-9 through stiffening of the plasma membrane[101]. The stimulation of exocytosis of TIMP-1 and MMP-9 represents positive and negative feedback loops respectively.

ECM homeostasis requires a fine balance of degradation and deposition, and reactions that control the activity of the key species are regulated through a variety of means. Both positive and negative feedback loops exist where matrix stiffness can regulate the presence of MMP-9 and TIMP-1 in the extracellular matrix.

1.5 GPER signalling

G-protein coupled receptor (GPER) belongs to the G-protein coupled receptors family and is embedded into the plasma membrane through 7-transmembrane domains. In its inactive state, it is coupled to Gαs, and upon activation stimulates Src, adenylate cyclase and EGFR signalling amongst others[102]. Apart from the activation by 17β-estradiol it can be activated or inhibited by a variety of natural and synthetic agonists and antagonists, such as the anticancer drug tamoxifen[103] and fulvestrant, some of the phytoestrogens, synthetic estrogen, diethylstilbestrol, and chemical compounds like bisphenol-a[104]. GPER localizes in plasma membrane, but it has been shown that it can also be detected in other organelles, such as endoplasmic reticulum[105]. In human breast cancer cell line T47D[106] and MCF-7[107] it also resides in plasma membrane. Experiments on T47D cell line showed GPER-dependant cAMP synthesis after 17β-estradiol stimulation, which is a membrane-specific event.

G-protein coupled estrogen receptor takes part in multiple cell signalling events, such as calcium influx, which is known to regulate i.e. hormone secretion and enzyme activity. In estrogen receptor α (ERα) negative cells Cos7 transfected with GPER, treatment with 17β-estradiol triggered intracellular calcium mobilisation, previously attributed to ERα[105]. Similar stimulation with 17β-estradiol in ERα and β negative SKBr3 cell line resulted in Erk phosphorylation[108], being a first step of a signalling cascade affecting cell proliferation via the transcription of c-fos and cyclinD1 genes[109,110]. In MDA-MB-231 cell line lacking the expression of GPER Erk phosphorylation was not observed after estradiol stimulation. Moreover, blocking the βγ subunit of this receptor resulted in estradiol sensitivity. These observations suggest that Erk phosphorylation and activation by estradiol is GPER dependant.

Proliferation related pathways are not the only targets of G-protein coupled estrogen receptor activation. Tamoxifen, one of GPER agonists, was shown to decrease the myofibroblast contractility, leading to a decreased ECM deformation[111]. Tamoxifen, in a GPER-dependent manner, can affect the pancreatic stellate cells in mouse pancreatic adenocarcinoma models. It suppresses fibrosis, inhibits cell proliferation and stroma remodelling, leading to an inhibition of cancer cell invasion[103]. In pancreatic stellate cells, tamoxifen, via GPER/RhoA, inhibits the activation of YAP and MLC-2 (Figure 1.7). GPER is also a mechanoregulator – its activation can affect cell response to mechanical stimuli, in vitro, but also to the stimuli by the forces exerted by ECM in the tumour.

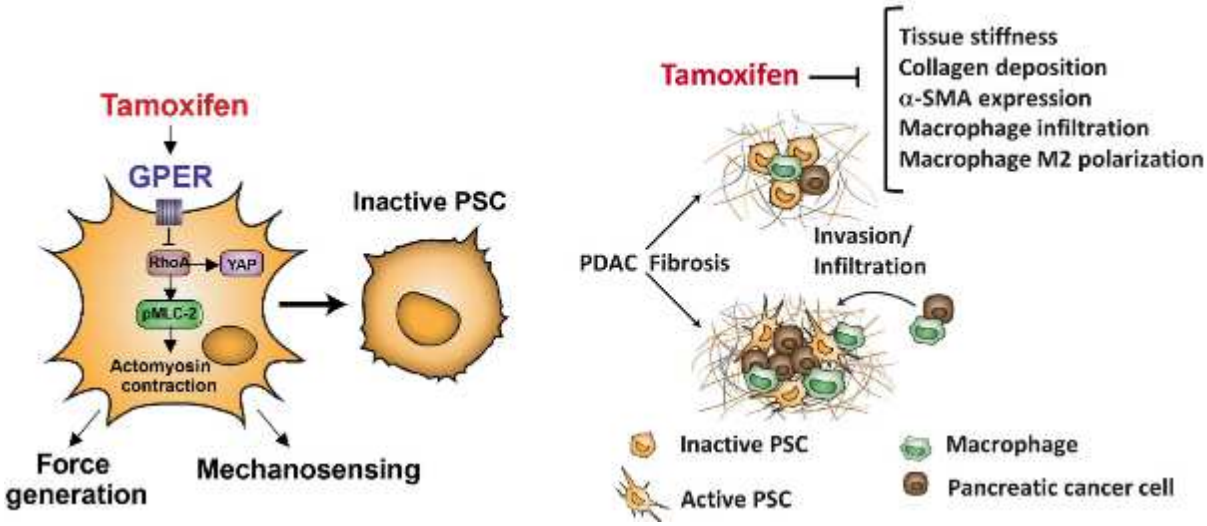

Figure 1.7 The effect of tamoxifen on GPER activation in pancreatic stellate cells. Adapted from Cortes 2019[103]

1.6 Pancreatic cancer

The pancreas is a digestive system organ, positioned in the upper right part of the abdomen. Structurally it can be divided in four parts: tail, body, neck and head. The body lies behind the stomach and the tail is adjacent to the spleen. The body contains two ducts: the main pancreatic duct and a smaller accessory duct. They join the common bile duct near the ampulla of Vater and open to the duodenum through the sphincter of Oddi[112].

Proper functioning of the pancreas is necessary for nutrient digestion and metabolism and functions both as an endocrine and exocrine organ. Exocrine function relies on pancreatic juice secretion by the acinar cells that is transported via the ductal system to the duodenum. Pancreatic juice is a cocktail of enzymes catalysing the digestion of lipids, proteins and carbohydrates. Endocrinally, pancreatic alpha cells release glucagon (in response to low glucose levels), beta cells secrete insulin to decrease the glucose levels inn blood and delta cells secrete somatostatin decreasing the release of insulin.

Pancreatic ductal adenocarcinoma (PDAC), comprising 80% of all pancreatic cancers, is currently the most common pancreatic malignancy and the 7th highest cause of cancer-related death in Europe and United States. In these regions the chance of developing PDAC stands at 1 in 64[113]. This type of cancer has an extremely poor prognosis - 5-year patient survival of ~5% and a median survival of less than 11 months. It is predicted to become the 2nd leading cancer-related cause of death in the United States. High mortality rate is related to the difficulty in early stage diagnosis, resulting in the majority of detected cases already being metastatic, with only 9.7% cases presenting at a local stage at time of diagnosis.

The microscopic PanIN lesions are the first symptom of the disease and due to their size, there is no early detection method. High grade lesions are observed only in the presence of carcinoma, suggesting that they are a source of malignancy and cancer cell invasion[114]. Both low grade and high grade lesions share common KRAS gene mutation, occurring in 95-97% of samples[115]. Other genetic alterations, such as INK4A/ARF, SMAD4, TP53 and CDKN2A are also common[116]. Based on genomic studies PDAC can be divided into two categories: tumour cells present in stroma surrounded by disrupted duct-like structures and sarcomatoid (with both epithelial and mesenchymal features) cells with less abundant stroma.

PDAC microenvironment possesses certain features affecting the behaviour of cancer cells. Excessive pancreatic cancer stroma is secreted by fibroblasts, including pancreatic stellate cells, constituting up to 90% of the tumour mass[117]. They produce excessive amounts of

collagens, fibronectin and laminin in a desmoplasia process. Under healthy physiological conditions extracellular matrix provides the scaffolding for the organ and can control cell proliferation, polarity and migration. However desmoplastic stroma can induce cell survival and invasiveness by the presence of dysregulated integrin subunits in the basement membrane of the cancer tissue[118] and secreted hyaluronan can bind to CD44 receptor on the cancer cells promoting their growth and prolonging survival[119].

Pancreatic stellate cells (PSCs) are extracellular matrix (ECM)-producing stromal cells found in the pancreatic cancer microenvironment and are a subtype of cancer associated fibroblasts (CAF). CAFs can derive from fibroblasts, PSCs, endothelial, epithelial and mesenchymal cells. They express typical markers upon activation, such as increased levels of α-smooth muscle actin[120], vimentin[121,122] and decreased levels of desmin[123]. Cancer associated fibroblasts can be activated by transforming growth factor β (TGF-β), sonic hedgehog, tumour necrosis factor α (TNF-α), platelet-derived growth factor (PDGF), and interleukin (IL)-1, -6, and -10[124]. Upon activation they increase collagen type-I and II and fibronectin secretion, leading to an increase in tumour stiffness and pressure exerted on cancer cells leading to further progression via increased epithelial-to-mesenchymal transition[125].

1.7 Liver fibrosis

The liver is the largest organ of human body – a vital organ responsible for the metabolism of carbohydrates, proteins, and lipids and the generation of bile acids that are essential for cholesterol homeostasis and the absorption of dietary lipid from the intestine. The liver removes toxins and drugs from the blood and also participates in the regulation of immune response[126]. It is the site of synthesis for major serum proteins, including albumin, complement and clotting factors, and of catabolism of amino acids and the generation of urea. Nutrients are transported to the liver via the portal tract, which originates from the gastrointestinal tract as well as from the spleen, pancreas, and gallbladder, then passing through sinusoidal lining cells. Finally, peptides, lipids and carbohydrates are taken up and metabolized by hepatocytes. These cells are responsible for most of the metabolic functions of the liver and constitute 80% of the whole liver mass and 70% of total liver cell fraction amongst endothelial cells, hepatic stellate cells Kupffer cells and bile duct cells[127,128]. The healthy, normal liver state is maintained with an organ size that provides substantial overcapacity. The liver also has an ability to regulate its growth and mass in response to functional parenchymal loss and can return to normal size and functional state, even when 70% of the parenchyma is lost.

Many factors are associated with the onset of chronic liver injury. This pathological state involves the accumulation of matrix proteins which results in fibrosis. During this process, there is a continued stimulus for regeneration. It leads to further distortion of hepatic structures and architecture. Fibrosis is a complex, multi-pathway event that involves biochemical and biomechanical signals processing. It appears in diseases, including Hepatocellular Carcinoma (HCC). HCC is the most common primary liver cancer and it is one of the most common cause of cancer-related deaths worldwide. In more than 80% of cases, HCC arises in the setting of highly progressed fibrosis – cirrhosis appearing 20 to 30 years after the first insult to the liver. Given the physiological, functional overcapacity of the liver, the cirrhotic liver can exhibit a normal, compensated function for long periods of time. In many cases there is high decompensation with catastrophic effects on the various strands of intermediary metabolism. Most therapies for chronic liver disease have targeted the aetiological agent like antiviral agents used in treatment of hepatitis C[129] or immunosuppressive agents that can be used in autoimmune hepatitis[130]. Agents mentioned above often have a beneficial side-effect on the degree of fibrosis, but the most promising treatments involve targeting cellular factors which are involved in creating the fibrotic tissue, for example targeting hepatic stellate cells activation.

Healthy, normal liver parenchyma consists of an epithelial component – hepatocytes and an endothelial lining that contains tissue macrophages – Kupffer cells and liver specific pericytes – hepatic stellate cells (HSC) which play an important role in liver tissue fibrosis. They were originally identified in 1876 by Carl von Kupffer as intralobular star-shaped cells that stained dark with selective gold chloride staining for retinol (vitamin A)[131]. The attention of many investigators was focused on their exceptional pathophysiological importance indicated by their ability to transdifferentiate into myofibroblasts despite confusion of using different names for these cells. Finally, in 1996, the scientific community decided to name this cell population hepatic stellate cells[132]. Hepatic stellate cells reside in subendothelial space of Disse and they constitute 6.35 ± 1.92 % of total liver cell content[133]. These cells express typical markers – the presence of cytoplasmatic triacylglycerol-rich droplets, low number of mitochondria and distinct rough endoplasmic reticulum. They also exhibit a near absence of cytosolic vesicles and vacuoles and interstitial collagen bundles in close apposition to the cell body.

In healthy liver tissue, hepatic stellate cells reside in a quiescent state possessing characteristics mentioned above. Following liver injury, hepatic stellate cells become activated. It is described by the conversion of a resting, quiescent (qHSC), vitamin A-rich cell into activated cells with loss of retinoic acid droplets. Activation is followed by increased cell contraction and proliferation. Activated hepatic stellate cells (aHSC) also exhibit the release of proinflammatory, promitogenic and profibrogenic cytokines. aHSC are also capable of enhanced migration and extracellular matrix components deposition[134] (Figure 1.8). HSC activation can be abstractly divided into two stages: initiation and perpetuation. Initiation (preinflammatory stage) reveals early changes in gene expression and cellular phenotype in response to paracrine stimulation from damaged parenchymal cells. Upkeep of these stimuli leads to a perpetuation phase regulated by autocrine and paracrine stimuli. At least six distinct changes in HSC behaviour, including proliferation, chemotaxis, contractility, fibrogenesis, matrix degradation, and retinoid loss, are involved in the perpetuation stage[135].

After activation, during, for example, an injury, qHSC gain characteristics mentioned above and they can be considered as a major source of myofibroblasts in hepatotoxic liver - cells that express high level of α smooth muscle actin (ASMA) and collagen type I[136,137]. It is also possible to reverse hepatic stellate cells activation by removal of the injury-causing agent[138]. This is one of the possible targets in anti-fibrotic therapy amongst others – suppression of HSC migration into fibrotic sites or alterations in the secretion of matrix metalloproteinases – enzymes capable of ECM degradation.

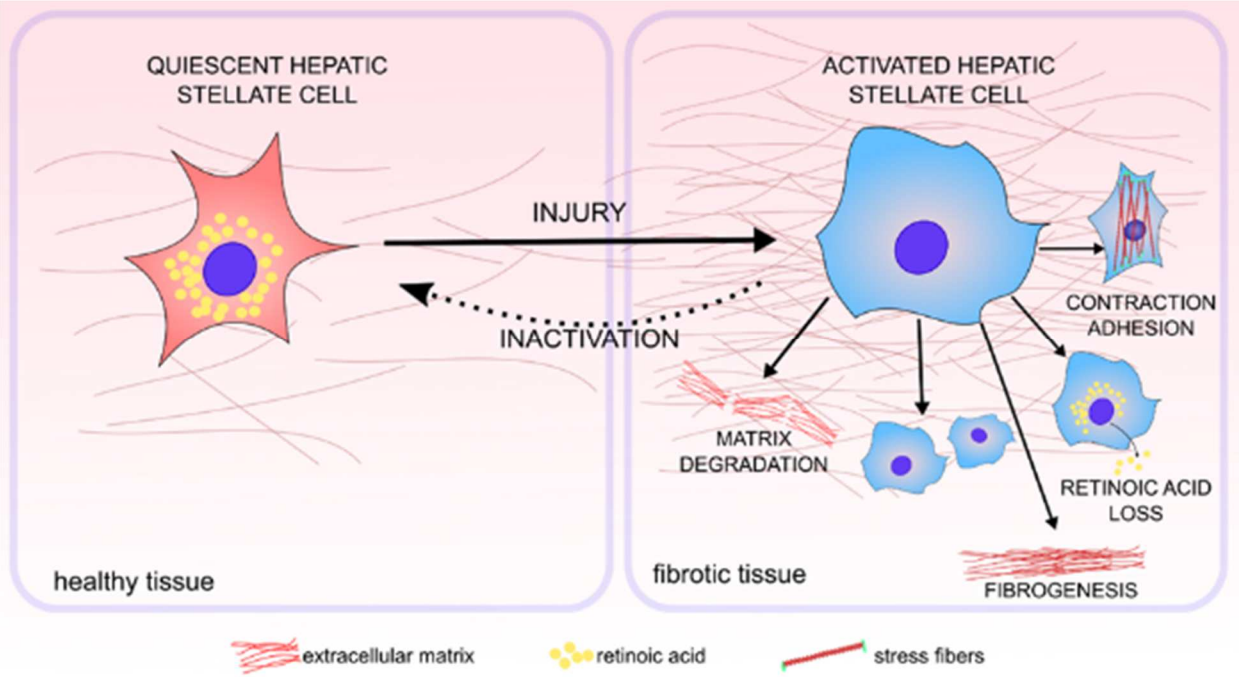

Figure 1.8 Hepatic stellate cells activation. Schematic of HSC activation in the result of an injury, showing activated HSC that gained myofibroblastic properties in fibrotic tissue.

2 Substrate rigidity controls activation and durotaxis in pancreatic stellate cells

2.1 Introduction

Pancreatic Ductal Adenocarcinoma (PDAC) is a highly aggressive malignancy characterised by rapid progression, invasiveness and resistance to treatment[139]. The cancer is almost uniformly lethal with a dismal 5-year survival rate of less than 5%[140] and a median survival time of 6 months from diagnosis[141]. Despite efforts over the past few decades, conventional treatment approaches such as chemotherapy, radiotherapy, and resection have had little impact on disease progression[142], owing to the extreme resistance of pancreatic malignancies to all extant treatments[139]. One of the unique and defining features of PDAC is the presence of remarkable stiffness and extensive desmoplasia surrounding the tumour[143], which is thought to generate a unique microenvironment that facilitates cancer growth[144], survival[144–147] and metastasis[148–150].

Through various in vivo and in vitro studies[143,148,151–155] pancreatic stellate cells (PSCs) have been identified as the cell type responsible for the production and maintenance of this growth permissive microenvironment. Under normal conditions, these myofibroblast-like cells play a role in maintaining the normal tissue architecture of the pancreas[152]. Upon pancreatic injury, PSCs transition from a quiescent, vitamin A lipid storing phenotype[156], to an activated state characterized by changes in migratory capacity and an increase in mitotic index and extracellular matrix secretion (ECM)[157]. In health, this ECM remodelling results in wound healing and the subsequent removal of activated PSCs through apoptosis[158]. In pancreatic cancer however, PSC activation is induced and maintained through the release of soluble growth factors and cytokines by cancer cells[152,159] resulting in the characteristic stromal 'reaction' around the tumour. Once produced, this leads to a vicious cycle of accelerated cancer proliferation and subsequent mitogen production, perpetuating PSC activity[144].

Given the role this desmoplastic stroma, and particularly PSCs, play in cancer progression and survival, research has accordingly switched to targeting aspects of the tumour microenvironment, such as PSCs and the pronounced fibrosis. Stromal ablation techniques however, have thus far been met with limited and somewhat contradictory results[160,161]. Unlike stromal depletion strategies, stromal reprogramming is an emerging concept gaining acceptance as an attractive alternative PDAC therapy[162]. Such an approach is supported through

a recent report showing that vitamin D analogues are capable of transcriptionally reprogramming pancreatic stellate cells and overall tumour-associated stroma into a more quiescent state, which resulted in reduced tumour volume and an increase in intratumoral gemcitabine[162].

It is well known that soluble profibrotic factors released from cancer cells activate both local[152,159] and distant[163] PSCs, which migrate from remote sites in the pancreas towards the tumour core. Here, crosstalk between activated PSCs and cancer cells promote PDAC carcinogenesis[144] and chemoresistance[144–147]. Activated PSCs have also been shown to play a key role in cancer metastasis[149,150], participating in the formation of distant metastatic sites through co-migration with cancer cells[149] and through the creation of 'tracks' within tissues, aiding in cancer cell migration[164]. Therefore, there is an urgent, currently unmet need in the field of pancreatic cancer to find therapies that induce PSC deactivation.

Interestingly, efforts thus far seem to overlook any potential role for the mechanical PDAC microenvironment in regulating PSC activity. The fact that PDAC is one of the most fibrotic and stroma-rich malignancies intuitively leads to the idea that extracellular matrix mechanics may play a key role in the development of fibrosis and PDAC progression. Studies that address the influence of mechanical force on PSC-PDAC interactions however, are severely lacking with some exceptions such as a recent study by Weaver and colleagues that has revealed that changes in matrix rigidity associated with PDAC fibrosis has a pronounced effect on the malignant epithelium, accelerating PDAC progression via changes in integrin-mediated mechanosignalling. This leads to the notion that ECM rigidity may also alter the ECM tensional homeostasis to influence the activity of PSCs in the stromal compartment of the tumour, therefore accelerating the development of fibrosis within a positive feedback loop[165].

In a first attempt to mechanically reprogram PDAC-associated stroma, the group reported that ATRA, an active metabolite of vitamin A, restores mechanical quiescence in PSCs, in an actomyosin dependent manner and inhibiting local cancer cell invasion in 3D organotypic models[166]. Such studies, however, involve analysis of cells cultured on glass – a substrate with rigidity in the order of GPa[167] – and as such fail to recapitulate a biologically relevant environment. It is a well-known phenomenon that transdifferentiation of PSCs to an active phenotype occurs during culture on glass[168], however the question of whether or not PSCs possess the ability to mechanically sense the rigidity of their local fibrotic environment and undergo phenotypic transition solely as a result of mechanical stress has never been addressed.

Furthermore, whilst the ability of PSCs to chemotactically migrate towards pancreatic neoplasms has been well defined[163], whether or not PSCs display durotactic behaviours within this microenvironment has not been explored.

Here, through the use of a physiomimetic system that recapitulates the mechanical microenvironment found within healthy and fibrotic pancreas, it is shown that matrices mirroring rigidities found within fibrotic pancreas activate PSCs, whilst matrices resembling healthy pancreas induce and maintain quiescence in previously activated PSCs. Moreover, activated PSCs were also observed to undergo durotactic migration towards stiffer, fibrotic-like regions; a response previously characterized in fibroblasts[169], but not reported before in PSCs.

Aims:

- To assess the effect of soft and stiff matrices on the induction and maintenance of pancreatic stellate cells quiescence or activation
- To investigate if pancreatic stellate cells undergo rigidity guided, durotactic migration

2.2 Results

2.2.1 Matrigel induces PSC quiescence

Transition of quiescent PSCs to an activated myofibroblast-like state is a well-documented phenomenon that occurs upon cell culture[168]. Indeed, all fibroblasts grown in standard culture conditions are myofibroblast by definition, given that contact with the stiff surface of culture flasks triggers the formation of contractile stress fibres[170]. As a result, the assessment of any potential mechano-sensory regulation of PSC activity is not possible using this setup. To address this issue, it has been sought to implement an in vitro model that allows us to culture PSCs in a quiescent state. Transdifferentiated culture-activated PSCs were grown on a layer of Matrigel for 6 days to induce cell quiescence, following an in vitro method identified by Jesnowski et al.[168]. Matrigel culture resulted in reversion of activated PSCs to a quiescent-like state. Cells lost their spindle morphology and Oil Red staining was used to confirm the presence of cytoplasmic lipid droplets characteristic of PSC quiescence (Figure 2.1).

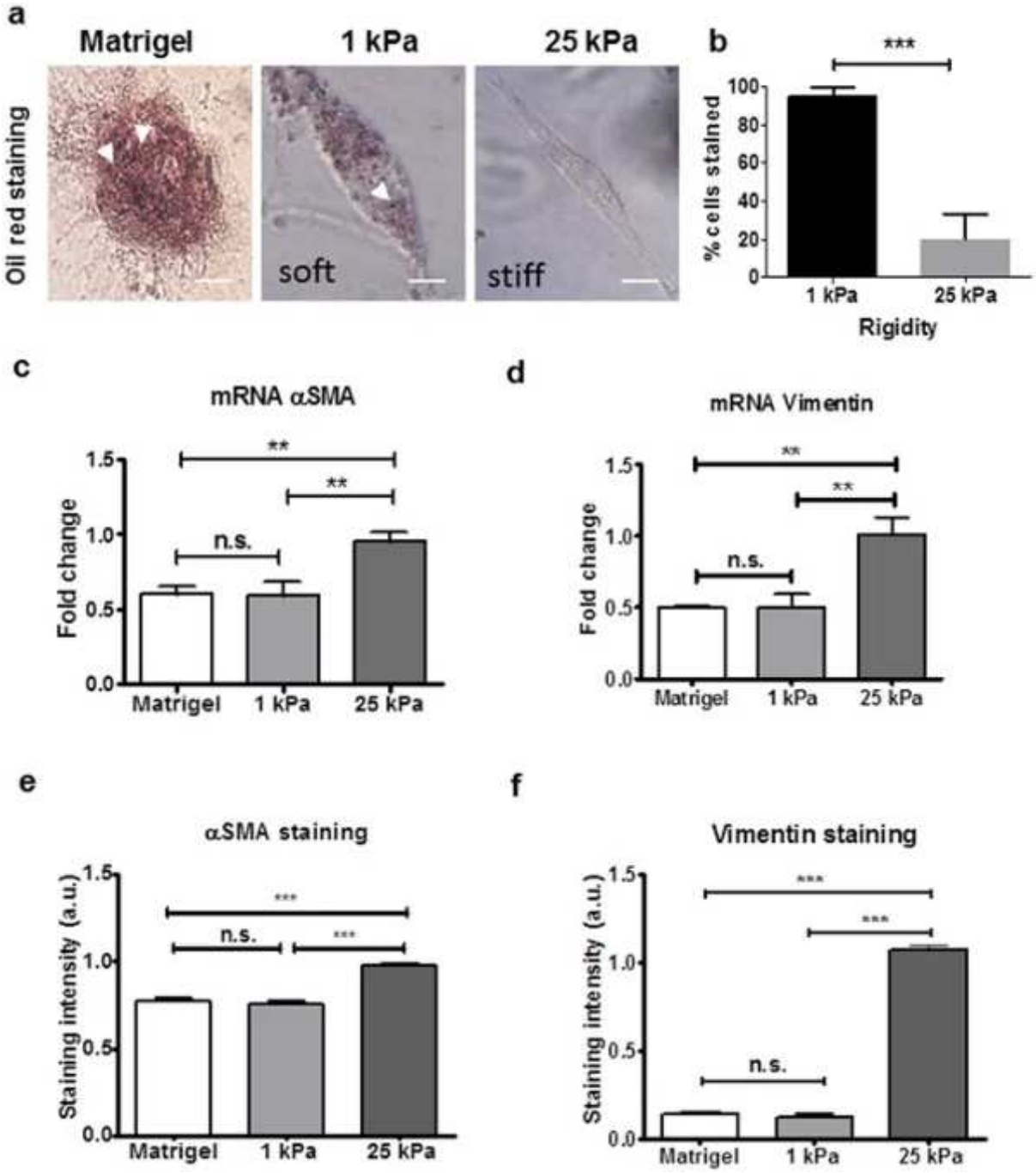

Figure 2.1 Stiff matrices induce PSC activation. (a) Bright-field images of Oil Red O stained PSCs on Matrigel, soft and stiff matrices for 6 days. Scale bar 25 μm. (b) Quantification of Oil Red O staining after 24-hour culture on soft or stiff PAA matrices showed a significant reduction in staining levels on stiff matrix when compared to soft matrix, indicating cellular activation almost entirely on stiff matrix rigidities. (c, d) qPCR mRNA levels of αSMA and vimentin for conditions represented in (a). (e, f) Quantification of staining intensity for αSMA and vimentin for conditions represented in (a), images in Fig. 2.4. In all cases, histogram bars represent mean ± SEM. Representative of 3 independent experiments with more than 20 cells analysed in (b, e, f), ***$p < 0.001$, **$p < 0.01$.

These observations are in agreement with previous results described by Jesnowski et al.[168], and confirm that Matrigel culture of activated PSCs results in the reversion of cells to a resting-like state. In addition to resumption of lipid storing ability, cells on Matrigel began to form cell clusters connected by a filamentous network (Figure 2.2) further mirroring earlier observations by Jesnowski et al.[168]. Taken together, these results indicate the ability of Matrigel to revert culture-activated PSCs to a state of quiescence, whilst indicating the matrix surrounding PSCs plays a pivotal role in the maintenance of PSC activation[168].

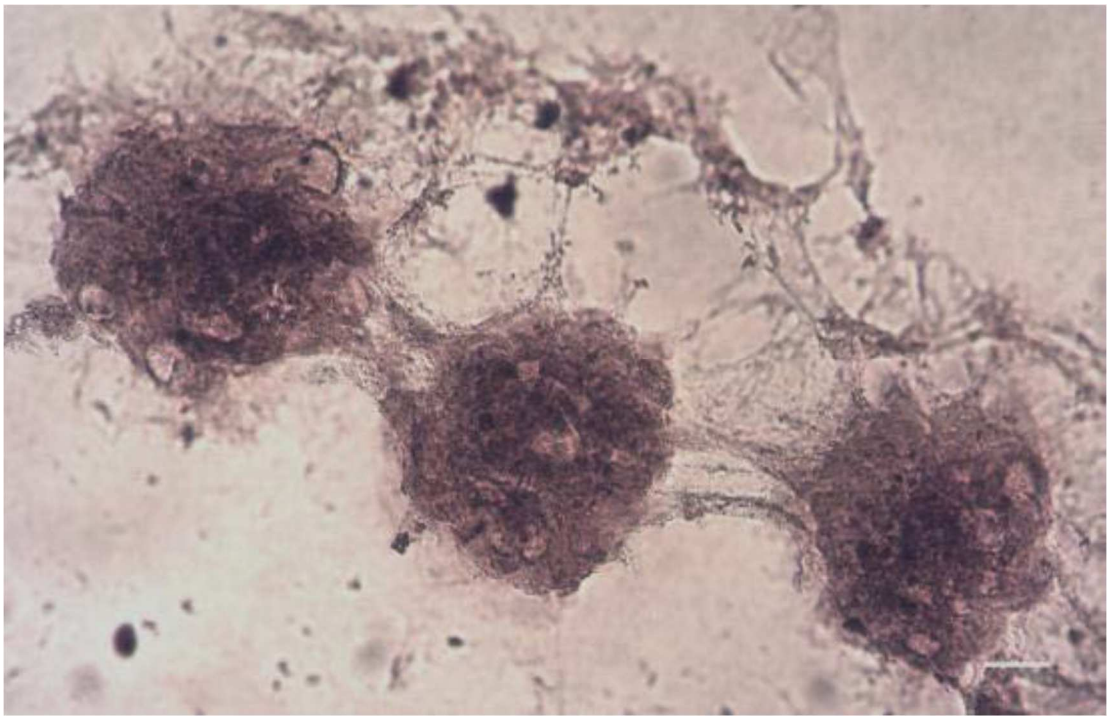

Figure 2.2 Bright field images of Oil Red O stained PSCs cultured on Matrigel for 6 days and showing the clusters connected by a filamentous network characteristic of PSCs quiescence. Scale bar 50 μm

2.2.2 Production of a physiomimetic model recapitulating soft and stiff substrates

The ability of cells to sense and respond to environmental mechanical force is a key determinant in tissue homeostasis[171]. Whilst activation of PSCs in physiological conditions is a well-regulated defined process, the unabated activation leads to sustained fibrosis[172]. Although prior observations are suggestive, there has of yet been no direct demonstration that PSCs are able to adapt behaviour based on the mechanical properties of their substrate. To

explore if the exogenous mechanical environment is enough in itself to regulate PSC activity, a physiomimetic model representing soft and stiff tissues was produced.

Polyacrylamide (PAA) gels of varying rigidity – 1 kPa (soft matrix) or 25 kPa (stiff matrix) – were prepared according to Engler's protocol[36], through alteration of gel acrylamide/bis-acrylamide ratios (Table 1), widely accepted as non-toxic and suitable for fibroblast culture[39,45,173–175]. Elastic modulus was measured with atomic force microscopy, using the Hertz contact model. Cell culture on these synthetic hydrogels requires the coupling of a cell-adhesive matrix protein in order to provide proper cell attachment to the gel surface[36]. Through the use of the substrate-protein crosslinker sulfo-SANPAH[37], gels were crosslinked with the ECM protein fibronectin (Figure 2.3), yielding a mechanically tuneable, chemically identical PAA hydrogel system, capable of providing a platform upon which to investigate how substrate stiffness regulates PSC behaviour.

stiffness [kPa]	acrylamide concentration %	total volume [µl]	PBS volume [µl]	acr/bisacr (29:1) 40% vol [µl]	TEMED [µl]	APS [µl]
1.3	2.7	500	459.1	34.9	1	2.5
4.16	4.6	500	434.6	59.4	1	2.5
12.93	6.1	500	415.2	78.8	1	2.5
14.8	7.6	500	395.8	98.2	1	2.5
25.5	9.7	500	378.7	125.3	1	2.5

Table 1 Reagent proportions required to obtain specific PAA hydrogel rigidities

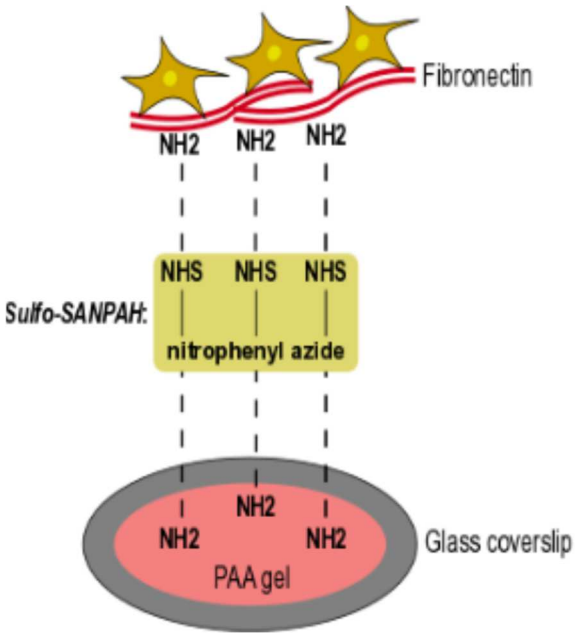

Figure 2.3 Schematic representation of surface preparation for cell attachment on soft and stiff PAA gels. Crosslinking of PAA hydrogels with fibronectin through the use of sulfo-SANPAH. sulfo-SANPAH is a heterobifunctional crosslinker containing an amine-reactive NHS and a photoactivatable nitrophenyl azide. Upon UV exposure, this nitrophenyl azide forms a nitrene group that binds to NH2 groups within the hydrogel, leaving an NHS group free at the gel surface to allow binding of fibronectin.

2.2.3 Stiff matrices induce PSC activation

PDAC is intrinsically one of the most fibrotic and rigid human malignancies, ascribed in part, to the dense collagenous stroma that surrounds the neoplasm[148]. To identify if this stiff mechanical microenvironment is enough alone to induce PSC activation, Matrigel-induced quiescent PSCs were seeded onto PAA hydrogels resembling soft (1 kPa) and stiff (25 kPa) tissues, referred hereafter as soft and stiff, respectively. After 24 hours of culture, Oil Red staining was used to identify the presence of any cytoplasmic lipid droplets characteristic of PSC quiescence (Figure 2.1 a). It was observed that quiescent PSCs seeded onto soft matrices retained the ability to store lipid droplets, suggesting maintenance of a resting-like state. Quantification of seeded cell populations revealed a statistically significant difference ($p < 0.001$) in total Oil Red staining levels between PSCs on soft (95% stained) and those on stiff (20%) hydrogels (Figure 2.1 b). To further validate the observations, the expression of alpha smooth muscle actin (αSMA) and vimentin was tested, two widely used markers for quiescence in PSCs, at the gene and protein levels[148,176]. No significant difference was observed in the mRNA levels of αSMA and vimentin of PSCs seeded on Matrigel (standard technique to induce PSCs quiescence) and soft matrices. Conversely, a two-fold increase was found in the mRNA levels of αSMA and vimentin of PSCs seeded on stiff matrices compared to soft matrices and Matrigel (Figure 2.1 c, d). At the protein level, a similar trend was observed, no significant differences in the expression of αSMA and vimentin between PSCs on Matrigel and soft matrix, and a significant increase in both proteins expressions when PSCs were on stiff matrices (Figure 2.1 e, f and Figure 2.4). It also has been observed that stiff substrates increase PSC proliferation and fibronectin expression (Figure 2.5).

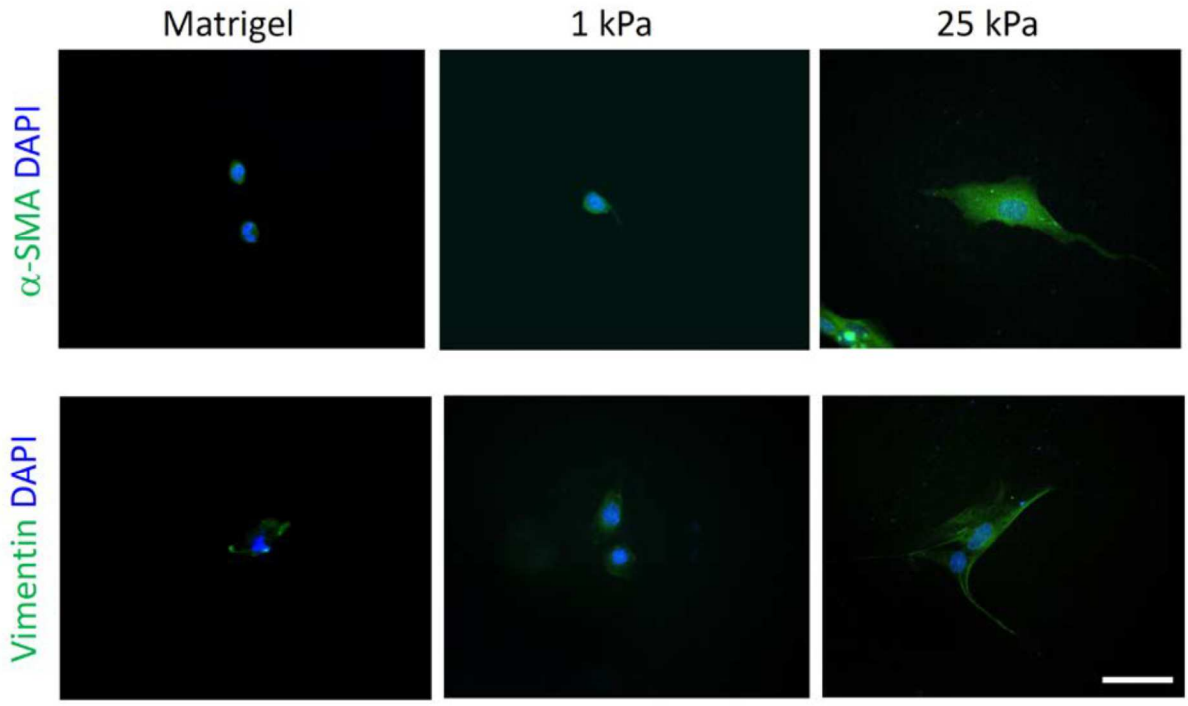

Figure 2.4 Immunofluorescent images of αSMA and vimentin of PSCs seeded on matrices represented in Fig. 1a. Scale bar 50 μm. Quantification in Figure 2.1 e, f.

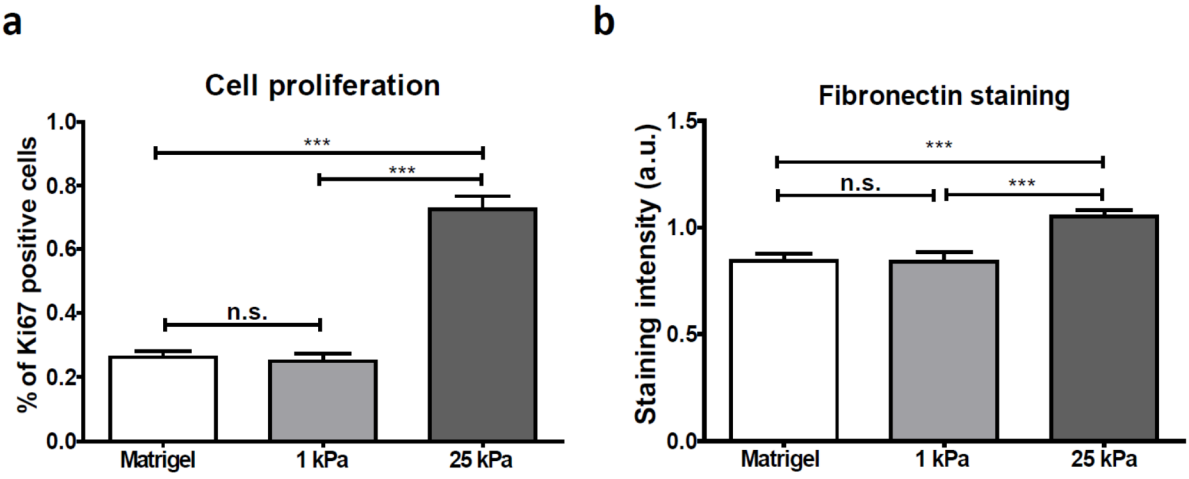

Figure 2.5 Mechanical activation of PSCs by stiff substrates increases cell proliferation and fibronectin production. (a, b) Quantification of Ki67 positive cells and fibronectin immunofluorescent staining as markers of cell proliferation and ECM production, respectively. Histogram bars represent mean ± SEM. Representative of 3 independent experiments. (Anova and Tukey posthoc test) *** $p<0.001$.

Taken together that quiescent PSCs seeded onto stiffer matrices were observed to lose lipid-storing capacity, express the canonical markers characteristic of PSC activation, and increase proliferation & ECM protein production, these observations indicate that substrate stiffness can, per se, induce phenotypic transition of PSCs to a matrix-secreting active state. Serum conditions were kept the same throughout the experiments, indicating that the observed changes occurred irrespective of the presence of any soluble factors.

2.2.4 Soft matrices induce and maintain PSC quiescence

Many conditions featuring pathological tissue fibrosis occur as a result of sustained myofibroblast activity[156]. This persistent activation is a consequence of the establishment of a mechanical feedback loop, which perpetuates myofibroblast matrix secretion through the sensing and promotion of a stiff microenvironment[166]. Restoring ECM mechanics to normalcy or the ability of the cell to perceive the elevated ECM rigidity is sufficient to terminate the feedback loop and abrogate myofibroblast activity, cells typically undergoing de-differentiation to a quiescent state[170]. To investigate whether PSCs exhibit this mechano-induced state 'fluidity', previously glass culture-activated PSCs were transferred and grown on soft or stiff PAA hydrogels for 3 days, with Oil Red staining employed to identify cell phenotypic state. Cells cultured on stiff matrices were shown to remain continually active, with PSCs lacking lipid-storing ability (Figure 2.6 a). Conversely, PSCs grown on soft matrices began to regain cytoplasmic lipid droplets (Figure 2.6 a), indicative of a resumption of quiescence.

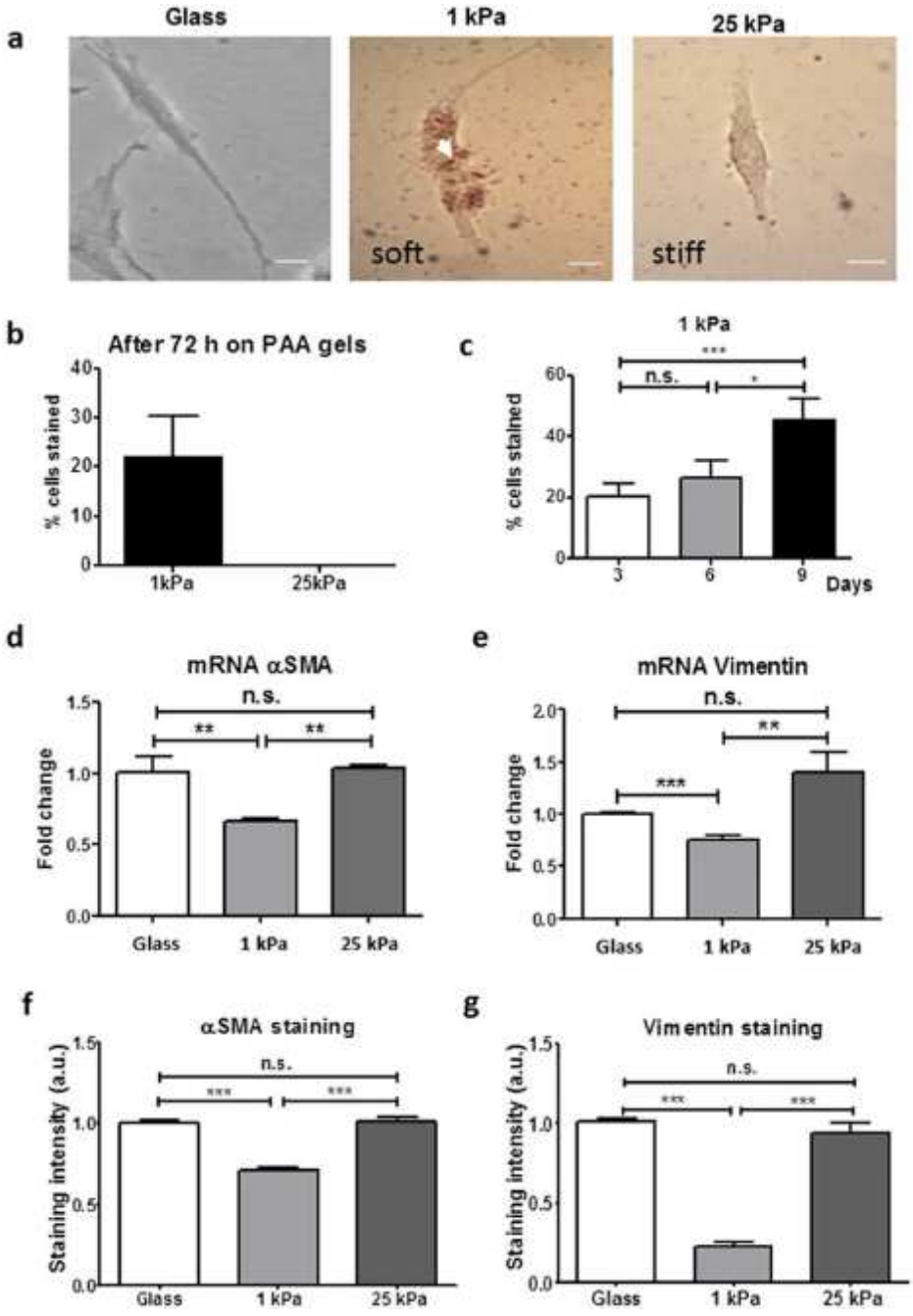

Figure 2.6 Soft matrices induce PSC deactivation. (a) Bright-field images of Oil Red O stained PSCs on glass, soft and stiff matrices for 6 days. Scale bar 25 μm. (b) Cell population Oil Red staining levels after 3 days on soft or stiff PAA matrices show that active PSCs on soft matrix begin to revert to quiescence. Representative of 3 independent experiments with 33 cells analysed. (c) Cell population Oil Red O staining levels after 3, 6 and 9 days on soft matrix confirm that culture of active PSCs on soft matrices reverts cells back into a resting state in a time-dependent manner. (d, e) qPCR mRNA levels of αSMA and vimentin for conditions represented in (a). (f, g) Quantification of staining intensity for αSMA and vimentin for conditions represented in (a), images in Supplementary Fig. 5. In all cases, histogram bars represent mean ± SEM. Data are representative of 3 independent experiments and 221 cells analysed in (c), *$p < 0.05$, **$p < 0.01$, ***$p < 0.001$, n.s. non-significant.

Quantification of these populations (Figure 2.6 b) revealed, as expected, the complete absence of any Oil Red staining on stiff matrices (0% stained), indicating a population-wide maintenance of PSC activation. On soft hydrogels however, after 3 days of culture 22% of the previously outright culture-active population had reverted to a state of quiescence; nearly a quarter of cells regaining lipid-storing capacity (Figure 2.6 b). Given these findings, it was next tested whether further prolonged growth on soft matrices would increase population phenotypic transition to a quiescent state. Glass culture-activated PSCs were grown on soft matrices for a total of 9 days, with Oil Red staining of samples occurring in 3-day intervals to assess PSC population quiescence (Figure 2.6 c). Staining levels at 3 days (21% stained) were in agreement with the earlier observations, with 6 days (26%) and 9 days (46%) yielding a significant increase in population quiescence.

To learn more about the effect of matrix rigidity on PSCs activation, next step was to investigate the expression of αSMA and vimentin at the gene and protein levels, as markers of PSCs activation. Consistent with the previous observation, the αSMA and vimentin mRNA levels in PSCs seeded onto stiff matrices were not statistically different from those plated on glass; while the expressions of these two markers on PSCs seeded onto soft matrices were markedly suppressed with regard to glass and stiff matrix (50% and 40% reduction for αSMA and vimentin, respectively) indicating the induction of quiescence on PSCs seeded on soft matrices (Figure 2.6 d, e). The same trend was observed at the protein level for both markers (Figure 2.6 f, g and Figure 2.7). Furthermore, it also was observed that soft substrates induce a decrease in PSC proliferation and fibronectin expression (Figure 2.8).

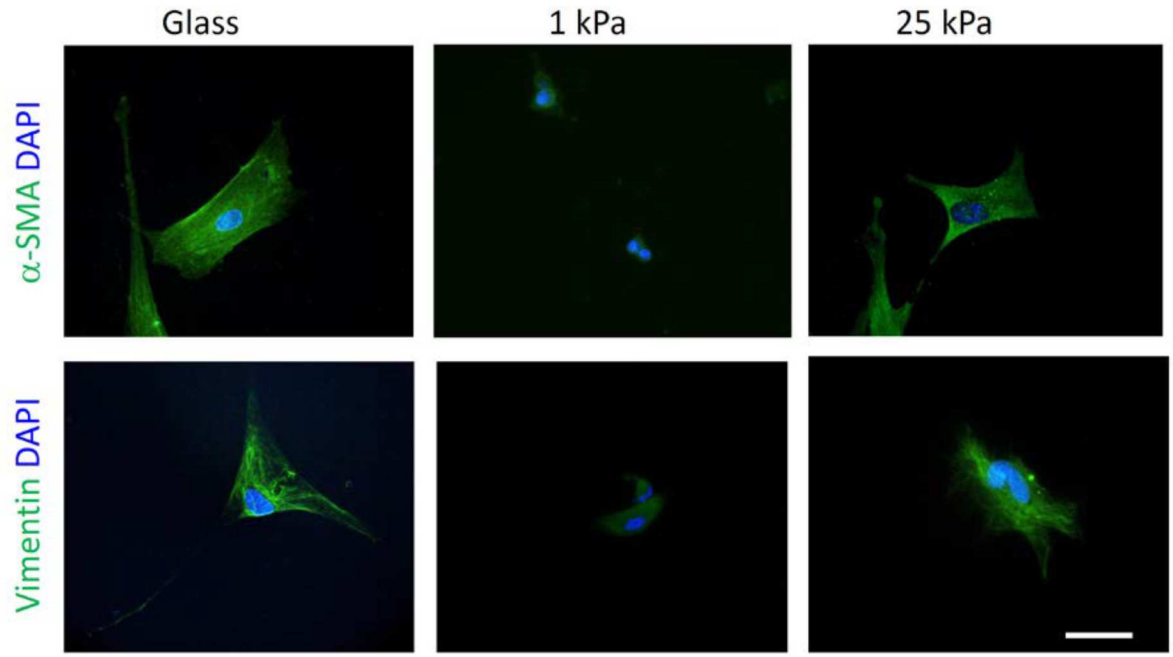

Figure 2.7 Immunofluorescent images of αSMA and vimentin of PSCs seeded on matrices represented in Fig. 2a. Scale bar 50 μm. Quantification in Figure 2.6 f, g.

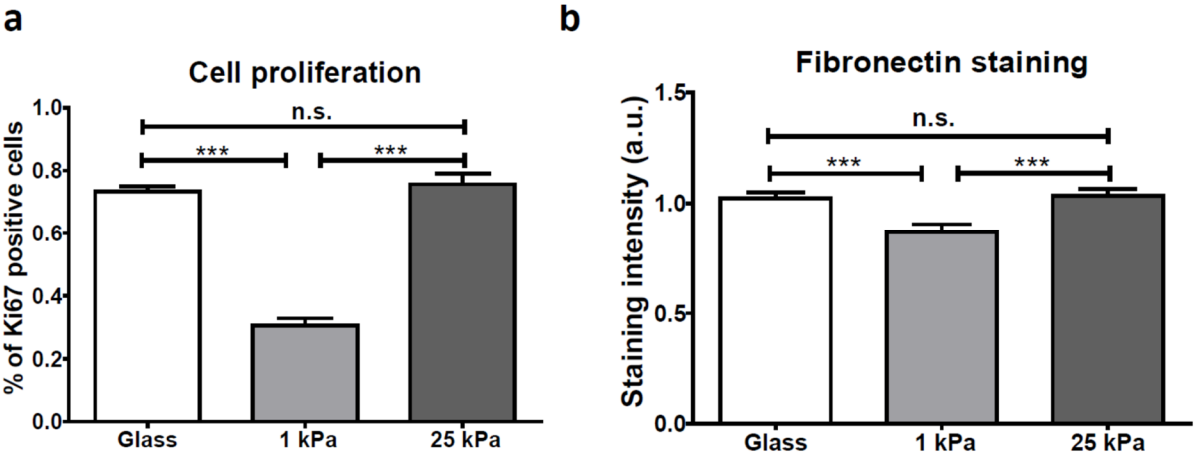

Figure 2.8 Mechanical deactivation of PSCs by soft substrates decreases cell proliferation and fibronectin production. (a, b) Quantification of Ki67 positive cells and fibronectin immunofluorescent staining as markers of cell proliferation and ECM production, respectively. Histogram bars represent mean ± SEM. Representative of 3 independent experiments. (Anova and Tukey posthoc test) *** $p<0.001$.

In order to explore the physiological relevance of thse findings, the activation levels of PSCs were investigated in normal (Pdx1-Cre) and fibrotic pancreas associated to PDAC (Pdx-1 Cre, LSL-Kras$^{G12D/+}$, LSL-Trp53$^{R172H/+}$) in mice models. Using immunofluorescence to detect αSMA, and second harmonic generation (SHG) to visualize collagen-I, abundant expression and co-localization of αSMA and collagen-I were observed in PDAC fibrotic tissues. This indicates the presence of active PSCs (αSMA expression used as a surrogate of PSC activation) secreting high levels of ECM proteins. In stark contrast with this, the αSMA expression and collagen deposition were only observed in ductal areas of normal pancreas tissues (Figure 2.9).

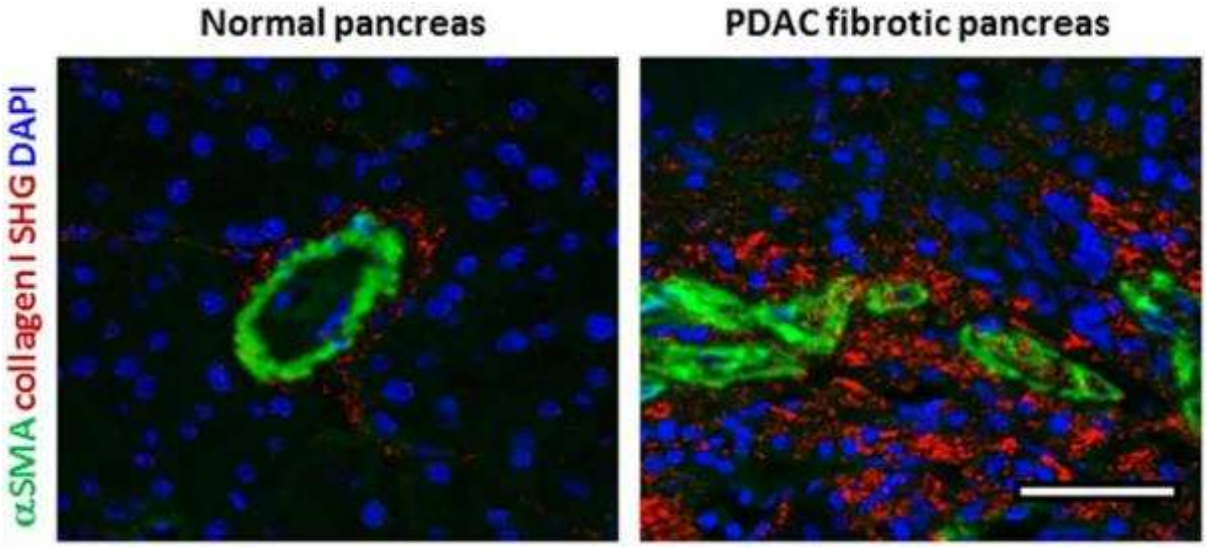

Figure 2.9 αSMA is highly expressed and co-localises with collagen-I in PDAC tissues but αSMA expression is markedly decreased in normal pancreatic tissues from mice. Immunofluorescence images combined with second harmonic generation (SHG) signal of normal and PDAC tissues from mice. Scale bar 100 μm. Collagen I SHG shown in red.

Thus, taken collectively, data indicate that PSCs are capable of returning to a resting state within a mechanically relevant model of pancreatic fibrosis. Furthermore, these observations directly highlight the importance of the mechanical microenvironment in regulating PSC behaviour, with the results identifying that the stiff microenvironment found within PDAC plays a pivotal role in maintaining the matrix secreting PSC phenotype.

2.2.5 PSCs exhibit directed migration across a stiffness gradient

Durotaxis, the ability of cells to detect and move along gradients in substrate stiffness[169], has been well characterized in fibroblasts[45]. Such migration provides a novel mechanism through

which gradients of matrix stiffness can facilitate and drive the progression of fibrosis[177]. Given the differences in matrix rigidity between the fibrotic PDAC microenvironment and normal pancreas, it was set out to identify if PSCs possess any durotactic behaviour. A double-rigidity PAA hydrogel system was produced through juxtaposition of functionalized soft and stiff matrices, resembling a model originally used to observe durotactic migration in fibroblasts[45]. Regions of different rigidities were outlined through embedding of fluorescent beads within the stiff region of substrate (Figure 2.10 a). Culture-active PSCs were seeded onto this dual-rigidity hydrogel and after 30 minutes (to allow attachment), observations were made through time-lapse phase contrast microscopy every 15 minutes over a period of 12 hours. Observations took place simultaneously within the soft, stiff and boundary regions of the hydrogel.

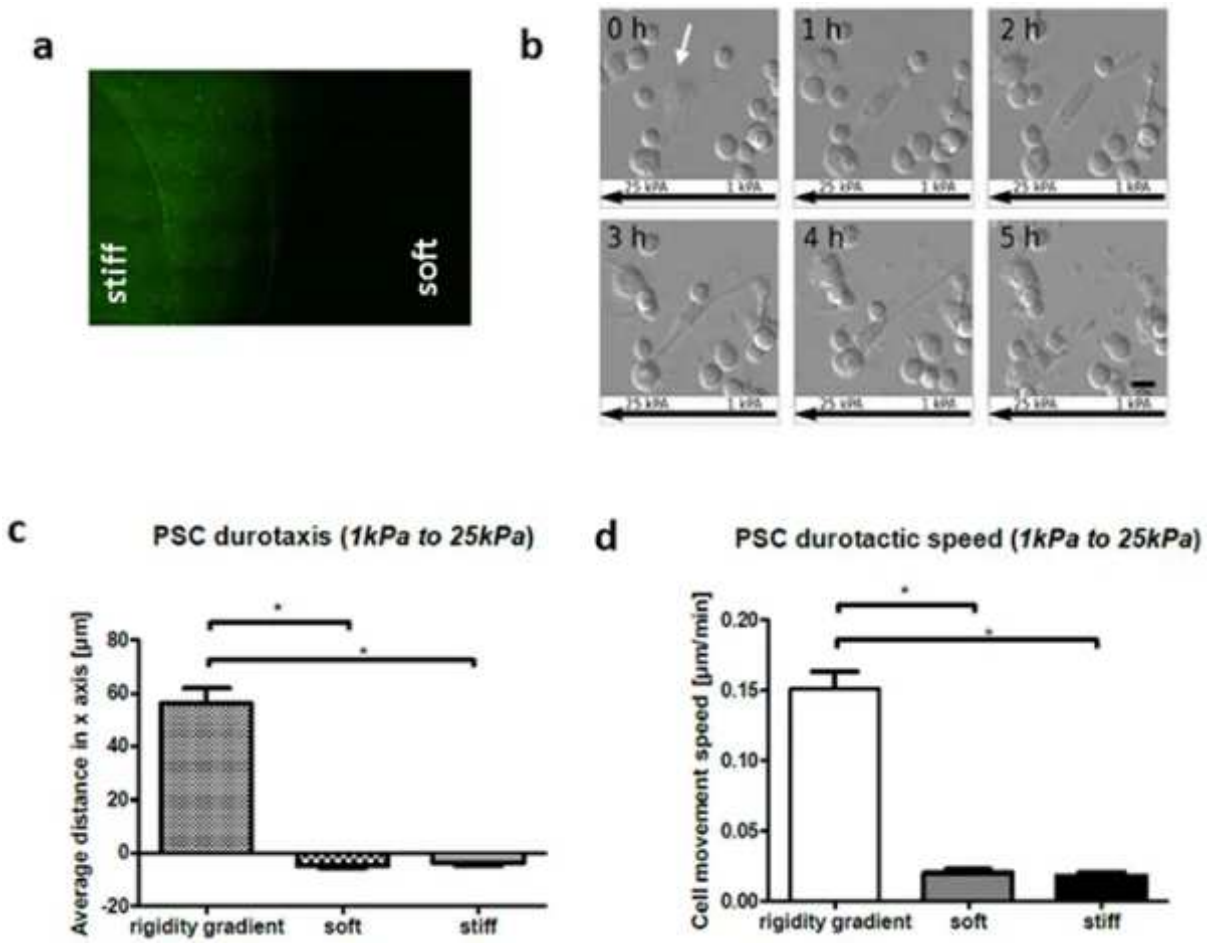

Figure 2.10 Durotactic response of PSCs. (a) Fluorescent image of rigidity boundary between soft (1 kPa) and stiff (25 kPa) PAA matrices. Yellow-green FluoSpheres were embedded into stiff hydrogels. (b) Representative example of PSC migration from soft to stiff regions over a 5-hour period. Scale bar 25 µm. Over time the cell (highlighted with a white arrow) moved towards the left (stiffer substrate). (c) Average cell migration distance observed at the rigidity boundary, soft region and stiff region of the hydrogel over a 12-hour period. Positive values indicate movement towards higher rigidity, values close to 0 indicate random, undirected movement. PSCs exposed to a stiffness gradient expressed a marked predilection towards stiff substrate, with those exposed to only a single rigidity exhibiting undirected, limited movement. Number of cells analysed per region: boundary – 51; soft – 67; stiff – 78. *$p < 0.05$. (d) Average cell movement speed observed at the rigidity boundary, soft region and stiff region of the hydrogel over a 12-hour period. PSCs exposed to a stiffness gradient exhibit markedly increased migratory speed when compared to PSCs exposed to only a single rigidity. Number of cells analysed per region: boundary – 51; soft – 67; stiff – 78. *$p < 0.05$, In all cases, histogram bars represent mean ± SEM. Data are representative of 3 independent experiments.

Cell movement distance within each region was calculated by subtraction of initial (0 hours) from final (12 hours) cell position coordinates along the 'x' axis, with migration only analysed when movement along the 'y' axis, perpendicular to the gradient axis, was 0. This allows for exclusion of factors other than rigidity gradient in affecting cell movement. Positive 'x' values indicate a preference of PSCs to migrate towards regions of fibrosis, whilst negative 'x' values indicate migration in the opposite direction. Values close to 0 highlight random, undirected cell movement. The preferential ability of PSCs to durotactically migrate from soft to stiff matrices (Figure 2.10 b) was observed, with quantification of average 'x' values outlining a marked predilection of PSCs to migrate from soft to stiff within the boundary region of hydrogels (Figure 2.10 c). Cells observed within single rigidity regions of the gel (solely soft or stiff), as expected, exhibited random movement along the 'x' axis, with PSCs present within these regions displaying no directed motility (Figure 2.10 c).

PSC movement speed was also assessed as a function of migration, determined in relation to cell movement distance over the experiment duration (12 hours). As to be expected, cells undergoing directed migration within the boundary region exhibited significantly increased migratory speed in comparison to cells residing within single rigidity regions (Figure 2.10 d).

Cell migration and hence durotaxis depend on very tightly coordinated processes of focal adhesion turnover and detachment of the adherent rear edge via myosin-II mediated contractile forces. Interfering with normal spatiotemporal focal adhesion dynamics or cell contractility impairs durotaxis in fibroblasts and mesenchymal stem cells[41,178]. To learn more about the mechanisms underlying durotaxis in PSCs, siRNA against focal adhesion kinase (siRNA FAK) and blebbistatin that inhibits myosin-II ATPase activity and cell contractility were used. As expected, down regulating FAK or cell contractility profoundly decreased durotaxis in PSCs, evidenced by close to null average of PSCs movement in the x-axis, which is indicative of random non-directed movement (Figure 2.11 a, b).

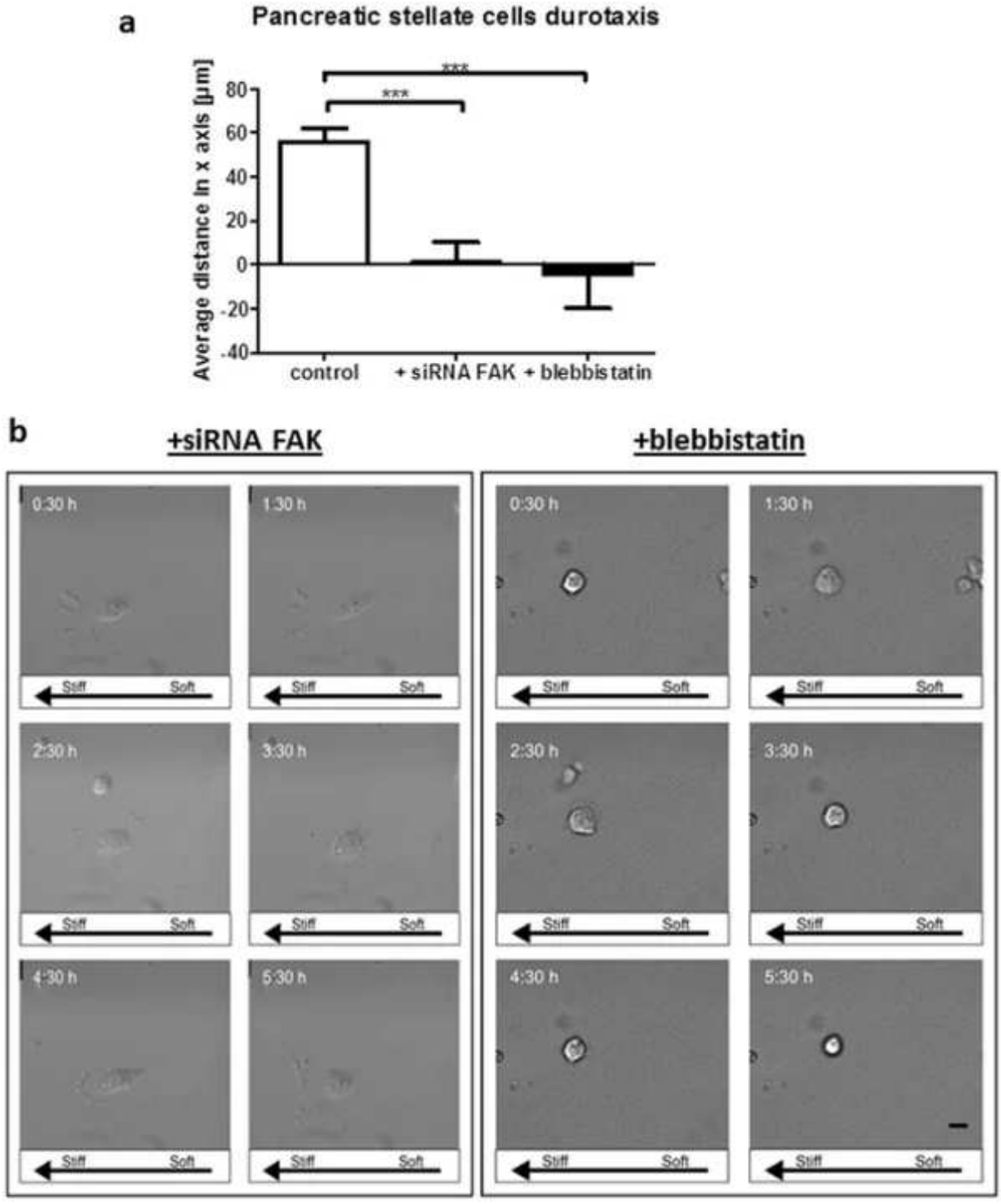

Figure 2.11 FAK and myosin-II activities are required for durotaxis in PSCs. (a) Average cell migration distance at the rigidity boundary over a 12-hour period for control PSCs, PSCs transfected with siRNA for FAK, and PSCs treated with blebbistatin. Positive values indicate movement towards higher rigidity, values close to 0 indicate random, undirected movement. Histogram bars represent mean ± SEM. ***$p < 0.001$. (b) Representative images of PSC migration over a 5 h period. Scale bar 25 µm.

Taken together, data show that PSCs possess the ability to durotactically migrate towards regions of fibrosis within a mechanically relevant model of PDAC. It is demonstrated that such motility occurs in the absence of any chemotactic stimuli, highlighting another avenue through which PSCs contribute to the production of desmoplasia around pancreatic neoplasms, whilst providing a potential additional mechanism through which PSCs play a role in cancer metastasis.

2.3 Discussion

PDAC is a highly aggressive malignancy characterised by persistent activation of pancreatic stellate cells (PSCs), resulting in excessive ECM deposition and secretion of soluble factors, which provides both mechanical and biochemical cues that in turn influence all aspects of tumour progression. Furthermore, the tumour-associated fibrosis in PDAC not only impedes intratumoural drug perfusion, but also alters the mechanical microenvironment by increasing matrix stiffness. This can in turn alter force transmission and deregulate the tensional homeostasis of resident PSCs leading to a perpetual cycle of fibrosis and aberrant PSC activation.

Given that activated PSCs are the main effector cells in pancreatic fibrosis, targeting PSCs can offer a novel therapeutic approach to normalise the tumour stroma. In the past, research has primarily focused on identifying soluble profibrogenic and pro-migratory factors – cytokines and growth factors that mediate PSC activation and migration, with most notable examples, transforming growth factor (TGF-β1) and platelet-derived growth factor (PDGF). Matrix stiffness has traditionally been thought of as a manifestation of disease rather than a contributor to fibrosis and as a result little attention was paid so far to the mechanical microenvironment as a stimulus for PSC activation and migration.

It has previously been shown that activated PSCs possess the ability to mechanically activate latent TGF-β stored within the ECM[179], producing an autocrine feedback loop that independently sustains PSC fibrotic activity[179]. Furthermore, as it was previously shown, using a 3-dimensional model of ECM, activated PSCs apply higher tension on collagen fibres, producing a greater degree of collagen alignment and fibre thickness[180] that ultimately perpetuates fibrosis and creates the collagen fibre tracks that are used by cancer cells to migrate[164]. Abrogating PSC activation through tuning matrix rigidity, cytoskeletal contractility, or normalising integrin-mediated mechanosensing thus holds the potential to both suppress

mechanical activation of latent TGF-β, and change the alignment of ECM architecture that is conducive to cancer cell invasion and survival[181].

Here, this research presents a newly identified PSC mechano-sensory regulation within an *in vitro* physiomimetic model of PDAC. Stiff PAA hydrogels, mimicking the PDAC mechanical microenvironment, were shown to induce PSC phenotypic transition to an activated, higher matrix secreting state. This force-mediated activation could explain the perpetuation of established fibrosis. Once resident PSCs are activated through soluble factors released by cancer cells, the matrix secreted by these PSCs creates higher tissue tension in the local microenvironment around the tumour. This increase in stiffness leads to the generation of a positive mechanical feedback loop that both induces and maintains PSC activation (Figure 2.12) in the stroma, irrespective of the presence of any soluble factors.

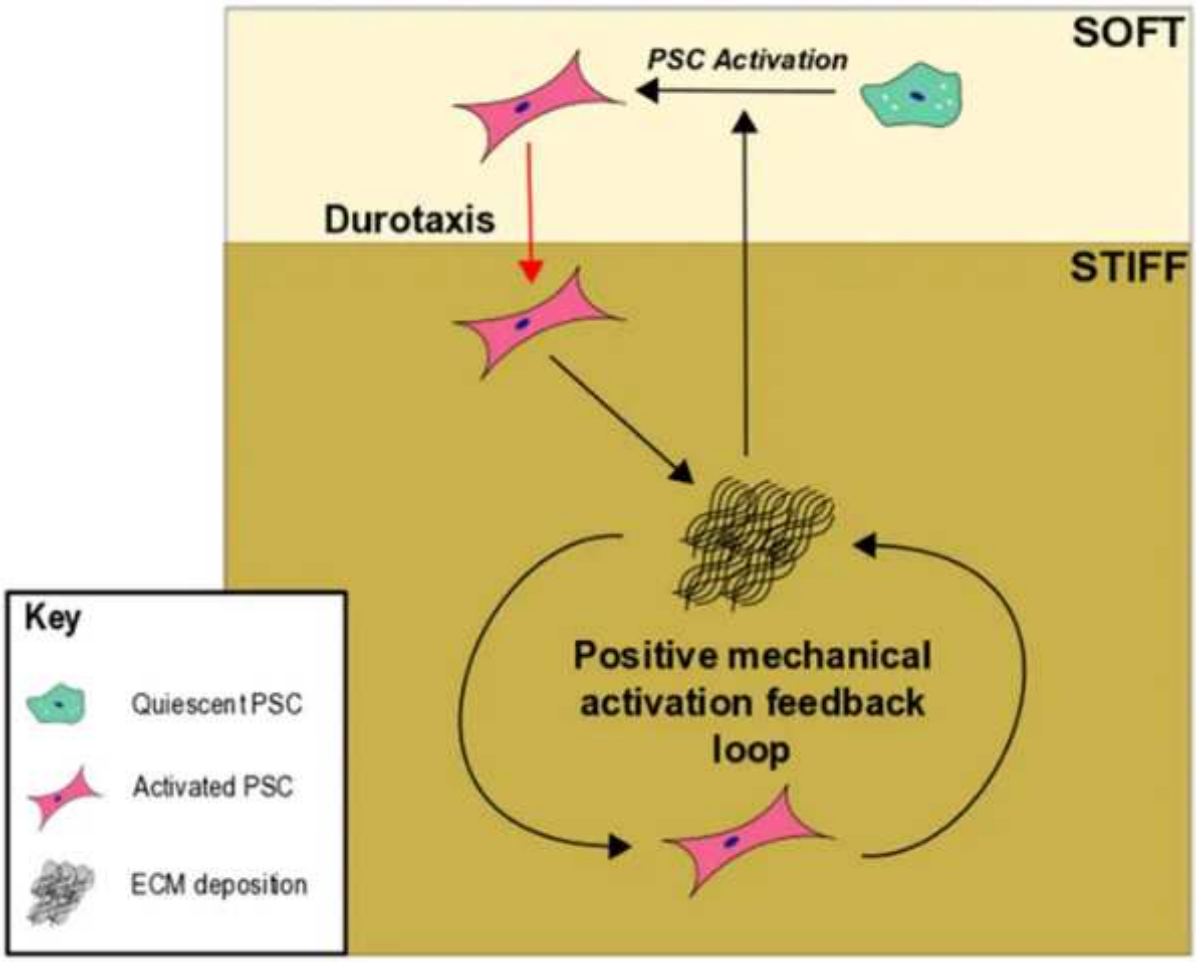

Figure 2.12 Illustration of PSC mechano-sensory driven regulation within a PDAC microenvironment. Under the effects of activating factors released from nearby cancer cells, local PSCs undergo phenotypic transition to a myofibroblast-like state, characterised by the secretion of vast amounts of ECM, providing a growth permissive environment for the neoplasm. Independently of PSC-cancer cell interactions, the generation of this highly stiff matrix mechanically activates local PSCs through mechanotransduction of the local microenvironment. This leads to increased matrix secretion and further PSC mechano-activation, resulting in the production of a positive mechanical activation feedback loop that produces a continually expanding region of fibrosis around the tumour. Such deposition leads to the generation of a stiffness gradient within the pancreas that is sensed by distant quiescent PSCs, causing them to undergo transition to an active state and begin durotactic migration towards the neoplasm, where upon they contribute to further matrix deposition. This accentuates the ever-growing area of fibrosis around the neoplasm through a vicious cycle of mechanically perturbed PSC activity.

Contrarily, soft matrices, recapitulating healthy pancreas modulus, were demonstrated to induce and maintain PSC quiescence, disproving the idea that apoptosis is solely responsible for termination of PSC activation[182]. The feasibility of stellate cell inactivation is also consistent with previous reports that suggest hepatic stellate cells can revert back to a quiescent state upon resolution of liver fibrosis, although still retaining an intermediate phenotype with enhanced capacity to respond to fibrogenic signals[138]. Such observations may also shed light as to why current therapies targeting the depletion of the myofibroblastic stroma have thus far yielded limited results[160,161].

Furthermore, a previously unobserved durotactic response within PSCs was identified, with cells preferentially migrating towards regions of fibrosis on a mechanically relevant dual-rigidity PAA hydrogel. Thus, it can be expected that within the PDAC pancreas, such durotactic behaviours complement the already characterised PSC chemotactic movement[163] in being responsible for the observed increase in activated PSC numbers around the neoplasm[183]. This increase leads to further matrix deposition and subsequent growth of desmoplasia that, in turn, increases durotactic capacity of yet more PSCs, leading to the generation of a positive durotactic feedback loop that complements the aforementioned mechanical loop (Figure 2.12).

Taken together, the findings suggest that matrix stiffness can induce myofibroblastic differentiation of PSCs, independently of soluble profibrotic factors (e.g. TGF-β), as well as promote durotactic migration to stiffer fibrotic regions independently of chemotactic stimuli, (e.g. PDGF). Targeting matrix stiffness and mechanotransduction could open new avenues for treatment of pancreatic fibrosis (PDAC and chronic pancreatitis) and fibroproliferative diseases in general. One such avenue includes the recent demonstration that aside from matrix rigidity, cells also sense the length of adhesive ligands that attach them to the matrix[184]. Such information opens up the possibility for engineering applications that make use of longer 'relaxed' artificial adhesive tethers that allow PSCs to perceive stiff environments as soft, abrogating fibrotic behaviour.

An alternative and currently more tangible option[166,179] is targeted deactivation of PSCs removing the growth permissive microenvironment which surrounds the tumour. Furthermore, through targeting of the mechanosensing properties of PSCs, such treatments have the potential to abrogate PSC mechanical activation of TGF-β[179], inhibit PSC durotactic migration towards the tumour core and suppress the ability of PSCs to create 'tracks' within tissues for further cancer cell invasion[164]. Inhibition of this migratory capacity not only inhibits the crosstalk

between PSCs and cancer cells, but also may play an important role in preventing the formation of metastatic niches[166].

2.4 Materials and methods

2.4.1 Cell culture and reagents

Human primary PSCs were purchased from ScienCell Research Laboratories (Carlsbad, USA) and cultured in DMEM/F-12 HAM (Sigma-Aldrich, USA) supplemented with 10% FBS (Gibco, USA), 1% penicillin/streptomycin (Sigma-Aldrich, USA) and 1% Fungizone (Gibco, USA). Cells were tested for contamination and cultured until passage 4–8 was reached.

2.4.2 Quiescence induction using Matrigel assay

PSC quiescence was induced through culture of cells on Matrigel for 6 days. Corning Matrigel Basement Membrane Matrix, LDEV-free (Scientific Laboratory Supplies, UK) was prepared on ice in a 1:2 ratio with serum-free DMEM/F-12 HAM. Homogenised solution was used to coat sterile positively charged microscope slides/13 mm sterile glass coverslips and left to polymerise for 24 hours at 37 °C. PSCs were then seeded on top of Matrigel and cultured at 37 °C, 5% CO_2 with media changed every 2–3 days.

2.4.3 Preparation of polyacrylamide hydrogels of tuneable stiffness

Single rigidity PAA hydrogels were prepared through homogenisation of a polymer solution containing PBS, acrylamide/bisacrylamide (29:1) 40% volume (Sigma-Aldrich, USA), TEMED (Sigma-Aldrich, USA) and 10% APS. Varying hydrogel rigidities were produced through alteration of acrylamide/bisacrylamide amounts (Table 1) based on Engler's protocol[36]. 8 µl (gel attachment to coverslips)/100 µl (microscope slide) drop(s) of desired polymer solution were then transferred to dichlorodimethylsilane (Sigma-Aldrich, USA) treated glass microscope slides before *'activated'* 13 mm glass coverslips/*'activated'* glass microscope slide treated with: 0.1 M NaOH, 4% APTES (Sigma-Aldrich, USA) and 2.5% glutaraldehyde (Sigma-Aldrich, USA), were placed on top. Gels were incubated for 45–60 minutes to allow polymerisation before gentle removal from the dichlorodimethylsilane

treated microscope slide using a sterile scalpel. Gels were then sterilized under 2 × 30 minutes of UV light and where necessary submerged in PBS and stored at 4 °C.

To produce double rigidity PAA hydrogels suitable for durotaxis analysis, 2.5 µl yellow-green 0.2 µm FluoSpheres carboxylate (Molecular Probes, USA) were added to one of two hydrogel polymer solutions so as to distinguish the boundary between rigidities. FluoSpheres were activated by sonication for 7 seconds. Two 4 µl droplets (one containing FluoSpheres) of varying hydrogel stiffness were placed adjacent to each other on an *'activated'* glass dish. A dichlorodimethylsilane treated coverslip was placed on top and gels allowed to polymerise for 45–60 minutes before gentle removal of coverslip.

To facilitate cell attachment to gels, 50 µl (coverslip)/200 µl (microscope slide) sulfo-SANPAH (SS) (Sigma-Aldrich, USA) solution (0.1 mg SS in 2 µl DMSO/50 µl PBS) was used to covalently bind native human fibronectin (Gibco, USA) to gel surface. Gel surface was covered in SS solution and exposed to 2 × 5 minutes UV light to activate sulfo-SANPAH before excess solution was removed through PBS washing. 50 µl (coverslip)/200 µl (microscope slide) of fibronectin solution (10 µl fibronectin/1 ml PBS) was added to gel surface and gels incubated at RT for 2 hours. Excess fibronectin was then removed with gentle PBS washing. Cells were then added and cultured.

2.4.4 Oil Red O staining

Oil Red O stock solution was prepared with 60 mg Oil Red O powder (Sigma-Aldrich, USA) dissolved in 20 ml 100% isopropanol and stored at RT in dark. Working solution was prepared by adding 3 parts stock to 2 parts dH_20, left to sit for 10 minutes, and then filtered through a 0.2 µm syringe filter. Cells were fixed with 1% PFA, washed with PBS, then incubated with 60% isopropanol for 5 minutes at RT. Isopropanol was removed and cells submerged in Oil Red O working solution for 20 minutes on a dish rocker. Samples were washed with distilled water until clear and stored in distilled water at 4 °C.

2.4.5 Immunofluorescence

Cells were fixed with 4% PFA, blocked and permeabilised with 2% BSA and 0.1% Triton X-100 (all Sigma-Aldrich, St. Louis, MO, USA) then incubated with primary antibodies (Vimentin M0725 DAKO, Alpha SMA M0851 DAKO, Ki67 ab15580 abcam, Fibronectin

ab2413 abcam) 1/100 diluted in 2% BSA/PBS for 1 hour at RT, then washed with PBS and incubated with secondary antibodies (Alexa Fluor® 488 anti-rabbit Life Technologies, USA) and phalloidin (Alexa Fluor® 546, A22283, Life Technologies, USA) 1/500 in PBS for 45 min in dark. Finally, the coverslips were mounted with ProLong® Gold Antifade with DAPI (Life Technologies, USA).

2.4.6 Image acquisition and quantitative analysis

Oil Red O images were taken with a Motic AE31 trinocular inverted microscope by Motic Images Plus 2.0 software using 20x objective. Oil Red O staining was analysed on Matrigel/PAA hydrogels through bright-field microscopy based on the presence/absence of red-stained lipid droplets within cell cytoplasm. Quantification of cell population quiescence per condition was assessed as the number of cells stained positively for Oil Red O within that condition. Immunofluorescent images were taken with Nikon Ti-e inverted microscope by NIS elements software using 40x objective. Immunofluorescent staining was analysed on Matrigel/PAA hydrogels through epifluorescence microscopy based on the mean fluorescence intensity. The immunofluorescent images of pancreas OCT frozen sections and collagen second harmonic generation images were taken with Leica SP5 MP/FLIM upright multiphoton microscope.

2.4.7 Quantification and analysis of durotaxis on polyacrylamide hydrogels

Durotactic responses of cells were analysed with a Nikon Ti-Eclipse microscope using 20x objective. After cell seeding (control, with 50 μM blebbistatin and with siRNA FAK sc-29310 Santa Cruz Biotechnology transfected with Neon Transfection System, ThermoFisher) onto double rigidity hydrogels, samples were transferred to microscope culture chamber (37 °C, 5% CO_2) and gently submerged in 5 ml of growth media. Rigidity boundary was identified through yellow-green fluorescence of FluoSpheres. ‘Regions of interest’ (ROI) across the sample were stitched together using NIS elements software to generate a representative image of the hydrogel surface. x- and y-axis were used to define these ROI within the ‘soft’, ‘stiff’, and ‘soft-stiff boundary’ regions of the hydrogel, whilst the z-axis was used to focus the camera onto the surface plane of the gel. A period of 1–2 hours was set to allow cells to fully attach to gel surface before time-lapse phase contrast images were taken every 15 minutes for 12 hours

within each designated ROI. Coordinates and distances of cell movement were calculated using the Fiji "Manual Tracking" plugin.

2.4.8 Real-time quantitative polymerase chain reaction

Total RNA was extracted with RNeasy Mini Kit (Qiagen, 74104) and 1 µg of total RNA was reverse transcribed by High-Capacity RNA-to-cDNA Kit (Applied Biosystems, 4387406) according to manufacturer's instructions. Q-PCR was performed with SYBR Green PCR Master Mix (Applied Biosystems, 4309155) with 100 ng cDNA input in 20 µl reaction volume. GAPDH expression level was used for normalisation as a housekeeping gene. The sequences were as following: GAPDH: forward-5′ACAGTTGCCATGTAGACC3′, reverse-5′TTTTTGGTTGAGCACAGG3′; a-SMA: forward-5′CATCATGAAGTGTGACATCG3′, reverse-5′GATCTTGATCTTCATGGTGC3′; vimentin: forward-5′GGAAACTAATCTGGATTCACTC3′, reverse-5′CATCTCTAGTTTCAACCGTC3′. All primers were used at 300 nM final concentration. The relative gene expression was analysed by comparative $2^{-\Delta\Delta Ct}$ method.

2.4.9 Mouse Tissues

Mouse tissues for healthy pancreas (Pdx-1-Cre) and PDAC (Pdx1-Cre; LSL-$Kras^{G12D/+}$ LSL-$Trp53^{R127H/+}$) were obtained from Dr. Jennifer Morton at the Beatson Institute in Glasgow. All experimental protocols were conducted in compliance with the UK Home Office guidelines under license and approved by the local ethical review committee (Beatson Cancer Research UK Institute, Glasgow).

2.4.10 Multiphoton Microscopy

All SHG images were obtained using a custom built multiphoton microscope incorporating an upright confocal microscope (SP5, Leica) and a mode-locked Ti:Sapphire Laser (Mai Tai, Newport Spectra-Physics). Images of the SHG signal from collagen I were collected using an 820 nm excitation with SHG signal obtained with a 414/46 nm bandpass filter and multiphoton autofluorescence signal obtained with a 525/40 nm bandpass filter. A 25X, 0.95 NA water-immersion objective (Leica) was used to deliver the excitation signal and to collect the SHG emission signal from the sample.

2.4.11 Statistical analysis

Results were analysed using Prism software. A two-tailed Student's t-test for unpaired data or ANOVA plus Tukey posthoc test was used to calculate the difference between means, with p-values less than 0.05 considered significant. Single asterisk show *$p < 0.05$, double asterisk show **$p < 0.01$, triple asterisk show ***$p < 0.001$. Data is presented as means, with error bars the standard error of the mean (SEM).

3 FAK controls the mechanical activation of YAP, a transcriptional regulator required for durotaxis

3.1 Introduction

Cells communicate with their environment through focal adhesion complexes, which are integrin-based structures that mediate interactions between the cell and the extracellular matrix (ECM). The ECM acts as a signalling hub whereby mechanical cues affect intracellular Signaling in health and disease[185]. Focal adhesion kinase (FAK), a key protein within focal adhesions, is known across many cell types to be sensitive to stiffness[186], becoming activated when recruited to focal adhesions after integrin attachment to the ECM in a high-stiffness environment[187]. FAK acts as an essential link between a myriad of extracellular signalling inputs and intracellular Signaling outputs, with the autophosphorylation of Tyr397 allowing effector proteins to recognize its activated state[188]. Downstream effects of FAK activation include cell survival, proliferation, and motility, and therefore FAK represents a suitable target in cancer therapeutics[185].

The transcriptional regulator and Hippo pathway effector protein Yes-associated protein (YAP) is well known as an intracellular transducer of mechanical stimuli[189]. Phosphorylation of YAP on Ser 127 by a wide variety of kinases, including CDK1 and PI3K, inactivates it and prevents it from translocating to the nucleus, where it would interact with transcription factors to promote the expression of genes associated with the cell cycle and proliferation[190,191]. Localization of activated YAP to the nucleus and up-regulation of multiple YAP-dependent genes have been shown to be sensitive to substrate stiffness[125,189] as well as other mechanical cues such as cyclic stretching, requiring Rho and a functional actin cytoskeleton[189]. Furthermore, YAP activation has been shown to promote cell migration of breast cancer cells[192].

Computational models have been used to describe the mechanical network controlling YAP activity[193]. These studies suggest that the level of activation of FAK mediates the effect of substrate rigidity on YAP nuclear translocation and further activation. Hence, abnormal FAK activation can override the external rigidity in facilitating YAP activation. Mechanosensing links between FAK and YAP have been studied in the context of breast[194] and liver cancer[195], but this link has not been examined in relation to cell migration.

In durotaxis, cells show directed movement based on the substrate stiffness, and mechanotransduction *via* FAK has been implicated in this process[196]. It has been shown that durotaxis requires individual focal adhesions to sample local substrate rigidity and that FAK signalling is critical for this process[41]. Here it is shown that a balance between active and inactive FAK is required for durotaxis, through mechanical activation of YAP. Deregulation of either of these mechanoregulatory proteins will fully abrogate directed migration along a rigidity gradient. These Signaling details are elucidated in hepatic stellate cells, the dominant contributor of liver fibrosis[197], and therefore these results may also have important implications in fibrosis.

Aims:

- To examine the role of FAK activation in mechanical YAP nuclear translocation in response to substrate stiffness
- To assess how FAK activation balance can affect the rigidity guided migration regulated via YAP

3.2 Results

3.2.1 Stiffness-induced YAP nuclear localization and activation requires FAK activity

YAP translocates from the cytoplasm (inactive form) to the nucleus (active form) in response to increased extracellular matrix rigidity[189,198]. FAK regulates the dynamics of focal adhesions and has been implicated in rigidity sensing[41]. To investigate the influence of FAK activity on YAP activation and localization to the nucleus, siRNA was used to knockdown the endogenous expression of FAK in hepatic stellate cells (HSCs) and subsequently transfected cells to express either the constitutively active myristoylated form of FAK (myrFAK)[199] or the FAK isoform with a mutation in the residue tyrosine 397 (Y397FAK), which is constitutively inactive[200].

Fibronectin-coated polyacrylamide gels were used to culture cells; the substrate stiffness could be altered by changing the acrylamide/bisacrylamide ratio without affecting the surface composition[125,174,201]. A significant increase in YAP nuclear localization was observed in wild-type HSCs with increasing rigidity (from 4 to 25 kPa) (Figure 3.1 c; Figure 3.2 a, b). Consistent

with this, the mRNA expression of the YAP target gene *CTGF* was found to significantly increase from 4 to 25 kPa (Figure 3.2 c), indicating that substrate rigidity can regulate YAP-mediated gene expression.

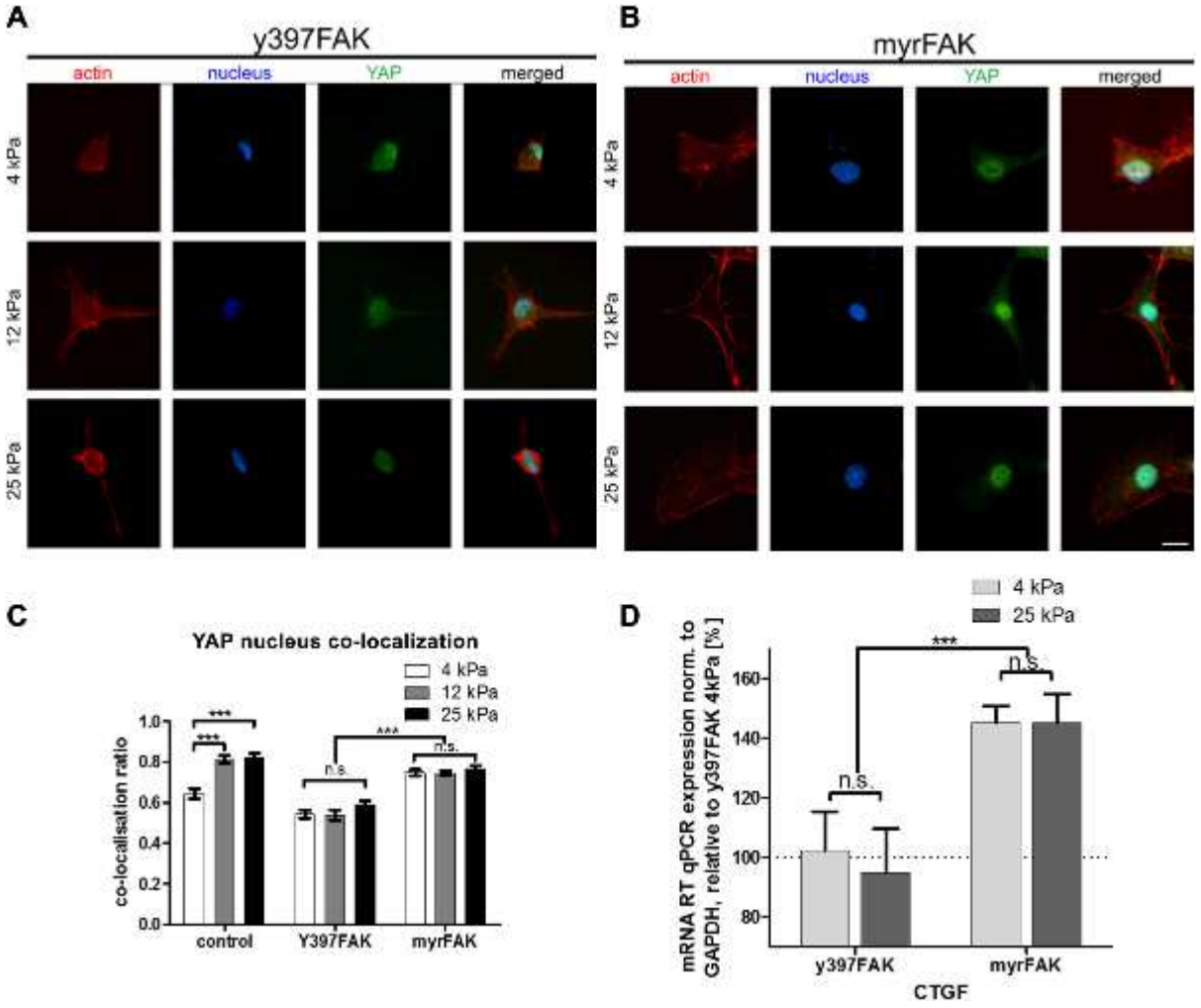

Figure 3.1 Active FAK is required for YAP translocation to the nucleus and further activation. (a, b) Immunofluorescence images of Y397FAK HSCs (a) and myrFAK HSCs (b) cultured on 4, 12, and 25 kPa polyacrylamide substrates. Scale bar, 20 µm. C, D) YAP/nucleus colocalization ratio (c) and CTGF mRNA relative expression (d) in cells cultured on 4, 12, and 25 kPa polyacrylamide gels (represented in a, b) (n = 3 independent experiments for c, d). Results are expressed as means ± sem.

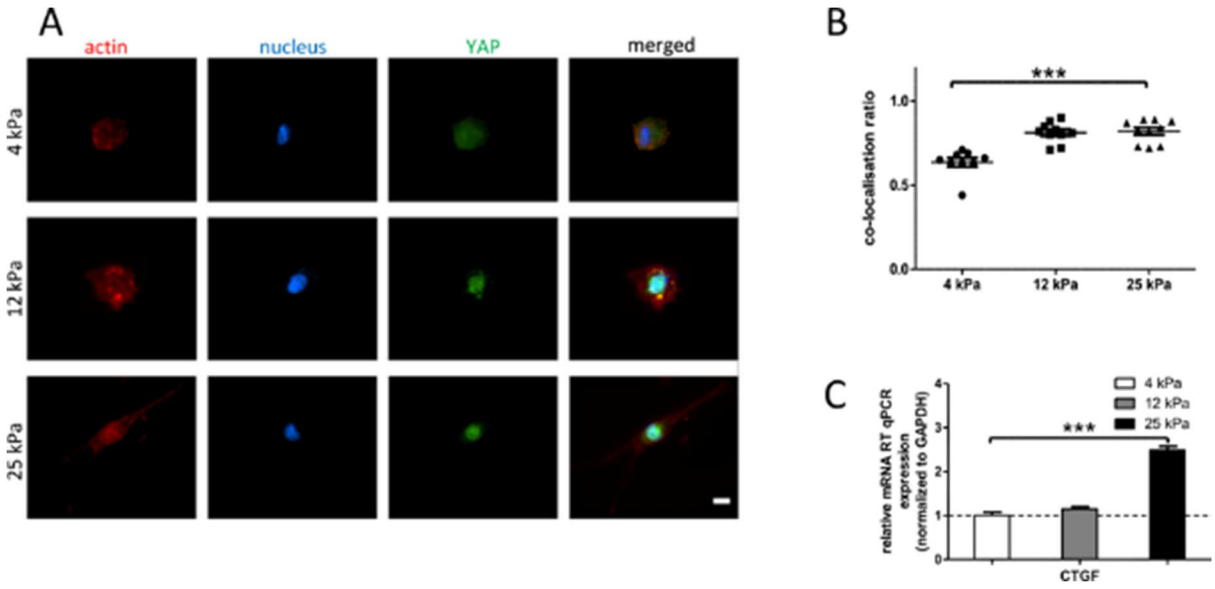

Figure 3.2 YAP nuclear localisation in HSCs cultured on different stiffness polyacrylamide gels (a) Immunofluorescence images of YAP (green) localisation to the nucleus (blue) in HSCs cultured on 4, 12 and 25 kPa polyacrylamide substrates. Scale bar represents 20 µm. (b) YAP/Nucleus co-localisation ratio and (c) CTGF mRNA expression relative to GAPDH in cells cultured on 4, 12, and 25 kPa polyacrylamide gels. n=10 Results are expressed as mean ± S.E.M

In contrast with this, no changes in YAP translocation to the nucleus were observed in response to increased rigidity in cells expressing only inactive Y397FAK. These cells showed lower levels of YAP in the nucleus in all matrix rigidities, comparable to wild-type cells on the softest matrix rigidity (4 kPa), indicating a lack of sensitivity to substrate stiffness (Figure **3.1** a, c). Cells that only had active myrFAK displayed higher levels of nuclear YAP in all matrix rigidities, comparable to wild-type cells with the stiffest rigidity (25 kPa), which were significantly higher than the levels of nuclear YAP in Y397FAK cells. Similar to the Y397FAK cells, no significant changes in YAP localization were observed between rigidities, indicating a lack of sensitivity to substrate stiffness (Figure 3.1 b, c).

To determine whether the dependence of YAP localization of FAK is an HSC-specific phenomenon, HFFs (human foreskin fibroblasts - model fibroblastic cells[202]) were used and a knock down the endogenous expression of FAK was performed using siRNA. Then, these cells were transfected with either Y397FAK (inactive FAK) or myrFAK (inactive FAK). Control wild-type HFFs are seen to be sensitive to stiffness, with higher nuclear localization of YAP in the 25 kPa condition compared with the 4 kPa condition (Figure 3.3 a, b). It was also observed that in Y397FAK HFFs, low levels of YAP nuclear localization are seen on both substrate

rigidities, comparable to control cells on a 4 kPa substrate. In myrFAK HFFs, higher levels of localization are seen on both substrate rigidities, comparable to control cells on a 25 kPa substrate (Figure 3.3 c, d). This parallels the results seen with HSCs, including the lack of sensitivity of these FAK mutants to stiffness, showing that FAK activation of YAP is not specific to HSCs but applies to other cell types.

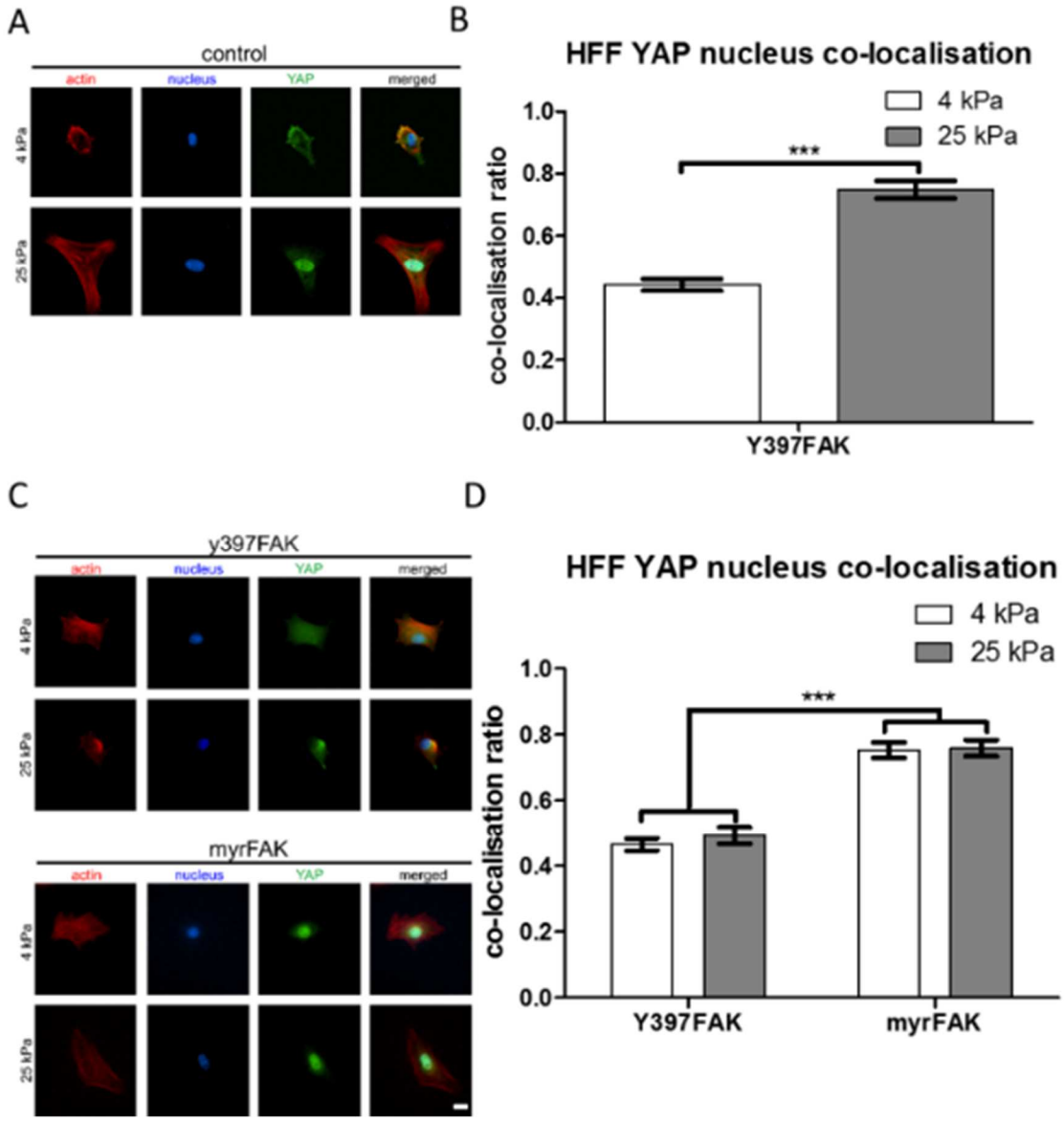

Figure 3.3 YAP nuclear localisation in y397FAK and myrFAK HFFs cultured on different stiffness polyacrylamide gels. Immunofluorescence images of (a) control HFFs and (c) Y397FAK HFFs and myrFAK HFFs cultured on 4 and 25 kPa polyacrylamide substrates. Scale bar represents 20 µm. YAP/Nucleus co-localisation ratio in (b) control and (d) Y397FAK HFFs and myrFAK cells cultured on 4 and 25 kPa polyacrylamide gels represented in n= 3 independent experiments. Results are expressed as mean ± S.E.M.

Furthermore, mRNA expression of CTGF in active myrFAK HSCs is 50% higher than in Y397FAK for both 4 and 25 kPa substrate rigidities. Changes in expression of CTGF have been observed in response to alterations in stiffness in other cell types to a similar extent[189,203,204]. The observed YAP nuclear localization correlates with the high CTGF expression in myrFAK cells and with the low expression in Y397FAK cells (**Figure 3.1** d).

Activation of FAK was seen through dual immunostaining of the active phosphorylated form of FAK and total FAK and subsequent quantification of the expression area. It was observed that the phosphorylated FAK/total FAK ratio, which is indicative of FAK activation, significantly increased with stiffness (Figure 3.4), confirming the mechanosensitivity of FAK. Collectively, these results suggest that FAK activation drives the nuclear localization of YAP and expression of YAP target genes in response to increased matrix rigidity.

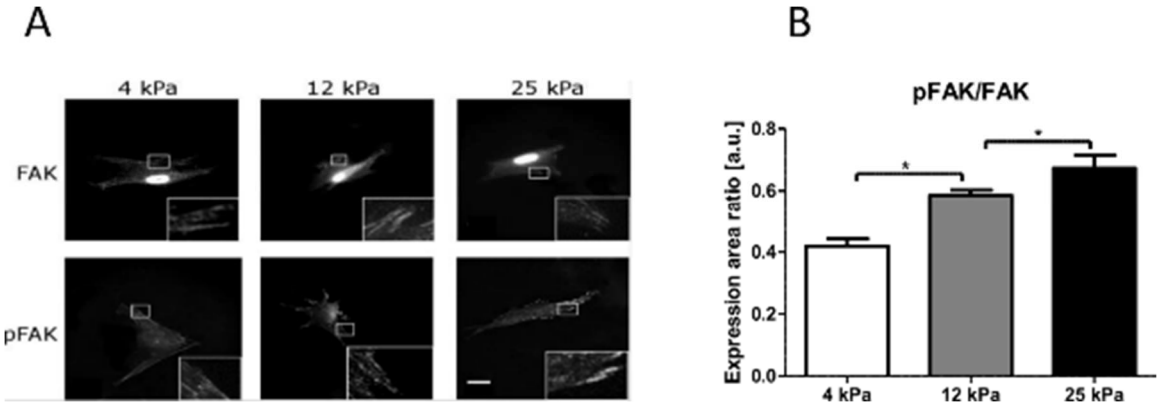

Figure 3.4 Focal adhesion kinase (FAK) expression and FAK inhibition in Hepatic Stellate Cell durotaxis. (a) Confocal immunofluorescence images of FAK and pFAK expression in cells on 4, 12m and 25 kPa polyacrylamide substrates. Scale bar represents 20 µm. (b) pFAK/FAK expression area ratio in cells cultured on 4, 12 and 25 kPa PAA substrates. Quantification was done for 60 cells. Results are expressed as mean ± S.E.M

3.2.2 Fabrication of a rigidity gradient for durotaxis assays

An *in vitro* rigidity gradient assay was prepared to assess durotaxis. Using polyacrylamide gels, a dual-rigidity gel was fabricated with the left side at 25 kPa (hereafter referred to as "stiff") and the right side at 4 kPa (hereafter referred to as "soft") (Figure 3.5 a). The stiff 25 kPa gel contained fluorescent nanobeads to identify the gel boundary and to verify that a boundary had been created (Figure 3.5 b).

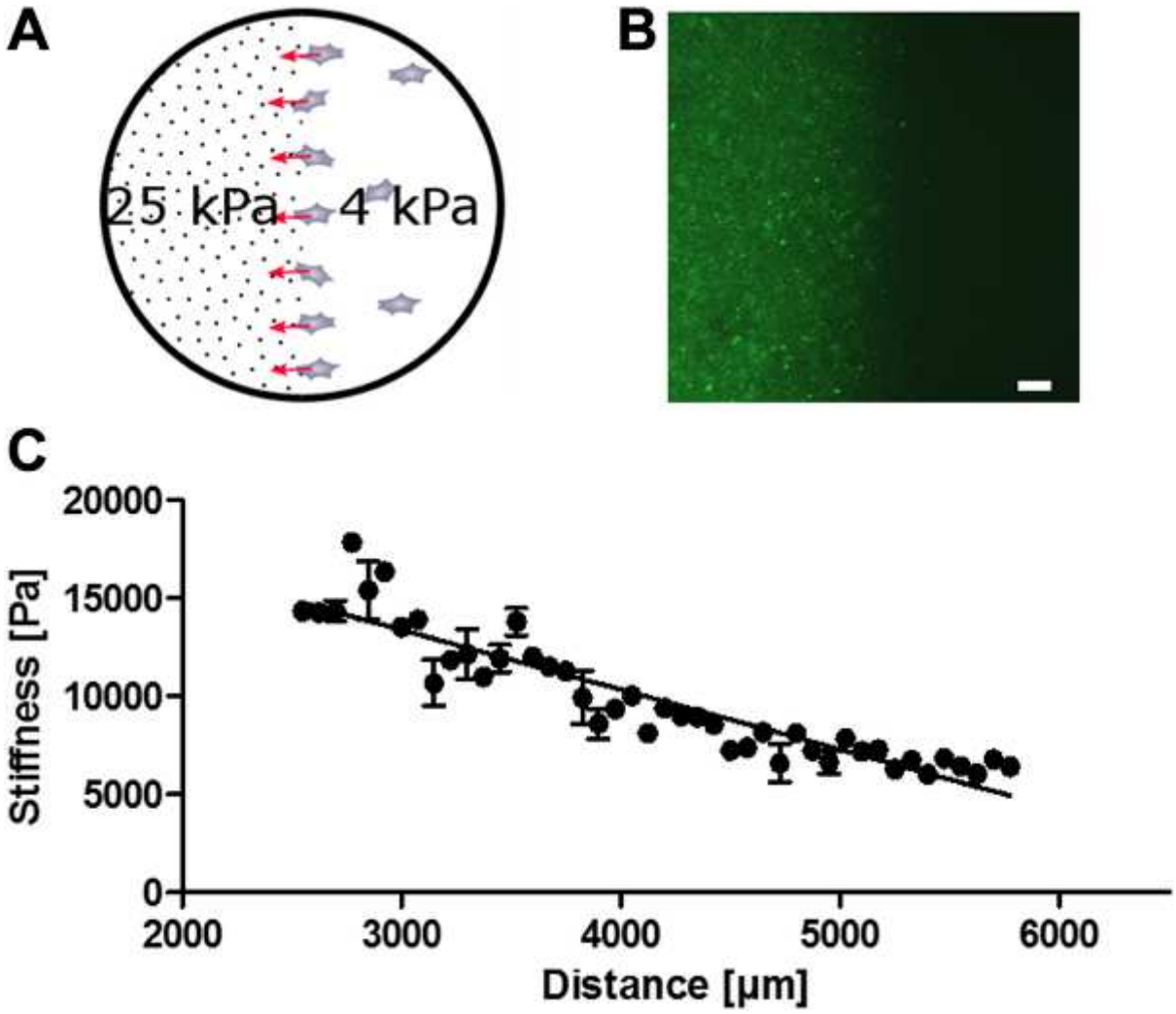

Figure 3.5 Stiffness transition boundary. (a) Diagram of dual-rigidity gel, indicating gradient from soft to stiff polyacrylamide substrate. (b) Epifluorescence image of stiff-soft rigidity gradient boundary. Stiff polyacrylamide gel labelled with fluorescent nanobeads; soft polyacrylamide gel is unlabelled. Scale bar, 100 µm. (c) Stiffness gradient ($a = -3.048 \pm 0.1926$ Pa/µm) across the durotaxis polyacrylamide gel. Presented as AFM stiffness (Young's modulus) measurements vs. length in the axis perpendicular to the boundary. Each point ($n = 5$ indentations) is represented as mean ± sem.

Atomic force microscope with a bare pyramidal tip was used to assess the stiffness profile of the boundary (Figure 3.5 c). The determined Young's modulus for points along the gradient was plotted against their distance from the edge of the stiff side of the substrate, perpendicular to the boundary. The stiffness gradient was determined to be −3.05 Pa/μm with an s.e.m of 0.20 Pa/μm. The negative gradient value indicates that stiffness increases moving left across the gel.

3.2.3 Directed migration in hepatic stellate cells

Durotaxis, or directed migration toward stiffer substrates, has been well characterized for fibroblasts[45,196]. Fabricated dual-rigidity gradient gel was used to test if HSCs perform durotaxis. Cells were seeded evenly across the gel, and an area of 8 mm^2 was used in capturing images of cells over 5 h and 30 min at 6 frames per hour. Cell movement was quantified by manually tracking the global position of the centre of cells across all frames of the video (Figure 3.6 a), the average distance travelled in the *x* axis (*i.e.*, perpendicular to the stiffness boundary) and the average speed was reported for 60 cells. For control conditions, cell movement on single-rigidity gels with stiffness values equal to each of the rigidities in the dual-rigidity gel was also analysed.

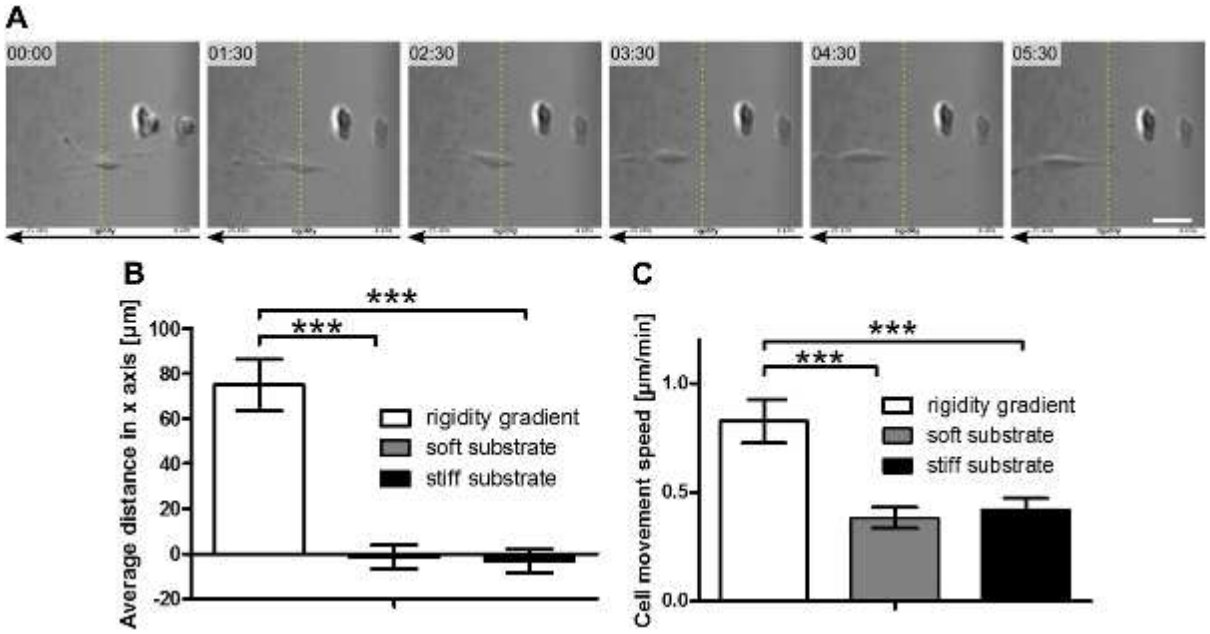

Figure 3.6 HSC-directed migration toward stiffer substrate in the rigidity gradient. (a) Cell migration from soft (light grey) to stiff (dark grey) polyacrylamide substrate during a 5.5-h observation. Scale bar, 50 µm. (b) Average cell movement distance on the soft-stiff rigidity gradient compared with single-rigidity soft and stiff substrates presented as an average displacement (positive values indicate directed movement toward stiff substrate, negative values indicate movement toward soft substrate, and 0 indicates random movement) (n = 3 independent experiments). Results are expressed as means ± sem. (c) Cell movement speed on the soft-stiff rigidity gradient compared with single-rigidity soft and stiff substrates. Quantification was done for 60 cells (n = 3 independent experiments). Results are expressed as means ± sem.

Where a rigidity gradient was present, directed movement of wild-type HSCs toward the stiffer substrate (positive value in average distance) was observed, with an average distance of 75 µm travelled over 5.5 h. This positive value is significantly different from the average distance travelled on both single-rigidity substrates (Figure 3.6 b), which contain the value of 0 within their 95% confidence limits, indicating a lack of mechanically driven directed movement. This indicates that HSCs can migrate along a rigidity gradient to a stiffer substrate and that the increased speed of movement depends on the presence of gradient rather than a single stiff or soft substrate.

Cell movement speed was also quantified and followed a similar trend in which cells showed a significantly higher average speed on a rigidity gradient (0.825 µm/min) than on soft (0.38 µm/min) or stiff (0.42 µm/min) gels (Figure 3.6 c). The durotaxis speed values are comparable to those measured by Wang *et al.* [196], where the migration speed of wild-type mouse embryonic fibroblasts (MEFs) on a similar dual-rigidity gel was 0.827 µm/min.

3.2.4 HSC durotaxis is dependent on a working FAK/YAP axis

To learn more about the mechanism underlying durotaxis in HSCs, the activity of FAK and YAP was altered and the ability of HSCs to undergo directed migration was assessed. All experiments were conducted on the dual-rigidity gel in which wild-type HSCs under control conditions show an average distance travelled of 75 µm, as was previously demonstrated (Figure 3.6 b). The intracellular signalling pathway was altered using agents known to induce constitutively inactive FAK (Y397FAK, FAK14 inhibitor) or YAP (siRNA YAP) or constitutively active FAK (myrFAK) or YAP (siRNA LATS1).

FAK inhibition and knockdown has been shown in MEFs to decrease cell speed and directional persistence (*i.e.*, durotaxis)[196], as was shown by using FAK inhibitors[205] and the inactive mutant Y397FAK[200]. In this study, wild-type cells treated with 500 µM FAK inhibitor FAK14 and cells expressing only inactive Y397FAK showed a significantly decreased average distance travelled (*i.e.*, close to 0), indicating a lack of durotaxis (Figure 3.7 a, c). This suggests that FAK inactivity prevents the cell from responding to the rigidity gradient due to the cell's perception of being on a soft, single-rigidity substrate (Figure 3.7 a, c).

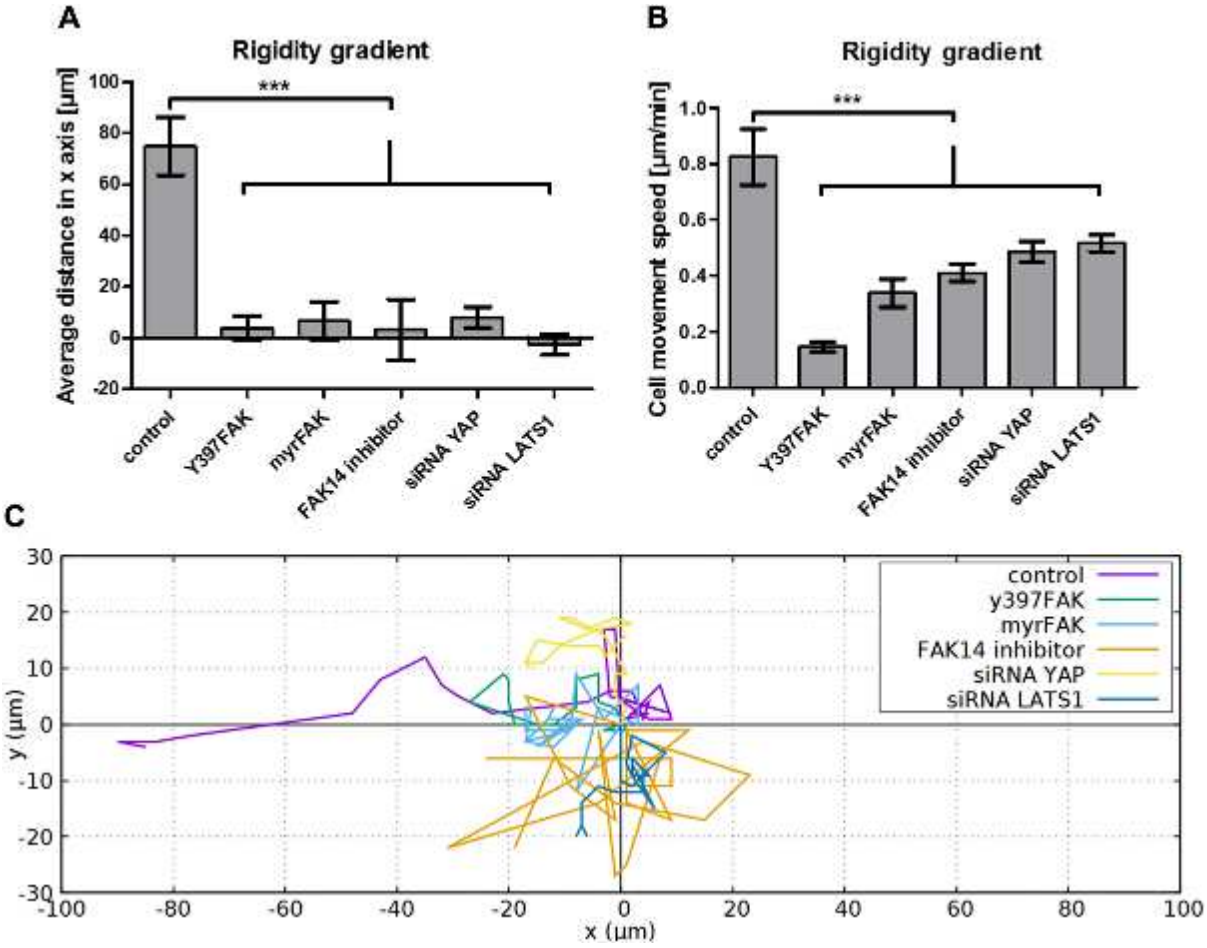

Figure 3.7 Durotaxis in HSCs depends on the FAK/YAP axis. (a) Average cell movement distance on the soft-stiff rigidity gradient compared with single rigidity soft and stiff substrates presented as an average displacement (positive values indicate directed movement toward stiff substrate, negative values indicate movement toward soft substrate, and 0 indicates random movement) (n = 3 independent experiments). (b) Cell movement speed on the soft-stiff rigidity gradient compared with single rigidity soft and stiff substrates (n = 3 independent experiments). (c) Representation of the average displacements of HSCs. Quantification was done for 60 cells. Results are expressed as means ± sem.

The cells expressing constitutively active myrFAK also showed a near-zero average distance travelled, suggesting that the constitutive activation of FAK prevents the sensing of the rigidity gradient due to the cell's perception of being on a stiff, single-rigidity substrate (Figure 3.7 a, c). Cell speed (control = 0.825 μm/min) is also decreased in all the modified FAK states (myrFAK, 0.338 μm/min; FAK14, 0.410 μm/min; Y397FAK, 0.144 μm/min) (Figure 3.7 b). These reduced speeds are comparable to those measured by Wang *et al.* [196], where FAK-null and Y397-mutated FAK MEFs travel at an average speed of 0.364 and 0.585 μm/min, respectively.

Modifications to YAP activity also affected HSC durotaxis. Cells treated with siRNA for YAP showed a significant decrease in durotaxis (Figure 3.7 a, c) and a significant decrease in cell speed (0.487 μm/min) (Figure 3.7 b). This indicates that YAP inactivation prevents directed movement and that YAP plays a role in promoting cell speed. Additionally, activation of YAP through knockdown of its negative regulator Lats1/2, which is part of the canonical Hippo signalling pathway[206], prevents durotaxis behaviour and reduces cell speed.

Control conditions of single-rigidity gels, both soft and stiff, were used to assess whether directed migration occurred due to any of the FAK or YAP modifications (Figure 3.8). It is shown that none of the modifications on any substrate allows movement in any particular direction. Cell speed was also quantified, and no significant differences in cell speed for any of the modified cells were observed between dual-rigidity and single-rigidity gels.

Constitutively active or inactive forms of YAP or FAK are unable to drive durotaxis. Taken together, these results suggest that the presence of active and inactive populations of YAP and FAK molecules is a requirement for durotaxis to occur.

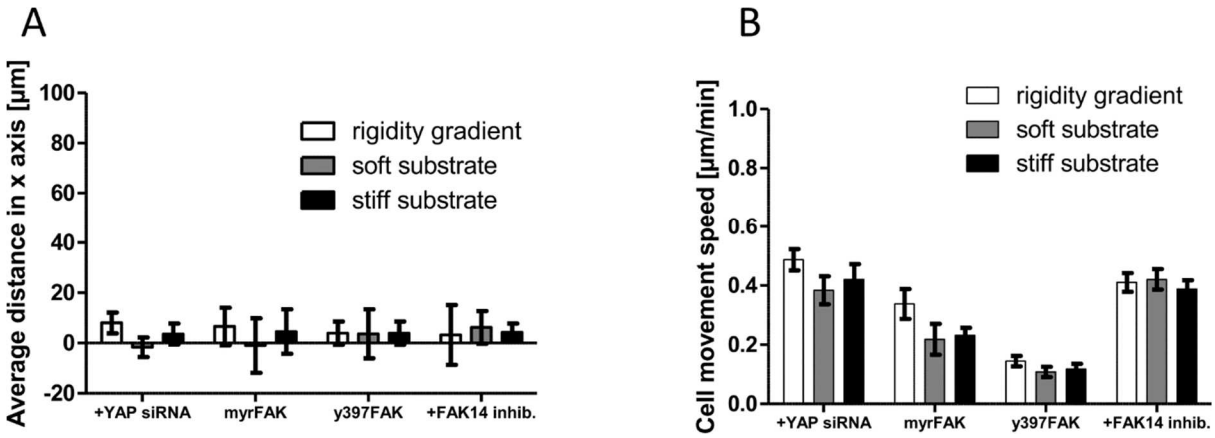

Figure 3.8 Durotaxis in HSCs depends on the FAK/YAP axis. (a) Average cell movement distance on the soft-stiff rigidity gradient compared to single rigidity soft and stiff substrates presented as an average displacement (positive values indicate directed movement towards stiff substrate, negative values towards soft substrate and 0 indicates random movement. (b) Cell movement speed on the soft-stiff rigidity gradient compared to single rigidity soft and stiff substrates. Quantification was done for 60 cells. Results are expressed as mean± S.E.M.

3.3 Discussion

Substrate stiffness is a driver of many different cell behaviours and can promote signalling through a variety of cell surface proteins and their intracellular effectors. Here it is shown that FAK activation in hepatic stellate cells is required for stiffness-induced YAP nuclear localization and activation and that, although these molecules are essential for durotaxis, their constitutive activation does not support durotaxis. It is proposed that both inactive and active subpopulations of FAK must exist for durotaxis to occur.

The observation that FAK is essential for directed migration in hepatic stellate cells is in agreement with previous studies in mouse embryonic fibroblasts[196] and studies that show the importance of focal adhesions in durotaxis[41]. It is propose that the difference in substrate rigidity across the cell generates a heterogeneous and asymmetrically distributed active focal adhesion population (Figure 3.9). The active fraction of these FAK molecules, present on the side of the cell attached to the more rigid substrate, facilitates mechanosensing and its intracellular downstream effects, including YAP nuclear localization.

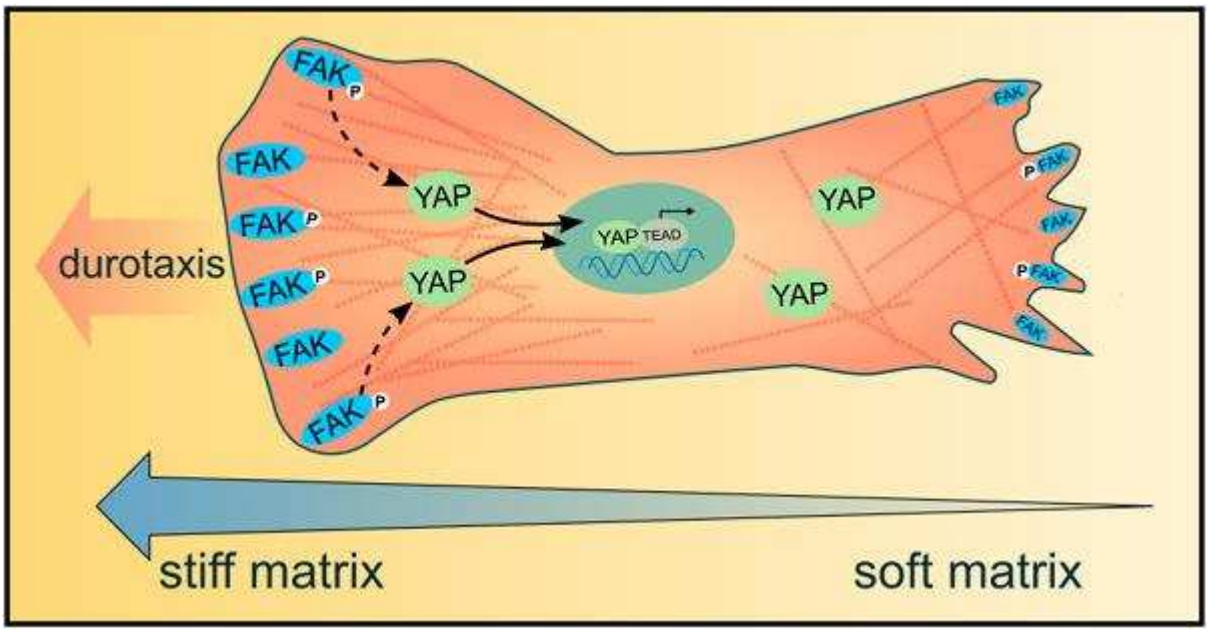

Figure 3.9 Model illustrating the roles of FAK/YAP in HSCs durotaxis.

Durotaxis has been previously linked with a balance between active and inactive forms of mechanosensitive proteins. In mesenchymal stem cells, durotaxis has been shown to rely on a finely tuned myosin distribution within the cell, requiring myosin II-A and phosphorylated myosin II-B to be present at certain amounts in the cell, both of which are sensitive to substrate rigidity[178]. The results, which reveal that constitutive FAK activation or inactivation fully abrogates durotaxis, show parallels with the study by Raab *et al.* [178] in that a balance in activation of mechanosensitive molecules is required for durotaxis.

YAP emerges as a key effector molecule in durotaxis, being essential in allowing cells to undergo directed migration, indicating that its function cannot be rescued by other mechanoresponsive transcriptional regulators present in the cells. YAP activation can occur either by the canonical Hippo pathway or by noncanonical signalling cascades, of which mechanotransduction is a noncanonical example[207]. The canonical Hippo pathway is dependent on MTS and LATS kinases. As a response to stimuli, the MST-activated LATS kinase phosphorylates Serine residue located in the amino-terminal region of YAP[208]. The motif around phosphorylated serine is then recognized and complexed by 14-3-3 protein, strongly anchoring it in the cytoplasm. LATS inhibition results in YAP translocation to the nucleus triggering a transcriptional cascade, via TEADs (transcriptional factors containing TEA domain)[209].

Regulation of YAP activity can also occur through an alternative, non-canonical pathway. Growing cells on stiff substrate can activate RhoA through FAK and therefore increase cytoskeleton and actomyosin contractility – this has been shown to regulate YAP translocation independently from LATS kinase. It has also been shown that YAP dephosphorylation is not necessary to enable entering the nucleus. This mechanical control occurs through the physical opening of nuclear pores by the cytoskeletal tension[210]. It has also been shown that LATS phosphorylation downstream of the Hippo cascade is not the main mediator of mechanical/physical cues in the regulation of YAP activity and it depends on still unidentified cytoskeleton-activated regulator[211].

Here, through use of Lats1/2 and myrFAK, it is demonstrated that alterations to the canonical and noncanonical pathways (through affecting the focal adhesion-cytoskeleton-YAP axis), respectively, prevent durotaxis, emphasizing the importance of YAP regulation.

This additionally indicates that canonical signalling is not made redundant by an active mechanical response but that the complex signalling network surrounding YAP needs to remain functional for durotaxis. Multiple kinases are known to directly regulate YAP activity through phosphorylation on residues other than the inactivating Ser 127, which can stabilize transcription complexes that promote particular gene expression profiles[212–214], opening up the possibility of direct phosphorylation of YAP by FAK.

The translocation of active YAP into the nucleus after induction by a subpopulation of dynamically active focal adhesions represents a loss of asymmetry in the signalling cascade. Therefore, it is proposed that expressed YAP target proteins interact with the polarized cytoskeleton that would form in this environment to promote directed migration. For example, focal adhesions are known to promote alignment of actin fibres on stiff substrates, whereas softer substrates show a more dynamic and isotropic distribution[215]. For a cell on a stiffness gradient, this would lead to a cell showing different actin fibre structures on different sides, and this could be the polarized environment required for motility in a specific direction. Future studies on specific YAP target proteins and their interactions with cytoskeletal components would shed light on this mechanism.

Knowledge of FAK and YAP as key molecules in durotaxis may reveal new therapeutic directions for diseases such as cancer and other diseases that are associated with fibrosis and tissue stiffening. For instance, liver injury and a deregulated wound healing process induce a fibrotic response. This fibrosis would increase local stiffness, and durotaxis of hepatic stellate

cells toward this area would lead to their accumulation at the wound site[216]. This would further increase fibrosis[217] and the reciprocal activation of cancer cells in the presence of HSCs[218,219]. Moreover, it is well established that myofibroblasts such as activated hepatic stellate cells have a role in the formation of the premetastatic niche by creating tracks in the ECM for the cancer cells to follow[164]. Therefore, inhibition of durotaxis in HSCs may have therapeutic potential in preventing the cross talk between hepatic stellate cells and cancer cells in tumours and in preventing the formation of metastatic niches; therefore, targeting YAP and FAK may be a suitable strategy. Because other malignant pathways, such as the epithelial–mesenchymal transition, have been associated with YAP[220] and FAK[185], this study provides further confirmation of the importance of these molecules in mechanically mediated tumour progression.

3.4 Materials and methods

3.4.1 Cell culture

Primary culture-activated human hepatic stellate cells (passage 3–6, HHStec 5300; ScienCell, Carlsbad, CA, USA) were cultured at 37°C, 5% CO_2 in culture medium containing DMEM/Nutrient Mixture F-12 Ham (D8437; Sigma-Aldrich, St. Louis, MO, USA), 10% foetal bovine serum (10270-106; Thermo Fisher Scientific, Waltham, MA, USA), 1% penicillin/streptomycin (Thermo Fisher Scientific), and 1% fungizone (15290-026; Thermo Fisher Scientific). Human foreskin fibroblasts (HFFs) were cultured in DMEM high glucose (D6429; Sigma-Aldrich) with the same supplements as previously described[184]. For the polyacrylamide substrate experiments, cells were detached from culture flasks and transferred to 4, 12, 25 kPa single-rigidity or 4/25 kPa dual-rigidity polyacrylamide gels.

3.4.2 Transfection

For mutant FAK expression, hepatic stellate cells were transfected with small interfering RNA (siRNA) FAK (sc-29310; Santa Cruz Biotechnology, Dallas, TX, USA) and either Tyr397 inactive FAK (Y397FAK) plasmid or myristoylated FAK (myrFAK) plasmid (both kindly donated by Dr. Andrew Gilmore, Wellcome Trust Centre for Cell-Matrix Research, University of Manchester, Manchester, United Kingdom).

3.4.3 Polyacrylamide substrate fabrication

Coverslips were dipped in 0.1 M NaOH and left to dry. Dried coverslips were coated with 4.0% (3-aminopropyl)triethoxysilane (281778; Sigma-Aldrich) and washed with distilled water. Coverslips were dried and transferred to 2.5% glutaraldehyde (G6257; Sigma-Aldrich)/PBS and incubated at room temperature for 30 min, washed twice in distilled water, and left to dry at room temperature. Polyacrylamide gels of 4, 12, and 25 kPa for the soft, medium stiff, and stiff substrates[221] were prepared according to the protocol adapted from Wen *et al.* [36]. Gel stiffness was varied by adding 29:1 acrylamide/*bis*-acrylamide to a final concentration ranging from 4.7 to 10%. PBS, acrylamide/*bis*-acrylamide (29:1) 40% volume (A7802; Sigma-Aldrich), *N,N,N′,N′*-tetramethylethylenediamine (T9281; Sigma-Aldrich), and 10% ammonium persulfate were mixed at concentrations to achieve a working solution with varying gel stiffness. A small drop of this working solution was applied to activated coverslips, which

were placed face down on hydrophobic, dichlorodimethylsilane (440272; Sigma-Aldrich)-treated glass microscope slides and left to polymerize at room temperature for 45 min. Gel-coated coverslips were removed and stored in PBS.

To allow polyacrylamide gels to be coated with ECM proteins, gels were functionalized to present *N*-hydroxysuccinimide groups. For functionalization, polyacrylamide gels were washed with PBS and coated with 50 µl sulfosuccinimidyl 6-(4′-azido-2′-nitrophenylamino) hexanoate (Sulfo-SANPAH; 803332; Sigma-Aldrich) (5 mg/ml, PBS) solution per coverslip and activated with UV light for 10 min. Polyacrylamide gels were washed with PBS and coated with human plasma fibronectin (PHE0023; Thermo Fisher Scientific) (10 µg/ml, PBS) and incubated for 1.5 h at room temperature. Gels were washed once with PBS, and cells were seeded on gels in culture medium. The same procedure was used for large-area microscope slide preparation for genetic analysis.

3.4.4 Immunofluorescence

Cells were fixed with 4% paraformaldehyde, blocked, and permeabilized with 2% bovine serum albumin and 0.1% Triton X-100 (all Sigma-Aldrich). Cells were incubated with primary antibodies (YAP sc-101199; Santa Cruz Biotechnology), 1/100 diluted in 2% bovine serum albumin/PBS for 1 h at room temperature, washed with PBS, and incubated with secondary antibodies (Alexa Fluor 488 Anti-Rabbit; Thermo Fisher Scientific) and phalloidin (Alexa Fluor 546, A22283; Thermo Fisher Scientific) 1/500 in PBS for 45 min in the dark. The coverslips were mounted with ProLong Gold Antifade with DAPI (Thermo Fisher Scientific). Immunofluorescent images were taken with Nikon Ti-e Inverted Microscope (Nikon, Kingston-upon-Thames, United Kingdom) with NIS elements software using a ×40 objective. Immunofluorescent staining was analysed on polyacrylamide hydrogels through epifluorescence microscopy based on the mean fluorescence intensity. YAP nuclear colocalization was calculated based on Pearson product-moment correlation coefficient obtained through Coloc2 ImageJ[222] plugin (National Institutes of Health, Bethesda, MD, USA).

3.4.5 Quantitative PCR

Total RNA was extracted from cells cultured on polyacrylamide gels for 24 h with the RNeasy Mini Kit (74104; Qiagen, Hilden, Germany). RNA template was reversed transcribed into

cDNA with the High-Capacity RNA-to-cDNA kit (4387406; Applied Biosystems, Loughborough, United Kingdom) per the manufacturer's instructions. Quantitative real-time PCR was performed on a StepOne Plus Real-Time PCR system (Applied Biosystems) using SYBR Green PCR Master Mix (4309155; Applied Biosystems). Relative gene expression was analysed by the ΔC_t method with the connective tissue growth factor (CTGF) target normalized to GAPDH mRNA. Primer sequences were as follows: CTGF (forward) 5′-TTAAGAAGGGCAAAAAGTGC-3′, (reverse) 5′-CATACTCCACAGAATTTAGCTC-3′; GAPDH (forward) 5′-ACAGTTGCCATGTAGACC-3′, (reverse) 5′-TTTTTGGTTGAGCACAGG-3′.

3.4.6 Atomic force microscopy

Measurements of polyacrylamide gel stiffness were conducted on a Nanowizard-1 (JPK Instruments, Berlin, Germany) atomic force microscope operating in force spectroscopy mode mounted on an inverted optical microscope (IX-81; Olympus, Tokyo, Japan). Atomic force microscopy (AFM) pyramidal cantilevers (MLCT; Bruker, Camarillo, CA, USA) with a spring constant of 0.03 N/m were used. Before conducting measurements, cantilever sensitivity was calculated by measuring the force–distance slope in the AFM software on an empty petri dish region. For each point, 3–5 force curves were acquired at an approach speed of 2 μm/s and a maximum set point of 0.1 V. The force–distance curves were used to calculate elastic moduli in the AFM software through the application of the Hertz contact model[223].

3.4.7 Quantification and analysis of durotaxis on polyacrylamide hydrogels

Durotaxis of cells was analysed with a Nikon Ti-Eclipse microscope using a ×20 objective. After cell seeding [control cells; cells transfected with siRNA FAK sc-29310 (Santa Cruz Biotechnology) and y397FAK plasmid or myrFAK plasmid, both kindly donated by Dr. Andrew Gilmore (Wellcome Trust Centre for Cell-Matrix Research, University of Manchester); and cells with 500 μM FAK14 inhibitor transfected with siRNA YAP (sc-38637; Santa Cruz Biotechnology)], cells were transfected with siRNA LATS1 sc-35797 (Santa Cruz Biotechnology) onto dual-rigidity hydrogels. Samples were transferred to a microscope culture chamber (37°C, 5% CO_2) and gently submerged in 5 ml of growth medium. The rigidity boundary was identified through yellow-green fluorescence of FluoSpheres. Regions of

interest across the sample were stitched together using NIS Elements software to generate a representative image of the hydrogel surface. The *x* and *y* axes were used to define these regions of interest within the soft, stiff, and rigidity gradient regions of the hydrogel, and the *z* axis was used to focus the camera on the surface plane of the gel. A period of 1–2 h was set to allow cells to fully attach to the gel surface before time-lapse phase contrast images were taken every 10 min for 5.5 h within each designated region of interest. Coordinates and distances of cell movement were calculated using the Fiji Manual Tracking plugin (ImageJ[222]).

3.4.8 Statistical analysis

Results were analysed using Prism software (GraphPad, La Jolla, CA, USA). A 2-tailed Student's *t-test* for unpaired data was used to calculate the difference between means (unless otherwise specified), with values of $p<0.05$ considered significant.

4 Matrix stiffness modulates the activity of MMP-9 and TIMP-1 in hepatic stellate cells to perpetuate fibrosis

4.1 Introduction

Liver fibrosis in hepatocellular carcinoma (HCC) is characterised by a remarkable extracellular matrix (ECM) stiffness, with extensive deposition and cross-linking of extracellular proteins, including fibrillar and basement membrane collagens. These proteins are primarily secreted by activated hepatic stellate cells (HSCs), myofibroblast-like cells that remodel the extracellular matrix and drive fibrosis in a disease state[197,224]. In healthy liver tissue, hepatic stellate cells reside in a quiescent state with cytoplasmic vitamin A-rich droplets, a low number of mitochondria, and a distinct rough endoplasmic reticulum. Following liver injury, HSCs become activated, and in addition to increased production of collagen and other ECM proteins, lose their vitamin A-rich droplets and become increasingly contractile and proliferative. Activated HSCs are also associated with increased inflammatory signalling and altered matrix degradation, all of which can contribute to perpetuation of fibrosis[225,226].

HSCs have a key role in remodelling and maintaining the ECM and achieve this through secretion of ECM proteins such as collagen, as well as ECM-degrading enzymes known as matrix metalloproteinases (MMPs). MMPs are calcium-dependent zinc-containing peptidases and are responsible for the degradation and turnover of most components in the ECM, including collagen[2]. Quiescent HSCs maintain ECM homeostasis by balancing the extracellular proteolytic activity of MMPs with the production of ECM proteins, but when HSCs are activated in disease or following injury, excess collagen production and altered matrix degradation leads to a stiff fibrotic state[227]. In fibrosis resolution, increased activity of MMPs leads to collagen degradation and ECM softening, with consequent reversion of activated HSCs to their quiescent phenotype. Conversely, perpetuation of the stiff fibrotic state occurs when characteristics of the environment, such as altered stiffness, amplify the activated HSC phenotype[225,226]

MMP activity can be regulated at multiple levels, such as transcription, translation, and regulation of proenzyme activation[228]. Additionally, cells can secrete tissue inhibitors of metalloproteinases (TIMPs) that inhibit the activity of MMPs outside the cell. Different MMPs are inhibited by different TIMPs in a complex interaction network and therefore the specific balance of MMPs with their cognate TIMPs dictates the activity of the extracellular MMP pool.

For example, TIMP-1 reacts with the zymogen form of MMP-9[98]. TIMPs bind to MMPs through both their N and C terminal domains. The N-terminal domain of TIMPs leads to MMP inhibition by chelating the zinc ion in the active site of MMPs. The C terminal domain binds with high affinity to the hemopexin domains of MMPs, and this interaction is likely to be inhibitory[229].

The pathological state of fibrosis is associated with an increased matrix stiffness due to the altered composition of the ECM, with stiffness dependent on both collagen abundance and cross-linking[230]. This increased rigidity is detected by HSCs through cell surface receptors known as integrins, leading to HSC activation[231–233]. HSC-mediated remodelling is a key process in ECM homeostasis, and it is known that the ECM can regulate its own composition through biochemical regulation of the secretion profile of resident fibroblasts[3]. Since many signalling pathways in HSCs have been shown to be highly mechanosensitive, e.g. rigidity inhibiting the HNF4α transcriptional network[231] or integrin-mediated activation of YAP[233], it is likely that external rigidity from fibrosis may affect HSC-mediated ECM remodelling at the protein expression and secretion levels. The matrix remodelling proteins matrix metalloproteinase 2 (MMP-2) and 9 (MMP-9) are two key MMPs secreted from HSCs that degrade collagen[234], and a sensitivity of MMP and TIMP secretion by HSCs to external rigidity may underlie an important feedback loop that regulates the composition of the ECM in fibrosis.

To investigate the role of matrix stiffness on the function of MMP-2, MMP-9 and TIMP-1, HSCs were cultured on substrates of varying rigidity (4, 12 and 25 kPa), mimicking healthy and fibrotic liver tissue stiffnesses[221]. Then, changes in mRNA and protein expression and secretion of MMP-2, MMP-9, and TIMP-1 in response to external stiffness were assayed to analyse the possible mechanotransduction network that surrounds MMP-mediated ECM homeostasis. The hypothesis that the rigid environment created by fibrosis can modulate the expression and secretion of proteins, specifically MMP-9 and TIMP-1, to alter the ECM in either resolution or perpetuation of fibrosis has been tested. The results indicate that rigidity promotes the perpetuation of fibrosis as external stiffness downregulates the activity of MMP-9.

Aims:

- To assess the role of matrix stiffness on the expression and secretion of MMP-2, MMP-9 and TIMP-1
- To investigate the MMP-9 expression in human hepatocellular carcinoma tumour tissue

4.2 Results

4.2.1 Substrate rigidity inhibits MMP-9 gene expression

Fibrosis in the liver is associated with specific rigidities, as determined through ultrasound based transient elastography. Liver stiffness values below 6 kPa are designated as normal, with values around 8–12 kPa designated as advanced fibrosis and cirrhosis. Further disease progressions including portal hypertension and oesophageal varices have been shown to increase the stiffness to greater than 20 kPa[221].

It is hypothesized here that substrate stiffness would affect MMP-2, MMP-9 and TIMP-1 gene expression. To alter substrate stiffness without altering ligand density, fibronectin-coated polyacrylamide substrates were fabricated, where rigidity could be tuned by altering the ratio of acrylamide to bis-acrylamide. Since these substrates were coated with the same amount of fibronectin, the ligand density was constant across samples so only the effect of rigidity was observed. 4, 12, and 25 kPa rigidities were chosen to represent the progression from healthy to fully developed liver fibrosis, based on *in vivo* measurements[221]. HSCs were cultured on these polyacrylamide substrates of tuneable rigidity for 24 hours. It was observed that HSCs became more elongated and less rounded with increasing rigidity (Figure 4.1).

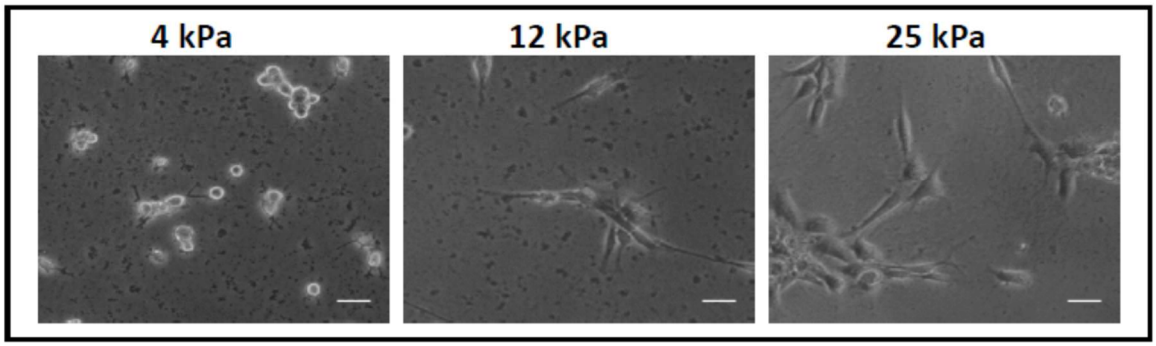

Figure 4.1 Changes in cell morphology are dependent on substrate stiffness. Hepatic stellate cells were cultured on 4 12 and 25 kPa substrates and after 24 hours the cell morphology was assessed. Scale bar represents 50 µm.

After cell collection, reverse transcription quantitative PCR was used to assess the relative mRNA levels of the target genes (Figure 4.2). GAPDH was chosen as a suitable housekeeping gene for normalization as its expression was unaffected by stiffness (Figure 4.3). It was observed that the expression of MMP-2 remained unchanged across rigidities. Interestingly, it

was observed that on 12 and 25 kPa substrates, expression of MMP-9 was greatly reduced in comparison to the 4 kPa substrate, indicating that MMP-9 expression is sensitive to external rigidity through mechanotransduction. Similar to MMP-2, it was observed that substrate stiffness did not significantly affect the TIMP-1 expression.

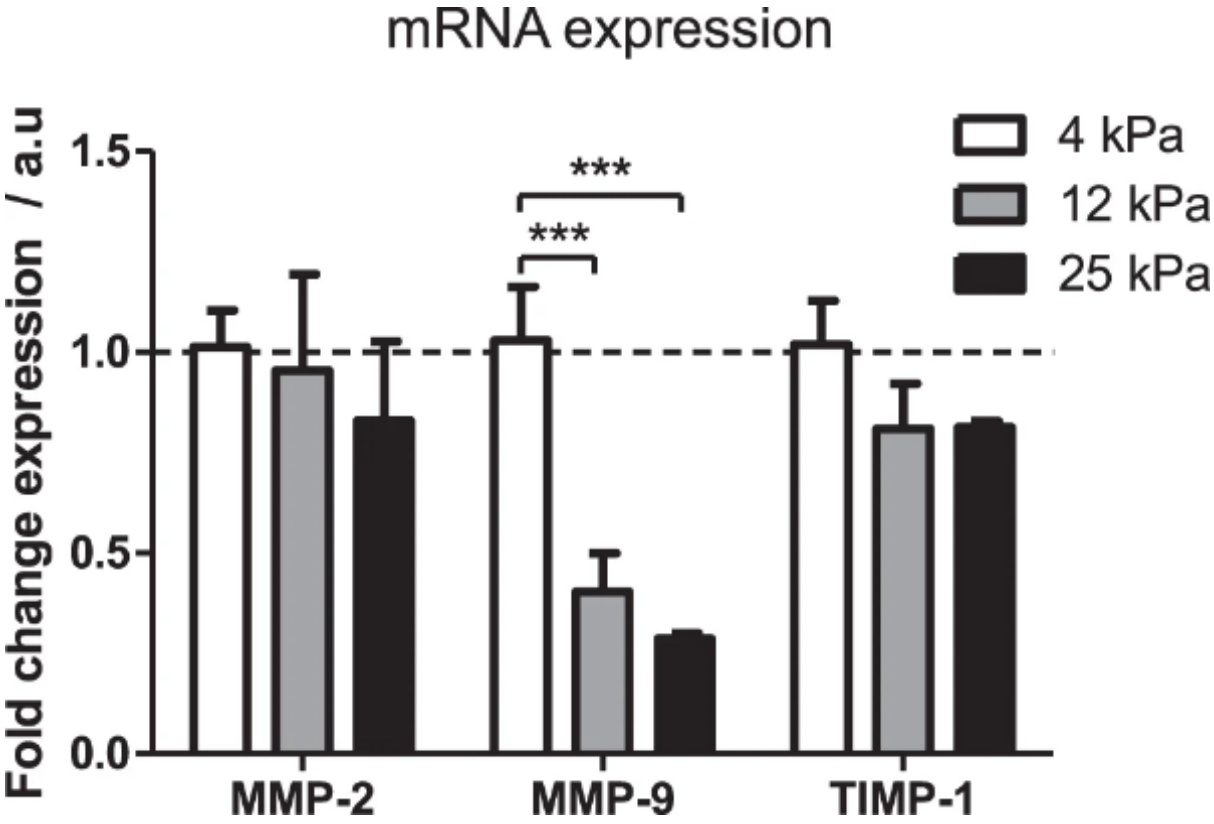

Figure 4.2 MMP-2, MMP-9 and TIMP-1 mRNA expression on different gel rigidities. mRNA expression of MMP-2, MMP-9, and TIMP-1 was assayed by RT-qPCR, normalised to control GAPDH mRNA and presented relative to 4 kPa sample. Data obtained from 3 separate experiments ($n = 3$). Results are expressed as mean ± s.e.m. ***Represents t-test, $p < 0.001$. Dashed line represents relative mRNA RT qPCR expression (normalized to GAPDH) value of 1.0.

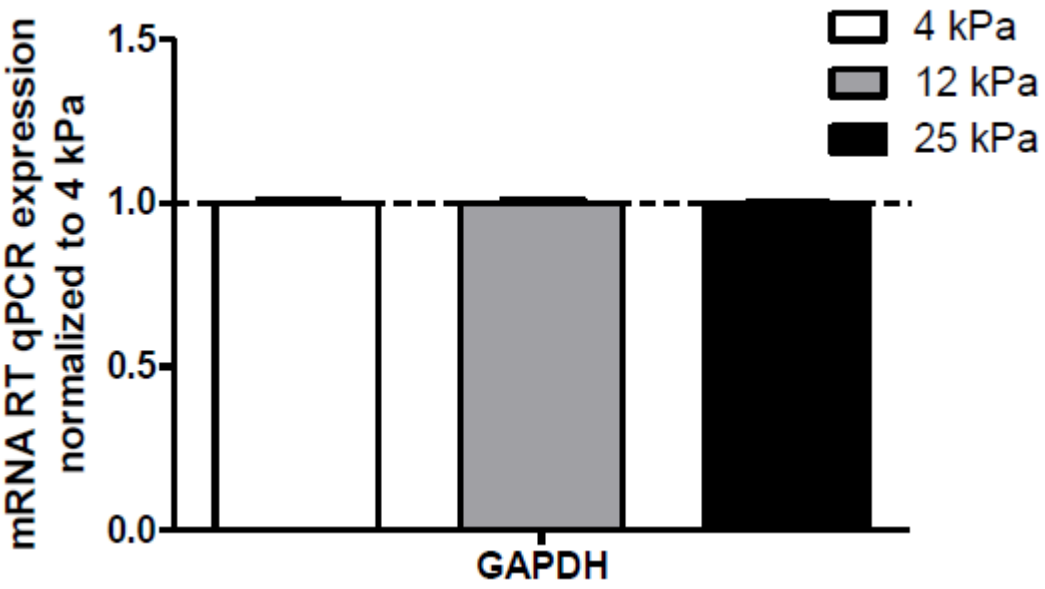

Figure 4.3 GAPDH mRNA expression in hepatic stellate cells does not change when cultured on different rigidity substrates. mRNA expression of GAPDH was assayed by RT-qPCR, relative to 4 kPa. Data obtained from 3 separate experiments (n=3). Results are expressed as mean ± s.e.m. *** represents t-test, $p < 0.001$

4.2.2 Substrate rigidity inhibits intracellular protein levels of MMP-9 and TIMP-1

The same experimental setup described in the previous section was used for Western Blot analysis, and performed to assess the intracellular protein expression of MMP-2, MMP-9 and TIMP-1 across different substrate rigidities (Figure 4.4, Figure 4.5). Though all these proteins have extracellular roles, the mechanical sensitivity of their intracellular protein abundance would indicate the breadth of the mechanotransduction network, and its ability to affect multiple points in ECM homeostasis signalling.

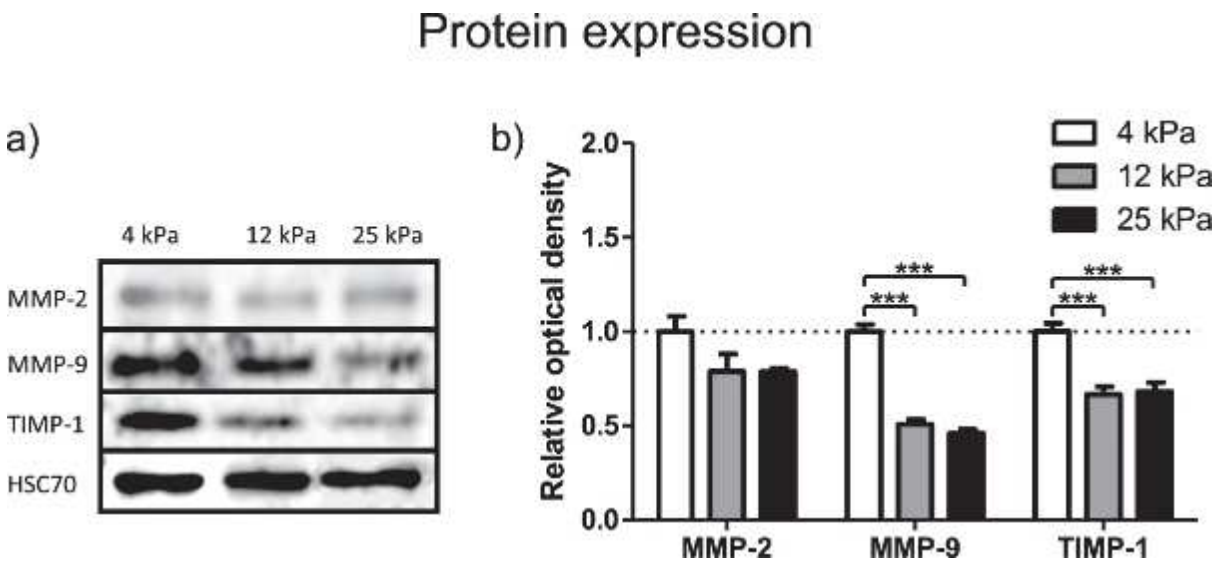

Figure 4.4 MMP-2, MMP-9 and TIMP-1 protein expression on different gel rigidities. (a) Protein expression of MMP-2, MMP-9 and TIMP-1 as assayed by Western Blot. HSC70 presented as control protein. (b) Optical density of Western Blot bands relative to 4 kPa sample. Data obtained from 3 separate experiments (n = 3). Results are expressed as mean ± s.e.m. ***Represents t-test, $p < 0.001$.

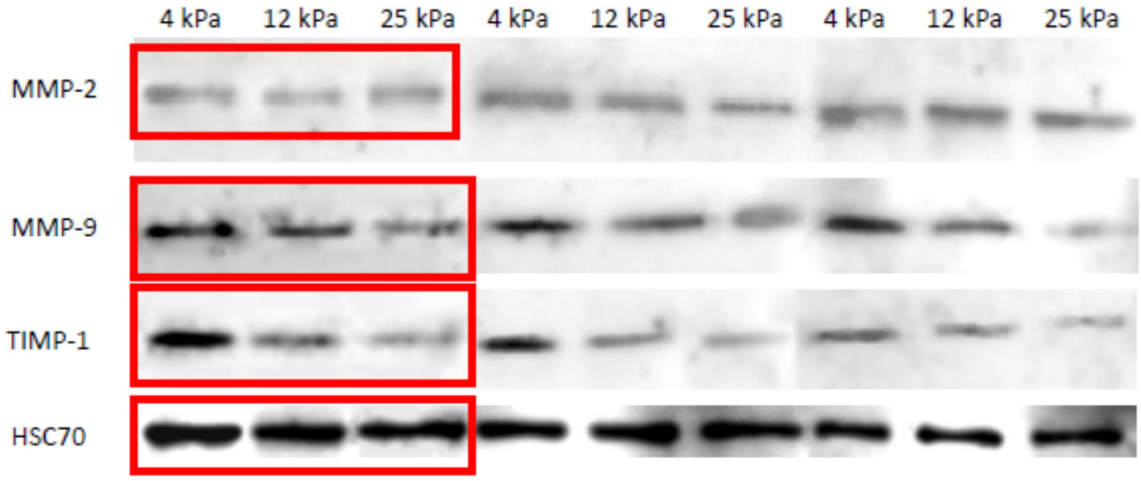

Figure 4.5 Western Blot analysis of protein expression in response to external rigidity. Full Western blot membrane images for MMP 2 MMP 9 TIMP 1 and loading control HSC 70. Rectangle marks the representative bands

The intracellular protein amount of MMP-2 was unchanged with increasing rigidity, equivalent to the trend observed in mRNA expression. Also, in agreement with mRNA expression, it was observed a marked and significant decrease (around 50%) of intracellular MMP-9 protein as rigidity increased from 4 to 25 kPa. Intriguingly, it was observed a significant decrease of 40% in the intracellular protein levels for TIMP-1 when rigidity was increased from 4 to 25 kPa, despite the observation that TIMP-1 mRNA levels were unresponsive to stiffness. This suggested to us a further mechanism by which TIMP-1 intracellular protein levels are regulated.

4.2.3 Substrate rigidity modulates the activity of secreted MMP-9 and TIMP-1

To learn more about the effect of matrix rigidity on the target enzyme's extracellular activity and to gain a more complete insight into the multi-level regulation of these proteins, enzyme activity assays were performed (Figure 4.6, Figure 4.7). After 24 hours of culture on 4, 12 or 25 kPa substrates, cell culture medium was changed to serum free medium for the next 24 hours and then collected for further examination. This medium therefore contained any secreted MMPs and TIMPs. Gelatin zymography was performed to assay MMP-2 and MMP-9 activity, where band intensity represents level of degradation. The inhibitory activity of TIMP-1 on MMP-9 was assayed by reverse gelatin zymography, where band intensity represents level of TIMP-1 activity i.e. inhibition of degradation. Recombinant MMP-2 and MMP-9 were used in adjacent lanes to confirm the position of MMP-2 and MMP-9 mediated degradation within the gel.

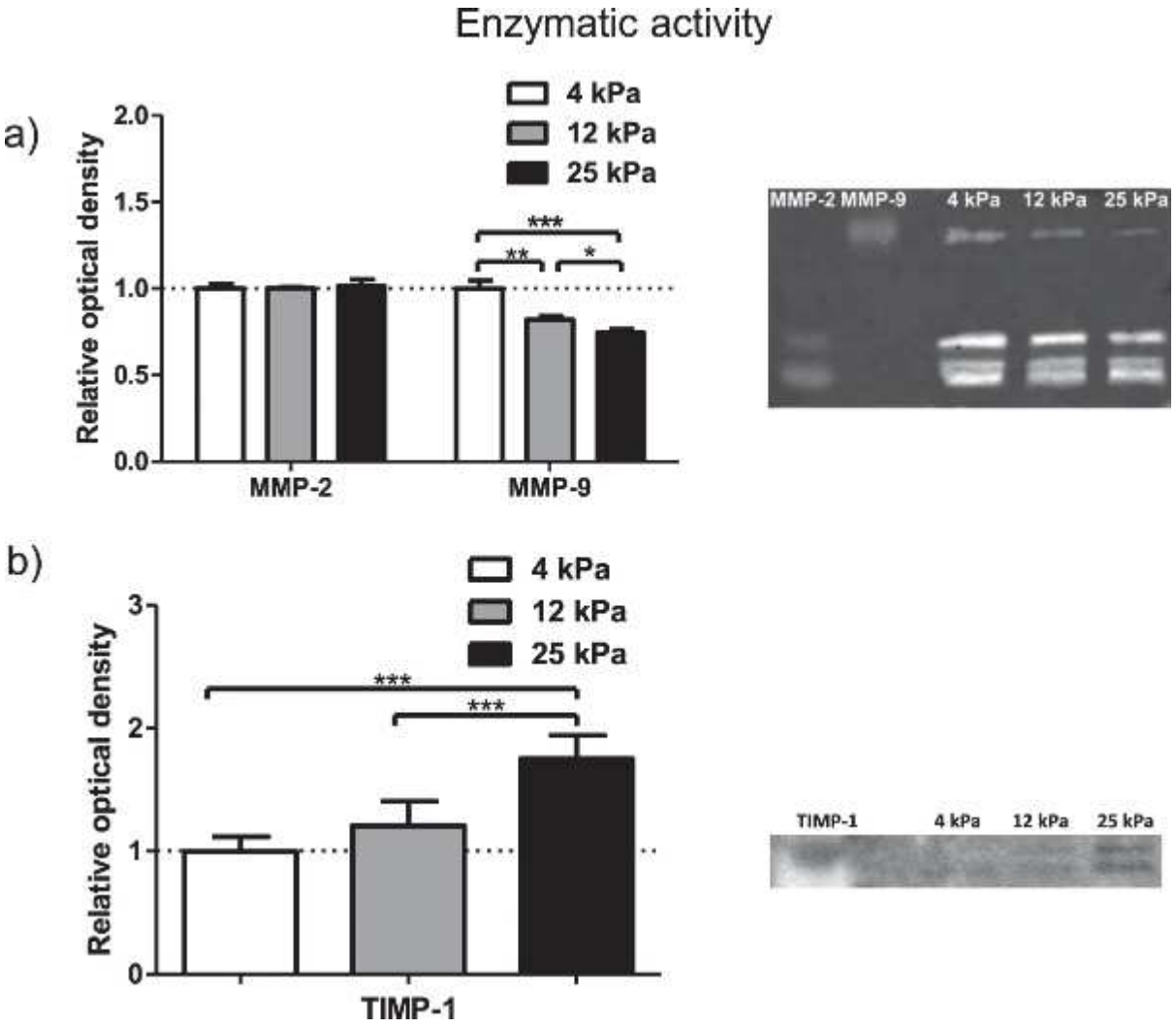

Figure 4.6 MMP-2, MMP-9 and TIMP-1 assayed activity on different gel rigidities. (a) Extracellular activity of MMP-2 and MMP-9 from HSC conditioned media assayed by gelatin zymography. Signal intensity of the bands presented relative to 4 kPa sample. Data obtained from 6 independent experiments. Results are expressed as mean ± s.e.m. *Represents t-test, $p < 0.05$, **$p < 0.01$, ***$p < 0.001$. (b) TIMP-1 activity assayed by reverse gelatin zymography. Signal intensity of the bands presented relative to 4 kPa sample. Data obtained from 6 independent experiments. Results are expressed as mean ± s.e.m. *** represents t-test, $p < 0.001$.

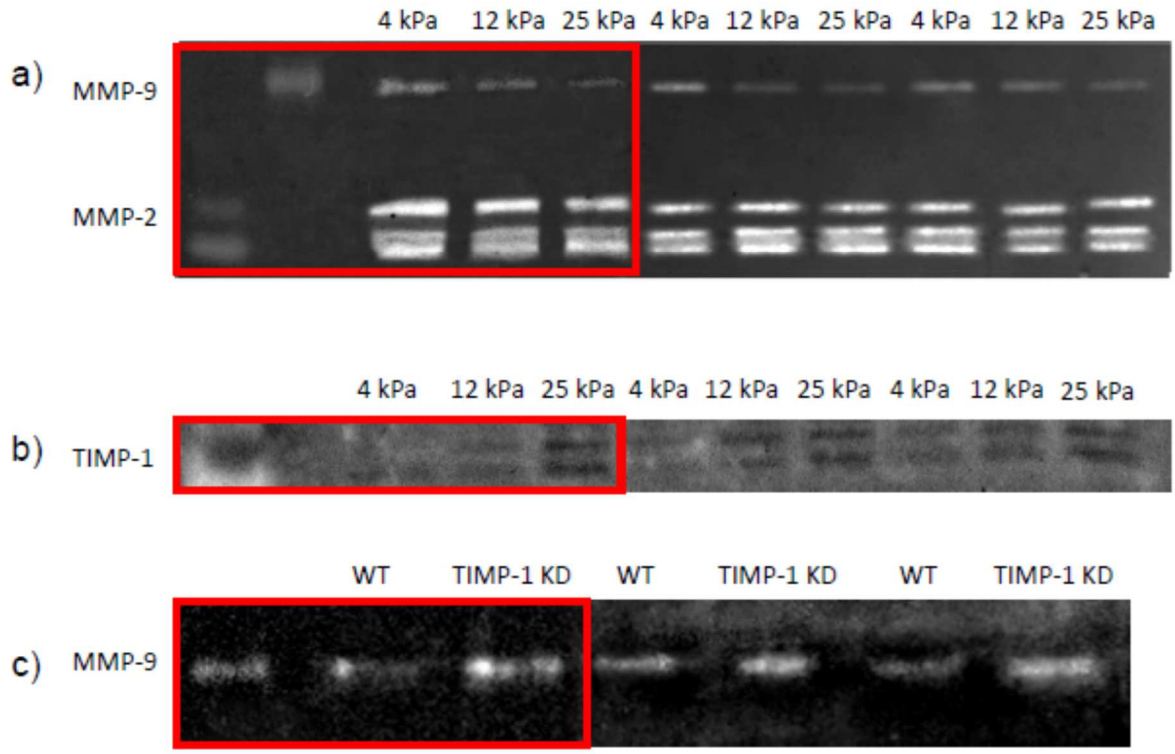

Figure 4.7 Enzymatic activity of MMP-9, MMP-2 and TIMP-1 in response to external rigidity assessed by zymography and reverse zymography Representative images of a) MMP-2 and MMP-9 zymography, b) reverse zymography of TIMP-1 in wildtype cells and c) MMP-9 zymography of TIMP 1 knockdown cells. Rectangle marks the representative bands

MMP-2 activity was constant on each substrate, in line with levels of mRNA and protein expression, showing a lack of mechanosensitivity. MMP-9 activity significantly decreased with increasing rigidity, with the 25 kPa condition showing 25% less activity than the 4 kPa condition. These observations are consistent with the previous results indicating that rigid substrates decreased MMP-9 expression at both the mRNA and protein levels, and this trend is continued through secretion. Furthermore, TIMP-1 activity was investigated and a significant increase was observed for 12 and 25 kPa substrate-cultured cells. These findings contrast with the decreased levels of intracellular TIMP-1 when rigidity increases. This difference suggests that the lower intracellular levels of TIMP-1 seen at 12 and 25 kPa may be caused by the higher TIMP-1 secretion observed at these rigidities, which depletes the intracellular pool but enriches the extracellular pool of TIMP-1.

4.2.4 TIMP-1 knockdown promotes extracellular MMP-9 activity

Since it was observed that TIMP-1 activity increased in response to increased matrix rigidity using reverse zymography, the relevance of this change in TIMP-1 activity with HSCs was

next quantitatively verified. HSCs were transfected with TIMP-1 siRNA to knockdown TIMP-1 (Figure **4.8**), and the enzyme activity of MMP-9 was assessed, to indicate how TIMP-1 directly affects the MMP-9 activity of the cells. A significant increase in MMP-9 activity of around 40% was observed when TIMP-1 siRNA was used (Figure 4.9), indicating that secreted TIMP-1 does indeed regulate MMP-9 activity in these cells. The large change in MMP-9 activity emphasises the importance of the observations that levels of both MMP-9 and TIMP-1 are mechanosensitive.

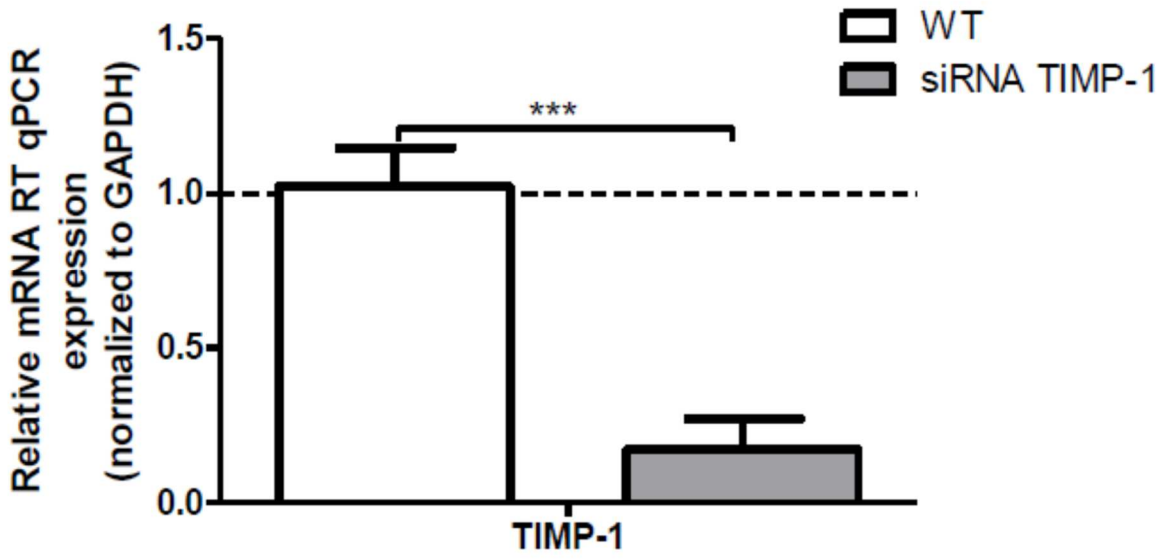

Figure 4.8 TIMP-1 mRNA expression in cells treated with TIMP-1 siRNA. mRNA expression of TIMP-1 was assayed by RT-qPCR, normalised to control GAPDH mRNA and presented relative to wildtype. Data obtained from 3 separate experiments (n=3). Results are expressed as mean ± s.e.m. *** represents t-test, $p < 0.001$

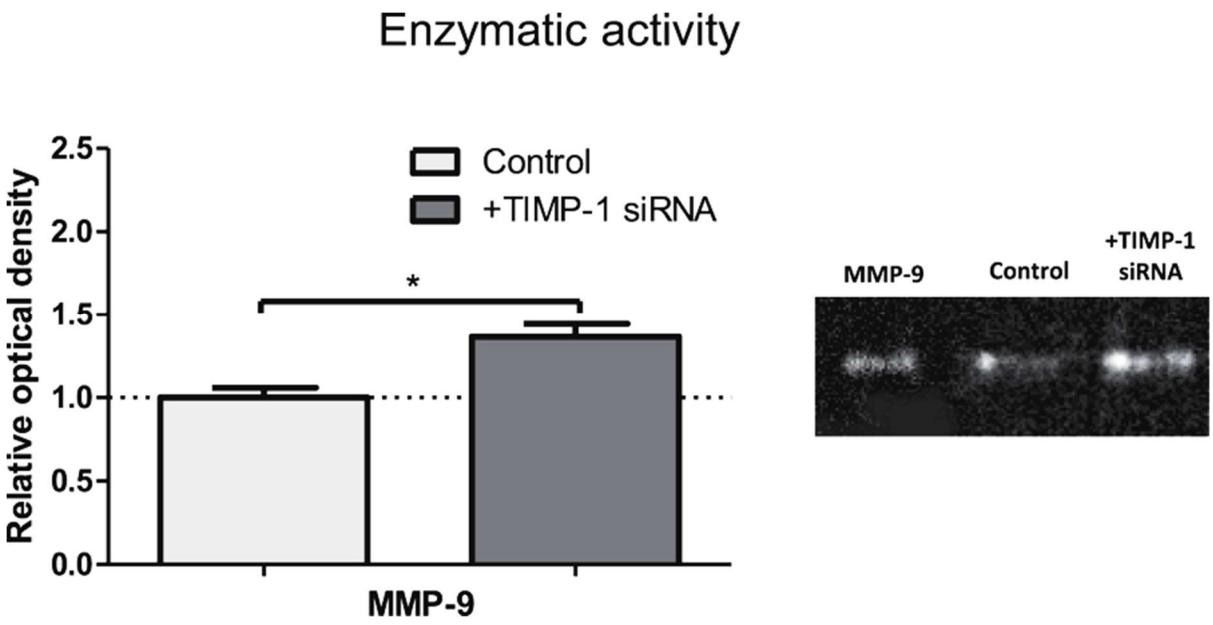

Figure 4.9 MMP-9 activity with TIMP-1 knockdown. MMP-9 zymography of HSC conditioned media from cell with or without TIMP-1 siRNA. Signal intensity of the bands presented relatively to untransfected control. Data obtained for 3 independent experiments. Results are expressed as mean ± s.e.m. * represents t-test, $p < 0.05$

4.2.5 MMP-9 is downregulated in HCC

Hepatocellular carcinoma (HCC) is characterised by fibrosis, with high levels of extracellular matrix proteins. This fibrosis is maintained within the disease state, often through upregulation of ECM protein production. Although it is known that upregulation of MMP-9 occurs with progression from healthy liver to HCC[235], the reported correlation between MMP-9 and HCC progression is related to the whole liver, and is not specific to HSCs. It was therefore tested whether downregulation of MMPs occurs in HSCs in HCC and would therefore promote the maintenance of the fibrotic stroma.

Immunofluorescence staining on human tissues was performed for control and HCC patients, using the activation marker α-SMA to identify activated stellate cells present within the tissue. Activated stellate cells were present in both healthy and HCC tissues, though at a lower level in healthy tissue (Figure 4.10). This increased presence of α-SMA in HCC correlates with previous studies that link α-SMA expression to HCC progression[236]. Significantly lower levels of MMP-9 were observed in activated HSCs in tissues from HCC patients than in healthy control patients, where the expression of MMP-9 in the activated HSCs present in HCC patients was almost negligible (Figure 4.10). This indicates that one of the methods by which HCC may

promote the disease state is through inhibition of MMP-9, which would otherwise degrade ECM components that contribute to fibrosis.

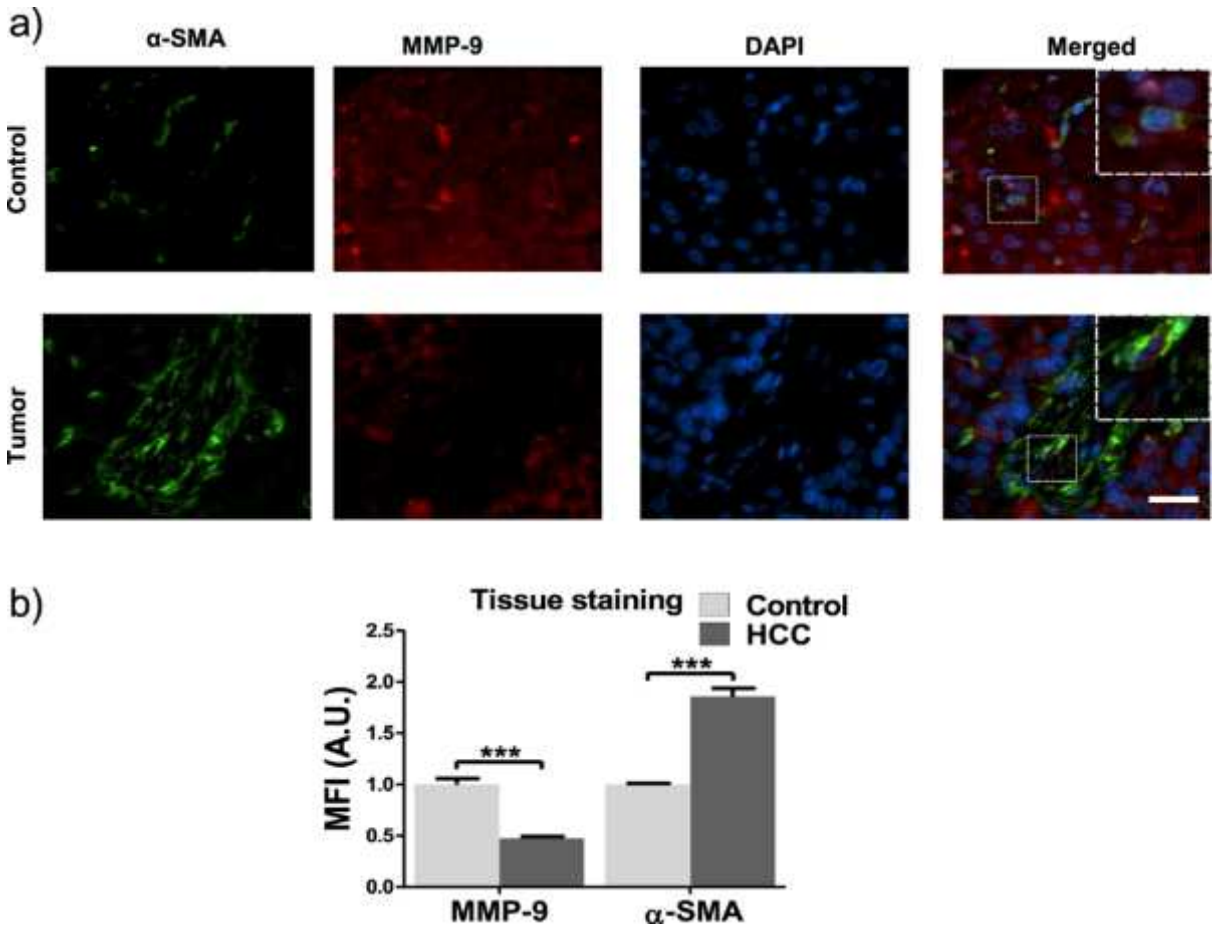

Figure 4.10 MMP-9 is downregulated in stromal tissues of HCC patients. (a) Representative images of tissue staining of stromal tissues from normal and HCC human patients, scale bar = 20 µm. Each image is a single slice as observed through immunofluorescence imaging. Inset represents magnification of area inside white square. (b) Quantification of MMP-9 and α-SMA (alpha smooth muscle actin) staining. Data was obtained from 20 HCC patients and 10 healthy patients. Bars represent mean ± s.e.m. ***Represents t-test, $p < 0.001$.

4.3 Discussion

Remodelling of the extracellular matrix (ECM) is a common occurrence in many processes that occur in the healthy liver, including wound healing and morphogenesis, and includes the regulated secretion of proteases that degrade the components of the ECM[237]. In disease states, including fibrotic diseases such as hepatocellular carcinoma (HCC), stromal remodelling is deregulated and the altered ECM influences disease progression[20]. An understanding of the sensitivity of remodelling enzymes, such as matrix metalloproteinases (MMPs), to

characteristics of this fibrotic ECM, such as rigidity, is of vital importance in understanding the disease[238].

Here, it is revealed that fibrotic matrix stiffness can decrease the activity of extracellular MMP-9 *in vitro* and achieves this through downregulation of MMP-9 at the gene expression level. Furthermore, rigidity promotes secretion of TIMP-1, without affecting its gene expression (Figure 4.11). This suggests a positive feedback loop in which the stiffness aspect of fibrosis, through mechanosignalling, promotes fibrosis perpetuation by inhibiting MMPs that catalyse ECM degradation. The evidence for this feedback loop was observerd at rigidities comparable to those in liver fibrosis[221]. The *in vivo* environment for HSCs is much more complex than the *in vitro* environment, where a multitude of biochemical and mechanical stimuli may promote or inhibit the proposed pro-fibrotic positive feedback loop. Tthe results are limited in that only the *in vitro* effect of matrix stiffness is analysed and should therefore be combined with future studies which analyse the role of other aspects of fibrosis, such as changes in ECM architecture, to fully resolve the mechanisms surrounding MMP-9 and TIMP-1 regulation.

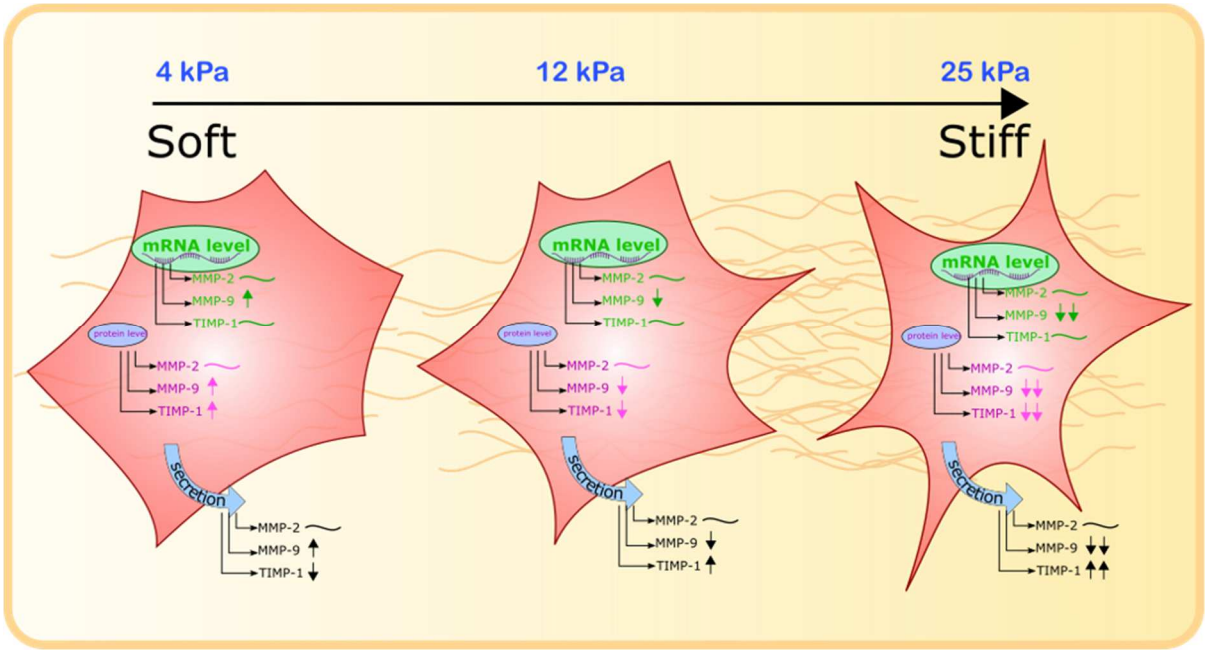

Figure 4.11 MMP-2, MMP-9 and TIMP-1 activity regulation on different gel rigidities. An illustration of matrix metalloproteinase 2 and 9 and tissue inhibitors of metalloproteinases 1 gene expression, protein expression and activity of secreted protein in cells cultured on different rigidity substrates. MMP-2 = matrix metalloproteinase 2, MMP-9 = matrix metalloproteinase 9, TIMP-1 = tissue inhibitor of metalloproteinases 1. ~ represents no change in levels, ↑ and ↓ represent up and downregulation respectively.

Though mechanisms that maintain MMP-9 and TIMP-1 levels in healthy homeostasis are not investigated here, it is proposed that in softer environments, the signalling pathways that modulate MMP-9 and TIMP-1 activity in response to high stiffness are not activated. Since MMP-9 expression at 25 kPa is still observed, albeit significantly reduced, this indicates that mechanotransduction of a soft substrate only partly promotes expression. *In vitro*, components of the cell culture medium likely promote a basal level of expression with further activation if the cell is on a soft environment. *In vivo*, the complex extracellular milieu also provides a wealth of possible signalling pathways promoting a basal level of expression, with external rigidity as an influencing factor.

Since it is shown that external rigidity alone affects MMP-9 and TIMP-1 activity, the importance of mechanotransduction of high rigidities is observed in liver fibrosis, in concurrence with studies that link the rigidity of the fibrotic liver to disease progression[239]. By using an *in vitro* system whereby culture conditions only differ in substrate rigidity, any difference in phenotype can only be described as a product of mechanotransduction. Though cells can also sense a soft environment through mechanotransduction, the results indicate that the activity of remodelling enzymes is sensitive to external rigidity. Mechanosensing of rigid substrates plays an important role in the progression of other cancers such as pancreatic ductal adenocarcinoma[240], as well as diseases such as cardiac hypertrophy and muscular dystrophy[241]. Therefore, the observed positive feedback system, i.e. increasing rigidity inhibits expression of MMP-9, may underlie the perpetuation of fibrosis in the liver.

The understanding of this previously unobserved mechanical network may have therapeutic applications, as drugs could be used that target either MMPs or TIMPs, or the specific proteins that link the mechanical environment to MMP or TIMP regulation. Overexpression of MMP-9 has been seen in animal models of abdominal aortic aneurysms, and treatment with doxycycline has been shown to downregulate this expression[242], suggesting the applicability of MMP-9 modulation in therapeutic approaches to other diseases. Therapeutics have also been developed against components of mechanosignalling networks[243], and therefore the results could be applicable in guiding therapeutic development that seeks to reduce fibrosis in the liver, by targeting the mechanical network linking the fibrotic environment to the mechanosensitive proteins that can degrade it.

The results reveal the mechanosensitivity of MMP-9 expression and secretion, as well as secretion of its inhibitor TIMP-1. This suggests a mechanosensitive feedback network in which

the rigid environment of fibrosis can prevent its own degradation by downregulating the activity of a protease that would otherwise degrade it.

4.4 Materials and methods

4.4.1 Tissues microarrays

Tissue microarray (TMA) blocks were constructed as previously described[244] using 20 archival paraffin-embedded HCC tissue blocks and 10 healthy controls retrieved from the Imperial College London Tissue Bank (Ethical Approval nr.R15058). A consultant histopathologist reviewed all the materials prior to inclusion on freshly cut haematoxylin & eosin (H&E) slides. TMA blocks were constructed using an MTA-1 Microarrayer (Mitogen, UK) following H&E-slide guided microdissection of target tumour and surrounding non-tumorous areas. The triplicates of 1 mm cores from separate central and peripheral areas of tumour and matching surrounding liver were obtained. Adequate sampling of target tissues was confirmed on a freshly cut H&E section from the recipient TMA block before downstream analysis.

4.4.2 Cell culture

Primary culture-activated human hepatic stellate cells (passage 3–6, HHStec #5300 – ScienCell) were cultured at 37 °C, 5% CO_2 in culture medium containing DMEM/Nutrient Mixture F-12 Ham (D8437, Sigma), 10% FBS (10270-106, Gibco), 1% penicillin/streptomycin (Sigma Aldrich, USA) and 1% fungizone (15290-026, Gibco). For the polyacrylamide substrate experiments, HSCs were detached from culture flasks with trypsin and i) seeded on polyacrylamide gels with different rigidities for zymography (or immunofluorescence) staining; ii) transfected with TIMP-1 siRNA (sc-29505, Santa Cruz Biotechnology) on glass for MMP-9 zymography. For this purpose, cells were transfected according to the manufacturer's protocol with 2.2 pmoles of TIMP-1 siRNA using interferIN (409-10, Polyplus) 24 hours after seeding.

4.4.3 Polyacrylamide substrate fabrication

Coverslips were dipped in 0.1 M NaOH and left to dry. Dried coverslips were coated with 4.0% (3-aminopropyl)triethoxysilane (281778, Sigma) and washed with dH_2O. Coverslips were dried and transferred to 2.5% glutaraldehyde (G6257, Sigma)/PBS and incubated at room temperature for 30 minutes, twice washed in dH_20 and left to dry at room temperature. Polyacrylamide gels of 4, 12 and 25 kPa mimicking healthy and fibrotic liver stiffnesses[221] were prepared according to the protocol adapted from Wen *et al*.[36] (Table 1). Gel stiffness was varied by adding 29:1 acrylamide/*bis*-acrylamide to a final concentration ranging from 4.7–10%. A working solution of PBS, acrylamide/*bis*-acrylamide (29:1) 40% vol (A7802, Sigma), TEMED (T9281, Sigma) and 10% ammonium persulfate were mixed at concentrations to achieve varying gel stiffness. A small drop of this working solution was applied to activated coverslips which were placed face down on hydrophobic, dichlorodimethylsilane (440272, Sigma) treated glass microscope slides and left to polymerise at room temperature for 45 minutes. Gel-coated coverslips were removed and stored in PBS at 4 °C.

To allow polyacrylamide gels to be coated with ECM proteins, gels were functionalised to expose NHS groups. For functionalisation, polyacrylamide gels were washed with PBS and coated with 50 µL Sulfo-SANPAH (sulfosuccinimidyl 6-(4′-azido-2′-nitrophenylamino)hexanoate) (803332, Sigma) (5 mg/mL, PBS) solution per coverslip and activated with UV light for 10 minutes. Polyacrylamide gels were washed with PBS and coated with human plasma fibronectin (F8095, Sigma) (10 µg/mL, PBS) and incubated for 1.5 hr at room temperature. Gels were washed once with PBS and cells were seeded on gels in culture medium. The same procedure was used for large area microscope slide preparation for proteoanalysis and genetic analysis.

4.4.4 Western blot

Cell lysates from cells cultured on polyacrylamide gels were prepared with radio immunoprecipitation assay (RIPA) buffer (89900, Thermo-Fisher) and a protease inhibitor cocktail (78440, Thermo-Fisher) for 10 minutes on ice. Lysates were sonicated and clarified by centrifugation at 9600 × G, at 4 °C for 10 minutes. Protein concentration was determined by DC protein assay (500-0116, Bio-Rad). Samples were separated by 12% SDS-polyacrylamide gel electrophoresis and transferred to a PVDF membrane. Membranes were blocked with 5% Bovine Serum albumin (BSA, A8022, Sigma) and 0.1% Tween-20 (P1379, Sigma) in PBS for

30 minutes. Primary antibodies were prepared in blocking solution and incubated overnight at 4 °C (MMP-2 – sc-10736, Santa Cruz, MMP-9 – sc-10737, Santa Cruz, TIMP-1 – sc-5538, Santa Cruz, HSC70 – sc-7298, Santa Cruz). The membrane was washed three times in 0.1% Tween-20/PBS and incubated with horseradish peroxidase (HRP) conjugated secondary antibodies for 1 hour. Following three washes in 0.1% Tween-20/PBS, membranes were developed using Luminata crescendo HRP substrate (WBLUR0100, Millipore) and Syngene GeneGnome. Band intensities were analysed via the band densitometry plugin in ImageJ.

4.4.5 Quantitative PCR

Total RNA was extracted from cells cultured on polyacrylamide gels for 24 hours with RNeasy Mini Kit (74104, Qiagen), according to the "RNeasy mini quick start protocol". RNA template was reversed transcribed into cDNA by High-Capacity RNA-to-cDNA kit (4387406, Thermo-Fisher) according to manufacturer's instructions. Quantitative real-time PCR was performed on a StepOne Plus Real-Time PCR system (Applied Biosystems) using SYBR Green PCR Master Mix (4309155, Thermo-Fisher). Relative gene expression was analysed by the ΔCt method with 3 targets: MMP-2, MMP-9, TIMP-1, and final values were normalised using ΔCt for GAPDH gene mRNA as a value of 1.0. Primer sequences were as followed: MMP-2 (F) TCTCCTGACATTGACCTTGGC, (R) CAAGGTGCTGGCTGAGTAGATC; MMP-9 (F) TTGACAGCGACAAGAAGTGG, (R) GCCATTCACGTCGTCCTTAT; TIMP-1 (F) TCAACCAGACCACCTTATACCA, (R) ATCCGCAGACACTCCAT; GAPDH (F) ACAGTTGCCATGTAGACC, (R) TTTTTGGTTGAGCACAGG.

4.4.6 Gelatin zymography and reverse zymography

The zymography resolving gel was prepared with 4.6 ml sterile distilled water, 2.7 ml 30% acrylamide, 2.5 ml 1.5 M Tris (pH 8.8), 100 µl 10%SDS, 285 µl 2.8 mg/ml gelatine (porcine skin type A gelatine, Sigma, G2500), 6 µl TEMED and 100 µl 10%APS to reach 8% acrylamide concentration. The reverse zymography gel was prepared by adding MMP-9 to the gel described before to reach 10 ng/ml concentration. Stacking gel was prepared with 3.4 ml sterile distilled water, 830 µl 30% acrylamide, 630 µl 1 M Tris (pH 6.8), 50 µl 10%SDS, 5 µl TEMED and 50 µl 10% APS. The conditioned medium was collected from HSCs cultured on polyacrylamide gels for 24 hours before replacing culture medium with serum free medium, DMEM/Nutrient Mixture F-12 Ham (D8437, Sigma) for a further 24 hours was added to non-

reducing Laemmli buffer. Control marker samples for the zymography were prepared from recombinant human MMP-2 (Calbiochem, PF037) and recombinant human MMP-9 (Calbiochem, PF038) 10 ng/ml and 20 ng/ml respectively and for the reverse zymography natural human TIMP-1 (Abcam, ab157282) 10 ng/ml, then added to non-reducing Laemmli buffer.

Samples and standards were loaded onto the gelatine gel and run for 50 minutes at 200 V using Novex® Tris-Glycine SDS Running Buffer (10X) (Novex, cat. LC2675). Sample volumes were the same for all samples, taken from conditioned media from culture of the same number of cells. Then, the gel was carefully removed from the cassette and placed in an airtight container and washed with 2.5% (v/v) Triton X-100, in sterile distilled water 4 times for 15 minutes. The gel was developed with developing buffer (10 ml 1 M Tris (pH 7,5), 8 ml 5 M NaCl (Fisher Scientific, cat. BP358), 1 ml 1 M $CaCl_2$ (Sigma, cat. C7902), 1.6 ml 2.5%Triton X-100 and 179.4 ml sterile distilled water). 20 ml developing buffer was added and incubated overnight at 37 °C. Coomasie blue staining solution was prepared with 0,5 g Brilliant Blue (Sigma, cat.27816-25G), 250 ml methanol, 100 ml acetic acid (Sigma, A6283-100 ml) and 150 ml sterile distilled water. After incubation, the gel was carefully transferred to a plastic box and stained with Coomasie blue for 1 hour, followed by decanting of the staining solution. The gel was rinsed with destaining solution containing 1.5 l methanol, 50 ml Formic acid (Sigma, cat. F0507) and 3.5 l sterile distilled water. After achieving the desired destaining grade, zymography = transparent, digested bands and blue background, reverse zymography = clear background and blue bands, the gel was photographed with a UVP Biospectrum 500 Imaging System. Band digestion intensity, representing potential MMPs activity, was calculated using the ImageJ densitometry plugin.

4.4.7 Immunostaining

For α-SMA and MMP-9 staining, FFPE blocks were sectioned, deparaffinised and rehydrated as described previously[245]. Antigen retrieval was performed by incubating the sections in boiling citrate buffer (pH 6) for 45 minutes and cooled down at room temperature for 25 minutes. α-SMA antibody (Abcam, UK, ab7817, 1/50), MMP-9 (Santa Cruz Biotechnology, sc-10737, 1/50) and secondary goat anti-mouse AlexaFluor 488 (Life Technologies, Paisley, UK; A-11029, 1/200) and goat anti-rabbit AlexaFluor 546 (Life Technologies, Paisley, UK; A-11003, 1/200). Antibodies were used following the abcam TBS based staining protocol

(https://www.abcam.com/protocols/immunostaining-paraffin-frozen-free-floating-protocol). Stained sections were mounted with ProLong® Gold Antifade with DAPI (Life Technologies, USA). Images from immunofluorescence staining were acquired using a Nikon Ti-e microscope. Mean fluorescence intensity was quantified using Fiji software by measuring the mean grey value in the MMP-9 channel for the randomly selected regions showing α-SMA positive staining. The values obtained from the different regions of the same tissue sections were averaged and treated as one experimental replicate. The final result was calculated for n = 20 HCC and 10 healthy patients per condition.

4.4.8 Statistics

Results were analysed using Prism software (GraphPad, La Jolla, CA,USA). A 2-tailed Student's t-test for unpaired data was used to calculate the difference between mean values, *$p < 0.05$, **$p < 0.01$, ***$p < 0.001$.

5 Matrix stiffness promotes membrane tension and caveolae-dependent exocytosis

5.1 Introduction

The cytoskeleton of a cell is linked to its physical environment through membrane protein complexes such as focal adhesions, and generates contractility to equilibrate the forces present in the extracellular matrix (ECM)[246]. Membrane-cytoskeletal adhesions, as well as hydrostatic pressure, generate tension within the plasma membrane and this can affect a wide range of cellular processes[247]. For example, the plasma membrane is highly dynamic during cell migration, and upregulation of membrane trafficking i.e. endocytosis and exocytosis, is required for control of membrane tension[248]. It is currently unknown whether the plasma membrane, with mechanical properties dictated by its composition and associated molecules[249], is itself mechanosensitive.

The transduction of environmental stimuli by cells is often performed by integrins, heterodimeric transmembrane receptors which attach to ECM proteins and mediate intracellular biochemical signalling. Integrins are also involved in mechanosensing, where they promote Rho-dependent actomyosin contractility and cytoskeletal stiffening in response to external stiffness[28]. The different isoforms of the α and β subunits provide variety in integrin function, e.g. β_1 integrins provide adhesive strength whereas β_3 integrins enable mechanotransduction[250]. β_1 integrins have even been shown to become activated in the absence of ligand interaction, through membrane tension-dependent signalling crosstalk when the uPAR receptor interacts with vitronectin[251].

Membrane tension can be buffered by regulation of membrane area, with exocytosis decreasing tension by providing greater area to the membrane[248]. Caveolae, small invaginations of the plasma membrane rich in the transmembrane protein caveolin-1, are known to rapidly flatten in response to increased membrane tension increasing membrane area[252]. The formation of caveolae occurs when exocytic caveolar carriers, rich in caveolin-1, cholesterol and glycosphingolipids, are trafficked from the Golgi complex to the plasma membrane[253]. The full incorporation of vesicles such as caveolae into the membrane is facilitated by the GTPase dynamin-1[254]. Furthermore, caveolin-1 expression has been shown to regulated by matrix stiffness.

Here it is shown that external rigidity increases membrane tension in hepatic stellate cells in a mechanism dependent on β_1 integrin and RhoA. Membrane tension is further observed to promote caveolae formation and exocytosis, achieving this by promoting the abundance of dynamin-1 at the plasma membrane.

Aims:

- To investigate the signalling pathway involved in plasma membrane stiffening in response to substrate rigidity
- To assess the effect of membrane stiffening on exocytosis and caveolae formation

5.2 Results

5.2.1 Substrate rigidity promotes membrane and cytoskeletal stiffening

Mechanosensing of ECM rigidity occurs in many cell types, including hepatic stellate cells (HSCs), which respond to liver injury with wound healing but can become dysregulated in hepatocellular carcinoma and promote desmoplasia and tumorigenesis[233].

Membrane tension is affected by the mechanical properties of the cytoskeleton[255], suggesting that matrix stiffness can promote membrane tension. To assess this, HSCs were seeded on fibronectin-coated polyacrylamide gels of tuneable rigidity[125,174] to analyse their response to external stiffness. These gels vary only in stiffness and not ligand density, and so allowed us to specifically assess mechanosensing.

Atomic force microscopy (AFM) was used to probe the elasticity of the plasma membrane[256,257]. By limiting the cantilever approach velocity to 2 μm/s and the voltage set point to 0.1 V, it was ensured that the fitting of the Hertz contact model would provide Young's modulus values relevant to membrane, and not cytoskeletal, stiffness (Figure 5.1 a). It was found that with cell membrane stiffness increased from 1 kPa on a 4 kPa substrate to around 3.6 kPa on a 25 kPa substrate, indicating mechanosensing (Figure 5.1 b). Similarly, it was confirmed that cytoskeletal stiffness also increased with substrate rigidity, with softer cells (0.6 kPa) on a 4 kPa substrate and stiffer cells (1.5 kPa) on a 25 kPa substrate. The results indicate that cytoskeletal stiffness is less than membrane stiffness, consistent with a previous study[258].

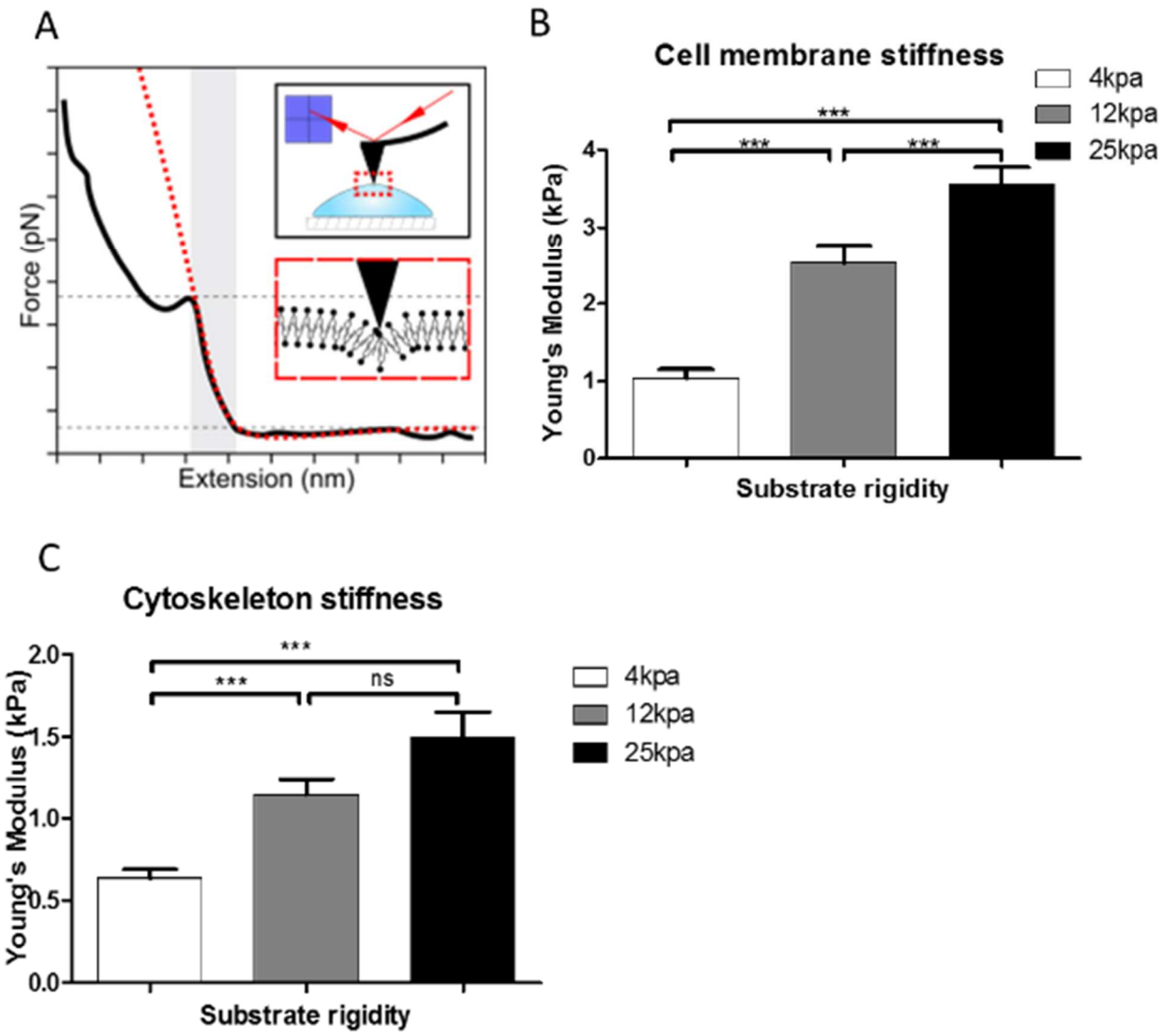

Figure 5.1 Substrate rigidity affects the membrane and cytoskeleton stiffness. (a) Schematics of the AFM cell membrane indentation for the Young's Modulus measurements. (b) Cell membrane stiffness and (c) cytoskeleton stiffness on 4, 12 and 25 kPa polyacrylamide substrates measured as Young's Modulus. Histogram bars represent mean ± SEM. Data are representative of 3 independent experiments and 100 cells analysed in (b) and (c), *$p < 0.05$, ***$p < 0.001$, n.s. non-significant.

5.2.2 Membrane mechanosensing requires β1 integrin

Integrins are key molecules in mechanosensing, and different isoforms of subunits generate variety in the specific function of integrins. β1 integrins are involved in sustaining adhesion with large forces whereas β3 integrins initiate mechanotransduction via intracellular signalling proteins such as talin[250].

To examine the roles of integrins in mechanosensing by plasma membranes, the membrane stiffness values for HSCs were determined in the presence or absence of integrin blocking antibodies. The membrane stiffness of control cells on a 4 kPa substrate was significantly reduced to around 700 Pa when β1 integrin was blocked. No significant difference from control was observed when a β3 blocking antibody was used, giving a membrane stiffness around 1000 Pa (Figure 5.2 a).

On a 25 kPa substrate, control HSCs showed a higher membrane stiffness (around 3.3 kPa) than on a 4 kPa substrate, indicating mechanosensitivity in concurrence with the results with HSCs. Blocking of β1 integrin significantly reduced the membrane stiffness to around 800 Pa, similar to that of control cells on a soft substrate. As before, a β3 blocking antibody did not significantly alter membrane stiffness, giving a value around 3.0 kPa (Figure 5.2 b). These results collectively indicate that HSCs require β1 integrin for robust mechanotransduction of external stiffness into membrane stiffness.

To confirm that β1 integrin is essential in dictating membrane stiffness in other cell types, primary epithelioid cell lines isolated from mice where β1 integrin was either knocked out or overexpressed were used. For cells on both 4 and 25 kPa polyacrylamide gels, β1 integrin knockout gave significantly reduced membrane stiffness values compared to values when β1 integrin was overexpressed (Figure 5.2 c). These results indicate that the link between membrane stiffness and β1 integrin is not specific to HSCs but may be generalisable to other cell types.

RhoA GTP-ase takes part in many actin-dependant cellular processes, such as adhesion, cell contraction or stress fibre formation[259]. It has also been shown to be regulated by β1 integrin to regulate actin cytoskeleton in myoblasts[260]. RhoA activity is required for cortical retraction and stiffening during the mitotic cell rounding, what indicates its potential role in membrane mechanosensing in conjunction with β1 integrin.

Here, it is hypothesized that by blocking or activating RhoA, altering the physiological response to the substrate stiffness[261], it is possible to affect the cell membrane stiffening. To examine it, membrane tension probe FLIPPER-TR was used for fluorescence lifetime measurements (FLIM microscopy) for the HFF cells on 4 and 25 kPa substrates in the presence of the RhoA activator or inhibitor. Wildtype control cells on a stiffer substrate showed increased fluorescence lifetime (around 5500 ps) and therefore higher membrane tension[262] in

compare to the 4900 ps lifetime of the cells on a softer substrate (Figure 5.2 d, e), confirming the AFM readouts.

To confirm the RhoA role in membrane response to the substrate stiffness, the fluorescence lifetime of the FLIPPER-TR probe was measured for the cells treated with the RhoA inhibitor or RhoA activator. For HFF cells on both substrates treatment with the RhoA activator resulted in an significant increase in fluorescence lifetime (the indicator of membrane tension), whereas RhoA inhibition on 25 kPa substrate significantly decreased the fluorescence lifetime, below the levels of the wildtype control and to the levels of 4 kPa control (Figure 5.2 d, e). RhoA inhibition in the cells on 4 kPa gave a value statistically indifferent to the wildtype control, indicating potential base threshold for the RhoA dependant membrane mechanosensing.

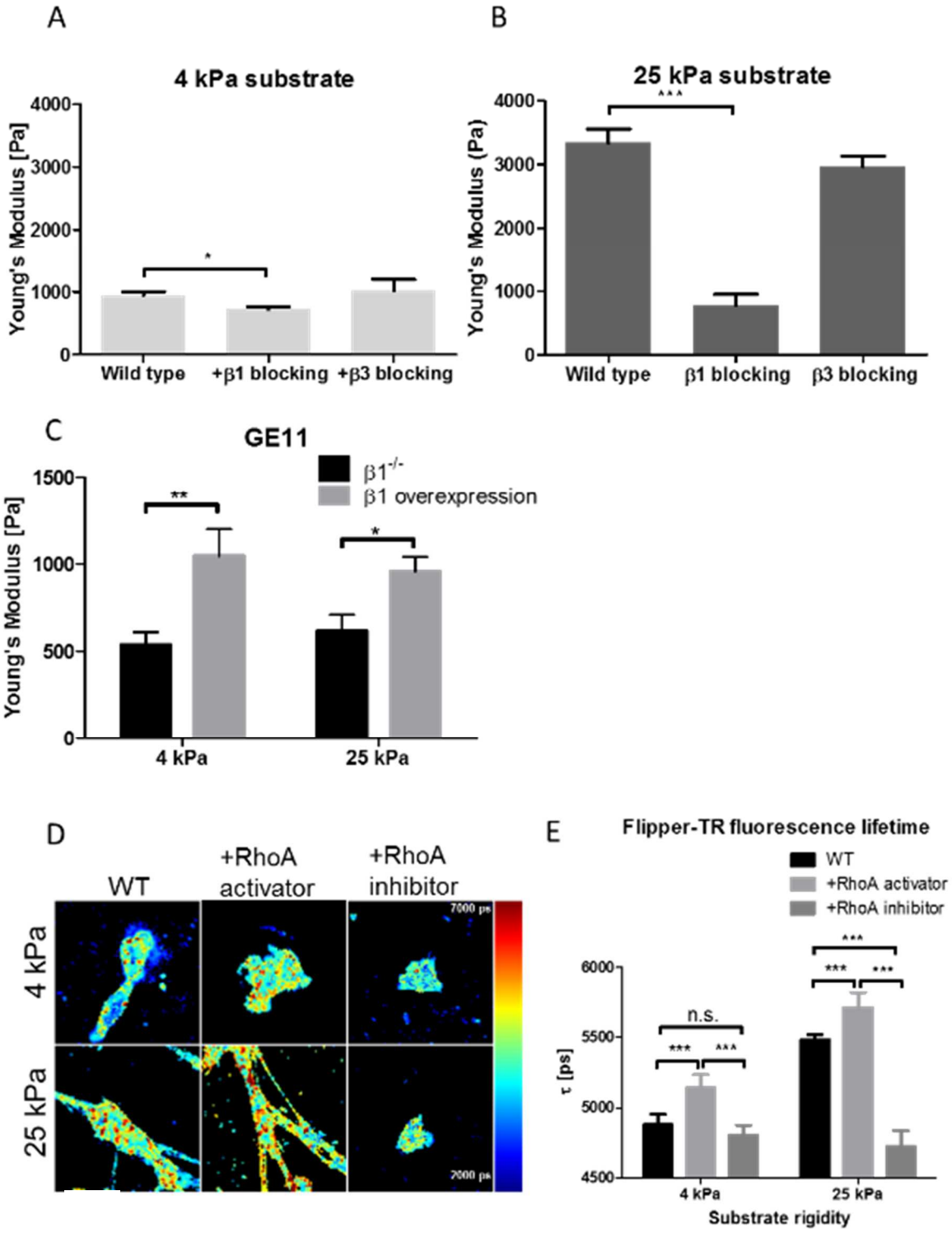

Figure 5.2 β1 integrin and RhoA activity are required for substrate-stiffness membrane mechanosensing. Cell membrane Young's Modulus with β1 or β3 integrin blocking in the HSC cells on (a) 4 kPa and (b) 25 kPa substrates. (c) Cell membrane stiffness of the GE11 cells with β1 integrin knockout or β1- overexpression. (d) Representative images and (e) quantification of the FLIPPER-TR membrane tension probe fluorescence lifetime in wildtype, with RhoA activator or with RhoA inhibitor treated HFF cells. Histogram bars represent mean ± SEM. Data are representative of 3 independent experiments and 15 cells analysed for each condition, *p < 0.05, **p < 0.01, ***p < 0.001, n.s. non-significant. Scale bar represents 50 µm.

5.2.3 Substrate rigidity and membrane tension promote caveolae formation

Since membrane tension increases with matrix stiffness, it is likely that a negative feedback loop to reduce membrane tension is also activated in response. Caveolae flattening is a rapid method (< 5 minutes) for increasing membrane surface area in response to tension and has been observed in HeLa cells, with regulation of endocytosis and exocytosis suggested as longer term regulators[252]. Caveolin-1 activity has been previously observed to be response to external stiffness, promoting intracellular signalling pathways such as β1 integrin internalisation[263] and YAP nuclear translocation[264]. Furthermore, caveolae formation has also been shown to be associated with cytoskeletal contractiltiy[265].

The above studies indicate the possibility of caveolae trafficking as a key response to matrix stiffness and membrane tension. As such, the presence of caveolae was analysed on cell membranes for different external conditions.

To count the number of caveolae present on cell membranes, focused ion beam scanning electron microscopy (FIB SEM) was used. For slices of each cell, the total number of visible invaginations was counted and normalised for the length of the slice (Figure 5.3 a). It was observed that on 4 kPa gels, HSCs showed a significantly reduced presence of invaginations (around 1 per micron) compared to HSCs on 25 kPa gels (around 2 per micron).

For further investigation, caveolin-1 was stained for, and TIRF imaging was used to measure the average vesicle size and density for cells on 4 and 25 kPa gels. It was observed that on the softer gels, vesicles were significantly smaller (0.5 µm2) compared to cells on the stiffer gels (0.8 µm2) (Figure 5.3 b). Similarly, stiffness increased the vesicle density from 0.035 µm-2 on soft to 0.055 µm-2 on stiff gels.

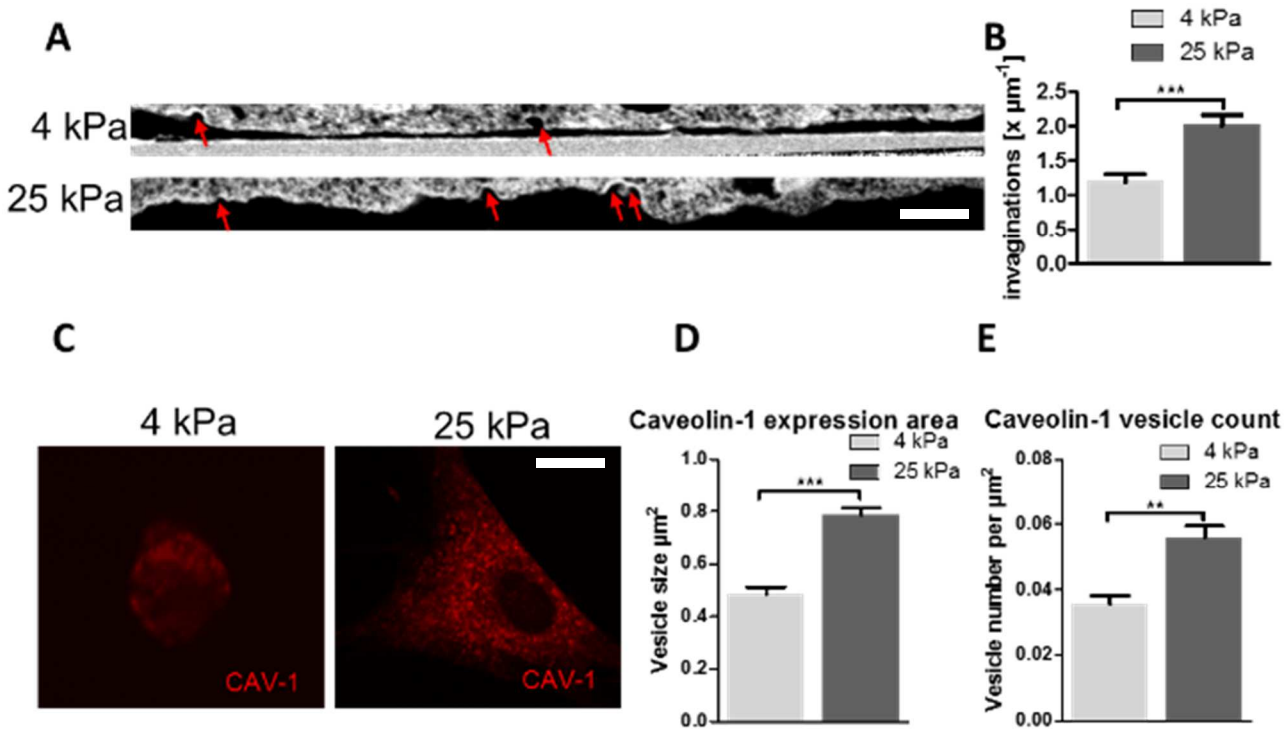

Figure 5.3 Substrate stiffness effect on caveolae formation. (a) FIB SEM images of the plasma membrane cross-sections, red arrows mark caveolae, and (b) quantification of the number of invaginations per µm of membrane cross-section for the cells on 4 and 25 kPa substrate. Scale bar in (a) represents 200 nm (c) Caveolin-1 mCherry TIRF microscopy images, (d) caveolin-1 expression area and (e) caveolae count per μm^2 for the cells on 4 and 25 kPa substrates. Scale bar in (c) represents 50 µm. Histogram bars represent mean ± SEM. Data are representative of 3 independent experiments and 15 cells analysed for each condition, $^{**}p < 0.01$, $^{***}p < 0.001$

To determine the specific contribution of membrane tension and rule out substrate stiffness effects that occur independently, the tonicity of the solution was altered. A hypotonic solution has a lower concentration of solutes than an isotonic solution, leading to osmosis of water into cells and an increased membrane tension. As such, hypotonic media is an established approach for altering membrane tension in vitro[266].

Using FIB SEM, it was observed that the number of invaginations present on cell membranes in hypotonic media (150 mOsm), i.e. high membrane tension, was significantly higher than in isotonic media, i.e. lower membrane tension (Figure 5.4 a). Furthermore, vesicle area and density were also higher in hypotonic media (Figure 5.4 b). This indicates that membrane tension promotes the formation of large vesicles and is likely to act downstream of matrix stiffness.

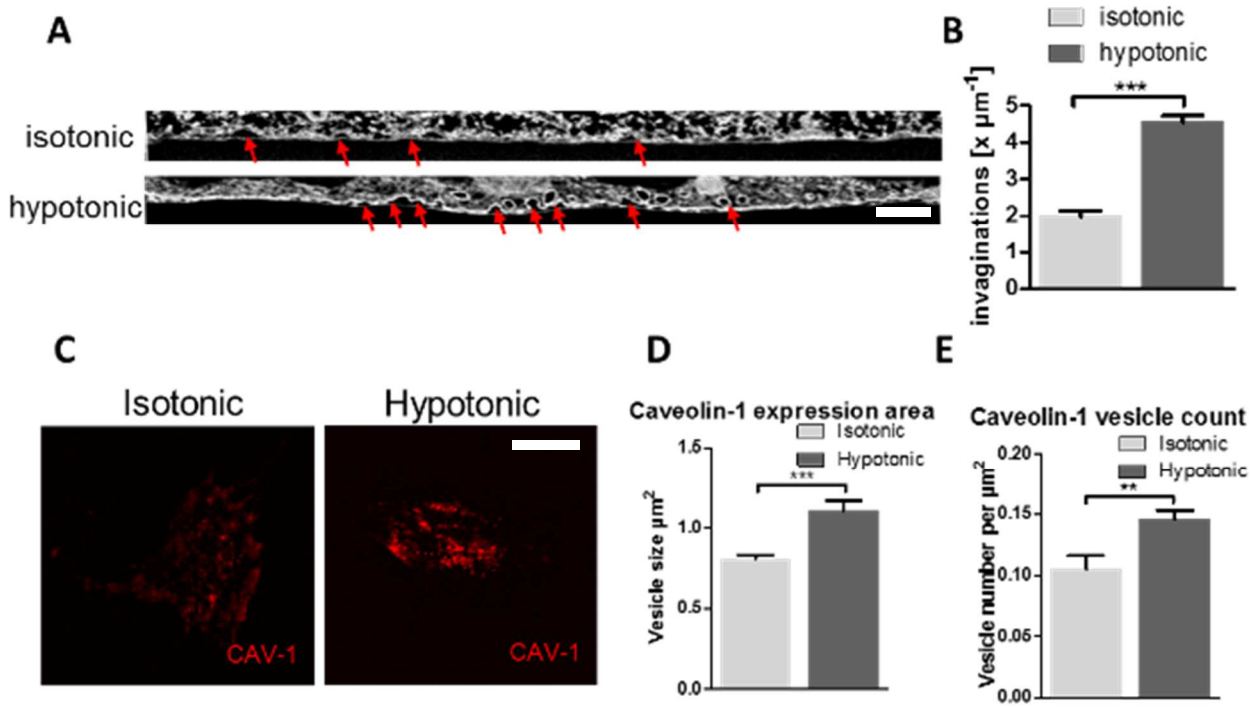

Figure 5.4 Media osmotic concentration effect on caveolae formation. (a) FIB SEM images of the plasma membrane cross-sections, red arrows mark caveolae, and (b) quantification of the number of invaginations per µm of membrane cross-section for the cells isotonic and hypotonic media. Scale bar in (a) represents 200 nm (c) Caveolin-1 mCherry TIRF microscopy images, (d) caveolin-1 expression area and (e) caveolae count per μm^2 for the cells isotonic and hypotonic media. Scale bar in (c) represents 50 µm. Histogram bars represent mean ± SEM. Data are representative of 3 independent experiments and 15 cells analysed for each condition, $^{**}p < 0.01$, $^{***}p < 0.001$

5.2.4 Substrate rigidity promotes exocytosis

Caveolae are involved in both endocytosis and exocytosis[253], so to assess whether the increased presence of caveolae at the cell membrane was associated with a positive or negative feedback loop for membrane tension regulation, levels of exocytosis were assessed. Increased membrane tension has been previously demonstrated in many cell lines to promote exocytosis, e.g. fibroblasts promote MMP secretion[267] and matrix stiffness has also been linked with regulation of clathrin-mediated endocytosis[268].

Studies presented here tested for the rate of exocytosis of TIMP-1, a negative regulator of various matrix metalloproteinases and therefore ECM remodelling[269]. Both the RFP plasma membrane (red) and intracellularly produced GFP TIMP-1 (green) in HSCs were labelled and TIMP-1 positive vesicles were identified as those where these fluorescent intensities co-localised (Figure 5.5 a). Then the lifetime of these vesicles was followed to determine the overall rate of exocytosis, and visualised TIMP-1 positive vesicles where each individual panel (Figure 5.5 b) represents 10 seconds.

It was observed that in hypotonic media, where membrane tension is increased, the average vesicle lifetime was significantly less than in isotonic media (150 s vs 270 s), indicating that a faster rate of exocytosis correlates with membrane tension. Exocytosis rate was visualised in a kymograph (Figure 5.5 c), where each horizontal line of pixels represents the cell membrane at a different time point, where time progresses vertically down. Slowly exocytosing vesicles produce long tracks whereas faster exocytosing vesicles produce shorter tracks (Figure 5.5 d).

To ensure that the increase in exocytosis was not due to an increase in intracellular TIMP-1 production, the expression of TIMP-1 mRNA was tested with qPCR. It was observed that mRNA expression was the same for both isotonic and hypotonic media (Figure 5.5 e), indicating that membrane tension likely underlies the increased rate of endocytosis.

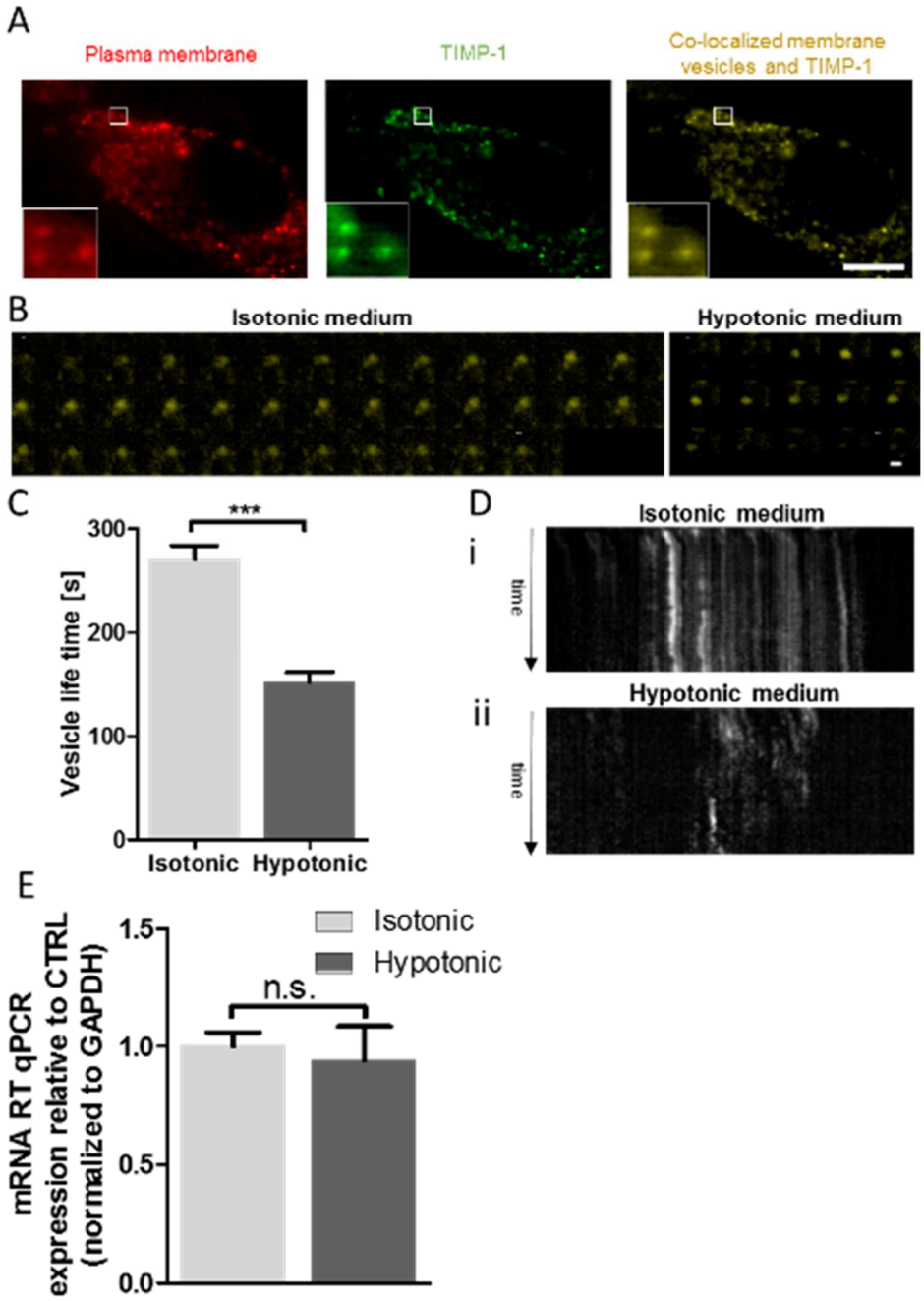

Figure 5.5 Hypotonic medium-induced plasma membrane stiffening affects the TIMP-1 exocytosis in HSC. (a) TIRF images of HSCs on glass with RFP tagged cell membrane, GFP tagged TIMP-1 and colocalised vesicles containing TIMP-1 for exocytosis analysis. (b) Representative TIRF images for TIMP-1 containing vesicles for isotonic and hypotonic medium used for (c) quantification of TIMP-1 vesicle lifetime. (d) Representative TIRF time-lapse kymographs of HSC TIMP-1 vesicles in (i) isotonic and (ii) hypotonic conditions. (e) mRNA expression of TIMP-1 assayed by RT-qPCR, normalised to control GAPDH mRNA and presented relative to isotonic conditions. Assay B and E were done for 3 separate experiments (n=3). Results are expressed as mean±SEM. Scale bars represent (a) 10 µm and (b) 1 µm. ***$p < 0.001$, n.s. non-significant

5.2.5 Dynamin-1 is required for caveolae formation in response to membrane stiffening

To gain a mechanistic insight into the increased rate of exocytosis, proteins that are intimately linked with membrane transport were investigated. Dynamin-1 is a GTPase often associated with endocytosis but has recently been implicated in promoting exocytosis. By forming a helical complex which binds to phosphatidylinositol-4,5-bisphosphate (PIP2)-rich membranes, dynamin promotes full distension, meaning the entire vesicle is incorporated into the membrane, over a 'kiss and run' event where vesicle incorporation is only partial[254].

It was observed, through immunofluorescence, that dynamin-1 expression was minimal in HSCs in isotonic media but was greatly increased in hypotonic media (Figure 5.6), indicating that membrane tension can promote changes in dyamin-1 abundance.

To test whether dynamin-1 was involved in promoting vesicle abundance in response to membrane tension, the dynamin-1 expression in HSCs was knocked down with siRNA. Dynamin-1 knockdown cells showed an insensitivity of vesicle size and density to changes in membrane tension, since it was observed that both these parameters were the same in both hypotonic and isotonic media (Figure 5.7).

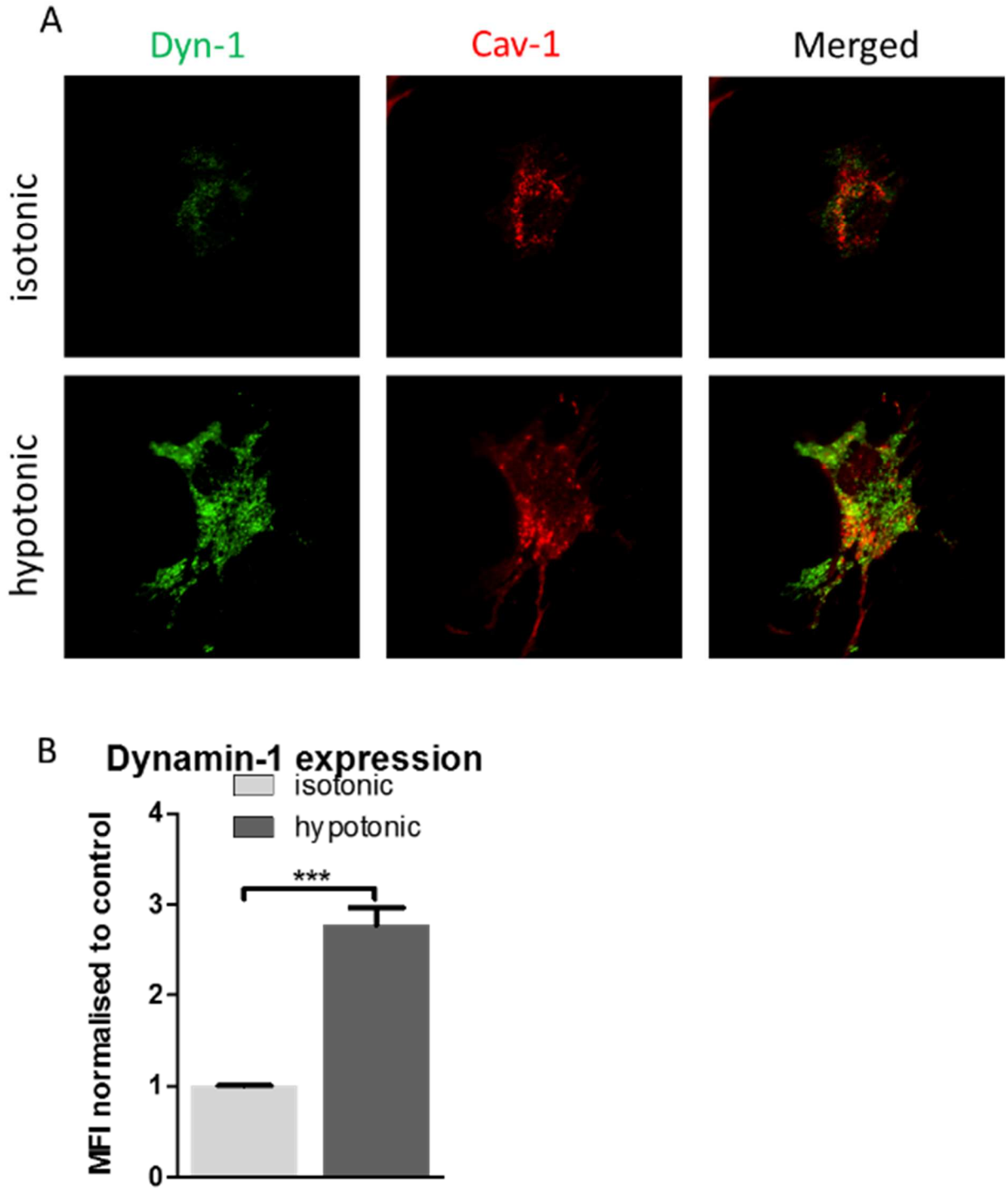

Figure 5.6 Dynamin-1 presence in the plasma membrane is membrane tension dependant. (a) Representative TIRF microscopy images of dynamin-1 (green), caveolin-1 (red) and merged in isotonic- and hypotonic-media treated HSC. (b) Quantification of dynamin-1 expression as mean fluorescence intensity (MFI). Histogram bars represent mean ± SEM. Data are representative of 3 independent experiments and 30 cells analysed, ***$p < 0.001$

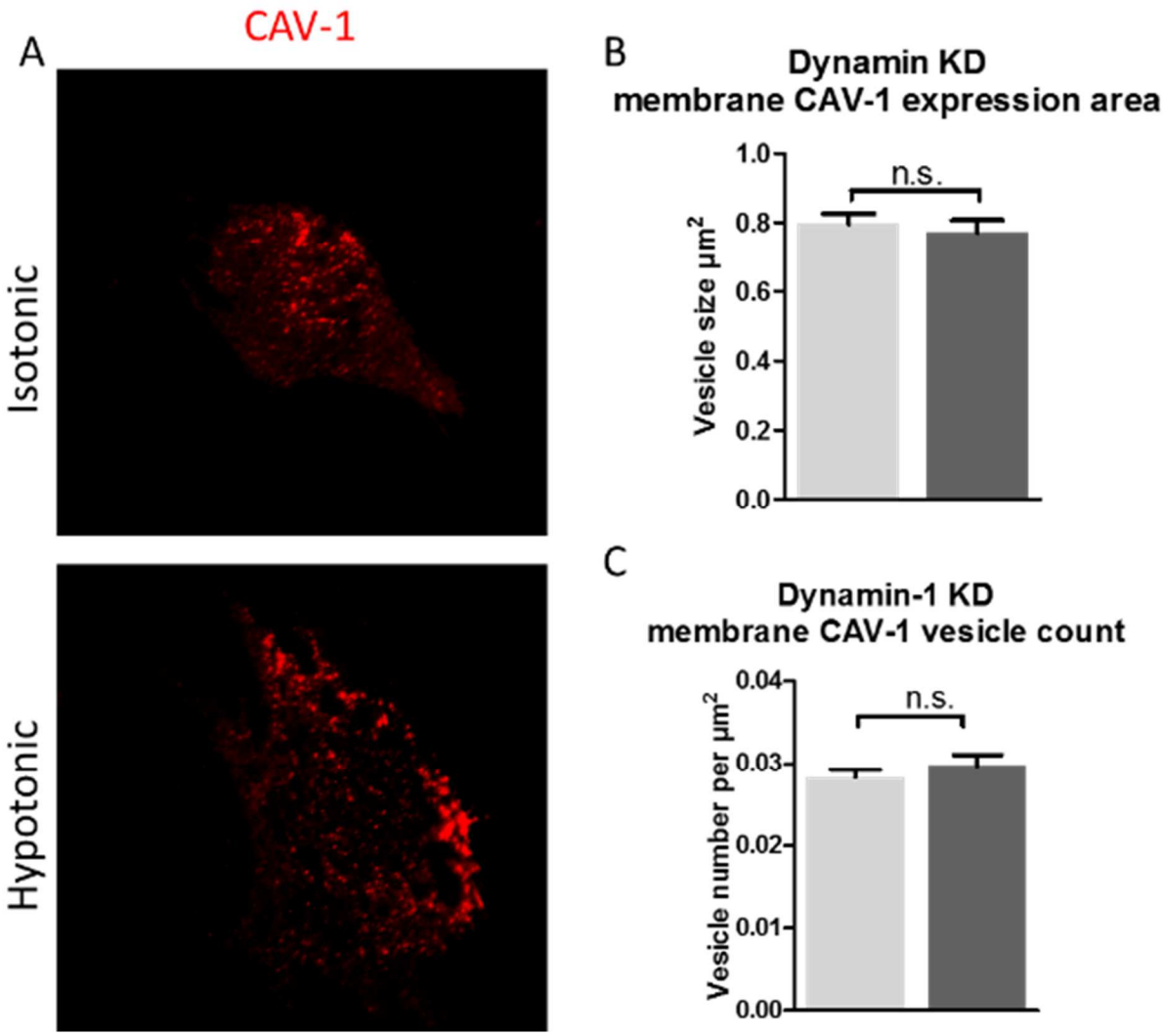

Figure 5.7 Dynamin-1 is required for increased caveolae presence in plasma membrane in response to high membrane tension. (a) Representative TIRF microscopy images of caveolin-1 isotonic and hypotonic media treated dynamin-1 knockdown HSC. Quantification of caveolin-1 (b) expression area and (c) vesicle count in dynamin-1 knockdown cells treated with isotonic and hypotonic media. Histogram bars represent mean ± SEM. Data are representative of 3 independent experiments and 30 cells analysed, n.s. non-significant

5.3 Discussion

Vesicular trafficking is important in the modulation of membrane tension, and exocytosis upregulation leads to a reduction in this tension by adding area to the membrane[248] and forcing water to leave the cells[270]. The results indicate that membrane tension in cells increases with matrix stiffness, and that the downstream effects of increasing membrane tension are consistent with a dynamin and caveolin dependent negative feedback loop which homeostatically regulates membrane tension.

The increased exocytosis involved in membrane tension homeostasis may also affect matrix stiffness through regulation of ECM remodelling, and therefore contribute to additional feedback within the signalling network. In HSCs, the increased secretion of TIMP-1 was observed, a protein which promotes matrix stiffening by inhibiting various MMPs which would otherwise degrade ECM components[269]. Given that HSCs are integral in determining ECM composition and organisation[271] and that this behaviour is sensitive to external stiffness[231], upregulation of TIMP-1 secretion by matrix stiffness would represent a negative feedback mechanism for ECM remodelling. It is unclear whether exocytosis of other secretory proteins would also be affected by matrix stiffness, since regulation of endocytosis by matrix stiffness has been shown to differ for clathrin and lipid raft-mediated endocytosis[268]. Future observations of whether secretion of MMPs or ECM proteins is affected by matrix stiffness and membrane tension would determine further details of this signalling network.

The observed exocytosis feedback loop is dependent on dynamin and caveolin-1, which are more commonly associated with endocytosis, and hence the results reframe the importance of these molecules. While dynamin and caveolin are known to interact in endocytic budding processes[272,273], and have been individually demonstrated to be important in exocytosis[253,254], the results indicate their co-operative importance in an exocytic context. Vesicle trafficking involves many budding and fusion events[274], and it is likely that the previously demonstrated roles of dynamin and caveolin in budding contribute to exocytosis by facilitating budding from the Golgi as well as fusion at the plasma membrane. This highlights the need to consider that other vesicle-related proteins commonly associated with one type of trafficking may be equally important in another type of trafficking in other contexts.

Vesicular trafficking regulation is not the only cellular strategy for regulating membrane tension, with actin assembly and cell shape changes also commonly used[270]. Actin contractility, known to be induced by matrix stiffness[47], opposes actin protrusion at the cell cortex by pulling

actin filaments away from the membrane and prevents further generation of tension by membrane extension[255]. Mechanosensitive ion channels, activated with high membrane tension, can promote the efflux of ions and therefore water by osmotic pressure, leading to a reduction in membrane tension[275]. Further mechanisms may therefore exist which transduce external rigidity into alterations in membrane tension, possibly co-operating with vesicular trafficking and regulating cell behaviour.

The presented signalling network involves negative feedback and this would contribute to homeostatic regulation in a healthy state, though could become dysregulated in various diseases. Many diseases involve alterations to ECM composition, such as fibrosis, which promote disease development, e.g. cancer and cardiovascular diseases[11]. Caveolae are considered as anti-fibrotic since caveolin-1 can inhibit fibrosis-promoting pathways such as TGF-β signalling[276], and various therapeutics such as tocotrienols and 17β-estradiol have been shown to be beneficial in cardiovascular diseases through caveolins[62]. Interestingly, 17β-estradiol and its mimetic tamoxifen have recently been shown to prevent mechanosensing in HSCs[277].

5.4 Materials and methods

5.4.1 Cell culture

Primary culture-activated human hepatic stellate cells (passage 3-6, HHStec #5300 – ScienCell) and human foreskin fibroblasts (HFF, kindly donated by Professor Molly Stevens, Imperial College London) were cultured at 37°C, 5% CO2 in culture medium containing DMEM/Nutrient Mixture F-12 Ham (D8437, Sigma), 10% FBS (10270-106, Gibco), 1 % penicillin/streptomycin (,Gibco) and 1% fungizone (15290-026, Gibco). Mouse epithelioid cell line GE11 (kindly donated by Professor Julien Gautrot, Queen Mary University of London) with β1 integrin knockout or overexpression was cultured at 37°C, 5% CO2 in culture medium containing DMEM/Nutrient Mixture F-12 Ham (D8437, Sigma), 20% FBS (10270-106, Gibco), 1 % penicillin/streptomycin (P4333, Sigma Aldrich), 1% fungizone (15290-026, Gibco) and 1% L-glutamine. Cell surface α5β1 and αvβ3 integrin were blocked by pre-treating cells with α5β1 integrin (75 μg/ml, MAB2514, Millipore) and αvβ3 integrin (10 μg/ml, LM609, Millipore) blocking antibody, respectively. For the AFM and TIRF microscopy experiments, HSCs and HFFs were detached from culture flasks with trypsin and seeded on fibronectin coated (10 μg ml^{-1}; Sigma) glass bottom dishes or fibronectin coated polyacrylamide gels with different rigidities and transfected. For the isotonic and hypotonic media experiments, standard culture medium (DMEM 10%FBS) was used as the former and 0.5x DMEM 10% FBS in distilled water was used as the latter (150 mOsm). For TIRF plasma membrane visualisation cells were transfected with CellLight™ Plasma Membrane-RFP, BacMam 2.0 (C10608, ThermoFisher) according to the standard manufacturer's protocol. For the plasmid requiring experiments, cells were transfected with 2 μg of caveolin-1 (#27705, Addgene), dynamin-1 (#34680, Addgene), TIMP-1 (RG201548, OriGene) plasmid using jetPRIME (114-01, Polyplus) according to manufacturer's protocol. For the gene silencing experiments cells were transfected with 2.2 pmoles of Dynamin-1 siRNA using interferIN (409-10, Polyplus) according to the manufacturer's protocol.

5.4.2 Polyacrylamide substrate fabrication

For the AFM experiments coverslips were dipped in 0.1 M NaOH and left to dry. Dried coverslips were coated with 4.0% (3-aminopropyl)triethoxysilane (281778, Sigma) and washed with dH_2O. Coverslips were dried and transferred to 2.5% glutaraldehyde (G6257, Sigma)/PBS and incubated at room temperature for 30 minutes, twice washed in dH_20 and left

to dry at room temperature. For the FLIM and confocal microscopy experiments glass bottom fluorodishes were treated as the coverslips. Polyacrylamide gels of 4, 12 and 25 kPa mimicking healthy and fibrotic liver stiffnesses[221] were prepared according to the protocol adapted from Wen *et al*.[36] (Table 1). Gel stiffness was varied by adding 29:1 acrylamide/*bis*-acrylamide to a final concentration ranging from 4.7–10%. A working solution of PBS, acrylamide/*bis*-acrylamide (29:1) 40% vol (A7802, Sigma), TEMED (T9281, Sigma) and 10% ammonium persulfate were mixed at concentrations to achieve varying gel stiffness. A small drop of this working solution was applied to activated coverslips or fluorodishes. Coverslips were placed face down on hydrophobic, dichlorodimethylsilane (440272, Sigma) treated glass microscope slides and left to polymerise at room temperature for 45 minutes. Fluorodishes had the dichlorodimethylsilane treated coverslips placed on the top of the working solution droplets and left for 45 minutes to polymerise. Gel-coated coverslips or fluorodishes were separated and stored in PBS at 4 °C.

To provide cell attachment to gels, 50 µl (coverslip)/200 µl (microscope slide) sulfo-SANPAH (SS) (Sigma-Aldrich, USA) solution (0.1 mg SS in 2 µl DMSO/50 µl PBS) was used to covalently bind native human fibronectin (Gibco, USA) to gel surface. Gel surface was covered in SS solution and exposed to 2 × 5 minutes UV light to activate sulfo-SANPAH before excess solution was removed through PBS washing. 50 µl (coverslip)/200 µl (microscope slide) of fibronectin solution (10 µl fibronectin/1 ml PBS) was added to gel surface and gels incubated at RT for 2 hours. Excess fibronectin was then removed with gentle PBS washing.

5.4.3 Quantitative PCR

Total RNA was extracted from cells cultured glass for 24 hours with RNeasy Mini Kit (74104, Qiagen), according to the "RNeasy mini quick start protocol". RNA template was reversed transcribed into cDNA by High-Capacity RNA-to-cDNA kit (4387406, Thermo-Fisher) according to manufacturer's instructions. Quantitative real-time PCR was performed on a StepOne Plus Real-Time PCR system (Applied Biosystems) using SYBR Green PCR Master Mix (4309155, Thermo-Fisher). Relative TIMP-1 gene expression was analysed by the ΔCt method and final values were normalised using ΔCt for GAPDH gene mRNA as a value of 1.0. Primer sequences were as followed: TIMP-1 (F) TCAACCAGACCACCTTATACCA, (R) ATCCGCAGACACTCCAT; GAPDH (F) ACAGTTGCCATGTAGACC, (R) TTTTTGGTTGAGCACAGG.

5.4.4 Atomic force microscopy

For AFM study, cell seeded polyacrylamide gels on coverslips were lifted from 24-well plates prior to measurement and immediately attached to a petri dish with a droplet of cyanoacrylate adhesive, applied with a 10 µL pipette tip. After coverslip attachment (~1 minute), 100 µL of culture medium (normal medium or integrin blocking media) was applied to the coverslip in order for the AFM measurements of cells to be conducted as soon as possible (<1 hour). Measurements of HSCs on polyacrylamide gels were conducted on a JPK Nanowizard-1 (JPK instruments) AFM operating in force spectroscopy mode, mounted upon an inverted optical microscope (IX-81, Olympus). AFM pyramidal cantilevers (MLCT, Bruker) with a spring constant of 0.03 N/m were used. Before conducting measurements, cantilever sensitivity was calculated by measuring the force-distance slope in the AFM software on an empty petri dish region. For cell indentation measurements the cantilever was aligned over a central region of a cell using a 20X objective and the optical microscope. For each cell 3-5 force curves were acquired at an approach speed of 2 µm/s and a maximum set point of 0.1 V to ensure that the cantilever only probed the cell membrane. The force-distance curves were used to calculate elastic moduli in the AFM software through the application of the Hertz contact model.

5.4.5 Fluorescence Lifetime Imaging Microscopy

HFF cells were plated on the polyacrylamide-coated fluorodishes 24 hour prior to the experiment. Culture media diluted 2.0 µg/ml Rho Inhibitor I (#CT04-A, Cytoskeleton) or 5 µl/ml RhoA Activator I (# CN01-A) were added to the cells on the gels 3 hours or 15 minutes respectively before the measurements. In order to fluorescently tag the cell membrane for the fluorescence lifetime imaging (FLIM) 1.5 µM FLIPPER-TR was added to the cells 5 minutes before the experiment.

The microscopy was carried on using Leica SP5 multiphoton inverted microscope (FLIM PMT detector and Becker & Hickl SPC-830 constant fraction discriminator) with a 488 nm pulsed laser for excitation and photons were collected through a 600/50 nm bandpass filter. To extract lifetime information, accumulated 1-minute acquisition high photon count histograms for single cells were fitted with a double exponential. Two decay times, $\tau 1$ and $\tau 2$ were extracted. The longest lifetime with the higher fit amplitude $\tau 1$ was used to report membrane tensions.

Longer lifetime means more tension in the membrane[262]. Data were analysed using FLIMFIT software[278].

5.4.6 Focused Ion Beam scanning electron microscopy

Sample preparation and microscopy was based on previously published methods[265,279]. Sample fixation of cells on polyacrylamide on glass coverslips or fibronectin coated glass coverslips was performed at room temperature for 15 min using a 4% v/v formaldehyde (Sigma, BioReagent, ≥ 36.0 %) with 0.2% v/v glutaraldehyde (Electron Microscopy Sciences) solution in PBS. Washing the samples three times with cacodilate buffer (Electron Microscopy Sciences) was followed with osmication with osmium tetroxide in 2% w/v cacodilate buffer for 30 min. Then, samples were washed five times with deionized water and then dehydrated through a graded ethanol (Sigma, ACS reagent 99.5%) series. Samples were incubated in a diluted series of ethanol-Epon Resin (Electron Microscopy Sciences) at a 3:1, 2:1 and 1:1 ratio for 1 h each, and then overnight at 1:2 ratio. After overnight incubation with pure resin the maximum amount of resin was removed and the samples were immediately placed in an oven at 60 °C and left to cure overnight. Then, samples were placed on a SEM aluminium sample holder with carbon tape and silver paint was applied to the surrounding area of the sample to maximize conductivity. Afterwards, sputter coater (QuorumTechnologies model K575X) was used to coat the samples with 5 nm layer of chromium. Following the coating procedure, samples were introduced into an SEM/focused ion beam (Carl Zeiss, Auriga) with gallium ion beam operated at 30 kV. A region over the cells with approximately $15 \times 5 \times 2$ µm (length × height × depth) was milled using 4 nA current. After that, the region exposed by the first milling was polished with 240 pA current and imaged by a backscattering detector with the electron beam operating at 1.5 V. Obtained dataset was reconstructed using MATLAB to obtain high resolution micrographs. Number of invaginations per length of the membrane cross-section was calculated by using the Image J software.

5.4.7 Total Internal Reflection Microscopy

For total internal reflection fluorescence (TIRF) microscopy, cells were cultured and transfected in glass bottom petri dishes with or without polyacrylamide gels to ensure high resolution and signal-to-noise. Prior to measurements, cell culture medium was changed for clear cell medium to reduce autofluorescence from the cell medium. Images of transfected cells

were obtained with an inverted microscope (Eclipse Ti; Nikon) operating in TIRF mode, under ambient temperature conditions of 37 °C. Multi-wavelength time lapse TIRF imaging was performed with a 63X oil immersion objective (1.3 NA, Nikon), a 488 nm diode laser and a 561 nm diode laser for excitation coupled with emission filters 525/50 nm and 600/50 nm respectively. Time lapse images were recorded at 0.1 Hz using a sCMOS camera (Neo, Andor) combined with the NIS elements (Nikon) control software to facilitate two colour imaging across multiple regions. To minimise drift in the focus across time and multiple regions, the perfect focus system (Nikon) was used to maintain axial focus. Measurements of hypotonic conditions followed the above imaging protocol directly after the culture medium was changed to hypotonic medium.

TIRF image sequences were analysed in ImageJ, using the bleaching correction plugin to allow visualisation of vesicles throughout the sequence. The coloc2 plugin was used to visualise TIMP-1 containing vesicles for analysis and vesicles were tracked from formation to disappearance from the focal plane, and thus emission into the surrounding medium. The kymography plugin was used to create the kymographs.

5.4.8 Statistical analysis

Results were analysed using Prism software (GraphPad, La Jolla, CA, USA). A 2-tailed Student's *t-test* for unpaired data was used to calculate the difference between means (unless otherwise specified), with values of $p<0.05$ considered significant.

6 Mechanoregulation in fibroblasts by the G protein-coupled estrogen receptor

6.1 Introduction

The G protein-coupled estrogen receptor (GPER) is an heptahelical transmembrane receptor that initiates rapid signalling cascades in response to both endogenous estrogens such as 17β-estradiol, as well as man-made compounds[104,105]. These GPER mediated events may involve the generation of second messengers such as Ca2+, as well as the activation of protein kinase A and tyrosine kinase receptors among others. Given that GPER is broadly expressed in eukaryotic cells and because of its potential to regulate multiple downstream signallings, including cell survival and proliferation, GPER has recently attracted significant attention in biology and medicine[280].

The small Rho GTPases are molecular switches that control a plethora of biological signalling in eukaryotic cells. They achieve this control by cycling between the GTP-active and GDP-inactive states[281]. The RhoA GTPase (RhoA) is one of the most prominent members of the Rho GTPase family, which controls and shapes actin cytoskeleton by promoting actin polymerisation via formins (mDia), and through actomyosin contractility by triggering the phosphorylation of the regulatory myosin light chain-2 (MLC-2) via ROCK[282]. This RhoA-dependent induction of cytoskeletal contractility is required for the nuclear translocation and activation of the transcriptional factor YAP, a mechanotransducer that has cardinal roles in development, tissue homeostasis and cell biology[189]. YAP activation has further mechanical influences such as genomic regulation of focal adhesion formation[283] YAP regulates cell mechanics by controlling focal adhesion assembly.

A robust cytoskeletal machinery, linked to a dynamic population of focal adhesions, is essential for transduction of mechanical signals within the cell. Reorganisation of the cytoskeleton is indispensable in multiple cellular events that require morphological changes such as cell adhesion and spreading, morphogenesis, migration, and phagocytosis[284]. These processes are promoted by the formation of structures such as actin stress fibres and focal adhesions[74]. The turnover rate of focal adhesions is also dependent on mechanical tension and contraction[285]. Rho-family GTPases are critical in the signalling pathways that link actin and adhesion dynamics[74,286], such as promoting polymerisation of G-actin into F-actin filaments[287].

Here, using two different, widely accepted model cell lines (human foreskin fibroblasts[202] and mouse embryonic fibroblasts[288]), it is shown that activation of GPER leads to cell line unspecific morphological changes in cells, inhibiting RhoA activation to consequently supress actomyosin dependent cell contractility, force generation and mechanosensing. It is also observed that GPER activation leads to a decrease in the number and assembly of actin ventral fibres. Furthermore, GPER activation retards actin polymerisation, and subsequently triggers a cellular negative feedback that transcriptionally suppresses the expression of monomeric G-actin. The dynamics of focal adhesions is also affected by GPER, whose activation reduces focal adhesion size and turnover. These cytoskeletal changes also drive RhoA-mediated deactivation of YAP.

Aims:

- To examine the effect of GPER activation on RhoA
- To assess how GPER activation affects regulates cellular mechanosensing, focal adhesion dynamics, actin polymerisation and force generation by fibroblasts

6.2 Results

6.2.1 GPER activation modifies cell morphology and supresses RhoA activation

The morphology of cells is highly dependent on the organisation of the actin cytoskeleton, which controls a very wide range of mechanical related processes in cells ranging from locomotion and cell adhesion to the formation of the mitotic spindle or the actin rings during mitosis and cytokinesis, respectively[284]. Specific morphological changes can dictate cell fate, such as lineage commitment in stem cells[289]. It was then sought to study if GPER plays a role in cell morphology.

First, it was confirmed that human foreskin fibroblasts (HFFs) and mouse embryonic fibroblasts (MEFs) express this type of receptor (Figure 6.2). Then, scanning electron microscopy was used to visualise the effect of GPER activation on the morphology HFFs, using a specifically designed selective GPER agonist, (G1)[290]. It was observed that control HFFs were highly spread with a large contact area with the substrate. Conversely, G1 treatment led

to rounding up of the cell to a more condensed morphology, with greater cell height and reduced contact area (Figure 6.1 a). Cell area and cell roundness were quantified and it was observed that G1 treated cells had a significantly smaller contact area (Figure 6.1 b) and were significantly rounder than control cells (Figure 6.1 c). Additionally, cell area and cell roundness were monitored in MEFs and the same trend was observed (Figure 6.3). This suggests a link between GPER and cytoskeletal dynamics, which manifests as alterations in cell morphology.

To understand the mechanism underpinning these morphological changes the levels of activation of RhoA were investigated. RhoA is known to control the actin cytoskeleton via actin polymerisation and cell contractility[291,292]. Immunoassays were used to measure the total and activated (GTP-bound) levels of RhoA. No significant changes were observed in the total amount of RhoA between control and G1 treated HFFs, but a significant 40% decrease was measured in the levels of GTP-bound active RhoA in cells treated with G1 compared to the levels of control HFFs (Figure 6.1 d). Guanine nucleotide exchange factors (GEFs) activate RhoA by promoting the exchange of GDP by GTP, while GTPase-activating proteins (GAPs) catalyse the substitution of GTP by GDP leading to the inactivation of RhoA. However, there is another layer of control for the activation of RhoA. The inactive pool of GDP-bound RhoA is complexed with guanine nucleotide dissociation factors (GDIs) and is prevented from activation[293]. It is well-documented that phosphorylation of the serine residue 188 in the C-terminal tail of RhoA prevents its dissociation from the complex with GDIs and therefore RhoA activation[294,295]. Using Western blot, it was confirmed that there was no change in the total levels of RhoA between the control and G1 treated HFFs, and around 30% increase in the levels of RhoA phosphorylated in Serine 188 (pRhoA-Ser188), and therefore inactive RhoA was observed in G1 treated HFFs compared to control HFFs (Figure 6.1 e and Figure 6.4). This data demonstrates that GPER activation induced pronounced morphological changes in HFFs and MEFs and suggests that these changes are mediated by the levels of activation of RhoA.

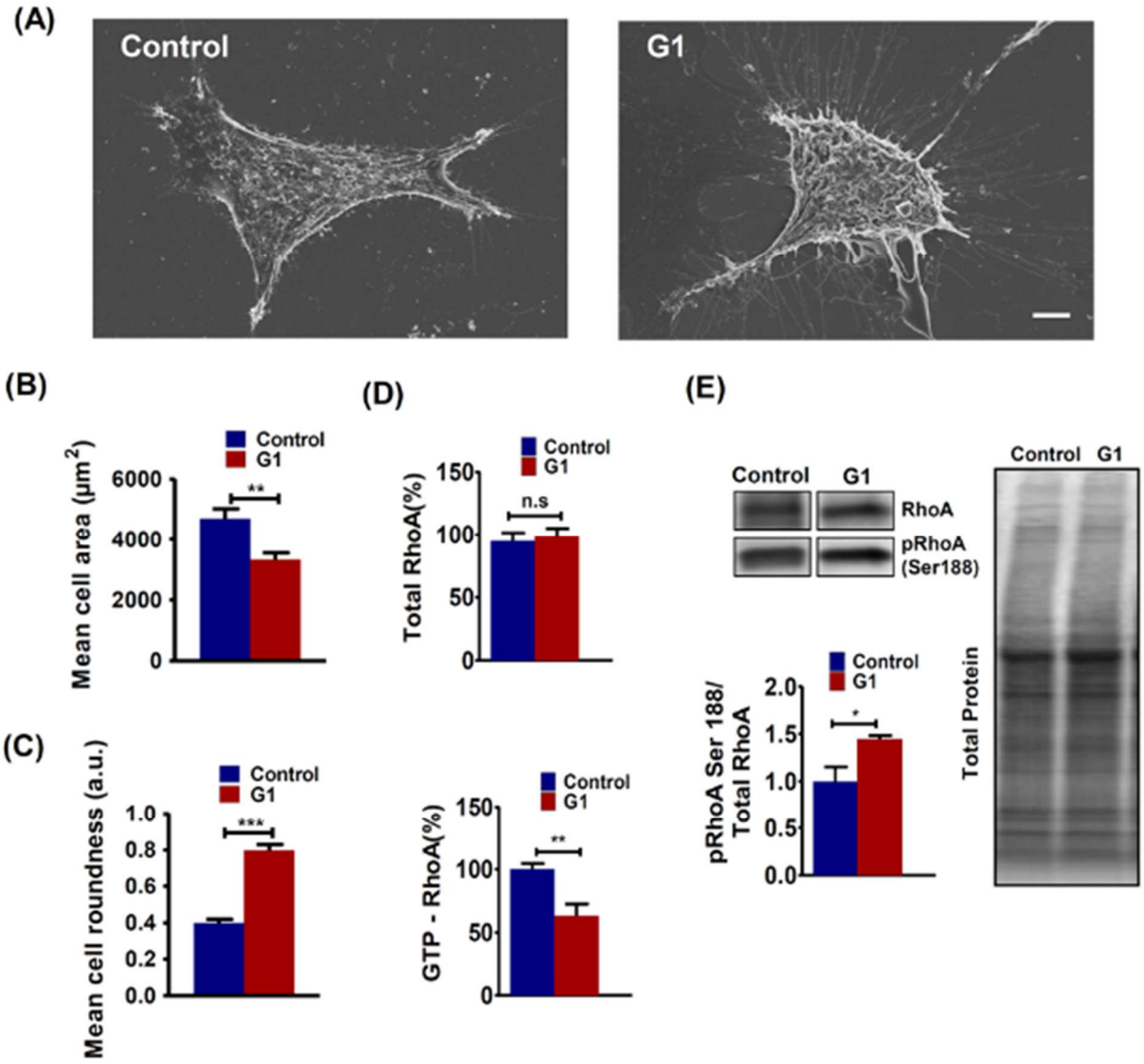

Figure 6.1 GPER activation changes the morphology of human foreskin fibroblasts (HFFs) and inhibits RhoA activation. (A) Scanning electron microscopy (SEM) photomicrographs of control and G1 treated HFFs. G1 is GPER agonist. The scale bar is 10 μm. (B, C) Quantification of HFF cell area and roundness. Number of cells: 10 control, 14 G1. (D) Quantification of total and active GTP-bound RhoA, normalised to the control condition. Three biological samples run in triplicate. (E) pRhoA Ser188 normalised to total RhoA expressed relative to control. Mean ± s.e.m., n=3. *** $p < 0.001$, ** $p < 0.01$, * $p < 0.05$, t-test. Histogram bars represent mean ± s.e.m.

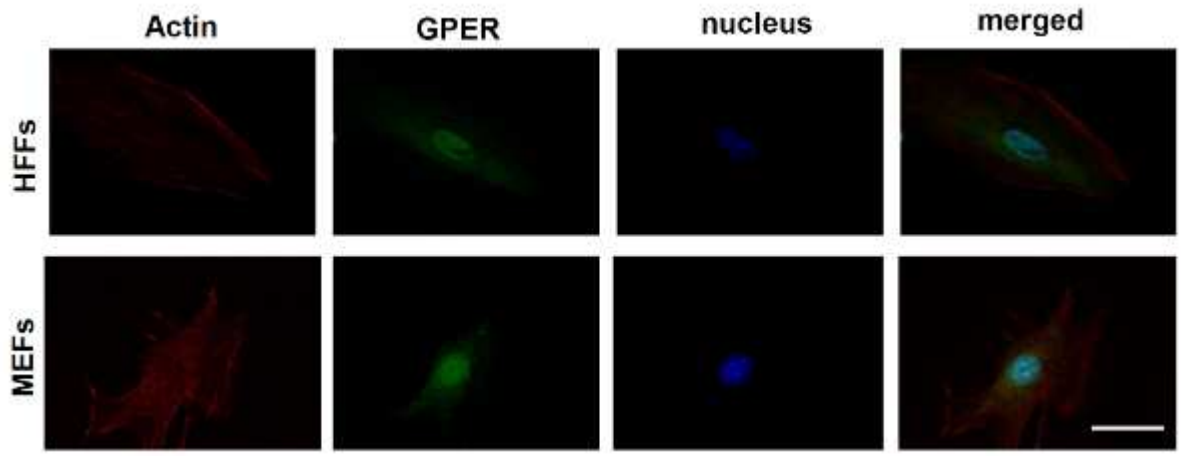

Figure 6.2 GPER expression in human foreskin fibroblasts (and mouse embryonic fibroblasts (Representative immunofluorescent images demonstrating that both cell lines express GPER Scale bar is 20 μm

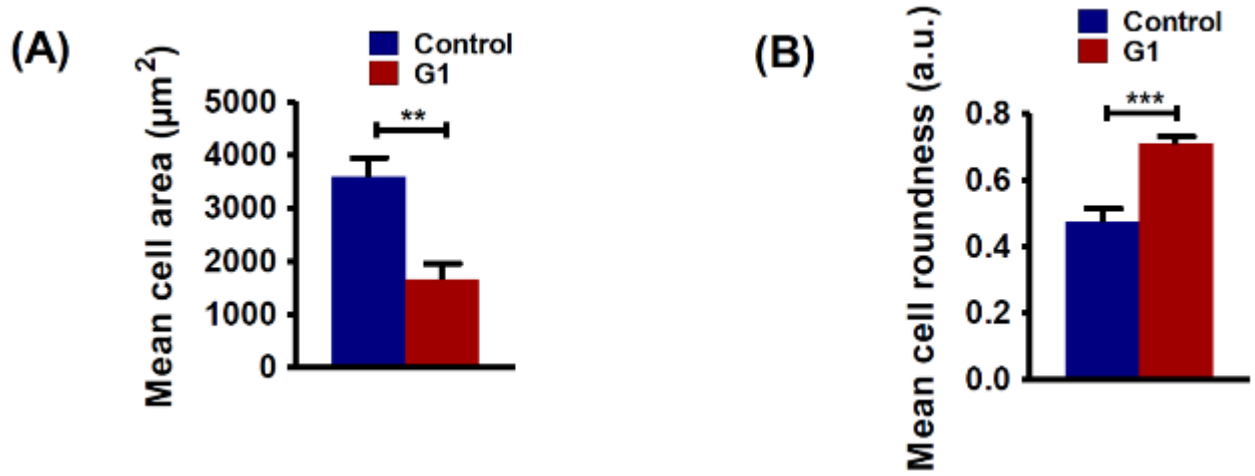

Figure 6.3 GPER activation changes morphology in mouse embryonic fibroblasts (MEFs). Quantification of MEF cell area (A) and cell roundness (B). Histogram bars represent mean ± s.e.m. 17 cells per condition. Three experimental replicates. T-test *** $p < 0.001$.

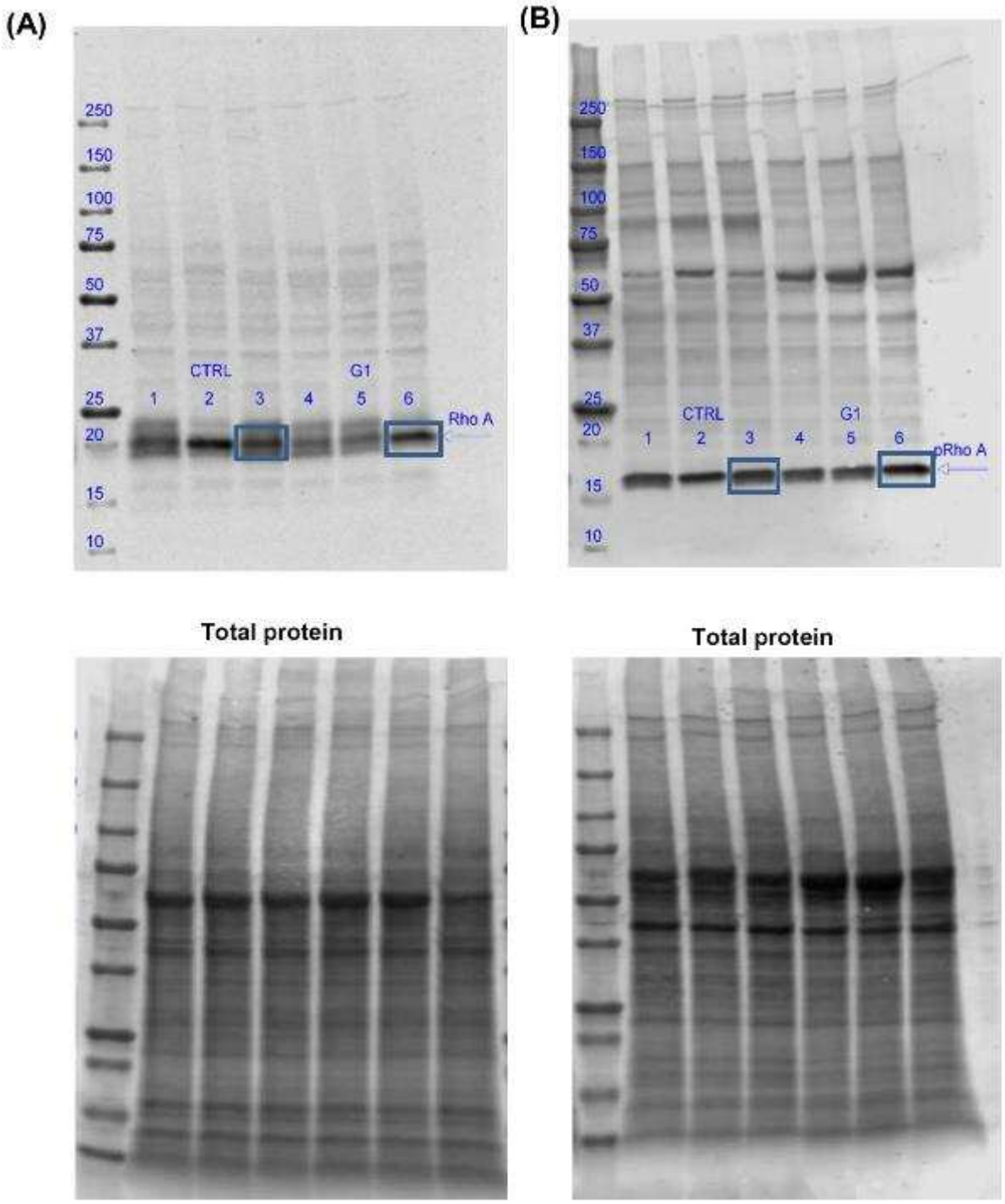

Figure 6.4 Images of the full membranes used in Western blots for RhoA (A) and pRhoA (B). HFFs Control and treated with GPER agonist (G1). 20 µg of protein was loaded per lane. Samples on each blot were normalised to control on the same blot before statistical analysis. Bands presented in figure are indicated by rectangle.

6.2.2 GPER activation reduces phosphorylation of myosin light chain 2 through RhoA

Actomyosin contraction regulates the organization of the actin cytoskeleton and therefore cell morphology. Fibroblasts, along with epithelial and endothelial cells, generate anisotropic stresses through a polarised cytoskeleton in order to remodel the extracellular matrix (ECM), which generates a non-rounded morphology[296]. To investigate the contractile changes in the actomyosin cytoskeleton that lead to morphological changes, the activation state of the cytoskeletal regulatory protein myosin light chain-2 (MLC-2) was assessed, which promotes actomyosin contractility in its phosphorylated state (pMLC-2). MLC-2 is a downstream effector of RhoA[291].

It was observed that G1 treatment of HFFs significantly reduced the phosphorylation of MLC-2 (pMLC-2). When G1 was combined with the selective GPER antagonist G15[297], or used in cells with GPER expression knocked down through siRNA, no reduction in pMLC-2 levels was observed, indicating that G1 is acting exclusively through GPER. Furthermore, introducing constitutively active RhoA (S188A/Q63L) after G1 treatment rescued the levels of pMLC-2 observed in control cells (Figure 6.5 a-c). All these conditions showed equivalent levels of the non-phosphorylated form, MLC-2 (Figure 6.5 c). The cell spreading area and roundness were not affected in control HFFs by using siRNA GPER. Also, G1 treated HFF cells after downregulating GPER using siRNA or followed by RhoA rescue show values of cell spreading area and roundness comparable to control HFFs (Figure 6.6). These trends were also validated in MEFs (Figure 6.7). These findings collectively show that GPER activation decreases MLC-2 phosphorylation and activation via RhoA signalling.

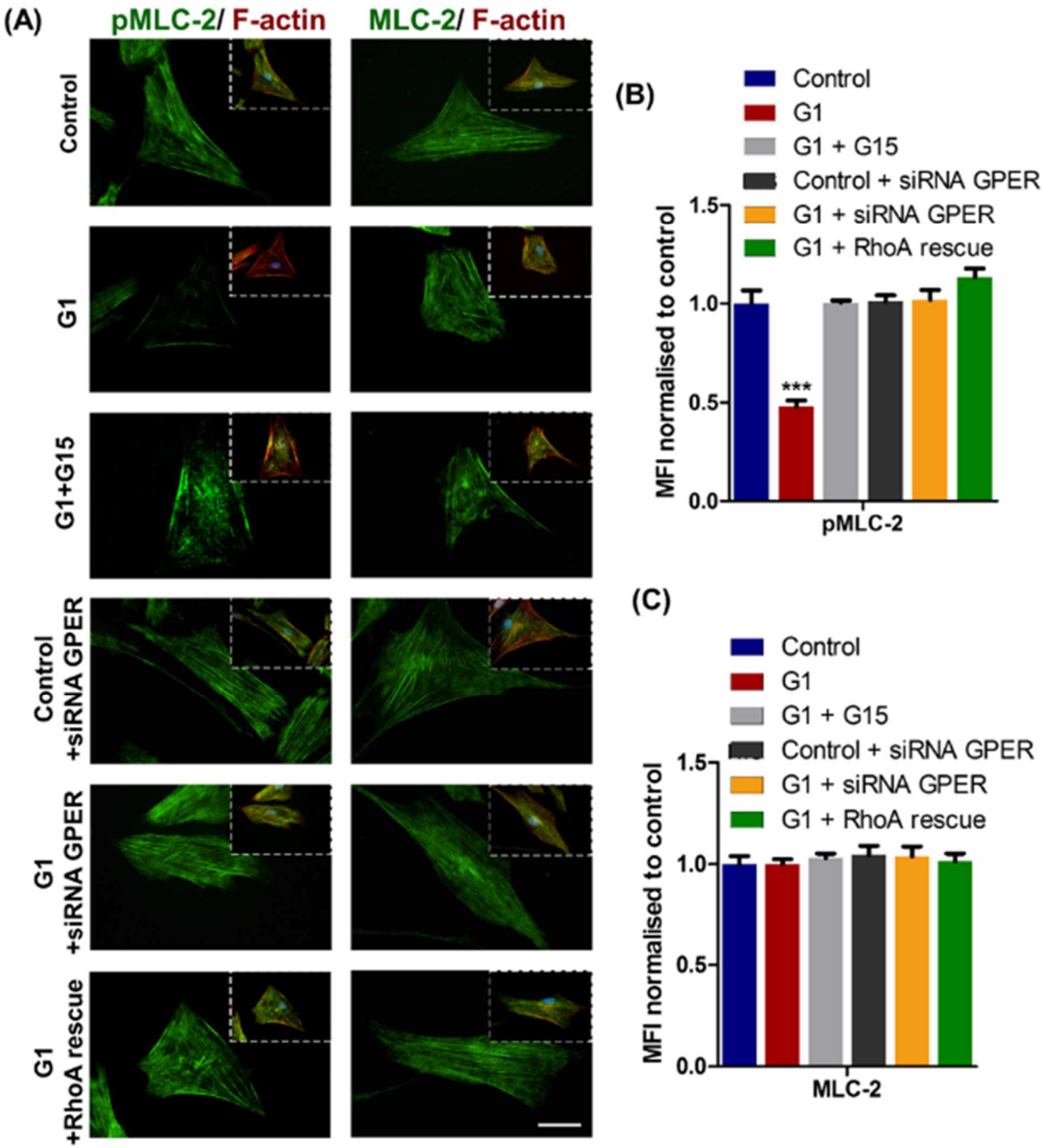

Figure 6.5 GPER activation supresses phosphorylation of myosin light chain 2 (MLC-2) but does not affect the expression of total MLC-2. (A) Representative images of human foreskin fibroblasts (HFFs), scale bar is 20 µm. (B, C) Quantification of pMLC-2 and MLC-2 staining intensity for panel a. Number of cells (control, G1, G1 + G15, control + siRNA GPER, G1 + siRNA GPER, G1 + RhoA rescue) for pMLC-2 29, 27, 17, 26, 53, 20 and for MLC-2 17, 22, 12, 19, 15, 16. G1 (GPER agonist) and G15 (GPER antagonist). Histogram bars represent mean ± s.e.m. Three experimental replicates. Anova and Tukey post hoc test. The marker denotes significant difference of G1 condition from the rest *** $p < 0.001$.

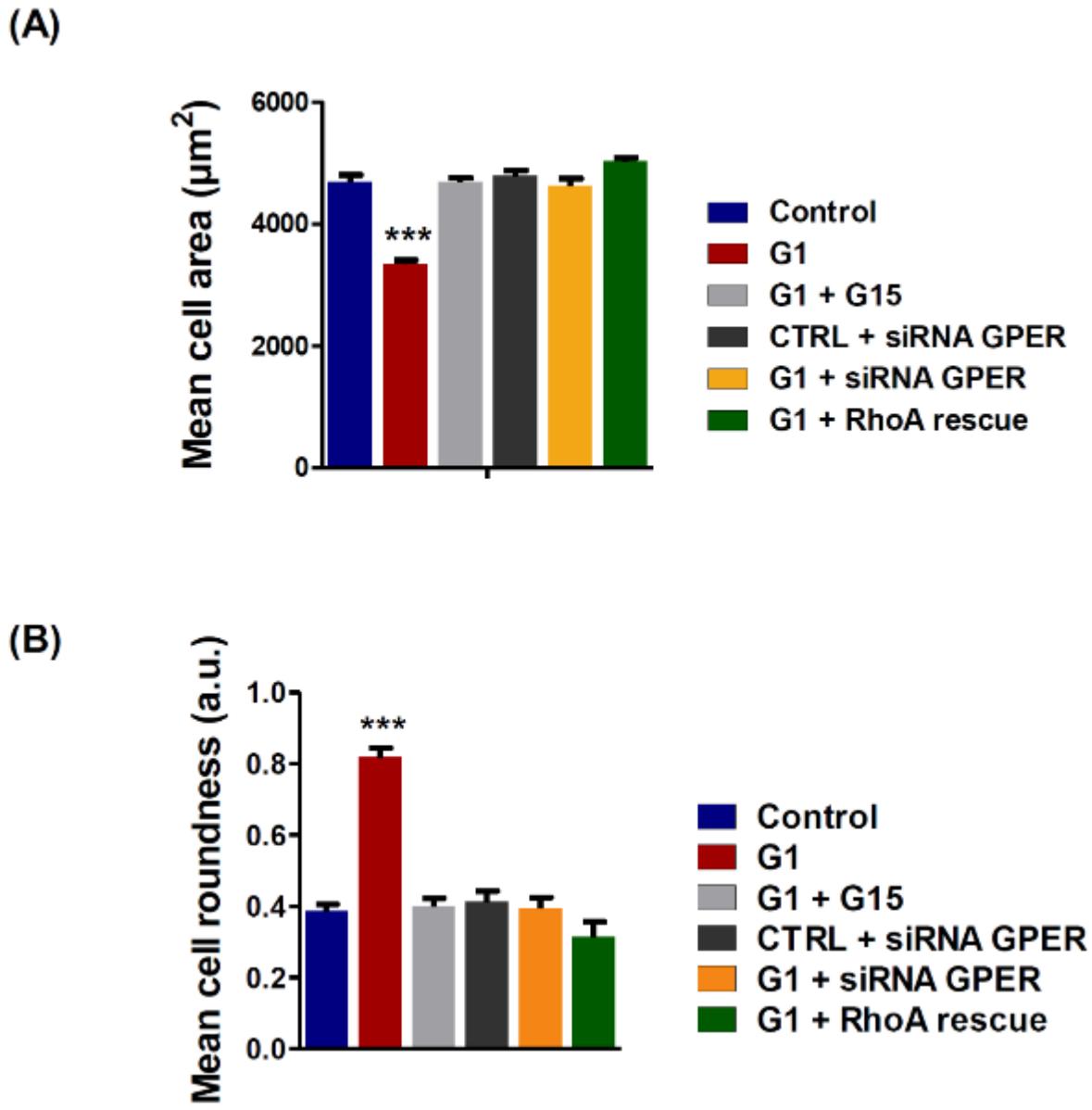

Figure 6.6 Characterization of cell morphology in human foreskin fibroblasts (HFFs). HFF cell area (A) and roundness (B) for control G1, G1+G15, control + siRNA GPER, G1 + siRNA GPER, G1 + RhoA rescue. These quantifications have been made based on the representative images of phalloidin staining in Fig 2. Histogram bars represent mean ± s.e.m. Anova and post-hoc Tukey test. The marker denotes significant difference of G1 condition from the rest *** $p < 0.001$. Number of cells: 10 control, 10 G1, 10 G1 + siRNA GPER, 10 G1 + RhoA rescue, 14 G1 + G15, and 11 control + siRNA GPER.

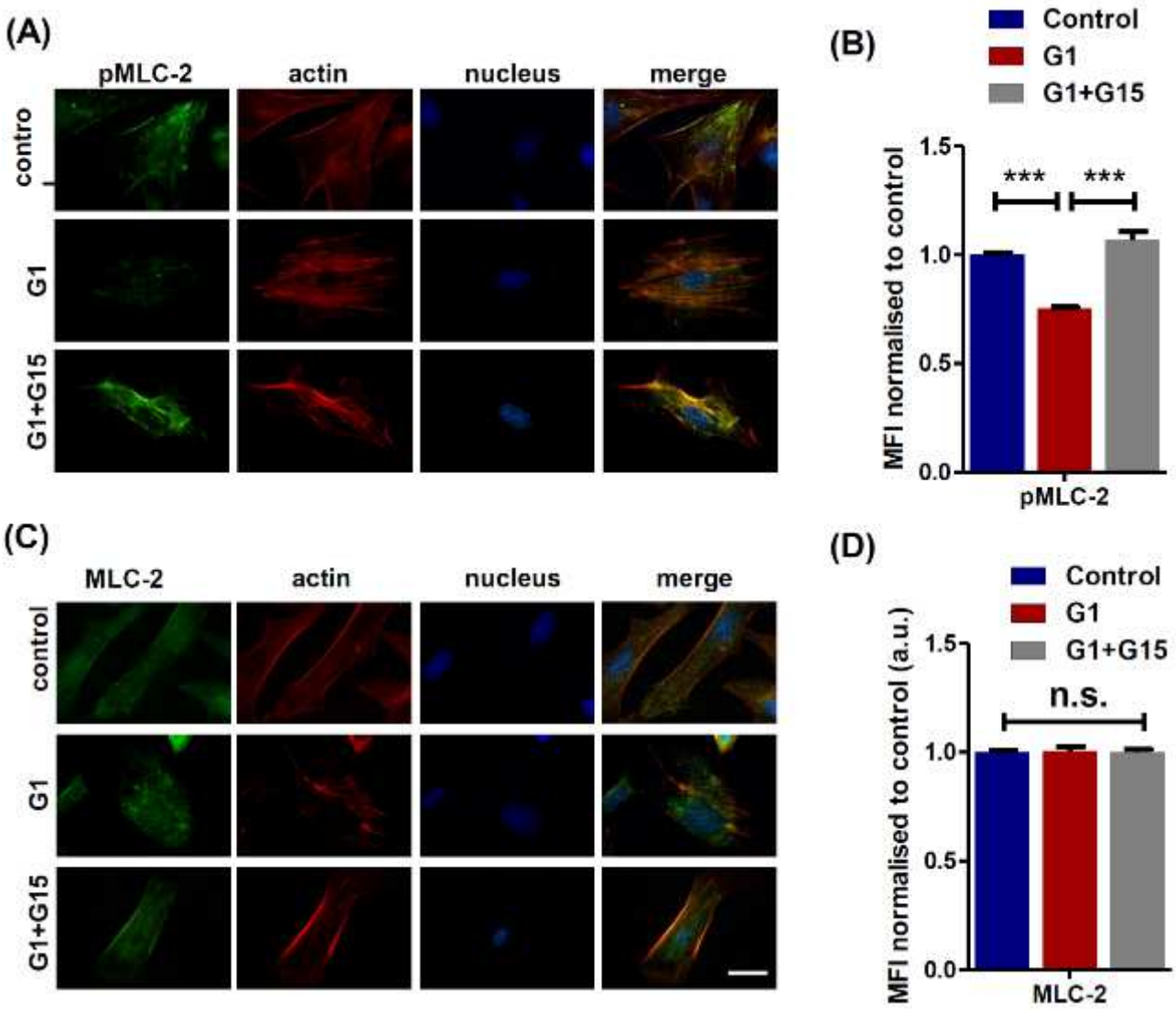

Figure 6.7 GPER activation supresses activation (phosphorylation) of MLC-2 but does not affect the expression of total MLC-2 in mouse embryonic fibroblasts (MEFs) cells. (A, C) Representative immunofluorescent images of MEFs, scale bar is 20 μm. (B, D) Quantification of mean fluorescence for panels a and c. Histogram bars represent mean ± s.e.m. Number of cells: 23 control, 21 G1, 11 G1 + G15, Three experimental replicates. Anova and post-hoc Tukey test ***$p < 0.001$.

6.2.3 GPER modulates force generation and mechanosensing

The reduced levels of pMLC-2 in G1 treated HFFs suggests that the cytoskeleton is significantly less contractile following GPER activation. The ability of cells to generate traction forces depends on the presence of a contractile actomyosin cytoskeleton, whose generated force is transmitted to focal adhesions that apply force to the substrate[298]. An elastic pillar array, a form of traction force microscopy, was used to measure traction forces generated by fibroblasts.

Time-lapse microscopy of the fibronectin-coated pillar array was used to analyse deflection of the elastic pillars, which is proportional to force applied by cells according to Hooke's law.

It was observed that control HFFs generated traction forces with a mean maximum force of around 1.5 nN, but G1 treated HFFs showed significantly less force generation, with a mean maximum force of around 0.7 nN. Co-incubation of G1 with G15 rescued force generation to around 1.4 nN, a value not significantly different from control HFFs. Similar forces to control were observed when HFFs were treated with G1 after knocking down GPER or when treated with G1 followed by introduction of a constitutively active RhoA in HFFs (Figure 6.8 a, b).

The elastic modulus of cells (a measure of cytoskeletal stiffness) is dependent on the structure of the cytoskeleton and its contractile state[299]. Nanoindentation atomic force microscopy was utilised to determine the Young's modulus of HFFs, using a cantilever with a 15 µm diameter polystyrene bead attached. It was observed that control HFFs showed a Young's modulus of around 6 kPa, a value within the expected range for fibroblasts[300]. The Young's modulus was significantly reduced to 1 kPa with G1 treatment. When G15 was used in conjunction with G1, the Young's modulus was significantly greater at 6 kPa, not significantly different from control HFFs (Figure 6.8 c, d), indicating that GPER activation is essential in modifying the rheological properties of the cell.

Furthermore, magnetic tweezers microrheology was used to assess the effect of GPER activation in the ability of cells to respond to external mechanical stimuli. Mechanical forces applied to mechanosensitive receptors such as integrins trigger an adaptive local stiffening, which is dependent on the RhoA/MLC-2 axis[301]. Mechanosensory response was quantified by applying a series of 12 successive force pulses of equal intensity to fibronectin-coated magnetic beads attached to the cell surface. Beads connected to cells with intact mechanosensory machinery will reduce their amplitudes of oscillation over time. The relative bead displacement was calculated by normalizing the displacement for each pulse to that observed during the first pulse.

It was observed that a robust mechanosensory response and cytoskeletal stiffening in control HFFs is demonstrated by the significant reduction of the bead oscillation after the 12th pulse compared to the first pulse (Figure 6.8 e, f). HFF cells treated with G1 showed an impaired ability to respond to mechanical forces (mechanosensing) as the oscillation of the beads after the 12th pulse did not significantly differ from the oscillation amplitude associated with the 1st

pulse of force. It was observed that the mechanosensory ability of HFFs was recovered and comparable to the levels shown in control HFFs in the following conditions: (1) The agonist G1 in the presence of the antagonist G15, (2) knocking down GPER expression via siRNA in control cells and in cells that were subsequently treated with G1, and (3) HFFs treated with G1 and subsequently rescued with constitutively active RhoA. These results show that GPER activation inhibits cellular mechanosensing via RhoA to adjust cell mechanics.

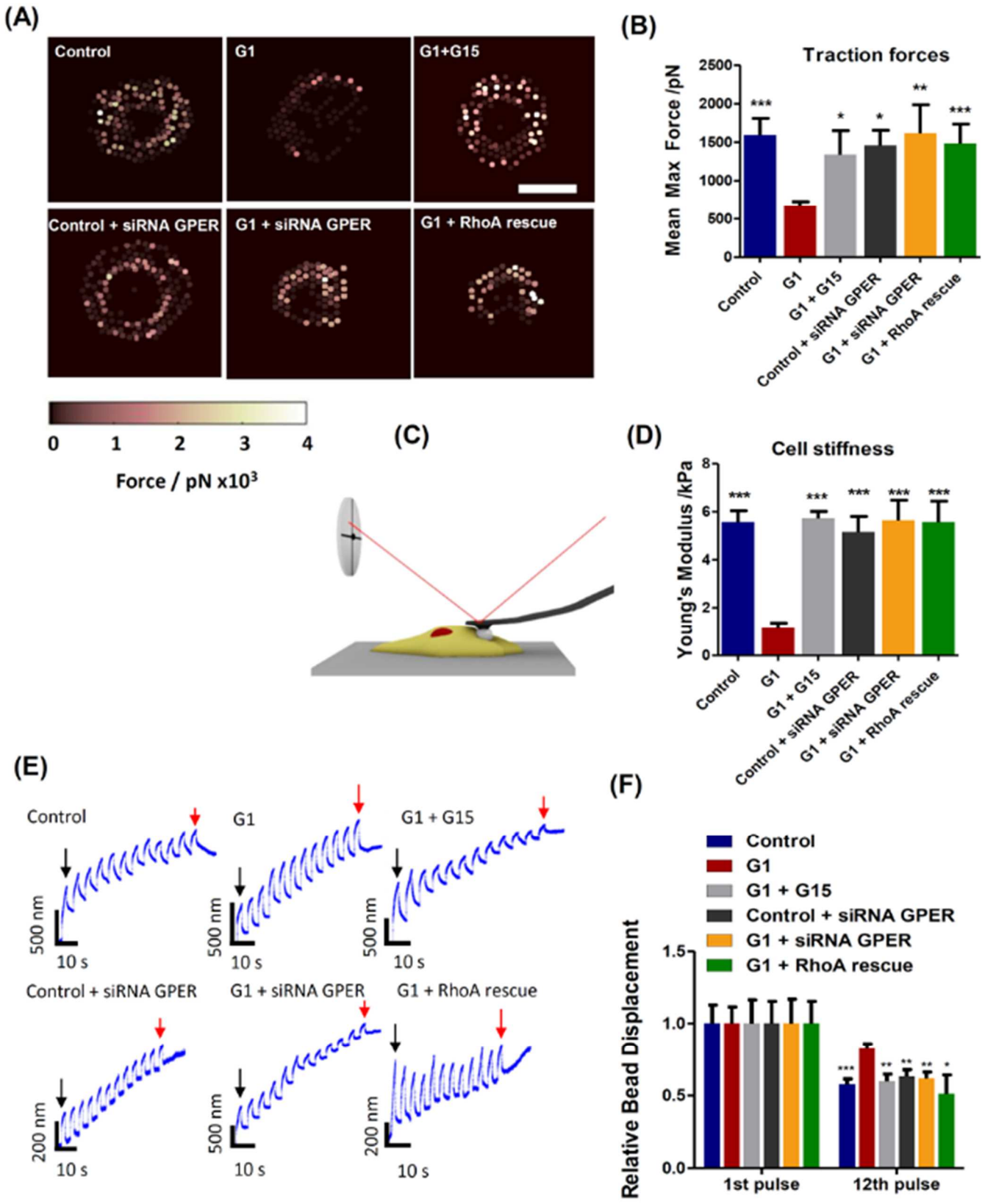

Figure 6.8 GPER activation reduces HFF force generation, cell stiffness, and mechanosensing. (A) Elastic pillars force maps for human foreskin fibroblasts (HFFs). Scale bar = 20 μm. (B) Mean maximum force calculated from elastic pillar force maps. Markers denote significant

difference from G1 condition by Mann-Whitney test, *p < 0.05, **p < 0.01 ***p < 0.001. For control, G1, G1+G15, control + siRNA GPER, G1 + siRNA GPER and G1 + RhoA rescue, n = 32, 34, 29, 30, 28, 20 cells. G1 (GPER agonist) and G15 (GPER antagonist). (C) Schematic illustrating the AFM used to measure cell stiffness. (D) Mean cell stiffness as determined by AFM. Markers denote significant difference from G1 condition by Mann-Whitney test, *p < 0.05, ***p < 0.001. For control, G1, G1+G15, control + siRNA GPER, G1 + siRNA GPER and G1 + RhoA rescue, n = 55, 41, 78, 25, 30, 28 cells. (E) Representative bead displacement curves for mechanosensing analysis of HFFs with magnetic tweezers, with 12 consecutive pulses of 1 nN of force. Black arrow indicates peak of 1st pulse, red arrow indicates peak of 12th pulse. (F) Mean of displacement of 1st and 12th pulse, relative to 1st pulse. For 1st pulse, error bars represent s.e.m for absolute values of bead displacement on the 1st pulse. For 12th pulse, error bars represent s.e.m for values of bead displacement on the 12th pulse as a proportion of their respective 1st pulse. Markers denote significant difference from G1 condition by Mann-Whitney test, *p < 0.05, **p < 0.01, ***p < 0.001. For control, G1, G1+G15, control + siRNA GPER, G1 + siRNA GPER and G1 + RhoA rescue, n = 23, 13, 18, 11, 14, 5 cells. All experiments were run at least in triplicate.

6.2.4 GPER activation suppresses the myofibroblast-like phenotype

The contractility of stress fibres, mediated by RhoA, and required for force generation and mechanotransduction, is a key feature of the myofibroblastic phenotype of activated fibroblasts[302]. This phenotype, characterised by increased expression of the intermediate filament protein vimentin and alpha smooth muscle actin (α-SMA)[303], is essential for fibroblasts to remodel the stroma in ECM homeostasis. The unabated activation of myofibroblasts lead to defective healing and fibrotic processes[302].

Following the immunofluorescence staining it was observed that G1 treated HFFs showed lower expression of the activated cell markers α-SMA and vimentin than control HFFs. G1 + G15 treated cells showed expression levels of these markers similar to control, i.e. significantly higher than in G1 treated cells (Figure 6.9 a-d). RT qPCR analysis of control, G1, and G1 + G15 treated HFFs also indicated the same trends with both α-SMA and vimentin showing reduced expression with G1, which could be rescued by also using G15 (Figure 6.9 e). These results were recapitulated using MEF cells (Figure 6.10). Together, these findings suggest that GPER activation inhibits the process of myofibroblastic trans-differentiation in fibroblasts.

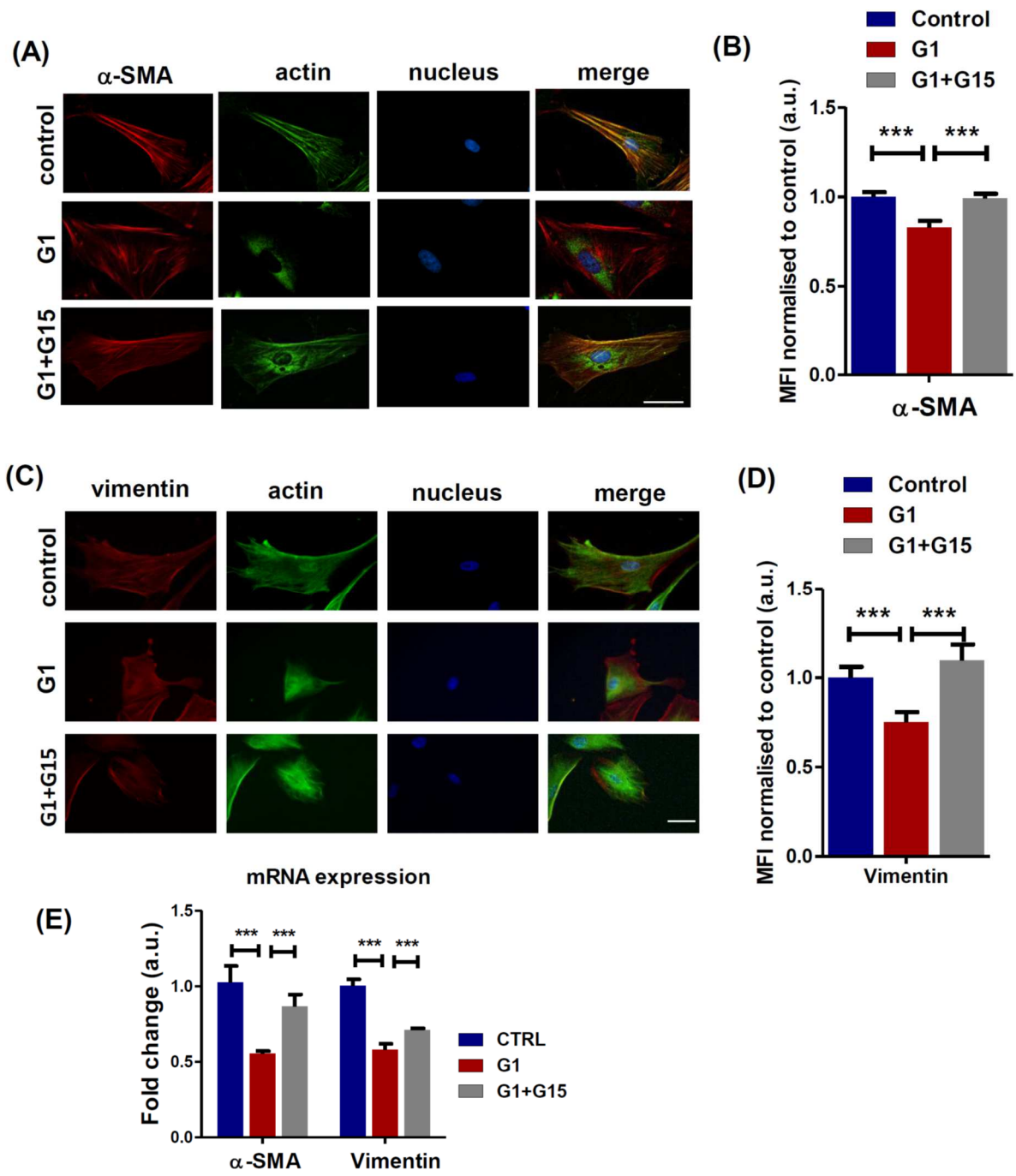

Figure 6.9 GPER activation induces HFF deactivation. (A, C) Representative immunofluorescent images of human foreskin fibroblasts (HFFs), scale bar represents 20 µm. (B, D) Quantification of mean fluorescence for panel a and c. (e) qPCR quantification of mRNA levels. Values are relative to control and normalised to RPL0 (60S acidic ribosomal protein). Histogram bars represent mean ± s.e.m. Number of cells: 24 control, 25 G1, 15 G1 + G15, Three experimental replicates. Anova and post-hoc Tukey test *** $p < 0.001$.

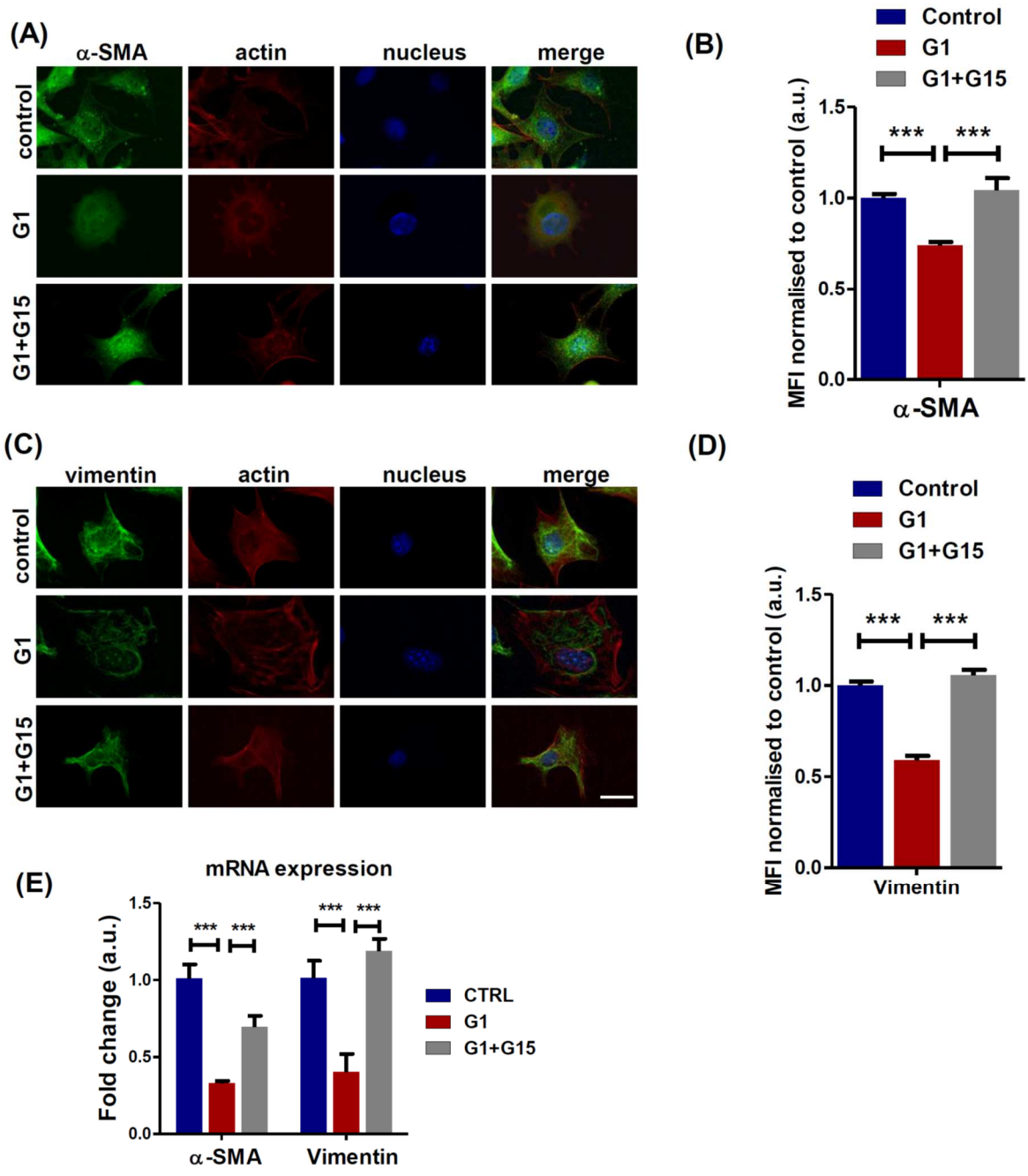

Figure 6.10 GPER activation induces MEF deactivation. (A, C) Representative immunofluorescent images of mouse embryonic fibroblasts (MEFs), scale bar represents 20 µm. (B, D) Quantification of mean fluorescence for panel a and c. Number of cells: Vimentin 24 control, 25 G1, 15 G1+G15/ a-SMA Vimentin 23 control, 12 G1, 22 G1+G15 (E) qPCR quantification of mRNA levels. Values are relative to control and normalised to (60S acidic ribosomal protein P0) RPL0. Histogram bars represent mean ± s.e.m. Three experimental replicates. Anova and post-hoc Tukey test *** $p < 0.001$.

6.2.5 GPER regulates cell polarization and assembly of actin stress fibres

Stress fibres are bundles of F-actin filaments that lies in the cell cortex beneath the plasma membrane. These structures are present in most animal cells and are particularly prominent in

fibroblasts. They have fundamental roles in cell adhesion, force generation, mechanosensing, and in general coordination of forces to drive tensional homeostasis in cells. Ventral stress fibres are attached to focal adhesions at both ends, are highly contractile, rich in MLC-2, and assemble in response to force generated by the RhoA/MLC-2 axis[304,305]. Thus, it was sought to study if/how GPER activation affects these cytoskeletal structures.

It was observed that control HFFs had numerous and thick ventral fibres widely distributed across the entire cell body particularly abundant in the posterior area of the well-polarized cells and less numerous in the leading edge (common localization of ventral fibres[305]). In stark contrast, G1 treated HFFs showed lack of polarization and a significant decrease in the number and thickness of ventral fibres (Figure 6.11 a-c). However, it was observed that G1 treatment did not affect the number and thickness of ventral fibres in HFFs that were previously treated with siRNA to knock down GPER expression. These cells showed values comparable to the ones observed in control HFFs. Likewise, HFFs that were treated with G1 and then rescued with constitutively active RhoA displayed marked polarization and the number and thickness of ventral fibres similar to control HFFs.

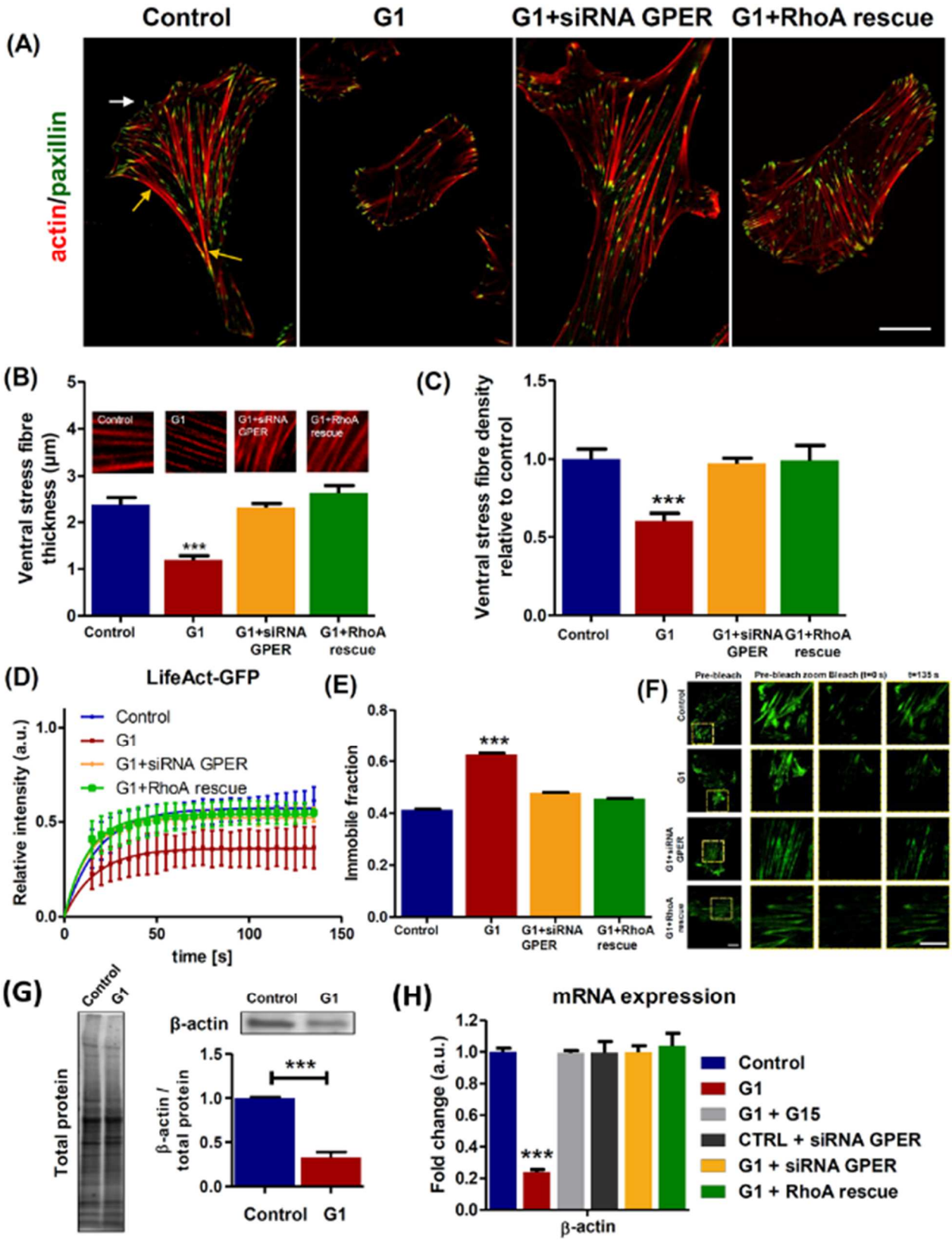

Figure 6.11 Actin polymerisation rate and fibre thickness are dependent on the GPER/RhoA axis. (A) Representative images of human foreskin fibroblasts (HFFs), scale bar is 20 µm. The white arrow indicates the lamellipodium and the yellow arrows, the localization of the ventral stress fibres. (B, C) Quantification of thickness and density of ventral fibres in HFFs. Number of cells: 23 control, 24 G1, 29 G1 + siRNA GPER, 24 G1 + active RhoA rescue. G1 (GPER

agonist). (D) FRAP curves for the recovery of lifeAct-EGFP in HFFs. (E) Immobile fraction data obtained from fit of FRAP curves in d. 50 cells per condition. (F) Representative images of actin fibres in human foreskin fibroblasts (HFFs), scale bar is 10 µm. (G) Western blot – β-actin expression levels in HFFs. (H) qPCR quantification of mRNA levels of □-actin in HFFs. Values are relative to control and normalised to RPL0 (60S acidic ribosomal protein). Histogram bars represent mean ± s.e.m. The marker denotes significant difference of G1 condition from the rest *** $p < 0.001$. Three experimental replicates. Anova and Tukey post hoc test *** $p < 0.001$.

6.2.6 GPER activation inhibits actin polymerisation and synthesis of β-actin

The actin cytoskeleton is highly dynamic, with continuous remodelling and polymerisation & disassembly of actin filaments. These two processes drive the formation of lamellipodia and facilitate cell detachment at the trailing edge of spreading and migrating cells. RhoA is known to activate the downstream effector formin protein mDia to induce actin polymerisation and drive the formation and assembly of stress fibres[292]. Using lifeAct-GFP, F-actin was visualised in living HFF cells. Then, fluorescence recovery after photobleaching (FRAP) was utilised to study the dynamics of actin polymerisation in control, G1 treated, siRNA GPER and G1 treated, and G1 treated and rescued with constitutively active RhoA HFF cells (Figure 6.11 d-f). The recovery of the GFP signal in the bleached region serves as a measure of the dynamics of the actin polymerisation in these fibres.

Comparable levels in the fluorescence recovery of lifeAct-GFP signal were observed in control, siRNA GPER and G1 treated, and G1 treated and rescued with constitutively active RhoA HFF cells (Figure 6.11 d, f). The recovery rate was significantly reduced 40% in G1 treated HFFs. Analysis of the recovery curves also showed a larger population of the immobile fraction of in G1 treated HFFs compared with the rest of conditions (Figure 6.11 e). These findings imply a lower polymerisation rate in G1 treated HFFs that is modulated by the GPER/RhoA axis.

To investigate if the GPER-mediated decrease in actin polymerisation affected the overall synthesis of β-actin monomers in cells, the expression of β-actin at the protein and gene levels were quantified using Western blot and RT qPCR, respectively. Interestingly, the levels of expression of β-actin protein were significantly downregulated in G1 treated HFF cells compared to control (Figure 6.11 g and Figure 6.12). Also, a pronounced decrease in the levels of mRNA for β-actin in G1 treated HFF cells was observed compared to control. Values comparable to controls were observed when G1 treatment was carried out in the presence of

the antagonist G15, or when siRNA GPER was used, or when cells were rescued with active RhoA after G1 treatment (Figure 6.11 h). Taken together these results show that GPER activation retards actin polymerisation via RhoA and suggest that this triggers a negative regulatory feedback that reduces the synthesis of β-actin at the gene level.

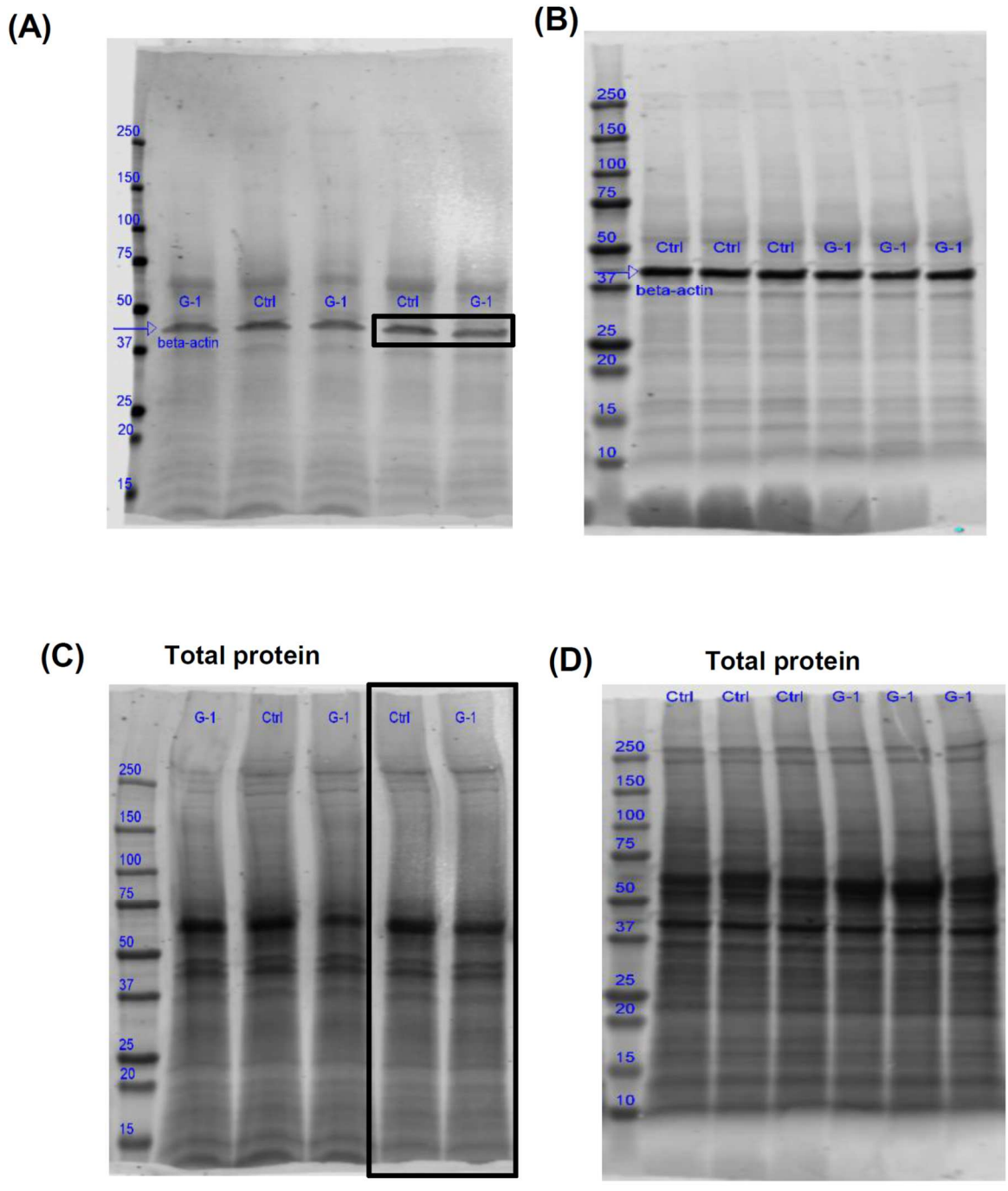

Figure 6.12 Full membranes for Western blot of β-actin (A, B) and total protein (C, D) in HFFs. Control (ctrl) and treated with GPER agonist (G1). 20 µg (A, C) or 9 µg (B, D) of protein was loaded per lane. Samples on each blot were normalised to control on the same blot before statistical analysis. Bands presented in figure are indicated by rectangle.

6.2.7 GPER modulates focal adhesion formation and dynamics through RhoA

The actomyosin cytoskeleton links to the extracellular environment through focal adhesions. These membrane-bound protein complexes are signalling hubs that allow the bi-directional communication of cells with the ECM and drive traction force generation and mechanosensing through regulation of Rho GTPases and modulation of myosin activity[306]. Using GFP-paxillin transfected HFFs, it was observed that focal adhesions in G1 treated HFFs were significantly smaller than in control HFFs. Knocking down GPER suppressed the G1 effect on the focal adhesion sizes in HFFs. G1 treatment followed by active RhoA rescue of HFFs showed a focal adhesion area not significantly different from control cells (Figure 6.13 a, b), suggesting a control of the focal adhesion size in HFFs through the GPER/RhoA axis.

Focal adhesions are highly dynamic structures, with formation, growth, and disassembly dependent on cytoskeletal properties such as mechanical tension and cell contractility[285]. The application of force to focal adhesions by the cytoskeleton promotes turnover of focal adhesion components such as paxillin[307]. The GFP-paxillin transfected HFF cells were used to image focal adhesions combining total internal reflection fluorescence (TIRF) with FRAP. It was observed that following photobleaching, G1 treated HFFs showed a reduced ability to recover paxillin fluorescence in the bleached area compared to control cells (Figure 6.13 c-e). This indicates that focal adhesion turnover is significantly reduced following G1 treatment. Knocking down GPER via siRNA before G1 treatment or rescuing the G1 treated HFFs with active RhoA recovered the focal adhesion dynamics seen in control HFFs, suggesting a control of focal adhesion dynamics by mechanical tension modulated by the coordinated action of GPER and RhoA.

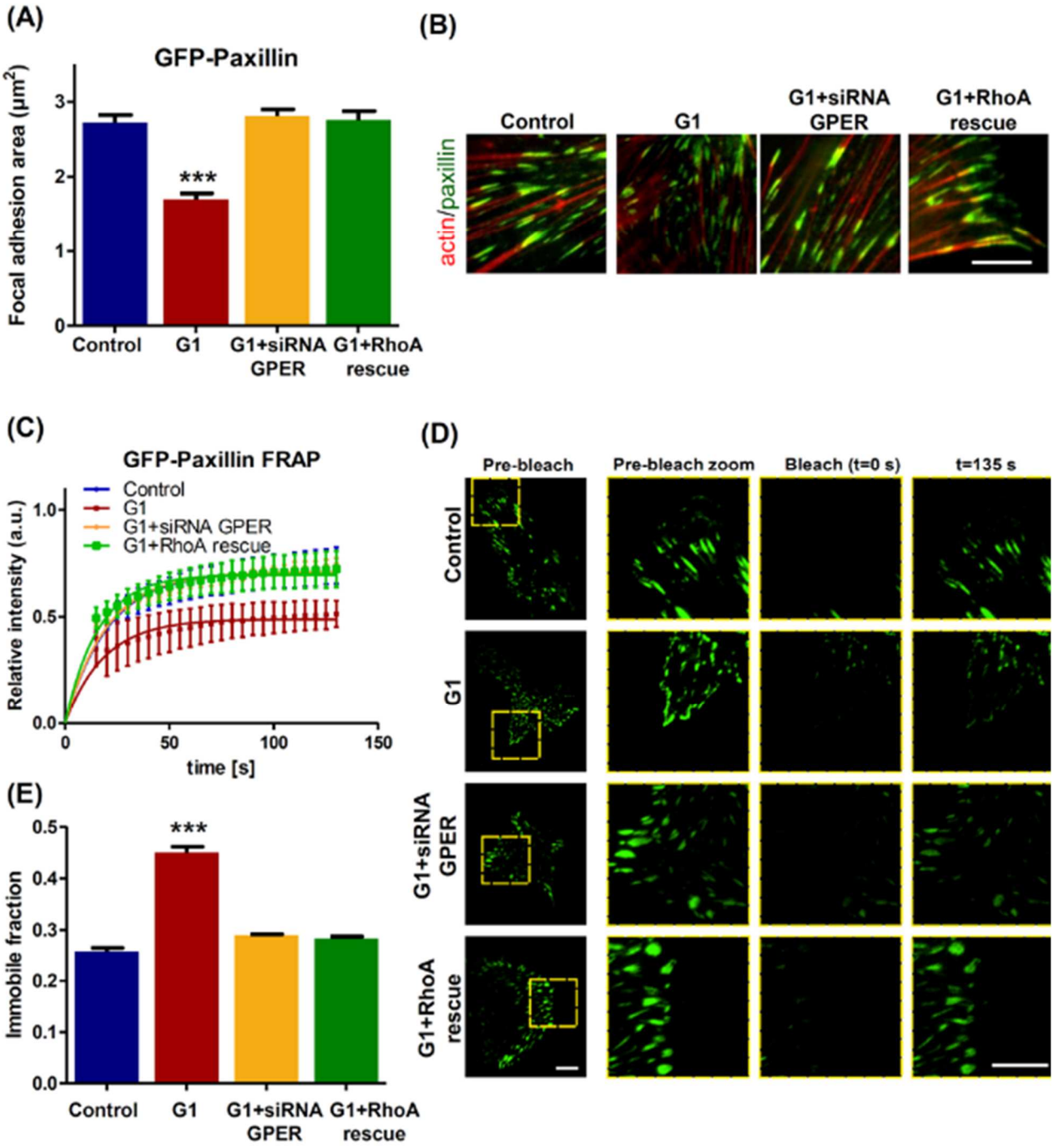

Figure 6.13 GPER activation regulates the size and dynamics of focal adhesions in human foreskin fibroblasts (HFFs). (A) Quantification of paxillin-based focal adhesion areas. Number of cells: 15 control, 16 G1, 21 G1 + siRNA GPER, 18 G1 + active RhoA rescue. G1 (GPER agonist). (B) Representative images of regions of interest in human foreskin fibroblasts (HFFs) cultured on fibronectin coated glass, scale bar represents 10 μm. (C) FRAP curves for the recovery of GFP-paxillin in focal adhesions of HFFs. (D) Representative TIRF-FRAP images of GFP-paxillin focal adhesions in HFFs, scale bar represents 10 μm. (e) Immobile fraction data obtained from fit of FRAP curves in d (number of cells: 34 control, 114 G1, 47 G1 + siRNA GPER, 64 G1 + RhoA rescue. Histogram bars represent mean ± s.e.m. The marker denotes significant difference of G1 condition from the rest *** $p < 0.001$. Three experimental replicates. Anova and Tukey post hoc test *** $p < 0.001$.

6.2.8 GPER inhibits YAP nuclear localisation and activation

The transcriptional regulator YAP is activated and translocates to the nucleus in response to mechanical cues, leading to regulation of gene expression. This mechanical activation of YAP is independent of the Hippo signalling cascade, and requires RhoA GTPase activity and actomyosin contractility[189]. It was observed through immunofluorescence staining that YAP is highly localised to the nucleus in control HFFs, and that this nuclear localisation is significantly reduced in G1 treated HFFs. G1 and G15 together show YAP localisation at a level not significantly different from control cells (Figure 6.14 a, b).

The downstream transcriptional activity of YAP was also assessed through RT qPCR, and expression of the YAP target genes ankyrin repeat domain 1 (ANKRD1) and connective tissue growth factor (CTGF)[189]. The expression levels of both genes were significantly reduced in G1 treated cells compared to control, and co-incubation with G15 rescued the expression of both genes to the levels comparable to control (Figure 6.14 c). Also, the same effects of GPER activation in YAP nuclear localisation and expression of downstream genes ANKRD1 and CTGF in MEFs were observed following G1 and G15 treatments (Figure 6.15).

HFFs then were seeded on polyacrylamide gels of differing stiffnesses (4 kPa and 25 kPa gels) following a previously reported procedure[308]. In 4 kPa gels, HFFs showed similar levels of nuclear and cytoplasmic YAP, and treatment with G1, or G1 after siRNA downregulation of GPER did not significantly alter the YAP nuclear to cytoplasmic ratio (Figure 6.14 d-e). In contrast, when active RhoA was overexpressed in G1 treated HFFs, the nuclear to cytoplasmic ratio increased 4-fold. In 25 kPa gels, this ratio in control HFFs was 6-fold increased compared to control HFFs on 4 kPa gels. This result is in agreement with previous observations that demonstrated that stiffer substrates induce YAP nuclear localisation[189]. G1 treatment of HFFs seeded on 25 kPa gels reduced the nuclear localization of YAP to values comparable to those in HFFs on 4 kPa. G1 treatment of HFFs on 25 kPa gels after siRNA downregulation of GPER or followed by active RhoA rescue recovered the nuclear to cytoplasmic ratios seen in control HFFs seeded on 25 kPa. Collectively, the results show that GPER activation induces a RhoA mediated mechanical activation of YAP.

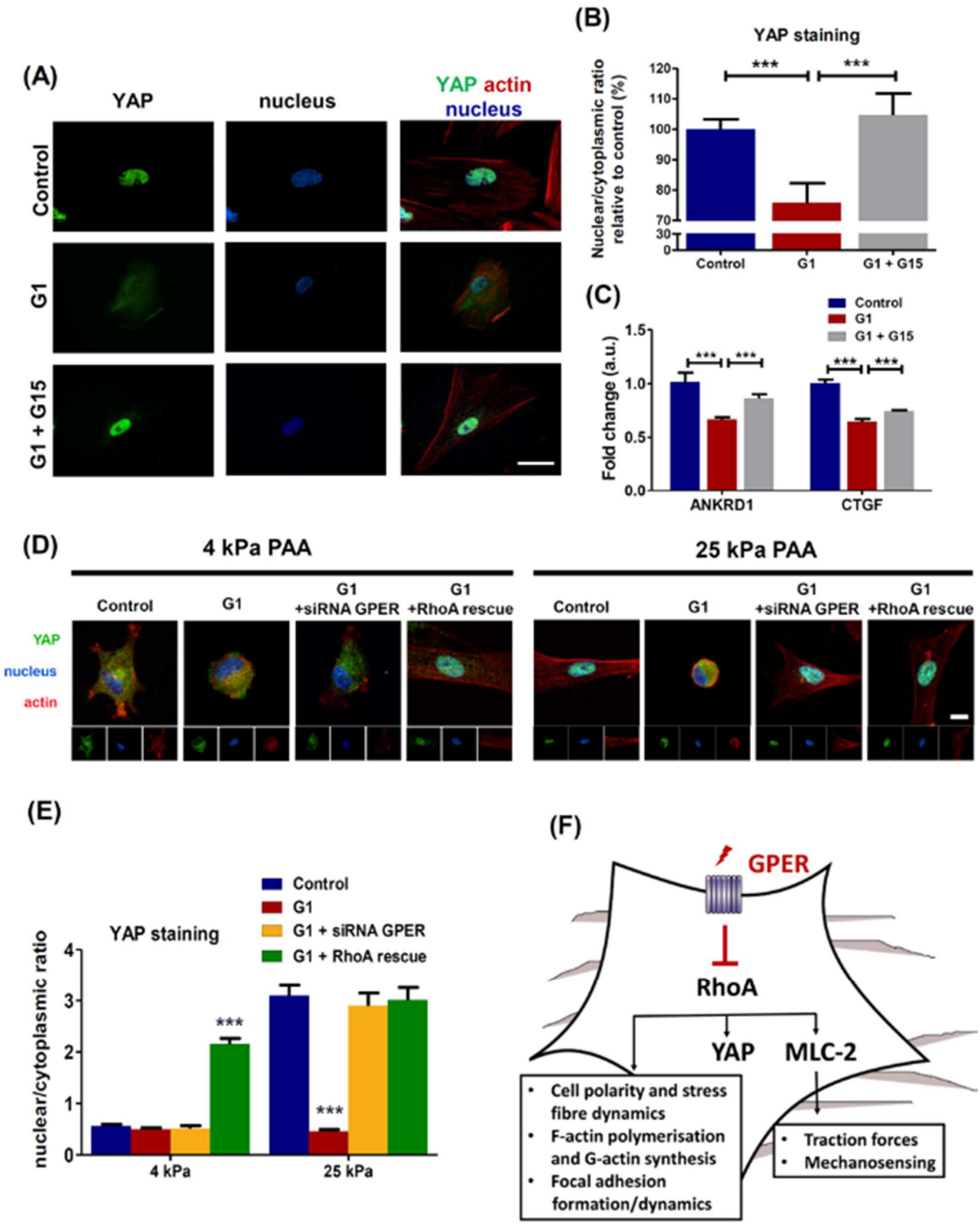

Figure 6.14 GPER activation decreases nuclear localisation of YAP in the nucleus and YAP activation. (A) Representative images of human foreskin fibroblasts (HFFs) cultured on fibronectin coated glass, control, G1, and G1+G15 treated cells. Scale bar is 20 µm (B) Quantification of YAP nuclear to cytoplasmic ratio. Number of cells: 11 control, 10 G1, 12 G1 + G15. G1 (GPER agonist) and G15 (GPER antagonist). (C) qPCR gene expression of Ankyrin Repeat Domain 1 (ANKRD1) and connective tissue growth factor (CTGF) – YAP downstream

genes. Values are relative to control and normalised to RPL0 (60S acidic ribosomal protein). (D) Representative images of human foreskin fibroblasts (HFFs) cultured on soft (4 kPa) and stiff (25 kPa) polyacrylamide gels. Scale bar is 10 μm. (E) Quantification of YAP nuclear to cytoplasmic ratio. Number of cells: 4 kPa/ 10 control, 10 G1, 11 G1 + siRNA GPER, 14 G1 + active RhoA rescue. 25 kPa/ 12 control, 12 G1, 11 G1 + siRNA GPER, 10 G1 + active RhoA rescue Histogram bars represent mean ± s.e.m., Three experimental replicates. Anova and Tukey post hoc test. The marker denotes significant difference of the condition from the rest *** $p < 0.001$. (F) Model illustrating the effect of GPER activation in fibroblasts.

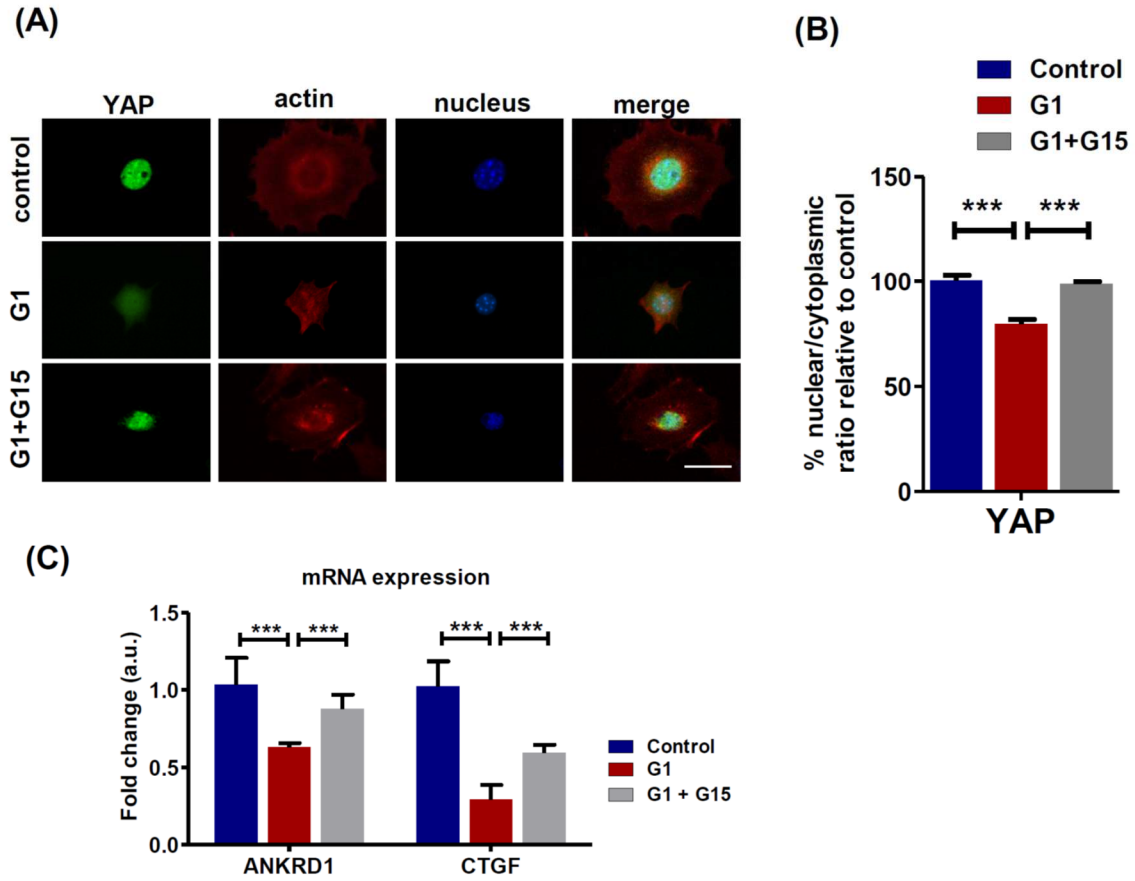

Figure 6.15 GPER activation decreases nuclear YAP location via mechanical pathway in mouse embryonic fibroblasts (MEFs) cells. (A) Representative images of MEFs cultured on fibronectin coated glass, Scale bar is 20 µm (B) Quantification of YAP nuclear to cytoplasmic ratio. Number of cells: 11 control, 10 G1, 12 G1 + G15. (C) qPCR gene expression of Ankyrin Repeat Domain 1 (ANKRD1) and connective tissue growth factor (CTGF) – YAP downstream genes. Values are relative to control and normalised to RPL0 (60S acidic ribosomal protein). Histogram bars represent mean ± s.e.m., Three experimental replicates Anova and post-hoc Tukey test *** $p < 0.001$

6.3 Discussion

The wealth of physiological and pathological roles of rapid estrogenic signalling through GPER underlies the importance of understanding its regulation and downstream signalling effects. In this work, a previously unidentified biomechanical mechanism is highlighted, by which the ubiquitous transmembrane receptor GPER regulates global cell mechanics and the activation of YAP-related genes in fibroblasts. It was found that activating GPER inhibits RhoA activation and consequently suppresses actomyosin contraction, traction force generation and mechanosensing. Accordingly, GPER controls the structure and dynamics of focal adhesion complexes and the actin cytoskeleton (Fig. 6.14 f).

This work positions GPER as another key player in regulating cellular mechanotransduction events and lay the ground for further investigation on how GPER mediated changes in the cytoskeleton may control other processes in cells such as adhesion, spreading, migration, membrane protrusion, endocytosis, phagocytosis, and organization of the actin rings at the end of mitosis among many others.

The broader implications of GPER mediated mechanotransduction events in fibroblasts will need to be established. For example, GPER could affect actomyosin-dependent ECM remodelling directly impacting on the regulation of connective tissue homeostasis in health and disease[309]. A stiff fibrotic ECM, generated by fibroblasts and fibroblast like cells, is also a major clinical hallmark of solid tumours, often associated with aberrant mechanotransduction[166] and this GPER mediated mechanism may provide a therapeutic target wherein mechanical deactivation of fibroblasts leads to a reduction in tumour permissive desmoplasia.

The physiology of many cells depends on generation and perpetuation of a defined mechanical phenotype, which is often altered in disease and therefore targeted by therapeutics. For example, inhibitors of Rho-associated kinase are proposed as potential therapeutic options for a range of diseases such as cancer, glaucoma and insulin resistance[310]. GPER, which is revealed to be a new mechanoregulator, has been investigated for its therapeutic effects in diseases such as cancer, cardiovascular disease, and atherosclerosis[311,312]. This suggests that therapeutics targeting GPER may also deregulate mechano-pathologies in addition to influencing biomechanical signalling.

The results also provide an additional dimension to GPER activation, as it can also mechanically modulate YAP activity. YAP, and its orthologue TAZ, are mechanoresponsive transcriptional regulators that are essential in development, tissue homeostasis and cancer[313]. YAP/TAZ signalling can reprogram cancer cells into cancer stem cells, and therefore promote tumour progression and metastasis[313]. Additionally, YAP/TAZ signalling is implicated in the pathogenesis of atherosclerosis and hemodynamic-induced mechanotransduction[314]. The data linking GPER to YAP activation may provide new therapeutic targets for cancer, cardiovascular disease and regenerative medicine and shed new insights into force-regulated processes in developmental biology.

Collectively, the results indicate the importance of GPER and RhoA in regulating the mechanical properties of fibroblasts, suggesting its wide applicability in other cell types. This mechanical regulation by this estrogen sensitive GPCR may allow development of therapeutics that target diseases in which altered mechanics play a pathological role.

6.4 Materials and methods

6.4.1 Cell culture, transfection, and antibodies

The human foreskin fibroblasts (HFFs) were from ATCC (catalogue number SCRC-1041). The mouse embryonic fibroblasts (MEFs) were a gift from Dr. Wolfgang Ziegler and has been previously described by Xu & Baribault, 1998[315]. Both cell lines were maintained in high-glucose DMEM supplemented with 10% FBS and 1% GlutaMax (Thermo Fisher Scientific, USA), 1% Penicillin/Streptomycin (Sigma Aldrich, P4333), and 1% Fungizone R Amphotericin (Gibco, 15290-026). A humidified 37 °C incubator with 5 % CO2 was used for culturing both cell lines. Cells were negative when tested for mycoplasma contamination. To prevent any estrogenic effects from phenol red, during the treatment with G1, HFFs (or MEFs) were transferred to clear medium with no phenol red (DMEM/ Nutrient Mixture F-12 Ham (DMEM/F-12, Sigma-Aldrich, D6434) supplemented with 5% Double Charcoal Foetal Calf Serum - DCSS (First Link UK, 02-46-850), 1% L-glutamine (Sigma Aldrich, G7513) and 1% Penicillin-Streptomycin solution (Sigma Aldrich , P4333), and 1% Fungizone R Amphotericin (15290-026, Gibco, USA). For subsequent experiments media (without phenol red) and DCSS were used. When cells reached 60-70% confluence in T-25 flasks, full culture medium was replaced by clear medium, and the cells were treated with G-1 (1μM) for 24hs. 2 μM of G15 was used simultaneously with G1 (1μM) to antagonize GPER activation. Total RhoA

(Millipore 04-822, WB 1/1000), pRhoA (Abcam ab41435, WB 1/100), MLC-2 (Millipore, MABT180, WB 1/100 and IF 1/200), pMLC-2 /Thr18/Ser19 (Cell Signalling, 3674, WB 1/100, IF 1/200), αSMA (Abcam, ab7817, 1/100), Vimentin (DAKO, M0725, 1/1000), GPER (abcam ab39742). Anti-Mouse HRP (Invitrogen, 626580, 1/2,000), Anti-Rabbit HRP (Abcam, ab137914, 1/2,000), and Anti-Mouse 488 (Invitrogen, A11029, 1/400). siRNA GPER was purchased from Santa Cruz Biotechnology (sc-60743). GPER agonist (G1) and GPER antagonist (G15) were purchased from Tocris, G1 (cat. 2577), G15 (cat. 3678). The constitutively active RhoA plasmid (pRK5-myc-RhoA-Q63L) was a gift from Gary Bokoch (Addgene plasmid # 12964). This plasmid was used as a template to create the plasmid RhoA (S188A/Q63L) by substitution of the serine amino acid in position 188 to alanine using site directed mutagenesis. Cells were transfected using the Neon Transfection system (Invitrogen, Thermofisher, UK) according to manufacturer's instructions with one pulse of 1300V and 30ms. 5 µg DNA and 10^6 cells were used per reaction. Measurements were performed within 72 h after transfection.

6.4.2 Scanning Electron Microscopy

The morphology of cells was analysed using scanning electron microscopy. Cells were fixed with 3% EM-grade glutaraldehyde in 0.1 M PBS for 15 min at 37°C and washed with 0.1 M PBS. Following fixation, cells were lipid contrast stained using 1% OsO4 in PBS for 1 hour at room temperature and dehydrated in ethanol with gradually increasing concentration. Samples were air dried overnight and coated with 10 nm Cr. The images were acquired using Zeiss Auriga Cross Beam SEM with 7.5 x 103 magnification, 5 kV. Images were analysed using FIJI by thresholding in order to detect the outline of at least 10 cells per condition. Obtained masks were measured using the Area and Roundness parameters.

6.4.3 Immunofluorescence staining

Cell immunofluorescence staining was done on coverslips coated with 10 µg ml^{-1} fibronectin (Gibco, phe0023). Following pertinent treatment, cells were fixed with 4% paraformaldehyde (Sigma, P6148) in D-PBS (Sigma, D8537) for 10 min, and then blocked and permeabilized with 0.2% BSA, 0.1%Triton (Sigma, T8787) in PBS for 30 min. After blocking, cells were incubated with primary antibodies prepared in blocking solution for 1 h at room temperature in a humidified chamber. Then, cells were washed in D-PBS and incubated with Alexa Fluor 488-

conjugated secondary antibodies and Phalloidin (Invitrogen, A22283, 1/1,000 dilution) prepared in PBS for 30 min at room temperature. Finally, coverslips were washed in PBS and mounted in mounting reagent with 4,6-diamidino-2-phenylindole (Invitrogen, P36931). Immunofluorescent images were taken with Nikon Ti-e Inverted Microscope (Nikon, Kingston-upon-Thames, United Kingdom) with NIS elements software.

6.4.4 YAP IF measurements

YAP immunofluorescence studies were conducted on 5 different samples incorporating 5 separate regions of interest to obtain images of single cells. IF images were obtained for cells in the 2 populations stained with Alexa Fluor 488, using a fluorescence microscope (AE31 trinocular, Motic) with a 480/30 nm excitation filter and a 535/40 nm emission filter. Images were obtained with a CMOS camera (Moticam 5, Motic) for 35 regions across the different coverslips with each population. Images for DAPI were also obtained with an excitation filter of 350/50 nm and emission of 460/50 nm in order to visualise the nucleus for the quantification of YAP staining regions. Images for the YAP and DAPI channels were combined to allow accurate location of the nucleus for the analysis of images in ImageJ. Measurements of the intensity of the fluorescence in the nucleus was obtained in ImageJ and compared against the total cell fluorescence intensity with the nuclear staining removed. Ratios of the nuclear to cytoplasm fluorescence intensities were calculated in order to analyse the localisation of YAP in the different cell populations and significances analysed via a non-parametric t-test in Prism (GraphPad).

6.4.5 Traction forces using elastic pillars

The micropillar arrays are based on the protocol as described previously[166]. Pillar arrays were created by mixing polydimethylsiloxane (PDMS) and a curing agent (Sylgard 184) in a 10:1 ratio and pouring this mixture into a pillar mould with holes of 5 µm depth and 1 µm diameter. This was incubated at 70 ºC for 12 hours for the PDMS to set, giving a Young's modulus of 2 MPa. Each pillar's spring constant was therefore 2.35 nN/µm. Once separated from the mould, PDMS pillars were coated with fibronectin (10 µl/mL PBS) for 1.5 hr at 37 ºC. The solution surrounding the pillars was replaced with PBS for washing, and then replaced by cell medium. Cells were trypsinised and resuspended in culture medium and seeded onto the pillars, then incubated for 1 hr at 37 degrees 5% CO2 before transfer to a Nikon Ti-e microscope in a 37 ºC

temperature-controlled chamber. Videos of different cells were taken at 1 frame per second for 60 seconds, and each pillar mould was imaged for a maximum time of 30 mins to ensure cell viability. The position of each pillar in the time-lapse videos was tracked using a custom MATLAB program to track the centre of a point spread function of the intensity of the pillars across all frames. By selecting a location free of cells, tracking of a small set of pillars allowed a measurement of the stage drift to be obtained and corrected for the data set. The time-dependent displacement of a given pillar was obtained by subtracting the initial position of the pillar (zero force) from the position in each frame. Traction forces were obtained by multiplying the pillar displacements by the pillar stiffness, determined from pillar height. The maxima for each pillar were found to obtain the average peak force across the cell.

6.4.6 Cell mechanosensing

HFFs were incubated with 4.5 µm fibronectin-coated magnetic beads coated for 30 minutes and then subjected to a pulsatile force regimen applied with magnetic tweezers, consisting of a 3 s, 1 nN pulse of force, followed by a 4 s period of rest, repeated for 12 total pulses over a 100 s time course. The ability of the cells to sense and respond to the applied tension was examined from the rapid cell stiffening response evident by the progressive decrease in amplitude of the bead movement.

6.4.7 Atomic force microscopy

Measurements of cell compliance were conducted on a Nanowizard-1 (JPK Instruments, Berlin, Germany) atomic force microscope operating in force spectroscopy mode mounted on an inverted optical microscope (IX-81; Olympus, Tokyo, Japan). Atomic force microscopy (AFM) pyramidal cantilevers (MLCT; Bruker, Camarillo, CA, USA) with a spring constant of 0.03 N/m (nominal stiffness reported by manufacturer) were used with a 15 µm diameter polystyrene bead attached at room temperature. Before conducting measurements, cantilever sensitivity was calculated by measuring the force–distance slope in the AFM software on an empty petri dish region. Cells were seeded on fibronectin-coated glass fluorodishes and allowed to spread for > 2 hours. For each cell analysed, force curves were acquired at an approach speed of 5 µm/s and a maximum set point of 1 nN. The force–distance curves were used to calculate elastic moduli in the AFM software through the application of the Hertz contact model.

6.4.8 Fluorescence Recovery After Photobleaching

The FRAP experiments were conducted on glass bottom Petri dishes (Mattek) coated with human plasma FN (10 μg ml^{-1}; Sigma) and incubated at 37 °C. Confocal photobleaching was carried out using an inverted microscope (Eclipse Ti; Nikon). Five confocal images were taken at 5 s intervals prior to bleaching for reference. Specified regions of the cells were then bleached using the confocal laser at 100% power. Images were taken at 5 s intervals for 100 s to capture fluorescent recovery. Images were analysed with FIJI[222], with the fluorescent signal normalised between the pre-bleach intensity and background. Statistical analysis was then carried out using Prism (GraphPad). Data was pooled from repeats. The significance between curves was measured using extra sum-of-squares F test on the best fit lines.

6.4.9 RT–PCR

Total RNA was extracted using the RNeasy Mini kit (Qiagen, 74104) and 1 μg of total RNA was reverse-transcribed using the High-Capacity RNA-to-cDNA kit (Applied Biosystems, 4387406) according to the manufacturer's instructions. qPCR was performed using the SYBR Green PCR Master Mix (Applied Biosystems, 4309155) with 100 ng cDNA input in 20 μl reaction volume. RPL0 (60S acidic ribosomal protein) expression level was used for normalization as a housekeeping gene. The primer sequences for were as follows: RPLP0 (F) 5'-CGGTTTCTGATTGGCTAC-3'; RPLP0 (R) 5'-ACGATGTCACTTCCACG-3'; MLC-2: forward, 5′-ATCCACCTCCATCTTCTT-3′ and reverse, 5′-AATACACGACCTCCTGTT-3′. CTGF: forward-5′-TTAAGAAGGGCAAAAAGTGC-3′, reverse-5′-CATACTCCACAGAATTTAGCTC-3′, ANKDR1: forward, 5′-TGAGTATAAACGGACAGCTC-3′ and reverse, 5′-TATCACGGAATTCGATCTGG-3′, ACTB: forward, 5′-GACGACATGGAGAAAATCTG-3' and reverse, 5′-ATGATCTGGGTCATCTTCTC-3'. All primers were used at 300 nM final concentration. The relative gene expression was analysed by comparative 2−ΔΔct method.

6.4.10 Western blotting

Cells were washed with chilled PBS and lysed in either Triton X-100 buffer (150 mM sodium chloride, 1% Triton X-100 and 50mM Tris-HCl, pH 8) or RIPA (Radioimmunoprecipitation Assay) buffer (150 mM sodium chloride, 1% NP-40, 0.5% sodium deoxycholate, 0.1% SDS and 50 mM Tris-HCl, pH 8) containing 1 mM activated Na3VO4 and protease inhibitors (Complete mini, Roche). Lysate was collected using a cell scraper, disrupted by repetitive

trituration through a 25-gauge needle, and incubated for 30 min on ice with periodic mixing. This was followed by centrifugation at 12,000g for 20 min at 4°C. The protein concentration in supernatant was determined using a BCA protein assay kit (Fisher Scientific, UK). Cell lysates were mixed with 4× Laemmli buffer (Bio-Rad) and denatured by heating at 100°C for 5 min. Samples then were loaded into a 4-20% Mini-PROTEAN TGX Precast Gel (Bio-Rad), and proteins were transferred to nitrocellulose membranes (Bio-Rad). Protein on membranes was stained using REVERT total protein stain (LI-COR) as per manufacturer's instructions, and blots were imaged using an Odyssey infrared imaging system. The stain was removed using REVERT Reversal Solution (LI-COR), followed by washing in tris-buffered saline (TBS). The membranes were blocked in Odyssey blocking buffer (LI-COR) for 1 hr followed by overnight incubation with primary antibodies in 0.1% Tween in TBS (TBST). After further washes in TBST, blots were incubated for 1 hr with secondary antibodies. Membranes were washed again in TBST and imaged using an Odyssey infrared Imaging system (LI-COR). Total protein for normalisation, and target protein expression were quantified using Image Studio Lite (Version 5.2, LI-COR). Target protein was normalised to total protein per lane and presented relative to the control group. The protein concentration was quantified by DC protein assay (Bio-Rad, 500-0113) according to manufacturer's instructions. Samples were separated by an SDS-PAGE gel under reducing conditions and transferred to a nitrocellulose membrane (GE Healthcare, 10401196) then blocked with 5% bovine serum albumin (BSA, Sigma, A8022) - 0.1% Tween20 (Sigma, P1379) in PBS. The membrane was washed and incubated with horseradish peroxidase (HRP) conjugated secondary antibodies in blocking solution for 1 hour at room temperature. Finally, the membrane was washed and developed with HRP substrate (Millipore, WBLUR0100). For the cases in which the total protein was used as reference.

6.4.11 G-LISA assay for RhoA

The intracellular amounts of total RhoA and RhoA-GTP were determined by using the total RhoA ELISA and G proteins-linked (G-LISA) assays (Cytoskeleton, Inc., Denver, CO, USA) according to the manufacturer's instructions. Briefly, cells were washed with cold PBS and homogenized gently in ice-cold lysis buffer. 20 µl was removed for protein quantification in order to adjust sample concentration to 0.5 mg/ml. After adding an equal volume of binding buffer, triplicate assays were performed using 1.5 µg protein per well. Samples were incubated for 30 minutes and then washed three times with washing buffer. Antigen-presenting buffer

was added for two minutes before removal; samples were then incubated with 1:250 dilution of anti-RhoA antibody at room temperature for 45 minutes, washed three times, and incubated with secondary antibodies for another 45 minutes. HRP detection reagent was added and signal was read by measuring absorbance at 490 nm using a microplate spectrometer.

6.4.12 Statistical analysis

All statistical analyses were conducted with the Prism graphical software (GraphPad, Software). Data were generated from multiple repeats of different biological experiments to obtain the mean values and s.e.m displayed throughout. P values have been obtained through t-tests on paired or unpaired samples with parametric tests used for data with a normal distribution and non-parametric tests conducted via the Mann–Whitney test where data had a skewed distribution. Anova and post-hoc Tukey test were used to analyse data including more than two groups. Significance was set at $p<0.05$ where graphs show significance through symbols (*$p<0.05$; **$p<0.01$; ***$p<0.001$).

7 Conclusions

Cellular mechanotransduction and ECM-cell interactions have been topics explored with an increasing interest over the past years[28,316–320]. Understanding the tumour stroma and fibrotic tissue biomechanics on a cellular level is crucial for the identification of signalling targets which may hold potential for the effective treatment of multiple diseases. The research presented here integrates cellular mechanotransduction mechanisms on fibrosis and/or cancer stroma-mimicking substrates with myofibroblast-ECM interactions on different levels: stellate cells activation, durotactic migration, ECM degradation, secretion, and finally, also proposes a way to interrupt the biomechanical response of the fibroblasts via GPER as a newly-discovered mechanoregulator.

Matrix stiffness plays a crucial role in pancreatic ductal adenocarcinoma[165]. Increased stiffness in the tumour can lead to the increased proliferation, survival and aggressiveness of the cancer cells[321]. The stroma properties are established and maintained, predominantly, by the cancer associated fibroblasts, i.e. pancreatic stellate cells (PSCs) . It has been known that biochemical signalling can induce the positive feedback loop of stellate cell activation[322], however the mechanical signalling has not been explored as a part of this loop. Substrate stiffness has been shown to be a factor capable of HSC activation, even in the absence of biochemical activators previously thought to be necessary, i.e. TGF-β[323]. Cells cultured on Matrigel and polyacrylamide of increasing rigidity exhibited elevated levels of α-smooth muscle actin expression and the typical myofibroblastic phenotype[324]. However, this has not been explored for pancreatic stellate cells, and whether changing the substrates back to soft can revert the mechanical activation. Results show that cells, once activated, can be reverted to the quiescent state. Thus, targeting ECM stiffness may be considered for future therapies.

Cells respond to tumour-mimicking, stiff polyacrylamide gels by transitioning to the activated state. As assayed previously by Phillips et al[163] those activated cells migrate with a higher rate than the freshly isolated, quiescent cells. However, this approach does not relate closely to the physiological conditions, especially in a cancer-related fibrosis context where tissue is heterogenous and its stiffness varies[125], potentially affecting cell movement. In the experiments presented in this thesis, the healthy-fibrotic tissue boundary was recreated showing that pancreatic stellate cells migrate in a durotactic manner, moving towards the stiffer side of the soft-stiff rigidity gradient biomimetic gel. It can lead to the positive feedback loop, perpetuating the fibrosis by increasing the number of activated stellate cells in the rigid area of the tumour.

These results provide another approach in stroma-targeting therapy, as it has been previously shown that using intratumoural collagenase injections to decrease the stroma stiffness can improve the therapeutic effect in melanoma treatment [325]. It would be insightful to assay, as a follow-up, the pancreatic stellate cells activation in a collagenase-treated tumour. Furthermore, the stroma softening would change the healthy tissue-tumour stiffness gradient, therefore in vitro experiments on different polyacrylamide stiffness gradient gels would show if the modulation of the substrate stiffness changes the cell durotaxis.

To further explore the mechanisms of durotaxis the polyacrylamide-based model of matrix rigidity gradient was used in application to hepatic stellate cells. It has been known that focal adhesion kinase (FAK) plays an important role in durotaxis[196] and YAP nuclear location changes in the rigidity guided migration[326], but the mechanism and connection between the two has been unclear. The results reveal the importance of the FAK and YAP activation balance in a polarity based migration. The difference in substrate rigidity across the cell generates an imbalance in mechanosensing focal adhesion protein activation. Therefore, optimal proportion of active and inactive protein is crucial for the cell orientation and guided migration. YAP, the key effector for durotaxis, also relies on the asymmetry of focal adhesion kinase, indicating a possible interaction between FAK and YAP activation. To get a better insight into the mechanism of durotaxis, based on the findings presented here, further research should focus on the changes in FAK expression area, length, turnover and activation together with cytoskeleton thickness and contractility within a single cell on a substrate stiffness gradient. Changes in the focal adhesions in the cell leading edge combined with the previously obtained results will clarify the mechanism behind the cell movement and further confirm the role of protein activation asymmetry in durotaxis.

The right balance of ECM secretion and degradation is necessary for the maintenance of healthy tissue homeostasis. However, stellate cells activation and durotaxis can contribute to the deregulation of the stromal remodelling. Results in this thesis reveal that increased matrix stiffness alone can negatively affect matrix metalloproteinase-9 (MMP-9) gene expression and protein secretion, together with an increased activity of tissue inhibitor of metalloproteinase 1 (TIMP-1). This combination can downregulate cells' ability to degrade the ECM, promoting fibrosis. Furthermore, a similar trend for MMP-9 decreased protein expression was observed in the tissues obtained from 20 hepatocellular carcinoma patients, confirming the in vivo occurrence of this mechanism. These results are in agreement with one of the hypotheses, that an increased ECM stiffness (here through the decrease in MMP-9) is associated with an

increased cancer malignancy[327,328]. However, there is also a contradictory hypothesis claiming that a decrease in stromal stiffness and an increase in ECM degradation by MMPs leads to faster and easier cancer cell migration and metastasis[329,330]. To assay the effect of decreased MMP-9 activity on hepatocellular carcinoma malignancy future experiments should include organotypic co-culture of hepatic stellate cells with TIMP-1 knockdown or inhibition (effecting in an increased ECM degradation) and SK-HEP1 liver cancer cells followed by the tracking of the cell migration.

Plasma membrane tension has been investigated as a key factor involved in cell spreading and migration, specifically as the cell forms lamellipodia. Gauthier et al showed that during this process local membrane tension increases, triggering exocytosis[248]. Another work, by Wen et al, further explored the mechanism and proposed cytoskeleton dynamics as a provider of the membrane tension necessary to merge the fusing vesicles[331]. Both pieces of research support the findings in which mechanosensing of the substrate stiffness via integrins is linked to RhoA controlled membrane stiffening and exocytosis. The observed increase in TIMP-1 exocytosis led to a set of experiments investigating the effect of substrate stiffness on vesicle trafficking and its modulation of plasma membrane tension. The results show that high substrate rigidity triggers an increase in membrane tension, via β1 integrin and RhoA pathway. As a downstream effect, homeostasis is maintained by increased dynamin1 and caveolin-1 dependent exocytosis which provides the additional membrane area leading to the reduction of its tension. This proposed negative feedback signalling network regulates membrane tension and secretion in a healthy tissue, however it can be altered in cancer and cardiovascular diseases. The research on modulating FAs and plasma membrane mechanosensing presented in this thesis is mostly focused on depicting the fundamental mechanism behind the process. The next logical steps in this direction should be focused on validating these results using in vivo models.

Myofibroblast activation, durotaxis, secretion and increased membrane tension on stiff substrates converged the final aim on targeting the biomechanical signalling in order to alter the cell response. Here, it is shown that GPER, known to be a receptor involved in cell signalling in both health and disease[280,311,312], is a key mechanotransduction regulator in myofibroblast cells. Previous research by Zilin et al indicated that GPER activation inhibits RhoA activation in vascular endothelial cells[332]. Results presented here reveal that G protein-coupled receptor activation inhibits myofibroblasts contraction, mechanosensing and focal

adhesion turnover through RhoA inhibition and it highlights GPER as a potential therapeutic target in cancer and fibrosis by affecting the stromal myofibroblast mechanotransduction. Therefore, more preclinical work using animal models should pave the way that lead to clinical trials opening the avenues to novel approaches based on targeting GPER in the tumour and the tumour microenvironment, including activating GPER to decrease the membrane stiffness through RhoA inhibition. Moreover, results shown here, together with the previous research[103,277], suggest a potential new role for GPER as a mechanosensor. Therefore, further work should involve a direct mechanical stimulation of the receptor with magnetic tweezers, followed by assaying the cellular response, for example as a calcium influx or potential RhoA inhibition. In addition, future research needs to focus on understanding the effect of GPER activation on other cytoskeletal structures such as intermediate filaments or microtubules and how this activation may affect cell polarization, migration and invasion in the context of cancer.

The results presented here prove that high microenvironmental stiffness triggers myofibroblast activation. For the first time it is observed in pancreatic and hepatic in stellate cells, fibroblasts responsible for the perpetuation of fibrosis and cancer progression. Cell activation is subject to many levels of control, including biochemical signalling, but in this work, it is stated that mechanical signalling through the cytoskeleton linkage between focal adhesions and regulators of cellular contractility is a major contributor to the change of cell phenotype and behaviour.

In addition, this thesis shows that fibroblast activation and ECM changes, similar to the stiff stroma formation, have a fundamental role in cellular migration and they affect cell ability to remodel the extracellular matrix. It is shown that fibroblasts, such as PSCs, HSCs and HFFs, are highly mechanosensitive; and mechanical cues are crucial for their activation.

Probing the physical features of the extracellular matrix occurs via focal adhesion complexes; substrate stiffness translates into mechanical tension exerted on cells and, via activation of FAK and therefore mechanoregulator YAP, it directs the cell movement towards the rigid microenvironment. Following the migration, high ECM stiffness decreases the cell ability to digest the matrix. This phenomenon is explained by the effect of rigid substrate on the cytoskeleton contractility orchestrated by RhoA. Small Rho GTPase RhoA is an important player in mechanotransduction that physical environmental cues to cellular responses through the regulation and remodelling of the actin cytoskeleton. Here, we show that RhoA activation in response to substrate stiffness occurs via β1 integrin and it is a key in an event discovered in

this work – rigidity dependant membrane stiffening. That, in turn, triggers the exocytosis, shown here as a mechanism of the maintenance of membrane tensional homeostasis.

RhoA signalling, as a key regulator of cell response to substrate stiffness, is a promising target to attenuate fibroblast activation in result to mechanical stimulation. This effect can be obtained, as it is presented in this thesis, by the activation of GPER, that consequently supresses RhoA mediated force response and force generation, as well as actomyosin contractility and focal adhesion dynamics. The analysis of the cascade of stiffness-triggered migration and changes in cell behaviour presented here provides an insight into the mechanism of fibroblast mechanosensing as well as suggests potential strategies for targeting stromal fibroblast mechanosensing and therefore potentially more efficient fibrosis and cancer treatment.

8 References

1. Frantz, C., Stewart, K. M. & Weaver, V. M. The extracellular matrix at a glance. *Journal of Cell Science* **123**, 4195–4200 (2010).

2. Duarte, S., Baber, J., Fujii, T. & Coito, A. J. Matrix metalloproteinases in liver injury, repair and fibrosis. *Matrix Biol* (2015). doi:10.1016/j.matbio.2015.01.004

3. Bonnans, C., Chou, J. & Werb, Z. Remodelling the extracellular matrix in development and disease. *Nature Reviews Molecular Cell Biology* (2014). doi:10.1038/nrm3904

4. Koohestani, F. *et al.* Extracellular Matrix Collagen Alters Cell Proliferation and Cell Cycle Progression of Human Uterine Leiomyoma Smooth Muscle Cells. *PLoS One* **8**, e75844 (2013).

5. Daley, W. P., Peters, S. B. & Larsen, M. Extracellular matrix dynamics in development and regenerative medicine. *Journal of Cell Science* **121**, 255–264 (2008).

6. Holle, A. W. *et al.* Cell-Extracellular Matrix Mechanobiology: Forceful Tools and Emerging Needs for Basic and Translational Research. *Nano Letters* **18**, 1–8 (2018).

7. Kular, J. K., Basu, S. & Sharma, R. I. The extracellular matrix: Structure, composition, age-related differences, tools for analysis and applications for tissue engineering. *Journal of Tissue Engineering* **5**, (2014).

8. Ross, T. D. *et al.* Integrins in mechanotransduction. *Current Opinion in Cell Biology* (2013). doi:10.1016/j.ceb.2013.05.006

9. Schwartz, M. A. Integrins and extracellular matrix in mechanotransduction. *Cold Spring Harb Perspect Biol* **2**, a005066 (2010).

10. Paluch, E. K. *et al.* Mechanotransduction: Use the force(s). *BMC Biol.* **13**, (2015).

11. Cox, T. R. & Erler, J. T. Remodeling and homeostasis of the extracellular matrix: implications for fibrotic diseases and cancer. *Dis. Model. Mech.* (2011). doi:10.1242/dmm.004077

12. Klingberg, F., Hinz, B. & White, E. S. The myofibroblast matrix: implications for tissue repair and fibrosis. *J Pathol* **229**, 298–309 (2013).

13. Spill, F., Reynolds, D. S., Kamm, R. D. & Zaman, M. H. Impact of the physical microenvironment on tumor progression and metastasis. *Current Opinion in Biotechnology* **40**, 41–48 (2016).

14. Jain, R. K., Martin, J. D. & Stylianopoulos, T. The Role of Mechanical Forces in Tumor Growth and Therapy. *Annu. Rev. Biomed. Eng.* **16**, 321–346 (2014).

15. Anari, F., Ramamurthy, C. & Zibelman, M. Impact of tumor microenvironment composition on therapeutic responses and clinical outcomes in cancer. *Future Oncology* **14**, 1409–1421 (2018).

16. DeClerck, Y. A. Desmoplasia: A response or a niche? *Cancer Discov.* **2**, 772–774 (2012).

17. Cannon, A. *et al.* Desmoplasia in pancreatic ductal adenocarcinoma: Insight into pathological function and therapeutic potential. *Genes and Cancer* **9**, 78–86 (2018).

18. Pandol, S., Edderkaoui, M., Gukovsky, I., Lugea, A. & Gukovskaya, A. Desmoplasia of Pancreatic Ductal Adenocarcinoma. *Clin. Gastroenterol. Hepatol.* **7**, (2009).

19. Lee, J. Il & Campbell, J. S. Role of desmoplasia in cholangiocarcinoma and hepatocellular carcinoma. *Journal of Hepatology* **61**, 432–434 (2014).

20. Affo, S., Yu, L.-X. & Schwabe, R. F. The Role of Cancer-Associated Fibroblasts and Fibrosisin Liver Cancer. *Annu. Rev. Pathol. Mech. Dis.* **12**, 153–186 (2016).

21. Li, S. *et al.* Targeting mechanics-induced fibroblast activation through CD44-RhoA-YAP pathway ameliorates crystalline silica-induced silicosis. *Theranostics* **9**, 4993–5008 (2019).

22. Huang, X. *et al.* Matrix stiffness-induced myofibroblast differentiation is mediated by intrinsic mechanotransduction. *Am. J. Respir. Cell Mol. Biol.* **47**, 340–348 (2012).

23. Berrier, A. L. & Yamada, K. M. Cell-matrix adhesion. *J Cell Physiol* **213**, 565–573 (2007).

24. Campbell, I. D. & Humphries, M. J. Integrin structure, activation, and interactions. *Cold Spring Harbor Perspectives in Biology* (2011). doi:10.1101/cshperspect.a004994

25. Danen, E. H. J. Integrins: An Overview of Structural and Functional Aspects. (2013).

26. Chen, W., Lou, J., Evans, E. A. & Zhu, C. Observing force-regulated conformational changes and ligand dissociation from a single integrin on cells. *J. Cell Biol.* **199**, 497–512 (2012).

27. Oria, R. *et al.* Force loading explains spatial sensing of ligands by cells. *Nature* (2017). doi:10.1038/nature24662

28. Humphrey, J. D., Dufresne, E. R. & Schwartz, M. A. Mechanotransduction and extracellular matrix homeostasis. *Nat Rev Mol Cell Biol* **15**, 802–812 (2014).

29. Swaminathan, V. *et al.* Actin retrograde flow actively aligns and orients ligand-engaged integrins in focal adhesions. *Proc. Natl. Acad. Sci.* (2017). doi:10.1073/pnas.1701136114

30. Gupta, M. *et al.* Adaptive rheology and ordering of cell cytoskeleton govern matrix rigidity sensing. *Nat. Commun.* (2015). doi:10.1038/ncomms8525

31. Chan, C. E. & Odde, D. J. Traction dynamics of filopodia on compliant substrates. *Science (80-.).* (2008). doi:10.1126/science.1163595

32. Schwarz, U. S., Erdmann, T. & Bischofs, I. B. Focal adhesions as mechanosensors: The

two-spring model. in *BioSystems* (2006). doi:10.1016/j.biosystems.2005.05.019

33. Wolfenson, H. *et al.* Tropomyosin controls sarcomere-like contractions for rigidity sensing and suppressing growth on soft matrices. *Nat. Cell Biol.* (2016). doi:10.1038/ncb3277

34. Yang, B. *et al.* Mechanosensing Controlled Directly by Tyrosine Kinases. *Nano Lett.* (2016). doi:10.1021/acs.nanolett.6b02995

35. Engler, A. *et al.* Substrate Compliance versus Ligand Density in Cell on Gel Responses. *Biophys. J.* **86**, 617–628 (2004).

36. Wen, J. H. *et al.* Interplay of matrix stiffness and protein tethering in stem cell differentiation. *Nat Mater* **13**, 979–987 (2014).

37. Pelham, R. J. & Wang, Y. -l. Cell locomotion and focal adhesions are regulated by substrate flexibility. *Proc. Natl. Acad. Sci.* (1997). doi:10.1073/pnas.94.25.13661

38. Yeung, T. *et al.* Effects of substrate stiffness on cell morphology, cytoskeletal structure, and adhesion. *Cell Motil Cytoskelet.* **60**, 24–34 (2005).

39. Peyton, S. R. & Putnam, A. J. Extracellular matrix rigidity governs smooth muscle cell motility in a biphasic fashion. *J Cell Physiol* **204**, 198–209 (2005).

40. Wang, H.-B., Dembo, M. & Wang, Y.-L. Substrate flexibility regulates growth and apoptosis of normal but not transformed cells. *Am. J. Physiol. - Cell Physiol.* **279**, C1345–C1350 (2000).

41. Plotnikov, S. V., Pasapera, A. M., Sabass, B. & Waterman, C. M. Force fluctuations within focal adhesions mediate ECM-rigidity sensing to guide directed cell migration. *Cell* **151**, 1513–1527 (2012).

42. Meredith JE Schwartz MA, F. B., Meredith, J. E., Fazeli, B. & Schwartz, M. A. The extracellular matrix as a cell survival factor. *Mol. Biol. Cell* **4**, 953–961 (1993).

43. Juliano, R. L., Haskill, S. & Juliano S. Haskill., R. L. Signal transduction from the extracellular matrix. *J Cell Biol* **120**, 577–585 (1993).

44. Bernstein, L. R. & Liotta, L. A. Molecular mediators of interactions with extracellular matrix components in metastasis and angiogenesis. *Curr Opin Oncol* **6**, 106–113 (1994).

45. Lo, C.-M. M., Wang, H.-B. B., Dembo, M. & Wang, Y. L. Cell Movement Is Guided by the Rigidity of the Substrate. *Biophys. J.* **79**, 144–152 (2000).

46. de Rooij, J., Kerstens, A., Danuser, G., Schwartz, M. A. & Waterman-Storer, C. M. Integrin-dependent actomyosin contraction regulates epithelial cell scattering. *J Cell Biol* **171**, 153–164 (2005).

47. Paszek, M. J. *et al.* Tensional homeostasis and the malignant phenotype. *Cancer Cell* **8**, 241–254 (2005).

48. Colombo, S. *et al.* Normal liver stiffness and its determinants in healthy blood donors. *Dig Liver Dis* **43**, 231–236 (2011).

49. Hu, K., Ji, L., Applegate, K. T., Danuser, G. & Waterman-Storer, C. M. Differential transmission of actin motion within focal adhesions. *Science (80-.).* **315**, 111–115 (2007).

50. Singer, S. J. & Nicolson, G. L. The fluid mosaic model of the structure of cell membranes. *Science (80-.).* (1972). doi:10.1126/science.175.4023.720

51. Nagle, J. F. & Tristram-Nagle, S. Structure of lipid bilayers. *Biochimica et Biophysica Acta - Reviews on Biomembranes* (2000). doi:10.1016/S0304-4157(00)00016-2

52. Chapman, D., Gómez-Fernández, J. C. & Goñi, F. M. Intrinsic protein--lipid interactions. Physical and biochemical evidence. *FEBS Lett.* **98**, 211–23 (1979).

53. Naqvi, K. R., Gonzalez-Rodriguez, J., Cherry, R. J. & Chapman, D. Spectroscopic technique for studying protein rotation in membranes. *Nature New Biology* (1973). doi:10.1038/newbio245249a0

54. Edidin, M. Rotational and translational diffusion in membranes. *Annu. Rev. Biophys. Bioeng.* **3**, 179–201 (1974).

55. Devaux, P. F., Herrmann, A., Ohlwein, N. & Kozlov, M. M. How lipid flippases can modulate membrane structure. *Biochim. Biophys. Acta* **1778**, 1591–600

56. Nakano, M. *et al.* Flip-flop of phospholipids in vesicles: kinetic analysis with time-resolved small-angle neutron scattering. *J. Phys. Chem. B* (2009). doi:10.1021/jp900913w

57. Daleke, D. L. Regulation of transbilayer plasma membrane phospholipid asymmetry. *J. Lipid Res.* **44**, 233–42 (2003).

58. Poulsen, L. R., López-Marqués, R. L. & Palmgren, M. G. Flippases: still more questions than answers. *Cell. Mol. Life Sci.* **65**, 3119–25 (2008).

59. Bassé, F., Stout, J. G., Sims, P. J. & Wiedmer, T. Isolation of an erythrocyte membrane protein that mediates Ca2+-dependent transbilayer movement of phospholipid. *J. Biol. Chem.* **271**, 17205–10 (1996).

60. Clark, M. R. Flippin' lipids. *Nature Immunology* (2011). doi:10.1038/ni.2024

61. Scherer, P. E. *et al.* Cell-type and tissue-specific expression of caveolin-2. Caveolins 1 and 2 co-localize and form a stable hetero-oligomeric complex in vivo. *J. Biol. Chem.* (1997). doi:10.1074/jbc.272.46.29337

62. Sellers, S. L., Trane, A. E. & Bernatchez, P. N. Caveolin as a potential drug target for cardiovascular protection. *Front. Physiol.* **3**, 280 (2012).

63. Thomas, C. M. & Smart, E. J. Caveolae structure and function: Caveolae Review Series.

J. Cell. Mol. Med. (2008). doi:10.1111/j.1582-4934.2008.00295.x

64. Pol, A. *et al.* Cholesterol and Fatty Acids Regulate Dynamic Caveolin Trafficking through the Golgi Complex and between the Cell Surface and Lipid Bodies. *Mol. Biol. Cell* (2005). doi:10.1091/mbc.e04-08-0737

65. Cheng, Z.-J. *et al.* Distinct mechanisms of clathrin-independent endocytosis have unique sphingolipid requirements. *Mol. Biol. Cell* **17**, 3197–210 (2006).

66. Parton, R. G. Caveolae: Structure, Function, and Relationship to Disease. *Annu. Rev. Cell Dev. Biol.* (2018). doi:10.1146/annurev-cellbio-100617-062737

67. Choudhury, A., Marks, D. L., Proctor, K. M., Gould, G. W. & Pagano, R. E. Regulation of caveolar endocytosis by syntaxin 6-dependent delivery of membrane components to the cell surface. *Nat. Cell Biol.* (2006). doi:10.1038/ncb1380

68. Singh, R. D. *et al.* Gangliosides and β1-integrin are required for caveolae and membrane domains. *Traffic* (2010). doi:10.1111/j.1600-0854.2009.01022.x

69. Örtegren, U. *et al.* Lipids and glycosphingolipids in caveolae and surrounding plasma membrane of primary rat adipocytes. *Eur. J. Biochem.* (2004). doi:10.1111/j.1432-1033.2004.04117.x

70. Fujimoto, T., Hayashi, M., Iwamoto, M. & Ohno-Iwashita, Y. Crosslinked plasmalemmal cholesterol is sequestered to caveolae: Analysis with a new cytochemical probe. *J. Histochem. Cytochem.* (1997). doi:10.1177/002215549704500903

71. Fujita, A., Cheng, J., Tauchi-Sato, K., Takenawa, T. & Fujimoto, T. A distinct pool of phosphatidylinositol 4,5-bisphosphate in caveolae revealed by a nanoscale labeling technique. *Proc. Natl. Acad. Sci.* (2009). doi:10.1073/pnas.0900216106

72. Pitto, M. *et al.* Use of a photoactivable GM1 ganglioside analogue to assess lipid distribution in caveolae bilayer. *Glycoconj. J.* (2000). doi:10.1023/A:1026593307882

73. del Rio, A. *et al.* Stretching single talin rod molecules activates vinculin binding. *Science (80-.).* **323**, 638–641 (2009).

74. Lee, S. H. & Dominguez, R. Regulation of actin cytoskeleton dynamics in cells. *Molecules and cells* (2010). doi:10.1007/s10059-010-0053-8

75. Blanchoin, L., Boujemaa-Paterski, R., Sykes, C. & Plastino, J. Actin Dynamics, Architecture, and Mechanics in Cell Motility. *Physiol. Rev.* (2014). doi:10.1152/physrev.00018.2013

76. Qian, H. Single-particle tracking: Brownian dynamics of viscoelastic materials. *Biophys. J.* (2000). doi:10.1016/S0006-3495(00)76278-3

77. Saarikangas, J., Zhao, H. & Lappalainen, P. Regulation of the Actin Cytoskeleton-Plasma Membrane Interplay by Phosphoinositides. *Physiol. Rev.* (2010). doi:10.1152/physrev.00036.2009

78. Goldschmidt-Clermont, P. J., Kim, J. W., Machesky, L. M., Rhee, S. G. & Pollard, T. D. Regulation of phospholipase C-γ1 by profilin and tyrosine phosphorylation. *Science (80-.).* (1991). doi:10.1126/science.1848725

79. Bezanilla, M., Gladfelter, A. S., Kovar, D. R. & Lee, W. L. Cytoskeletal dynamics: A view from the membrane. *Journal of Cell Biology* (2015). doi:10.1083/jcb.201502062

80. Campellone, K. G. & Welch, M. D. A nucleator arms race: Cellular control of actin assembly. *Nature Reviews Molecular Cell Biology* (2010). doi:10.1038/nrm2867

81. Tsuji, T. *et al.* ROCK and mDia1 antagonize in Rho-dependent Rac activation in Swiss 3T3 fibroblasts. *J. Cell Biol.* (2002). doi:10.1083/jcb.200112107

82. Yamaguchi, Y., Katoh, H., Yasui, H., Mori, K. & Negishi, M. RhoA Inhibits the Nerve Growth Factor-induced Rac1 Activation through Rho-associated Kinase-dependent Pathway. *J. Biol. Chem.* (2001). doi:10.1074/jbc.M100254200

83. Takefuji, M. *et al.* Rho-kinase modulates the function of STEF, a Rac GEF, through its phosphorylation. *Biochem. Biophys. Res. Commun.* (2007). doi:10.1016/j.bbrc.2007.02.028

84. Truschel, S. T. Stretch-regulated Exocytosis/Endocytosis in Bladder Umbrella Cells. *Mol. Biol. Cell* (2002). doi:10.1091/mbc.01-09-0435

85. Johnson, J. L., Monfregola, J., Napolitano, G., Kiosses, W. B. & Catz, S. D. Vesicular trafficking through cortical actin during exocytosis is regulated by the Rab27a effector JFC1/Slp1 and the RhoA-GTPase-activating protein Gem-interacting protein. *Mol. Biol. Cell* (2012). doi:10.1091/mbc.e11-12-1001

86. Klein, I. K. *et al.* Intersectin-2L regulates caveola endocytosis secondary to Cdc42-mediated actin polymerization. *J. Biol. Chem.* (2009). doi:10.1074/jbc.M109.035071

87. Bedossa, P. & Paradis, V. Liver extracellular matrix in health and disease. *J Pathol* **200**, 504–515 (2003).

88. Hernandez-Gea, V. & Friedman, S. L. Pathogenesis of liver fibrosis. *Annu Rev Pathol* **6**, 425–456 (2011).

89. Iimuro, Y. *et al.* Delivery of matrix metalloproteinase-1 attenuates established liver fibrosis in the rat. *Gastroenterology* **124**, 445–458 (2003).

90. Takahara, T. *et al.* Dual expression of matrix metalloproteinase-2 and membrane-type 1-matrix metalloproteinase in fibrotic human livers. *Hepatology* **26**, 1521–1529 (1997).

91. Harty, M. W. *et al.* Repair after cholestatic liver injury correlates with neutrophil infiltration and matrix metalloproteinase 8 activity. *Surgery* **138**, 313–320 (2005).

92. Kessenbrock, K., Plaks, V. & Werb, Z. Matrix metalloproteinases: regulators of the tumor microenvironment. *Cell* **141**, 52–67 (2010).

93. Arthur, M. J. P., Friedman, S. L., Roll, F. J. & Bissell, D. M. Lipocytes from normal rat liver release a neutral metalloproteinase that degrades basement membrane (type IV) collagen. *J Clin Invest* **84**, 1076–1085 (1989).

94. Radisky, E. S., Raeeszadeh-Sarmazdeh, M. & Radisky, D. C. Therapeutic Potential of Matrix Metalloproteinase Inhibition in Breast Cancer. *J. Cell. Biochem.* (2017). doi:10.1002/jcb.26185

95. Bode, W. *et al.* Insights into MMP-TIMP interactions. in *Annals of the New York Academy of Sciences* (1999). doi:10.1111/j.1749-6632.1999.tb07675.x

96. Bigg, H. F., Rowan, A. D., Barker, M. D. & Cawston, T. E. Activity of matrix metalloproteinase-9 against native collagen types I and III. *FEBS J.* (2007). doi:10.1111/j.1742-4658.2007.05669.x

97. Gioia, M. *et al.* The Collagen Binding Domain of Gelatinase A Modulates Degradation of Collagen IV by Gelatinase B. *J. Mol. Biol.* (2009). doi:10.1016/j.jmb.2008.12.021

98. Vempati, P., Karagiannis, E. D. & Popel, A. S. A biochemical model of matrix metalloproteinase 9 activation and inhibition. *J Biol Chem* **282**, 37585–37596 (2007).

99. Takahara, T. *et al.* Modulation of matrix metalloproteinase-9 in hepatic stellate cells by three-dimensional type I collagen: Its activation and signaling pathway. *Hepatol. Res.* (2003). doi:10.1016/S1386-6346(03)00169-4

100. Han, Y. P. Matrix metalloproteinases, the pros and cons, in liver fibrosis. in *Journal of Gastroenterology and Hepatology (Australia)* (2006). doi:10.1111/j.1440-1746.2006.04586.x

101. Lachowski, D. *et al.* Matrix stiffness modulates the activity of MMP-9 and TIMP-1 in hepatic stellate cells to perpetuate fibrosis. *Sci. Rep.* (2019). doi:10.1038/s41598-019-43759-6

102. Molina, L., Bustamante, F. A., Bhoola, K. D., Figueroa, C. D. & Ehrenfeld, P. Possible role of phytoestrogens in breast cancer via GPER-1/GPR30 signaling. *Clin. Sci. (Lond).* **132**, 2583–2598 (2018).

103. Cortes, E. *et al.* GPER is a mechanoregulator of pancreatic stellate cells and the tumor microenvironment. *EMBO Rep.* (2019). doi:10.15252/embr.201846556

104. Prossnitz, E. R. & Barton, M. The G-protein-coupled estrogen receptor GPER in health and disease. *Nature Reviews Endocrinology* (2011). doi:10.1038/nrendo.2011.122

105. Revankar, C. M., Cimino, D. F., Sklar, L. A., Arterburn, J. B. & Prossnitz, E. R. A transmembrane intracellular estrogen receptor mediates rapid cell signaling. *Science* **307**, 1625–30 (2005).

106. Sanden, C. *et al.* G Protein-Coupled Estrogen Receptor 1/G Protein-Coupled Receptor 30 Localizes in the Plasma Membrane and Traffics Intracellularly on Cytokeratin

Intermediate Filaments. *Mol. Pharmacol.* (2011). doi:10.1124/mol.110.069500

107. Samartzis, E. P. *et al.* The G protein-coupled estrogen receptor (GPER) is expressed in two different subcellular localizations reflecting distinct tumor properties in breast cancer. *PLoS One* (2014). doi:10.1371/journal.pone.0083296

108. Filardo, E. J., Quinn, J. A., Bland, K. I. & Frackelton, A. R. Estrogen-Induced Activation of Erk-1 and Erk-2 Requires the G Protein-Coupled Receptor Homolog, GPR30, and Occurs via Trans-Activation of the Epidermal Growth Factor Receptor through Release of HB-EGF. *Mol. Endocrinol.* (2014). doi:10.1210/mend.14.10.0532

109. Maggiolini, M. *et al.* The G protein-coupled receptor GPR30 mediates c-fos up-regulation by 17beta-estradiol and phytoestrogens in breast cancer cells. *J. Biol. Chem.* **279**, 27008–16 (2004).

110. Girgert, R., Emons, G. & Gründker, C. Inactivation of GPR30 reduces growth of triple-negative breast cancer cells: Possible application in targeted therapy. *Breast Cancer Res. Treat.* (2012). doi:10.1007/s10549-012-1968-x

111. Kuhn, M. A., Wang, X., Payne, W. G., Ko, F. & Robson, M. C. Tamoxifen decreases fibroblast function and downregulates TGFβ2 in Dupuytren's affected palmar fascia. *J. Surg. Res.* (2002). doi:10.1006/jsre.2001.6350

112. Standring, S. Gray's Anatomy. in *Gray's Anatomy* (2016).

113. Key Statistics for Pancreatic Cancer. Available at: https://www.cancer.org/cancer/pancreatic-cancer/about/key-statistics.html.

114. Hruban, R. H., Goggins, M., Parsons, J. & Kern, S. E. Progression model for pancreatic cancer. *Clin. Cancer Res.* **6**, 2969–72 (2000).

115. Cancer, P. *et al.* Pancreatic cancer genomes reveal aberrations in axon guidance pathway genes. *Nature* (2012). doi:10.1038/nature11547

116. Witkiewicz, A. K. *et al.* Whole-exome sequencing of pancreatic cancer defines genetic diversity and therapeutic targets. *Nat. Commun.* **6**, 6744 (2015).

117. Karagiannis, G. S. *et al.* Cancer-associated fibroblasts drive the progression of metastasis through both paracrine and mechanical pressure on cancer tissue. *Mol. Cancer Res.* (2012). doi:10.1158/1541-7786.MCR-12-0307

118. Giancotti, F. G. & Ruoslahti, E. *Integrin Signaling*.

119. Whatcott, C. J., Han, H., Posner, R. G., Hostetter, G. & Von Hoff, D. D. Targeting the tumor microenvironment in cancer: Why hyaluronidase deserves a second look. *Cancer Discov.* (2011). doi:10.1158/2159-8290.CD-11-0136

120. Von Ahrens, D., Bhagat, T. D., Nagrath, D., Maitra, A. & Verma, A. The role of stromal cancer-associated fibroblasts in pancreatic cancer. *Journal of Hematology and Oncology* (2017). doi:10.1186/s13045-017-0448-5

121. Quail, D. F. & Joyce, J. A. Microenvironmental regulation of tumor progression and metastasis. *Nature Medicine* (2013). doi:10.1038/nm.3394

122. Sugimoto, H., Mundel, T. M., Kieran, M. W. & Kalluri, R. Identification of fibroblast heterogeneity in the tumor microenvironment. *Cancer Biol. Ther.* (2006). doi:10.4161/cbt.5.12.3354

123. Sun, Q. *et al.* The impact of cancer-associated fibroblasts on major hallmarks of pancreatic cancer. *Theranostics* (2018). doi:10.7150/thno.26546

124. De Wever, O. *et al.* Critical role of N-cadherin in myofibroblast invasion and migration in vitro stimulated by colon-cancer-cell-derived TGF-beta or wounding. *J. Cell Sci.* **117**, 4691–703 (2004).

125. Rice, A. J. J. *et al.* Matrix stiffness induces epithelial-mesenchymal transition and promotes chemoresistance in pancreatic cancer cells. *Oncogenesis* **6**, (2017).

126. Protzer, U., Maini, M. K. & Knolle, P. A. Living in the liver: hepatic infections. *Nat Rev Immunol* **12**, 201–213 (2012).

127. Ma MH, B. L. The normal human liver cell. Cytochemical and ultrastructural studies. *Am. J. Pathol.* **62**, 353–390 (1971).

128. Si-Tayeb, K., Lemaigre, F. P. & Duncan, S. A. Organogenesis and development of the liver. *Dev Cell* **18**, 175–189 (2010).

129. Sise, M. E. *et al.* Treatment of Hepatitis C Virus-Associated Mixed Cryoglobulinemia with Sofosbuvir-Based Direct-Acting Antiviral Agents. *Hepatology* (2015). doi:10.1002/hep.28297

130. Manns, M. P., Lohse, A. W. & Vergani, D. Autoimmune hepatitis - Update 2015. *Journal of Hepatology* (2015). doi:10.1016/j.jhep.2015.03.005

131. Wake, K., Motomatsu, K., Senoo, H., Masuda, A. & Adachi, E. Improved Kupffer's gold chloride method for demonstrating the stellate cells storing retinol (vitamin A) in the liver and extrahepatic organs of vertebrates. *Stain Technol* **61**, 193–200 (1986).

132. Hepatic stellate cell nomenclature. *Hepatology* **23**, 193 (1996).

133. Giampieri, M. P., Jezequel, A. M. & Orlandi, F. The lipocytes in normal human liver. A quantitative study. *Digestion* **22**, 165–169 (1981).

134. Reynaert, H., Thompson, M. G., Thomas, T. & Geerts, A. Hepatic stellate cells: role in microcirculation and pathophysiology of portal hypertension. *Gut* **50**, 571–581 (2002).

135. Friedman, S. L. Mechanis of hepatic fibrogenesis. *Gastroenterology* (2008). doi:10.1053/j.gastro.2008.03.003

136. Bataller, R. & Brenner, D. A. Liver fibrosis. *J. Clin. Invest.* **115**, 209–218 (2005).

137. Friedman, S. L., Roll, F. J., Boyles, J., Bissell, D. M. & Friedman SL Boyles J, Bissell

DM., R. F. J. Hepatic lipocytes: the principal collagen-producing cells of normal rat liver. *Proc Natl Acad Sci* **82**, 8681–8685 (1985).

138. Kisseleva, T. *et al.* Myofibroblasts revert to an inactive phenotype during regression of liver fibrosis. *Proc Natl Acad Sci U S A* **109**, 9448–9453 (2012).

139. Bardeesy, N. & DePinho, R. A. Pancreatic cancer biology and genetics. *Nature Reviews Cancer* (2002). doi:10.1038/nrc949

140. Bramhall, S. R., Rosemurgy, A., Brown, P. D., Bowry, C. & Buckles, J. A. C. Marimastat as first-line therapy for patients with unresectable pancreatic cancer: A randomized trial. *J. Clin. Oncol.* (2001). doi:10.1200/JCO.2001.19.15.3447

141. Winter, J. M. *et al.* Survival after resection of pancreatic adenocarcinoma: Results from a single institution over three decades. *Ann. Surg. Oncol.* (2012). doi:10.1245/s10434-011-1900-3

142. Li, (D *et al. Pancreatic cancer. THE LANCET* • **363**, (2004).

143. Apte, M. V. *et al.* Desmoplastic reaction in pancreatic cancer: Role of pancreatic stellate cells. *Pancreas* (2004). doi:10.1097/00006676-200410000-00002

144. Erkan, M. *et al.* Periostin Creates a Tumor-Supportive Microenvironment in the Pancreas by Sustaining Fibrogenic Stellate Cell Activity. *Gastroenterology* (2007). doi:10.1053/j.gastro.2007.01.031

145. Edderkaoui, M. *et al.* Extracellular matrix stimulates reactive oxygen species production and increases pancreatic cancer cell survival through 5-lipoxygenase and NADPH oxidase. *Am. J. Physiol. Liver Physiol.* (2005). doi:10.1152/ajpgi.00197.2005

146. Harris, A. L. Hypoxia — a key regulatory factor in tumour growth. *Nat. Rev. Cancer* (2002). doi:10.1038/nrc704

147. Vaquero, E. C. *et al.* Extracellular matrix proteins protect pancreatic cancer cells from death via mitochondrial and nonmitochondrial pathways. *Gastroenterology* (2003). doi:10.1016/S0016-5085(03)01203-4

148. Omary, M. B., Lugea, A., Lowe, A. W. & Pandol, S. J. The pancreatic stellate cell: A star on the rise in pancreatic diseases. *Journal of Clinical Investigation* (2007). doi:10.1172/JCI30082

149. Xu, Z. *et al.* Role of pancreatic stellate cells in pancreatic cancer metastasis. *Am. J. Pathol.* (2010). doi:10.2353/ajpath.2010.090899

150. Kikuta, K. *et al.* Pancreatic stellate cells promote epithelial-mesenchymal transition in pancreatic cancer cells. *Biochem. Biophys. Res. Commun.* (2010). doi:10.1016/j.bbrc.2010.11.040

151. Apte, M. V., Wilson, J. S., Lugea, A. & Pandol, S. J. A starring role for stellate cells in the pancreatic cancer microenvironment. *Gastroenterology* **144**, 1210–1219 (2013).

152. Bachem, M. G., Zhou, S., Buck, K., Schneiderhan, W. & Siech, M. Pancreatic stellate cells - Role in pancreas cancer. *Langenbeck's Archives of Surgery* (2008). doi:10.1007/s00423-008-0279-5

153. Yen, T. W. F. *et al.* Myofibroblasts are responsible for the desmoplastic reaction surrounding human pancreatic carcinomas. *Surgery* (2002). doi:10.1067/msy.2002.119192

154. Vonlaufen, A. *et al.* Pancreatic stellate cells: Partners in crime with pancreatic cancer cells. *Cancer Res.* (2008). doi:10.1158/0008-5472.CAN-07-2477

155. Wilson, J. S., Pirola, R. C. & Apte, M. V. Stars and stripes in pancreatic cancer: Role of stellate cells and stroma in cancer progression. *Frontiers in Physiology* (2014). doi:10.3389/fphys.2014.00052

156. Erkan, M. *et al.* StellaTUM: Current consensus and discussion on pancreatic stellate cell research. *Gut* (2012). doi:10.1136/gutjnl-2011-301220

157. Apte, M. V., Pirola, R. C. & Wilson, J. S. Pancreatic stellate cells: A starring role in normal and diseased pancreas. *Frontiers in Physiology* (2012). doi:10.3389/fphys.2012.00344

158. Jaster, R. Molecular regulation of pancreatic stellate cell function. *Molecular Cancer* (2004). doi:10.1186/1476-4598-3-26

159. Bachem, M. G. *et al.* Pancreatic carcinoma cells induce fibrosis by stimulating proliferation and matrix synthesis of stellate cells. *Gastroenterology* (2005). doi:10.1053/j.gastro.2004.12.036

160. Özdemir, B. C. *et al.* Depletion of carcinoma-associated fibroblasts and fibrosis induces immunosuppression and accelerates pancreas cancer with reduced survival. *Cancer Cell* **25**, 719–734 (2014).

161. Rhim, A. D. *et al.* Stromal elements act to restrain, rather than support, pancreatic ductal adenocarcinoma. *Cancer Cell* **25**, 735–747 (2014).

162. Sherman, M. H. *et al.* Vitamin D receptor-mediated stromal reprogramming suppresses pancreatitis and enhances pancreatic cancer therapy. *Cell* (2014). doi:10.1016/j.cell.2014.08.007

163. Phillips, P. A. *et al.* Cell migration: a novel aspect of pancreatic stellate cell biology. *Gut* **52**, 677–682 (2003).

164. Gaggioli, C. *et al.* Fibroblast-led collective invasion of carcinoma cells with differing roles for RhoGTPases in leading and following cells. *Nat. Cell Biol.* **9**, 1392–1400 (2007).

165. Laklai, H. *et al.* Genotype tunes pancreatic ductal adenocarcinoma tissue tension to induce matricellular fibrosis and tumor progression. *Nat. Med.* (2016).

doi:10.1038/nm.4082

166. Chronopoulos, A. *et al.* ATRA mechanically reprograms pancreatic stellate cells to suppress matrix remodelling and inhibit cancer cell invasion. *Nat Commun* **7**, 12630 (2016).

167. Makishima, A. & Mackenzie, J. D. Calculation of bulk modulus, shear modulus and Poisson's ratio of glass. *J. Non. Cryst. Solids* (1975). doi:10.1016/0022-3093(75)90047-2

168. Jesnowski, R. *et al.* Immortalization of pancreatic stellate cells as an in vitro model of pancreatic fibrosis: Deactivation is induced by matrigel and N-acetylcysteine. *Lab. Investig.* (2005). doi:10.1038/labinvest.3700329

169. Lagares, D. Feedback amplification of lung fibrosis through matrix stiffness gradient-induced fibroblast durotaxis via αtat1-mediated microtubule acetylation. *Am J Respir Crit Care Med* **191**, A5329 (2015).

170. Hinz, B. The myofibroblast: Paradigm for a mechanically active cell. *J. Biomech.* (2010). doi:10.1016/j.jbiomech.2009.09.020

171. Calvo, F. *et al.* Mechanotransduction and YAP-dependent matrix remodelling is required for the generation and maintenance of cancer-associated fibroblasts. *Nat. Cell Biol.* **15**, 637–646 (2013).

172. Apte, M. V. & Wilson, J. S. Dangerous liaisons: pancreatic stellate cells and pancreatic cancer cells. *J Gastroenterol Hepatol* **27 Suppl 2**, 69–74 (2012).

173. Ferruti, P. Poly(amidoamine)s: Past, present, and perspectives. *J. Polym. Sci. Part A Polym. Chem.* **51**, 2319–2353 (2013).

174. Tse, J. R. & Engler, A. J. Preparation of hydrogel substrates with tunable mechanical properties. *Current Protocols in Cell Biology* (2010). doi:10.1002/0471143030.cb1016s47

175. Gray, D. S., Tien, J. & Chen, C. S. Repositioning of cells by mechanotaxis on surfaces with micropatterned Young's modulus. *J. Biomed. Mater. Res. - Part A* (2003). doi:10.1002/jbm.a.10585

176. Apte, M. V. *et al.* Pancreatic stellate cells are activated by proinflammatory cytokines: Implications for pancreatic fibrogenesis. *Gut* (1999). doi:10.1136/gut.44.4.534

177. DG Lagares, P. P. C. E. A. T. A. T. targeting of fibroblast durotaxis: a novel class of anti-fibrotic therapies for Ipf. *Am J Respir Crit Care Med* **193**, A4582 (2016).

178. Raab, M. *et al.* Crawling from soft to stiff matrix polarizes the cytoskeleton and phosphoregulates myosin-II heavy chain. *J. Cell Biol.* (2012). doi:10.1083/jcb.201205056

179. Sarper, M., Cortes, E., Lieberthal, T. J. & Del Río Hernández, A. ATRA modulates

mechanical activation of TGF-β by pancreatic stellate cells. *Sci. Rep.* (2016). doi:10.1038/srep27639

180. Robinson, B. K., Cortes, E., Rice, A. J., Sarper, M. & del Río Hernández, A. Quantitative analysis of 3D extracellular matrix remodelling by pancreatic stellate cells. *Biol. Open* (2016). doi:10.1242/bio.017632

181. Provenzano, P. P., Inman, D. R., Eliceiri, K. W., Trier, S. M. & Keely, P. J. Contact guidance mediated three-dimensional cell migration is regulated by Rho/ROCK-dependent matrix reorganization. *Biophys. J.* (2008). doi:10.1529/biophysj.108.133116

182. Klonowski-Stumpe, H., Fischer, R., Reinehr, R., Lüthen, R. & Häussinger, D. Apoptosis in activated rat pancreatic stellate cells. *Am. J. Physiol. Liver Physiol.* (2015). doi:10.1152/ajpgi.00073.2002

183. Keogh, G. W. *et al.* Activation of Pancreatic Stellate Cells in Human and Experimental Pancreatic Fibrosis. *Am. J. Pathol.* (2011). doi:10.1016/s0002-9440(10)65211-x

184. Attwood, S. J. *et al.* Adhesive ligand tether length affects the size and length of focal adhesions and influences cell spreading and attachment. *Sci. Rep.* (2016). doi:10.1038/srep34334

185. Sulzmaier, F. J., Jean, C. & Schlaepfer, D. D. FAK in cancer: mechanistic findings and clinical applications. *Nat Rev Cancer* **14**, 598–610 (2014).

186. Handorf, A. M., Zhou, Y., Halanski, M. A. & Li, W. J. Tissue stiffness dictates development, homeostasis, and disease progression. *Organogenesis* (2015). doi:10.1080/15476278.2015.1019687

187. Levental, K. R. *et al.* Matrix Crosslinking Forces Tumor Progression by Enhancing Integrin Signaling. *Cell* (2009). doi:10.1016/j.cell.2009.10.027

188. Mitra, S. K., Hanson, D. A. & Schlaepfer, D. D. Focal adhesion kinase: In command and control of cell motility. *Nature Reviews Molecular Cell Biology* (2005). doi:10.1038/nrm1549

189. Dupont, S. *et al.* Role of YAP/TAZ in mechanotransduction. *Nature* **474**, 179–183 (2011).

190. Varelas, X. The Hippo pathway effectors TAZ and YAP in development, homeostasis and disease. *Development* (2014). doi:10.1242/dev.102376

191. Zanconato, F. *et al.* Genome-wide association between YAP/TAZ/TEAD and AP-1 at enhancers drives oncogenic growth. *Nat. Cell Biol.* (2015). doi:10.1038/ncb3216

192. Zhang, X., Milton, C. C., Humbert, P. O. & Harvey, K. F. Transcriptional output of the Salvador/Warts/Hippo pathway is controlled in distinct fashions in Drosophila melanogaster and mammalian cell lines. *Cancer Res.* (2009). doi:10.1158/0008-5472.CAN-08-4592

193. Sun, M., Spill, F. & Zaman, M. H. A Computational Model of YAP/TAZ Mechanosensing. *Biophys. J.* (2016). doi:10.1016/j.bpj.2016.04.040

194. Kim, N. G. & Gumbiner, B. M. Adhesion to fibronectin regulates Hippo signaling via the FAK-Src-PI3K pathway. *J. Cell Biol.* (2015). doi:10.1083/jcb.201501025

195. Chakraborty, S. *et al.* Agrin as a Mechanotransduction Signal Regulating YAP through the Hippo Pathway. *Cell Rep.* (2017). doi:10.1016/j.celrep.2017.02.041

196. Wang, H.-B. B., Dembo, M., Hanks, S. K. & Wang, Y. -l. Focal adhesion kinase is involved in mechanosensing during fibroblast migration. *Proc Natl Acad Sci U S A* **98**, 11295–11300 (2001).

197. Mederacke, I. *et al.* Fate tracing reveals hepatic stellate cells as dominant contributors to liver fibrosis independent of its aetiology. *Nat Commun* **4**, 2823 (2013).

198. Johnson, R. & Halder, G. The two faces of Hippo: Targeting the Hippo pathway for regenerative medicine and cancer treatment. *Nature Reviews Drug Discovery* (2014). doi:10.1038/nrd4161

199. Yujiri, T. *et al.* MEK kinase 1 interacts with focal adhesion kinase and regulates insulin receptor substrate-1 expression. *J. Biol. Chem.* (2003). doi:10.1074/jbc.M206087200

200. Michael, K., Dumbauld, D., Burns, K., Hanks, S. K. & García, A. FAK Modulates Cell Adhesion Strengthening via Integrin Activation. *Mol Biol Cell* (2009). doi:10.1091/mbc.E08-01-0076

201. Lachowski, D. *et al.* Substrate Rigidity Controls Activation and Durotaxis in Pancreatic Stellate Cells. *Sci. Rep.* **7**, (2017).

202. Ichim, T. E., O'Heeron, P. & Kesari, S. Fibroblasts as a practical alternative to mesenchymal stem cells. *Journal of Translational Medicine* **16**, 1–9 (2018).

203. Rinschen, M. M. *et al.* YAP-mediated mechanotransduction determines the podocyte's response to damage. *Sci. Signal.* (2017). doi:10.1126/scisignal.aaf8165

204. Thomasy, S. M., Morgan, J. T., Wood, J. A., Murphy, C. J. & Russell, P. Substratum stiffness and latrunculin B modulate the gene expression of the mechanotransducers YAP and TAZ in human trabecular meshwork cells. *Exp. Eye Res.* (2013). doi:10.1016/j.exer.2013.05.014

205. Golubovskaya, V. M. *et al.* A small molecule inhibitor, 1,2,4,5-benzenetetraamine tetrahydrochloride, targeting the y397 site of focal adhesion kinase decreases tumor growth. *J Med Chem* **51**, 7405–7416 (2008).

206. Meng, Z., Moroishi, T. & Guan, K. L. Mechanisms of Hippo pathway regulation. *Genes and Development* (2016). doi:10.1101/gad.274027.115

207. Low, B. C. *et al.* YAP/TAZ as mechanosensors and mechanotransducers in regulating organ size and tumor growth. *FEBS Lett* **588**, 2663–2670 (2014).

208. Oka, T., Mazack, V. & Sudol, M. Mst2 and Lats kinases regulate apoptotic function of Yes kinase-associated protein (YAP). *J. Biol. Chem.* (2008). doi:10.1074/jbc.M804380200

209. Li, Z. *et al.* Structural insights into the YAP and TEAD complex. *Genes Dev.* (2010). doi:10.1101/gad.1865810

210. Elosegui-Artola, A. *et al.* Force Triggers YAP Nuclear Entry by Regulating Transport across Nuclear Pores. *Cell* (2017). doi:10.1016/j.cell.2017.10.008

211. Dupont, S. Role of YAP/TAZ in cell-matrix adhesion-mediated signalling and mechanotransduction. *Experimental Cell Research* (2016). doi:10.1016/j.yexcr.2015.10.034

212. Rosenbluh, J. *et al.* β-Catenin-driven cancers require a YAP1 transcriptional complex for survival and tumorigenesis. *Cell* (2012). doi:10.1016/j.cell.2012.11.026

213. Li, Y.-W. W. *et al.* Phosphorylation of Tyr188 in the WW domain of YAP1 plays an essential role in YAP1-induced cellular transformation. *Cell Cycle* **15**, 2497–2505 (2016).

214. Keshet, R., Reuven, N. & Shaul, Y. c-Abl forces YAP to switch sides. **2**, e995006 (2015).

215. Ladoux, B., Mège, R. M. & Trepat, X. Front-Rear Polarization by Mechanical Cues: From Single Cells to Tissues. *Trends in Cell Biology* (2016). doi:10.1016/j.tcb.2016.02.002

216. Friedman, S. L. Molecular regulation of hepatic fibrosis, an integrated cellular response to tissue injury. *J Biol Chem* **275**, 2247–2250 (2000).

217. Wells, R. G. *The role of matrix stiffness in regulating cell behavior. Hepatology* **47**, 1394–1400 (2008).

218. Carloni, V., Luong, T. V. & Rombouts, K. Hepatic stellate cells and extracellular matrix in hepatocellular carcinoma: more complicated than ever. *Liver Int* **34**, 834–843 (2014).

219. Mann, D. A. & Marra, F. Fibrogenic signalling in hepatic stellate cells. *J Hepatol* **52**, 949–950 (2010).

220. Zhao, B. *et al.* TEAD mediates YAP-dependent gene induction and growth control. *Genes Dev.* (2008). doi:10.1101/gad.1664408

221. Mueller, S. Liver stiffness: a novel parameter for the diagnosis of liver disease. *Hepatic Med. Evid. Res.* 49 (2010). doi:10.2147/hmer.s7394

222. Schindelin, J. *et al.* Fiji: An open-source platform for biological-image analysis. *Nature Methods* (2012). doi:10.1038/nmeth.2019

223. Harris, A. R. & Charras, G. T. Experimental validation of atomic force microscopy-

based cell elasticity measurements. *Nanotechnology* (2011). doi:10.1088/0957-4484/22/34/345102

224. Cassiman, D., Libbrecht, L., Desmet, V., Denef, C. & Roskams, T. Hepatic stellate cell/myofibroblast subpopulations in fibrotic human and rat livers. *J Hepatol* **36**, 200–209 (2002).

225. Tsuchida, T. & Friedman, S. L. Mechanisms of hepatic stellate cell activation. *Nature Reviews Gastroenterology and Hepatology* (2017). doi:10.1038/nrgastro.2017.38

226. Lee, U. E. & Friedman, S. L. Mechanisms of hepatic fibrogenesis. *Best Pract. Res. Clin. Gastroenterol.* (2011). doi:10.1016/j.bpg.2011.02.005

227. Moreira, R. Hepatic stellate cells and liver fibrosis. *Arch Pathol Lab Med* **131**, 1728–1734 (2007).

228. Fanjul-Fernández, M., Folgueras, A. R., Cabrera, S. & López-Otín, C. Matrix metalloproteinases: Evolution, gene regulation and functional analysis in mouse models. *Biochimica et Biophysica Acta - Molecular Cell Research* (2010). doi:10.1016/j.bbamcr.2009.07.004

229. Löffek, S., Schilling, O. & Franzke, C. W. Series 'matrix metalloproteinases in lung health and disease' edited by J. Müller-Quernheim and O. Eickelberg number 1 in this series: Biological role of matrix metalloproteinases: A critical balance. *European Respiratory Journal* (2011). doi:10.1183/09031936.00146510

230. Wells, R. G. Tissue mechanics and fibrosis. *Biochimica et Biophysica Acta - Molecular Basis of Disease* (2013). doi:10.1016/j.bbadis.2013.02.007

231. Caliari, S. R. *et al.* Stiffening hydrogels for investigating the dynamics of hepatic stellate cell mechanotransduction during myofibroblast activation. *Sci Rep* **6**, 21387 (2016).

232. Desai, S. S. *et al.* Physiological ranges of matrix rigidity modulate primary mouse hepatocyte function in part through hepatocyte nuclear factor 4 alpha. *Hepatology* (2016). doi:10.1002/hep.28450

233. Zhubanchaliyev, A., Temirbekuly, A., Kongrtay, K., Wanshura, L. C. & Kunz, J. Targeting mechanotransduction at the transcriptional level: YAP and BRD4 are novel therapeutic targets for the reversal of liver fibrosis. *Frontiers in Pharmacology* (2016). doi:10.3389/fphar.2016.00462

234. Li, Y.-L., Sato, M., Kojima, N., Miura, M. & Senoo, H. Regulatory Role of Extracellular Matrix Components in Expression of Matrix Metalloproteinases in Cultured Hepatic Stellate Cells. *Cell Struct. Funct.* (1999). doi:10.1247/csf.24.255

235. Chen, R. *et al.* The significance of MMP-9 over MMP-2 in HCC invasiveness and recurrence of hepatocellular carcinoma after curative resection. *Ann. Surg. Oncol.* (2012). doi:10.1245/s10434-011-1836-7

236. Yamaoka, K., Nouchi, T., Marumo, F. & Sato, C. α-Smooth-muscle actin expression in normal and fibrotic human livers. *Dig. Dis. Sci.* (1993). doi:10.1007/BF01308606

237. Nagase, H., Visse, R. & Murphy, G. Structure and function of matrix metalloproteinases and TIMPs. *Cardiovasc Res* **69**, 562–573 (2006).

238. Haage, A. & Schneider, I. C. Cellular contractility and extracellular matrix stiffness regulate matrix metalloproteinase activity in pancreatic cancer cells. *FASEB J* **28**, 3589–3599 (2014).

239. Sakurai, T. & Kudo, M. Molecular Link between Liver Fibrosis and Hepatocellular Carcinoma. *Liver Cancer* (2013). doi:10.1159/000343851

240. Chronopoulos, A., Lieberthal, T. J. & del Río Hernández, A. E. Pancreatic cancer: a mechanobiology approach. *Converg. Sci. Phys. Oncol.* (2017). doi:10.1088/2057-1739/aa5d1b

241. Jaalouk, D. E. & Lammerding, J. Mechanotransduction gone awry. *Nature Reviews Molecular Cell Biology* (2009). doi:10.1038/nrm2597

242. Lindeman, J. H. N., Abdul-Hussien, H., van Bockel, J. H., Wolterbeek, R. & Kleemann, R. Clinical Trial of Doxycycline for Matrix Metalloproteinase-9 Inhibition in Patients With an Abdominal Aneurysm. *Circulation* (2009). doi:10.1161/circulationaha.108.806505

243. Zanconato, F., Battilana, G., Cordenonsi, M. & Piccolo, S. YAP/TAZ as therapeutic targets in cancer. *Current Opinion in Pharmacology* (2016). doi:10.1016/j.coph.2016.05.002

244. Pinato, D. J. *et al.* Programmed cell death ligands expression in phaeochromocytomas and paragangliomas: Relationship with the hypoxic response, immune evasion and malignant behavior. *Oncoimmunology* (2017). doi:10.1080/2162402X.2017.1358332

245. Sethna, S. & Finnemann, S. C. Analysis of Photoreceptor Rod Outer Segment Phagocytosis by RPE Cells In Situ. in 245–254 (2012). doi:10.1007/978-1-62703-080-9_17

246. Discher, D. E., Janmey, P. & Wang, Y. L. Tissue cells feel and respond to the stiffness of their substrate. *Science* (2005). doi:10.1126/science.1116995

247. Gauthier, N. C., Masters, T. A. & Sheetz, M. P. Mechanical feedback between membrane tension and dynamics. *Trends Cell Biol.* **22**, 527–35 (2012).

248. Gauthier, N. C., Fardin, M. A., Roca-Cusachs, P. & Sheetz, M. P. Temporary increase in plasma membrane tension coordinates the activation of exocytosis and contraction during cell spreading. *Proc Natl Acad Sci U S A* **108**, 14467–14472 (2011).

249. Yesylevskyy, S. O., Rivel, T. & Ramseyer, C. The influence of curvature on the properties of the plasma membrane. Insights from atomistic molecular dynamics

simulations. *Sci. Rep.* (2017). doi:10.1038/s41598-017-16450-x

250. Roca-Cusachs, P., Gauthier, N. C., Del Rio, A. & Sheetz, M. P. Clustering of alpha(5)beta(1) integrins determines adhesion strength whereas alpha(v)beta(3) and talin enable mechanotransduction. *Proc Natl Acad Sci U S A* **106**, 16245–16250 (2009).

251. Ferraris, G. M. S. *et al.* The interaction between uPAR and vitronectin triggers ligand-independent adhesion signalling by integrins. *EMBO J.* (2014). doi:10.15252/embj.201387611

252. Ruez, R. *et al.* Cells respond to mechanical stress by rapid disassembly of caveolae. *Cell* (2011). doi:10.1016/j.cell.2010.12.031

253. Parton Robert & Kai, S. The multiple faces of caveolae. *Nat. Rev. Mol. Cell Biol.* (2007). doi:10.1038/nrm2122

254. Trouillon, R. & Ewing, A. G. Amperometric measurements at cells support a role for dynamin in the dilation of the fusion pore during exocytosis. *Chemphyschem* **14**, 2295–301 (2013).

255. Diz-Muñoz, A., Fletcher, D. A. & Weiner, O. D. Use the force: Membrane tension as an organizer of cell shape and motility. *Trends in Cell Biology* (2013). doi:10.1016/j.tcb.2012.09.006

256. Meister, A. *et al.* FluidFM: combining atomic force microscopy and nanofluidics in a universal liquid delivery system for single cell applications and beyond. *Nano Lett* **9**, 2501–2507 (2009).

257. Hategan, A., Law, R., Kahn, S. & Discher, D. E. Adhesively-tensed cell membranes: Lysis kinetics and atomic force microscopy probing. *Biophys. J.* (2003). doi:10.1016/S0006-3495(03)74697-9

258. Pegoraro, A. F., Janmey, P. & Weitz, D. A. Mechanical Properties of the Cytoskeleton and Cells. *Cold Spring Harb. Perspect. Biol.* **9**, (2017).

259. Van Aelst, L. & D'Souza-Schorey, C. Rho GTPases and signaling networks. *Genes and Development* (1997). doi:10.1101/gad.11.18.2295

260. Wei, L., Zhou, W., Wang, L. & Schwartz, R. J. β 1 -Integrin and PI 3-kinase regulate RhoA-dependent activation of skeletal α-actin promoter in myoblasts . *Am. J. Physiol. Circ. Physiol.* (2017). doi:10.1152/ajpheart.2000.278.6.h1736

261. Keung, A. J., De Juan-Pardo, E. M., Schaffer, D. V. & Kumar, S. Rho GTPases mediate the mechanosensitive lineage commitment of neural stem cells. *Stem Cells* (2011). doi:10.1002/stem.746

262. Colom, A. *et al.* A fluorescent membrane tension probe. *Nat. Chem.* (2018). doi:10.1038/s41557-018-0127-3

263. Du, J. *et al.* Integrin activation and internalization on soft ECM as a mechanism of

induction of stem cell differentiation by ECM elasticity. *Proc. Natl. Acad. Sci.* (2011). doi:10.1073/pnas.1106467108

264. Moreno-Vicente, R. *et al.* Caveolin-1 Modulates Mechanotransduction Responses to Substrate Stiffness through Actin-Dependent Control of YAP. *Cell Rep.* **25**, 1622-1635.e6 (2018).

265. Von Erlach, T. C. *et al.* Cell-geometry-dependent changes in plasma membrane order direct stem cell signalling and fate. *Nat. Mater.* (2018). doi:10.1038/s41563-017-0014-0

266. Sheetz, M. P., Sable, J. E. & Dobereiner, H. G. Continuous membrane-cytoskeleton adhesion requires continuous accommodation to lipid and cytoskeleton dynamics. *Annu Rev Biophys Biomol Struct* **35**, 417–434 (2006).

267. Apodaca, G. Modulation of membrane traffic by mechanical stimuli. *Am J Physiol Ren. Physiol* **282**, F179-90 (2002).

268. Missirlis, D. The effect of substrate elasticity and actomyosin contractility on different forms of endocytosis. *PLoS One* (2014). doi:10.1371/journal.pone.0096548

269. Arpino, V., Brock, M. & Gill, S. E. The role of TIMPs in regulation of extracellular matrix proteolysis. *Matrix Biol.* **44–46**, 247–54

270. Saha, S., Nagy, T. L. & Weiner, O. D. Joining forces: crosstalk between biochemical signalling and physical forces orchestrates cellular polarity and dynamics. *Philos. Trans. R. Soc. Lond. B. Biol. Sci.* **373**, (2018).

271. Cortes, E. *et al.* Retinoic Acid Receptor-β Is Downregulated in Hepatocellular Carcinoma and Cirrhosis and Its Expression Inhibits Myosin-Driven Activation and Durotaxis in Hepatic Stellate Cells. *Hepatology* (2019). doi:10.1002/hep.30193

272. Nabi, I. R. & Le, P. U. Caveolae/raft-dependent endocytosis. *Journal of Cell Biology* (2003). doi:10.1083/jcb.200302028

273. Henley, J. R., Krueger, E. W. A., Oswald, B. J. & McNiven, M. A. Dynamin-mediated internalization of caveolae. *J. Cell Biol.* (1998). doi:10.1083/jcb.141.1.85

274. Bonifacino, J. S. & Glick, B. S. The Mechanisms of Vesicle Budding and Fusion. *Cell* (2004). doi:10.1016/S0092-8674(03)01079-1

275. Zhang, X. C., Liu, Z. & Li, J. From membrane tension to channel gating: A principal energy transfer mechanism for mechanosensitive channels. *Protein Sci.* **25**, 1954–1964 (2016).

276. Shihata, W. A., Putra, M. R. A. & Chin-Dusting, J. P. F. Is There a Potential Therapeutic Role for Caveolin-1 in Fibrosis? *Front. Pharmacol.* (2017). doi:10.3389/fphar.2017.00567

277. Cortes, E. *et al.* Tamoxifen mechanically deactivates hepatic stellate cells via the G

protein-coupled estrogen receptor. *Oncogene* (2019). doi:10.1038/s41388-018-0631-3

278. Warren, S. C. *et al.* Rapid Global Fitting of Large Fluorescence Lifetime Imaging Microscopy Datasets. *PLoS One* (2013). doi:10.1371/journal.pone.0070687

279. Herrmann, I. K. *et al.* Differentiating sepsis from non-infectious systemic inflammation based on microvesicle-bacteria aggregation. *Nanoscale* **7**, 13511–20 (2015).

280. Zimmerman, M. A., Budish, R. A., Kashyap, S. & Lindsey, S. H. GPER-novel membrane oestrogen receptor. *Clin. Sci. (Lond).* **130**, 1005–16 (2016).

281. Etienne-Manneville, S. & Hall, A. Rho GTPases in cell biology. *Nature* (2002). doi:10.1038/nature01148

282. Sadok, A. & Marshall, C. J. Rho gtpases masters of cell migration. *Small GTPases* (2014). doi:10.4161/sgtp.29710

283. Nardone, G. *et al.* YAP regulates cell mechanics by controlling focal adhesion assembly. *Nat. Commun.* (2017). doi:10.1038/ncomms15321

284. Hall, A. Rho family GTPases. *Biochem. Soc. Trans.* **40**, 1378–82 (2012).

285. Geiger, B., Spatz, J. P. & Bershadsky, A. D. Environmental sensing through focal adhesions. *Nat. Rev. Mol. Cell Biol.* **10**, 21–33 (2009).

286. Gardel, M. L. *et al.* Mechanical Integration of Actin and Adhesion Dynamics in Cell Migration. *Annu. Rev. Cell Dev. Biol.* **26**, 315–333 (2010).

287. Sit, S.-T. S.-T. & Manser, E. Rho GTPases and their role in organizing the actin cytoskeleton. *J. Cell Sci.* **124**, 679–683 (2011).

288. Yusuf, B. *et al.* Embryonic fibroblasts represent a connecting link between mesenchymal and embryonic stem cells. *Dev. Growth Differ.* **55**, 330–340 (2013).

289. McBeath, R., Pirone, D. M., Nelson, C. M., Bhadriraju, K. & Chen, C. S. Cell shape, cytoskeletal tension, and RhoA regulate stem cell lineage commitment. *Dev. Cell* (2004). doi:10.1016/S1534-5807(04)00075-9

290. Bologa, C. G. *et al.* Virtual and biomolecular screening converge on a selective agonist for GPR30. *Nat. Chem. Biol.* **2**, 207–212 (2006).

291. Kimura, K. *et al.* Regulation of Myosin Phosphatase by Rho and Rho-Associated Kinase (Rho-Kinase). *Science (80-.).* **273**, 245–248 (1996).

292. Watanabe, N., Kato, T., Fujita, A., Ishizaki, T. & Narumiya, S. Cooperation between mDia1 and ROCK in Rho-induced actin reorganization. *Nat. Cell Biol.* **1**, 136–143 (1999).

293. Lessey, E. C., Guilluy, C. & Burridge, K. From Mechanical Force to RhoA Activation. *Biochemistry* **51**, 7420–7432 (2012).

294. FORGET, M.-A., DESROSIERS, R. R., GINGRAS, D. & BÉLIVEAU, R.

Phosphorylation states of Cdc42 and RhoA regulate their interactions with Rho GDP dissociation inhibitor and their extraction from biological membranes. *Biochem. J.* **361**, 243–254 (2002).

295. Lang, P. *et al.* Protein kinase A phosphorylation of RhoA mediates the morphological and functional effects of cyclic AMP in cytotoxic lymphocytes. *EMBO J.* **15**, 510–519 (1996).

296. Murrell, M., Oakes, P. W., Lenz, M. & Gardel, M. L. Forcing cells into shape: the mechanics of actomyosin contractility. *Nat. Rev. Mol. Cell Biol.* **16**, 486–498 (2015).

297. Dennis, M. K. *et al.* In vivo effects of a GPR30 antagonist. *Nat. Chem. Biol.* **5**, 421–427 (2009).

298. Fournier, M. F., Sauser, R., Ambrosi, D., Meister, J.-J. & Verkhovsky, A. B. Force transmission in migrating cells. *J. Cell Biol.* **188**, 287–297 (2010).

299. Brückner, B. R. & Janshoff, A. Elastic properties of epithelial cells probed by atomic force microscopy. *Biochim. Biophys. Acta - Mol. Cell Res.* **1853**, 3075–3082 (2015).

300. Solon, J., Levental, I., Sengupta, K., Georges, P. C. & Janmey, P. A. Fibroblast Adaptation and Stiffness Matching to Soft Elastic Substrates. *Biophys. J.* **93**, 4453–4461 (2007).

301. Guilluy, C. *et al.* The Rho GEFs LARG and GEF-H1 regulate the mechanical response to force on integrins. *Nat. Cell Biol.* **13**, 722–727 (2011).

302. Hinz, B. & Gabbiani, G. Mechanisms of force generation and transmission by myofibroblasts. *Curr. Opin. Biotechnol.* **14**, 538–546 (2003).

303. Goodpaster, T. *et al.* An Immunohistochemical Method for Identifying Fibroblasts in Formalin-fixed, Paraffin-embedded Tissue. *J. Histochem. Cytochem.* **56**, 347–358 (2007).

304. Kovac, B., Teo, J. L., Mäkelä, T. P. & Vallenius, T. Assembly of non-contractile dorsal stress fibers requires α-actinin-1 and Rac1 in migrating and spreading cells. *J. Cell Sci.* **126**, 263–273 (2012).

305. Tojkander, S., Gateva, G. & Lappalainen, P. Actin stress fibers - assembly, dynamics and biological roles. *J. Cell Sci.* **125**, 1855–1864 (2012).

306. Parsons, J. T., Horwitz, A. R. & Schwartz, M. A. Cell adhesion: integrating cytoskeletal dynamics and cellular tension. *Nat Rev Mol Cell Biol* **11**, 633–643 (2010).

307. Wolfenson, H., Bershadsky, A., Henis, Y. I. & Geiger, B. Actomyosin-generated tension controls the molecular kinetics of focal adhesions. *J. Cell Sci.* **124**, 1425–1432 (2011).

308. Lachowski, D. *et al.* FAK controls the mechanical activation of YAP, a transcriptional regulator required for durotaxis. *FASEB J* (2017). doi:10.1096/fj.201700721R

309. Scott, L. E., Mair, D. B., Narang, J. D., Feleke, K. & Lemmon, C. A. Fibronectin fibrillogenesis facilitates mechano-dependent cell spreading, force generation, and nuclear size in human embryonic fibroblasts. *Integr. Biol.* **7**, 1454–1465 (2015).

310. Feng, Y., LoGrasso, P. V, Defert, O. & Li, R. Rho Kinase (ROCK) Inhibitors and Their Therapeutic Potential. *J. Med. Chem.* **59**, 2269–2300 (2015).

311. Feldman, R. D. & Limbird, L. E. GPER (GPR30): A Nongenomic Receptor (GPCR) for Steroid Hormones with Implications for Cardiovascular Disease and Cancer. *Annu. Rev. Pharmacol. Toxicol.* **57**, 567–584 (2017).

312. Barton, M. & Prossnitz, E. R. Emerging roles of GPER in diabetes and atherosclerosis. *Trends Endocrinol. Metab.* **26**, 185–192 (2015).

313. Piccolo, S., Dupont, S. & Cordenonsi, M. The Biology of YAP/TAZ: Hippo Signaling and Beyond. *Physiol. Rev.* (2014). doi:10.1152/physrev.00005.2014

314. Wang, L. *et al.* Integrin-YAP/TAZ-JNK cascade mediates atheroprotective effect of unidirectional shear flow. *Nature* **540**, 579–582 (2016).

315. Xu, W., Baribault, H. & Adamson, E. D. Vinculin knockout results in heart and brain defects during embryonic development. *Development* (1998).

316. Bruckner-Tuderman, L., von der Mark, K., Pihlajaniemi, T. & Unsicker, K. Cell interactions with the extracellular matrix. *Cell Tissue Res.* **339**, 1–5 (2010).

317. Liu, A. P., Chaudhuri, O. & Parekh, S. H. New advances in probing cell-extracellular matrix interactions. *Integr. Biol. (Camb).* **9**, 383–405 (2017).

318. Vogel, V. Unraveling the Mechanobiology of Extracellular Matrix. *Annu. Rev. Physiol.* **80**, 353–387 (2018).

319. Rosso, F., Giordano, A., Barbarisi, M. & Barbarisi, A. From cell-ECM interactions to tissue engineering. *J. Cell. Physiol.* **199**, 174–80 (2004).

320. Puklin-Faucher, E. & Sheetz, M. P. The mechanical integrin cycle. *J Cell Sci* **122**, 179–186 (2009).

321. Rg Schrader, J. *et al.* Matrix Stiffness Modulates Proliferation, Chemotherapeutic Response, and Dormancy in Hepatocellular Carcinoma Cells. (2011). doi:10.1002/hep.24108

322. Charrier, A. *et al.* Connective tissue growth factor (CCN2) and microRNA-21 are components of a positive feedback loop in pancreatic stellate cells (PSC) during chronic pancreatitis and are exported in PSC-derived exosomes. *J. Cell Commun. Signal.* (2014). doi:10.1007/s12079-014-0220-3

323. Kordes, C., Brookmann, S., Häussinger, D. & Klonowski-Stumpe, H. Differential and synergistic effects of platelet-derived growth factor-BB and transforming growth factor-beta1 on activated pancreatic stellate cells. *Pancreas* **31**, 156–67 (2005).

324. Olsen, A. L. *et al.* Hepatic stellate cells require a stiff environment for myofibroblastic differentiation. *Am J Physiol Gastrointest Liver Physiol* **301**, G110-8 (2011).

325. McKee, T. D. *et al.* Degradation of fibrillar collagen in a human melanoma xenograft improves the efficacy of an oncolytic herpes simplex virus vector. *Cancer Res.* **66**, 2509–2513 (2006).

326. Hadden, W. J. *et al.* Stem cell migration and mechanotransduction on linear stiffness gradient hydrogels. *Proc. Natl. Acad. Sci. U. S. A.* **114**, 5647–5652 (2017).

327. Chaudhuri, O. *et al.* Extracellular matrix stiffness and composition jointly regulate the induction of malignant phenotypes in mammary epithelium. *Nat Mater* **13**, 970–978 (2014).

328. Leifler, K. S. *et al.* Inflammation Induced by MMP-9 Enhances Tumor Regression of Experimental Breast Cancer. *J. Immunol.* **190**, 4420–4430 (2013).

329. Egeblad, M. & Werb, Z. New functions for the matrix metalloproteinases in cancer progression. *Nature Reviews Cancer* **2**, 161–174 (2002).

330. Köhrmann, A., Kammerer, U., Kapp, M., Dietl, J. & Anacker, J. Expression of matrix metalloproteinases (MMPs) in primary human breast cancer and breast cancer cell lines: New findings and review of the literature. *BMC Cancer* **9**, (2009).

331. Wen, P. J. *et al.* Actin dynamics provides membrane tension to merge fusing vesicles into the plasma membrane. *Nat Commun* **7**, 12604 (2016).

332. Li, Z. *et al.* GPER inhibits diabetes-mediated RhoA activation to prevent vascular endothelial dysfunction. *Eur. J. Cell Biol.* **95**, 100–113 (2016).